https://doi.org/10.1070/RCR4932

# Supercritical fluids in chemistry

**Evgenii S. Alekseev,[a] Alexander Yu. Alentiev,[b] Anastasia S. Belova,[c] Viktor I. Bogdan,[a, d] Tatiana V. Bogdan,[a] Aleksandra V. Bystrova,[c, e] Elvira R. Gafarova,[f] Elena N. Golubeva,[a] Ekaterina A. Grebenik,[f] Oleg I. Gromov,[a] Vadim A. Davankov,[c] Sergei G. Zlotin,[d] Mikhail G. Kiselev,[g] Aleksei E. Koklin,[d] Yuriy N. Kononevich,[c] Alexey E. Lazhko,[h] Valerii V. Lunin (deceased),[a] Sergey E. Lyubimov,[c] Oleg N. Martyanov,[i] Igor I.Mishanin,[d] Aziz M. Muzafarov,[c, e] Nikolay S. Nesterov,[i] Alexander Yu. Nikolaev,[c] Roman D. Oparin,[g] Olga O. Parenago,[h] Oleg P. Parenago,[b] Yana A. Pokusaeva,[d] Inga A. Ronova,[c] Anna B. Solovieva,[j] Maxim N. Temnikov,[c] Peter S. Timashev,[f, j, k] Olga V. Turova,[d] Evgeniya V. Filatova,[d] Alexey A. Philippov,[i] Andrey M. Chibiryaev,[i] Anton S. Shalygin[i]**

*[a] Lomonosov Moscow State University, Faculty of Chemistry, Leninskiye Gory, stroenie 3, 119991 Moscow, Russian Federation,*
*[b] A.V.Topchiev Institute of Petrochemical Synthesis of the Russian Academy of Sciences, Leninsky prosp. 29, 119991 Moscow, Russian Federation,*
*[c] A.N.Nesmeyanov Institute of Organoelement Compounds of the Russian Academy of Sciences, ul. Vavilova 28, 119991 Moscow, Russian Federation,*
*[d] N.D.Zelinsky Institute of Organic Chemistry of the Russian Academy of Sciences, Leninsky prosp. 47, 119991 Moscow, Russian Federation,*
*[e] Enikolopov Institute of Synthetic Polymeric Materials of the Russian Academy of Sciences, ul. Profsoyuznaya 70, 117393 Moscow, Russian Federation,*
*[f] I.M.Sechenov First Moscow State Medical University, Institute for Regenerative Medicine, ul. Trubetskaya 8, stroenie 2, 119991 Moscow, Russian Federation,*
*[g] G.A.Krestov Institute of Solution Chemistry of the Russian Academy of Sciences, ul. Akademicheskaya 1, 153045 Ivanovo, Russian Federation,*
*[h] Kurnakov Institute of General and Inorganic Chemistry of the Russian Academy of Sciences, Leninsky prosp. 31, 119991 Moscow, Russian Federation,*
*[i] Boreskov Institute of Catalysis, Siberian Branch of the Russian Academy of Sciences, prosp. Akademika Lavrentieva 5, 630090 Novosibirsk, Russian Federation,*
*[j] Semenov Institute of Chemical Physics of the Russian Academy of Sciences, ul. Kosygina 4, 117977 Moscow, Russian Federation,*
*[k] Institute of Photonic Technologies, Federal Research Center 'Crystallography and Photonics' of the Russian Academy of Sciences, ul. Pionerskaya 2, 108840 Moscow, Troitsk, Russian Federation*

Dedicated the memory of Akademician Valery Vasilievich Lunin, a friend, colleague, teacher, founder and leader of the research into application of supercritical fluids in chemistry.

**Received 13 December 2019**

© 2020 Uspekhi Khimii, ZIOC RAS, Russian Academy of Sciences and IOP Publishing Limited

This review analyzes the rapidly developing applications of supercritical fluids, mainly supercritical carbon dioxide, in catalysis, chemistry of high-molecular-weight compounds, and medicinal chemistry in Russia and abroad. It considers the methods of catalyst preparation based on impregnation of inorganic and organic supports with metal-containing compounds, immobilization of organometallic and metal complex reagents in matrices of oxide and polymer supports, and deposition processes employing supercritical fluids. An analysis is presented of the prospects for applying $CO_2$ and some organic compounds, such as aliphatic alcohols, in sub- and supercritical states as reactants and (or) solvents for catalytic reactions of hydrocarbon isomerization and cracking, hydrogenation, dehydrogenation, oxidation, *etc.*, including the asymmetric reactions. The review discusses processes of synthesizing and modifying polymer materials for various purposes, including aerogels, foams, and composites impregnated with photochromes, in a supercritical fluid medium. Special attention is paid to supercritical one-pot processes, which make the techniques of obtaining new materials simpler, less expensive, and more efficient. The work investigates the effect of supercritical $CO_2$ on the morphology, gas separation characteristics, and dielectric properties of polymers. One of the promising applications of supercritical fluids in medicine is the use in transplantology and pharmacology, for example, for the preparation of drug polymorphs with higher bioavailability. The review also provides an overview of the recent data on the use of EPR spectroscopy for studying the properties of supercritical fluids, including those exhibited in the vicinity of the critical point and identifying the intermediates of chemical reactions in such media.
The bibliography includes 1151 references.

## Contents

1. Introduction 1339
2. Supercritical fluids in catalysis 1341
2.1. Formation of active sites of heterogeneous catalysts in supercritical carbon dioxide 1342
2.1.1. General principles of creating catalysts in sc-$CO_2$ 1342
2.1.2. Oxide supports 1343
2.1.3. Carbonaceous supports 1344
2.1.4. Polymer supports 1345
2.2. Supercritical solvents in the synthesis of heterogeneous catalysts and in chemical reduction processes 1346
2.2.1. Precipitation and drying in supercritical conditions as a promising method of synthesizing heterogeneous catalysts, adsorbents and supports 1346
2.2.2. Reducing properties of supercritical alcohols as a fundamental basis for innovative chemical processes 1351
2.3. Heterogeneous catalytic reactions in supercritical fluids 1357
2.3.1. Reactions with solid acid and base catalysts 1357
2.3.2. Hydrogenation and dehydrogenation 1359
2.3.3. Oxidation 1361
2.4. Enantioselective catalytic reactions in supercritical fluids 1363
2.4.1. Asymmetric hydrogenation 1363
2.4.2. Enantioselective reactions accompanied by the formation of a carbon – carbon bond 1369
2.4.3. Enantioselective reactions accompanied by the formation of a carbon – heteroatom bond 1373
2.4.4. Asymmetric tandem and domino reactions 1373
3. Supercritical fluids in the chemistry of polymers 1375
3.1. Preparation of advanced polymer materials in supercritical fluids 1375
3.1.1. Synthesis of polymers in supercritical carbon dioxide 1375
3.1.2. Chemical modification of polymers in sc-$CO_2$. Preparation of cross-linked polymers 1379
3.1.3. Preparation of aerogels by traditional and alternative methods 1379
3.1.4. Polymer foam materials obtained by supercritical methods 1381
3.2. Modification of glassy polymers and polymeric membranes by supercritical carbon dioxide 1383
3.2.1. Pore formation in $CO_2$ desorption processes 1384
3.2.2. Modification of gas separation properties of nonporous polymer membranes by sc-$CO_2$ 1385
3.3. Impregnation of polymers with photoactive compounds in supercritical $CO_2$ 1391
3.3.1. SCF-modification of polymers by compounds that are poorly soluble and insoluble in sc-$CO_2$ 1392
3.3.2. Impregnation of polymers with photochromic indoline derivatives in sc-$CO_2$ 1393
3.3.3. Matrix SCF immobilization of spiro indoline compound – polymer systems 1394
4. Supercritical fluids for medicine 1396
4.1. Formation of decellularized biological tissues in sc-$CO_2$: chemical aspects 1396
4.1.1. Decellularization of biological tissues in sc-$CO_2$ in combination with chemical agents 1396
4.1.2. Sterilization of biological tissue implants in sc-$CO_2$ 1398
4.2. Polymorphism screening of biologically active substances in a supercritical fluid medium 1400
4.2.1. Types of polymorphism 1400
4.2.2. Methods of polymorph preparation 1400
4.2.3. SCF technologies for obtaining crystalline forms of active pharmaceutical ingredients 1401
4.2.4. Polymorphism of drug compounds in sc-$CO_2$ 1401
4.2.5. Polymorphism of micronized forms of active pharmaceutical ingredients 1402

5. EPR spectroscopy of supercritical fluids 1403
5.1. EPR spectroscopy at a high pressure 1404
5.2. EPR spectroscopy of supercritical fluids *in situ*: the main results 1404
5.2.1. Local increase in supercritical fluid density 1404
5.2.2. Heisenberg spin exchange. Bimolecular processes 1405
5.2.3. Clustering of substances dissolved in supercritical fluids 1405
5.2.4. Micelle formation in supercritical fluids 1406
5.2.5. Polymers in sub- and supercritical solvents 1406
5.3. EPR spectroscopy of intermediates of chemical reactions in supercritical fluids 1406
6. Conclusion 1407

## 1. Introduction

The supercritical (sc) state of matter was discovered in 1822 by Charles Cagniard de la Tour, who noticed that alcohols sealed in a glass tube lost their transparency on heating in a particular temperature region. At still higher temperatures, the substances became transparent again, and the fluid filled the whole tube volume. It was later found that such transformations were caused by second-order phase transitions. According to the IUPAC definition, the maximum temperature at which a gas can turn into a liquid following a pressure increase is called critical temperature of the phase transition to the sc state ($T_c$), whereas the minimum pressure at which a substance at its critical temperature can be condensed is referred to as critical pressure ($P_c$). Supercritical fluid (SCF) is defined as the state of matter in which the thermodynamic parameters of a substance are higher than its critical pressure and temperature. A substance in the sc state has specific physicochemical properties. The fluid surface tension above the critical point is equal to zero, but its dissolving capacity and ability to penetrate into pores (swelling) significantly increase, and its viscosity decreases. Importantly, SCF properties can be easily controlled by changing the parameters of state.

Carbon dioxide is the most promising SCF, since its critical point parameters are easy to achieve ($T_c$ = 31.1 °C, $P_c$ = 72.8 atm), it is inexpensive, nontoxic, non-explosive, and nonflammable, and it can be readily removed from the reaction mixture by simply reducing the pressure. Supercritical carbon dioxide (sc-$CO_2$) has a perfect combination of properties of gases at high pressure (low density and high diffusion coefficient) and liquids (high dissolving capacity), which ensures, on the one hand, a fast mass transfer and, on the other hand, better (compared to liquids) penetration into porous supports. Some other compounds, including water, lower alcohols, and some hydrocarbons are also thought to be promising SCFs.

Despite such good application prospects of SCFs in chemical processes, they had been rarely used in industry until the mid-20th century. The situation changed radically when the green chemistry concept was introduced. The SCF chemistry is fully in line with this concept. The increasing environmental pollution stimulated the development of supercritical fluid technologies (SCFTs) in the early 1990s, and now this branch of chemistry is the leader in creating new materials by green chemistry methods. The unique physicochemical properties of SCFs have allowed scientists to carry out numerous reactions in a supercritical medium, to obtain materials with unique characteristics, to selectively extract organic compounds from mixtures and various specimens, including those of natural origin (plants), *etc*. At the same time, SCFTs offer the highest level of environmental safety.

This review provides a summary of some results achieved in the last few years by Russian and foreign scientists in the field of SCF application in catalysis, chemistry of polymers, and medicinal chemistry. It discusses the SCF method of obtaining catalysts by impregnation of inorganic and organic supports with metal-containing compounds. The review also analyzes a promising approach to creating highly active catalysts of hydroprocesses that are widely used in organic chemistry and petrochemistry. This

**A.Yu.Alentiev**. Doctor of Chemical Sciences, Professor, Leading Researcher, TIPS RAS.
E-mail: Alentiev@ips.ac.ru; Alentiev1963@mail.ru
**V.I.Bogdan**. Doctor of Chemical Sciences, Leading Researcher, ZIOC RAS.
E-mail: bogdan@ioc.ac.ru, vibogdan@gmail.com
**A.V.Bystrova**. Researcher, ISPM RAS and INEOS RAS.
E-mail: bystrova@ispm.ru
**E.N.Golubeva**. Doctor of Chemical Sciences, Leading Researcher, Faculty of Chemistry, MSU.
E-mail: legol@mail.ru
**E.A.Grebenik**. PhD in Biophysics, Leading Researcher, Institute for Regenerative Medicine, First Moscow State Medical University.
E-mail: grebeneka@gmail.com
**O.I.Gromov**. Candidate of Chemical Sciences (PhD), Researcher, Faculty of Chemistry, MSU.
E-mail: aalchm@gmail.com
**S.G.Zlotin**. Doctor of Chemical Sciences, Professor, Head of Laboratory, ZIOC RAS.
E-mail: zlotin@ioc.ac.ru
**M.G.Kiselev**. Doctor of Chemical Sciences, Director, ISC RAS.
E-mail: mgk@isc-ras.ru
**O.N.Martyanov**. Doctor of Chemical Sciences, Professor of the Russian Academy of Sciences, Deputy Director and Head of Laboratory, BIC SB RAS.
E-mail: oleg@catalysis.ru
**A.M.Muzafarov**. Academician, Doctor of Chemical Sciences, Chief Researcher, ISPM RAS and INEOS RAS.
E-mail: aziz@ispm.ru
**O.O.Parenago**. Candidate of Chemical Sciences (PhD), Senior Researcher, IGIC RAS.
E-mail: oparenago@scf-tp.ru
**O.P.Parenago**. Doctor of Chemical Sciences, Professor, Chief Researcher, TIPS RAS.
E-mail: parenago@ips.ac.ru
**A.B.Solovieva**. Doctor of Chemical Sciences, Professor, Head of Laboratory, FRCCP RAS.
E-mail: ann.solovieva@gmail.com
**P.S.Timashev**. Doctor of Chemical Sciences, Director, Institute for Regenerative Medicine, First Moscow State Medical University; Chief Researcher, Institute of Photonic Technologies and FRCCP RAS.
E-mail: timashev.peter@gmail.com
**A.M.Chibiryaev**. Candidate of Chemical Sciences (PhD), Associate Professor, Senior Researcher, BIC SB RAS.
E-mail: chibirv@catalysis.ru

Translation: E.G.Mancheva

approach is based on immobilization of organometallic and metal complex compounds in oxide and polymer support matrices in sc-$CO_2$. An interesting application of SCFs is their use as selective antisolvents for obtaining active catalysts, including multicomponent ones, by the precipitation method. Many catalytic reactions, including asymmetric ones, have higher rates and selectivities when conducted in sc-$CO_2$ than in conventional organic solvents. Other SCFs can also exhibit useful properties in catalytic processes. For example, aliphatic alcohols in the sc state act as highly active H-donors in catalytic transfer hydrogenation, transfer hydrogenolysis, hydrodesulfurization, hydrodeoxygenation, and other reactions.

Good results are achieved when a SCF is used as a medium for obtaining polymer materials, such as aerogels, foams and composites. The one-pot reactions are thought to be among the most promising types of supercritical processes, as they make the techniques of obtaining new materials simpler, less expensive, and more efficient. As a rule, processing of polymer with sc fluids leads to polymer swelling. The review presents a detailed study of the sc-$CO_2$ effect on the morphology and dielectric properties of polymers, their ability to act as membranes and to separate gas mixtures into individual components. It also discusses the use of SCFs for preparation of micronized forms of materials.

An important and promising area of SCF application in modern chemistry is preparation and modification of compounds and materials for medical purposes in such media. An analysis is presented of the data on the use of SCFs for making tissue grafts and their effect on polymorphic transformations of drug compounds. An important feature of chemical processes in sc fluids is that they can be studied by conventional spectroscopic methods, including electron paramagnetic resonance (EPR) techniques. The EPR techniques adjusted to sc conditions make it possible to investigate the properties of SCFs, including those exhibited in the vicinity of the critical point and the structure of intermediates of chemical reactions in such media.

Despite the fact that the list of references includes over 1100 entries, it is non-exhaustive since one review cannot provide a detailed analysis of all the aspects of SCF applications in chemistry and chemical engineering. However, the authors hope that the multidimensional and multidisciplinary character of this review will help the reader to get a better understanding of this promising research field and will probably be useful for the formation of new ideas and development of new branches of green chemistry.

The following abbreviations are used in this review:

AcAc — acetylacetonate;
AIBN — azobis(isobutyronitrile);
API — active pharmaceutical ingredient;
BARF — tetrakis[3,5-bis-(trifluoromethyl)phenyl]borate;
BINAP — 2,2′-bis(diphenylphosphino)-1,1′-binaphthyl;
BINOL — 1,1′-binaphthyl-2,2′-diol;
BMIM — 1-n-butyl-3-methylimidazolium;
BTC — benzene-1,3,5-tricarboxylate;
BTX — benzene–toluene–xylenes (fraction);
BzONO — 4-benzoyloxy-2,2,6,6-tetramethylpiperidine-1-oxyl;
CFA — chemical foaming agent;
CNT — carbon nanotubes;
COD — cycloocta-1,5-diene;
CuFod — copper 2,2,3-trimethyl-6,6,7,7,8,8,8-heptafluorooctane-5,5-dionate;
CXL phase — saturated sc-$CO_2$ phase;
DBA — dibenzylideneacetone;
*de* — diastereomeric excess;
DMG — dimethylglyoxime;
DMAP — 4-dimethylaminopyridine;
DNOZ — 2,2-di-n-nonyl-5,5-dimethyloxazolidine-3-oxyl;
*dr* — diastereomeric ratio;
DSC — differential scanning calorimetry;
DTBN — di-*tert*-butyl nitroxide;
DTBP — di-*tert*-butyl peroxide;
DVB — divinylbenzene;
ECM — extracellular matrix;
EMIM — 1-ethyl-3-methylimidazolium;
*ee* — enantiomeric excess;
$F_6$AcAc — hexafluoroacetylacetonate;
6FDA — (4,4′-hexafluoroisopropylidene)diphthalic anhydride;
FF — functional filler;
FFV — polymer fractional free volume;
FVE — free volume elements.
GO — graphene oxide;
Hdaib — 3-*exo*-(dimethylamino)isoborneolate;
HFC — hyperfine coupling;
HP + SS — high pressure and shear strain;
TH — transfer hydrogenation;
IL — ionic liquid;
LDPE — low-density polyethylene;
MDS — molecular dynamics simulation;
MOF — metal-organic framework;
MPV — Meerwein— Ponndorf–Verley (reaction);
Naph — naphthyl;
(P)AA — (poly)acrylic acid;
(P)AN — (poly)acrylonitrile;
PAC — photoactive compound;
PC — polycarbonate;
PDMS — polydimethylsiloxane;
PEEK — polyetheretherketone;
PEG — polyethylene glycol;
PEI — polyetherimide;
PFA — physical foaming agent;
PFPE — carboxy-perfluoropolyether;
(P)GA — (poly)glycolide;
PHFP — polyhexafluoropropylene;
(P)HEMA — (poly)2-hydroxyethyl methacrylate;
PIM-1 — polybenzoxane;
PI — polyimide;
(P)LA — (poly)lactide;
PLGA — a copolymer of lactic and glycolic acids;
(P)MMA — polymethyl methacrylate;
(P)NEAM — poly-*N*-ethylacrylamide;
PP — polypropylene;
PS — polystyrene;
PTA — phosphotungstic acid;
PTQD — phenanthrene-9,10-quinonedioxime;
(P)VDF — polyvinylidene fluoride;
PVC — polyvinyl chloride;
QD — quantum dots;
RESS — rapid expansion of supercritical solution;
RGO — reduced graphene oxide;
*rr* — regioisomeric ratio;
SAO — spiroanthroxazine;
SAS — supercritical antisolvent precipitation;

SBP — spirobenzopyran;
sc — supercritical;
SCF — supercritical fluid;
SCFT — supercritical fluid technology;
SCW — supercritical water;
SDS — sodium dodecyl sulfate;
SEM — scanning electron microscopy;
SIC — spiro indoline compound
SIO — spiro-indoline-oxazine;
SNO — spironaphthoxazine;
SPO — spirophenanthroxazine;
STP — standard temperature and pressure;
TBPS — 4-*tert*-butylbenzenesulfonyl;
TEM — transmission electron microscopy;
TEMPO — 2,2,6,6-tetramethylpiperidine-1-oxyl;
Tf — trifluoromethanesulfonyl (triflyl);
Tmhd — 2,2,6,6-tetramethylheptane-3,5-dionate;
TON — catalyst turnover number per catalytic cycle;
TMPDA — 2,3,5,6-tetramethylphenylene-1,4-diamine;
VP — 1-vinyl-2-pyrrolidone;
Xyl — 3,5-xylyl;
$a^{N}$ — hyperfine coupling constant with a $^{14}N$ atom;
$D$ — diffusion coefficient;
$d_{in}$ — inner diameter;
$d_{out}$ — outer diameter;
$k_e$ — spin exchange rate constant;
$\tilde{P}$ — permeability coefficient;
$P$ — pressure;
$P_c$ — critical pressure;
$P_r$ — reduced pressure;
$T$ — temperature;
$T_c$ — critical temperature;
$T_g$ — glass transition temperature;
$T_r$ — reduced temperature;
$\alpha_{ij}$ — selectivity (separation factor) for gases $i$ and $j$;
$\alpha_{ij}^{D}$ — diffusion selectivity for gases $i$ and $j$;
$\rho_r$ — reduced medium density;
$\rho_{loc}$ — local medium density;
$\rho_c$ — critical medium density;
$\tau$ — rotational correlation time;

## 2. Supercritical fluids in catalysis

Catalytic processes make up the basis of most modern processes for extentive processing of fossil and renewable hydrocarbon raw materials and are used for obtaining functional materials.[1] They are an integral part of the green chemistry paradigm,[2–4] as they speed up chemical reactions, increase their selectivity, and help to avoid the formation or reduce the amount of side products.

Owing to the development of nanochemical and nanoengineering approaches and methods, great progress has been made in the last few decades in the field of preparation and application of heterogeneous catalysts, including metal nanoparticles.[5–7] Smaller particle sizes considerably increase the ratio of the particle surface area to volume, which results in higher surface energy, whereas the presence of coordinatively unsaturated metal atoms on the nanoparticle surface can potentially significantly enhance the catalytic activity. At the same time, the small size and high surface energy of the particles make them thermodynamically unstable and more prone to aggregation, increase their sensitivity to catalyst poisoning, and promote side reactions. The most common techniques used to inhibit nanoparticle aggregation and increase their stability include introduction of inorganic or organic surfactants for protection of the nanoparticle surface or immobilization of nanoparticles on porous supports.

Supported nanocatalysts are obtained by impregnation, deposition–precipitation,[8] ultrasonic reduction,[9] chemical vapour deposition,[10] and sol–gel process.[11,12] Many of the conventional methods, such as impregnation or deposition–precipitation use solutions for deposition of active components, which may not only lead to particle agglomeration, but also cause the destruction of fragile supports, such as aerogels.[13] The chemical vapour deposition method also has some shortcomings concerning the precursor vapour pressure, process temperature, and mass transfer kinetics.[14] Unfortunately, such approaches do not always produce stable particles of the desired size and geometry. Besides, the use of organic solvents leads to the formation of a lot of waste, which requires further purification, neutralization or recovery, thus decreasing the environmental safety of the process.[4] In the last few decades, chemists have paid considerable attention to the engineering capabilities offered by the application of SCFs, especially sc-$CO_2$.[15–17] For example, application of sc-$CO_2$ at various stages of catalyst preparation (support impregnation, deposition, drying, *etc.*) makes it possible to considerably reduce the amount of organic solvents used, which makes these approaches quite attractive in terms of the environmental safety and complies with the key green chemistry principles defined by Noyori[3] in 2005.

Supercritical fluids have good prospects as solvents in large-scale reactions with heterogeneous catalysts, such as isomerization of alkanes and alkenes, hydrogenation and dehydrogenation, hydrocarbon cracking, oxidation and some other processes.† Carrying out such reactions in SCF increases the yield of target products and selectivity of their formation, ensures stability of catalyst performance by reducing the amount of deposits on the catalyst surface. Besides, aliphatic alcohols in the sc state can serve as effective H-donors in reduction of inorganic compounds and in hydrogenolysis and hydrogenation reactions of organic substrates.‡

There are good prospects for application of liquid and supercritical carbon dioxide as solvent in low-tonnage chemistry processes used for regio-, stereo-, and enantioselective preparation of complex organic compounds, such as drugs, aromatic substances, crop protection chemicals and their precursors.§ A lot of reactions require homogeneous transition metal catalysts or organocatalysts or their analogues immobilized on inorganic or organic substrates. Such catalytic transformations in a $CO_2$ medium, including those occurring in the vicinity of the critical point, make it possible to avoid the use of undesirable toxic organic solvents, which are unacceptable in the resulting pharmaceutical products. Besides, they can be employed to control the phase composition of the system and thus to achieve high selectivity values, and to regenerate valuable chiral catalysts.

These and some other aspects of SCF application in heterogeneous and homogeneous catalysis are discussed in this part of the review.

† See S.Saim, B.Subramaniam. *J. Catal.*, **131**, 445 (1991).
‡ See E.Y.Buslaeva, Y.F.Kargin, K.G.Kravchuk, S.A.Sigachev, S.P.Gubin. *Russ. J. Inorg. Chem.*, **46**, 323 (2001).
§ See monograph *Handbook of Green Chemistry. Supercritical Solvents*. Vol. 4. (Eds P.G.Jessop, W.Leitner). (Weinheim: Wiley-VCH, 2010).

### 2.1. Formation of active sites of heterogeneous catalysts in supercritical carbon dioxide

The problem of preparing, using, and recovery of catalysts remains extremely important virtually for all processes of petrochemistry, crude oil refining, organic synthesis, chemistry of polymers, *etc*. The decisive factor for ensuring the high activity, selectivity and stability of catalyst performance is the catalyst synthesis, which should not only provide the necessary technical properties of the systems formed, but also meet the constantly growing safety requirements. [4]

Great prospects in this field are offered by the use of supercritical carbon dioxide, which has undeniable environmental advantages over traditional organic solvents and make reactions in which it is used compliant with the green chemistry principles. One of the most promising areas of sc-$CO_2$ application is synthesis of supported heterogeneous catalysts for a number of important processes of modern chemical science and engineering.

The first review [18] on this subject focused solely on the preparation of supported metal nanoparticles using supercritical fluids. Another review [19] summarized the results of studies of the synthesis of metal nanoparticles and their use in catalysis and provided a brief description of the preparation of metal nanoparticles in supercritical fluids. Later, the use of supercritical carbon dioxide as the reaction medium became a common method of heterogeneous catalyst synthesis.[20–24]

#### 2.1.1. General principles of creating catalysts in sc-$CO_2$

According to the detailed description given in the review,[18] the synthesis of heterogeneous catalysts includes several stages. The first stage is dissolution of metal-containing compounds — organic complexes or metal salts, most often, with organic anions — in supercritical $CO_2$. It should be said that the properties of sc-$CO_2$ as a reaction medium, namely its density and viscosity, differ a lot from those of conventional organic liquids or gases and can be easily changed by varying pressure and temperature. This fluid, which normally has a higher density than liquid media, is a good solvent for organic and organometallic compounds. Their solubility values in sc-$CO_2$ are given in a review of Smart *et al.*,[25] Prof. Erkey's monograph, [26] and a number of other works.[27–29] For example, Smart *et al.* [25] analyzed the solubility data for 49 metal-containing compounds and 15 types of ligands for metal complexes and showed that fluorinated derivatives of metals have better solubility in sc-$CO_2$, while substitution in the phenyl groups leads to a noticeable solubility decrease. Better solubility can be achieved by increasing the metal oxidation state and ligand size.

After dissolution in sc-$CO_2$, the compounds get into contact with inorganic or polymeric supports on variation of the deposition conditions (temperature, pressure, and time). There are several ways to transform metal-containing compounds acting as catalyst precursors into metal particles (Fig. 1):[18]

1) chemical reduction in sc-$CO_2$ by reducing agents such as hydrogen or alcohols;

2) thermal reduction in sc-$CO_2$;

3) thermal decomposition in an inert atmosphere or reduction by hydrogen after decompression.

Supercritical $CO_2$ was first used as a reaction medium for obtaining polymer-supported platinum nanoparticles in 1995.[30] Poly(4-methylpent-1-ene) or polytetrafluoroethylene was used as the support, and dimethyl(cycloocta-1,5-diene)platinum [Pt(COD)$Me_2$] served as the precursor. The complex was reduced to the metal by the three methods described above. It was found that the particles obtained by the thermal method (see method 2) were somewhat larger ($< 100$ nm) than those prepared by hydrogen reduction in sc-$CO_2$ ($< 50$ nm) or after decompression (15 nm).

Watkins and McCarthy,[30] who pioneered this field of research, inspired a series of studies on sc-$CO_2$ application in the synthesis of supported nanocomposites of various metals for microelectronics, optics, and catalysis.[20, 21, 31–33] Most of these works used inorganic supports such as alumina, silica, aerogels, zeolites, carbon materials, *etc*.

Besides traditional methods of deposition of active components, there is another interesting technique for synthesizing heterogeneous catalysts based on laser ablation of metal targets in the presence of various supports, which serve as matrices for metal particle deposition. A review [34]

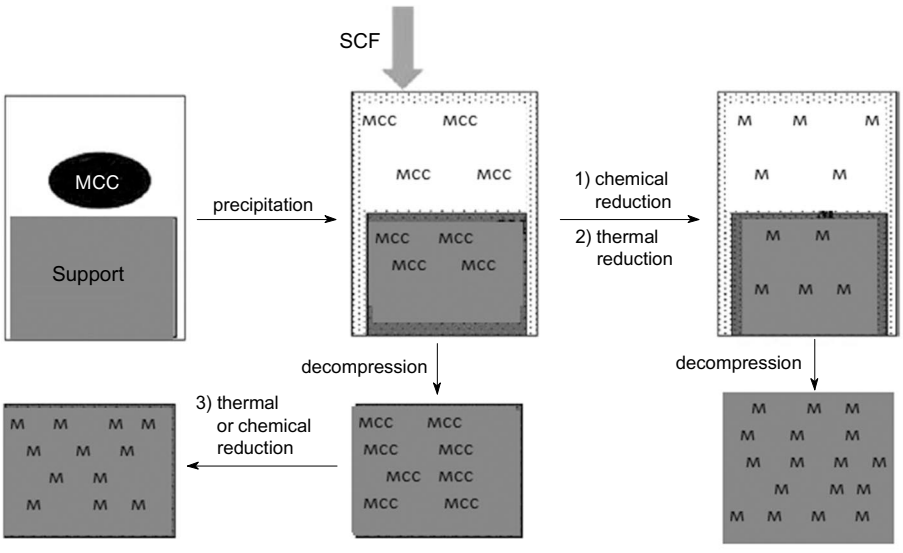



**Figure 1.** Diagram of using SCF solvent for the preparation of supported metal particles.[18] MCC is a metal-containing compound, M is a metal particle. Reproduced with the permission of Elsevier.

published in 2016 discusses the distinguishing features of this approach, mainly focusing on the most recent works, in which the authors obtained supported metal nanoparticles by laser ablation in a liquid medium (usually in water) instead of the gas phase. It is worth noting that the laser ablation method can produce high-purity metal nanoparticles, unlike the method described above, in which supported metal particles after reduction may contain residual amounts of the original anions or ligands.

Of special interest is preparation of metal particles deposited by laser ablation in sc-$CO_2$, as in this case, the drift of metal particles towards the support surface and the properties of the deposited particles (their size and size distribution, morphology, *etc.*) can be controlled by varying the SCF parameters (pressure and temperature). Some results concerning laser ablation in sc-$CO_2$ with various supports have been reported.[35–38] One of the first examples of using sc-$CO_2$ in laser ablation of metal targets for preparation of heterogeneous catalysts was described by Epifanov *et al.*,[39,40] who deposited palladium particles on alumina.

#### 2.1.2. Oxide supports

Oxide type supports (usually metal oxides) belong to the class of porous materials, like ceramics, carbon materials, and membranes. Such materials are characterized by macro-, meso-, and microporosity or their combination and by textural and physical properties, which are determined by their structure. Metal oxides are the biggest class of porous materials. They posses high thermal and chemical stability combined with a well-developed porous structure and a large specific surface area ($>100$ $m^2\,g^{-1}$). One of the advantages of these materials is also the simplicity of their preparation and functionalization. Supported catalysts are most often prepared on silica, alumina, titania, ceria, zirconia, and iron oxide.

After the first publication of Watkins and McCarthy,[30] quite a few studies dealing with metal deposition on oxide supports in sc-$CO_2$ medium appeared in the beginning of the 21st century. For example, some of the works described palladium particle deposition on alumina samples with different specific surface areas: $\alpha$-$Al_2O_3$ (13 $m^2\,g^{-1}$) and $\gamma$-$Al_2O_3$ (207 $m^2\,g^{-1}$).[41–43] Palladium hexafluoroacetylacetonate $Pd(F_6AcAc)_2$ served as the starting compound. After hydrogen reduction of the palladium complex, electron microscopy examination showed that in the case of $\alpha$-$Al_2O_3$, the palladium content in the support was 0.15 mass % – 1.54 mass % and the particles were 13 – 60 nm in size. In the case of $\gamma$-$Al_2O_3$, the palladium content was 0.58 mass % – 3.94 mass % and the particle size was 3 – 7 nm.

Deal *et al.*[44] also deposited platinum on alumina by impregnating alumina with platinum acetylacetonate in sc-$CO_2$. In some of the experiments, before deposition of the complex, ceria was applied on alumina and subsequently used to catalyze the water shift reaction. In another study,[45] devoted to the preparation of $\gamma$-alumina-supported catalysts, palladium complexes $Pd(PTQD)_2$ and $Pd(DMG)_2$ with fluorine-free ligands — phenanthrene-9,10-quinone dioxime (PTQD) and dimethylglyoxime (DMG) — served as the precursors. For the former compound, the palladium particles were 2 nm in size. For the latter compound, the particle size was 7 nm. The obtained nanocomposites were used as catalysts in the Suzuki – Miyaura coupling reaction. Mention should be made of the study[46] in which dimethyl(acetylacetonate)gold(III) $Au(AcAc)Me_2$ was deposited on silica gel in sc-$CO_2$. The gold particles formed after the complex reduction were 3.7 – 6.6 nm in size. Interestingly, the use of a fluorinated acetylacetonate ligand did not lead to the formation of any supported gold particles that could be identified by transmission electron microscopy (TEM) or X-ray diffraction methods. Deposition of gold particles in sc-$CO_2$ on the titania support has been reported.[47] The obtained catalyst was used in the mild oxidation of alcohols to aldehydes and ketones.

Of special interest are mesoporous supports, whhich have an ordered structure and narrow pore size distribution. Besides, in catalytic processes, mesoporous supports, unlike microporous materials, minimize the diffusion limitations associated with the transport of reacting molecules to the active sites and with low yield of reaction products. The fundamental problems of mesoporous silicates have been considered in a review[48] published in 2012; another review[49] published recently addresses various aspects of studying mesoporous materials (silica gels and zeolites), ranging from their synthesis and structure to practical use, including catalytic applications.

In most of the studies, various forms of silicon-containing oxides such as SBA-15, MCM-41, HMS and other silicates, which are most common in catalytic processes, were used as mesoporous supports for metal deposition in sc-$CO_2$. For example, Morère *et al.*[50] reported deposition of $Pd(F_6AcAc)_2$ on the SBA-15 support in sc-$CO_2$ followed by reduced with hydrogen. The size of clusters of Pd particles was limited by the support pore size and tended to increase with increasing impregnation time. The obtained composites could act as catalysts of hydrogenation of 4-nitrophenol to 4-aminophenol. It should be emphasized that palladium was used as the metal to be deposited in a large number of studies. For example, Hunt *et al.*[51] deposited tris(dibenzylideneacetone)dipalladium $Pd_2(DBA)_3$ was deposited on SBA-15 support. The authors noted that in this case, it was possible to avoid palladium nanoparticle agglomeration observed in many other cases. This composite appeared to be active in alkene hydrogenation. Palladium supported on SBA-15, which was deposited in sc-$CO_2$ from a bipyridine complex, had metal particles as large as 13.7 nm and could act as a catalyst in the Suzuki – Miyaura coupling reaction.[52] Palladium deposition on the MCM-41 silica was described.[53] This composite was characterized by uniform dispersion of small nanoparticles and high activity in liquid-phase conversion of biomass processing products.

A number of studies focused on obtaining nanocomposites by deposition of rhodium compounds on mesoporous supports. One of the early works[54] describes the deposition of rhodium acetate $[Rh(OAc)_2]_2$ on FSM-16, a mesoporous support of the silicate type. Hydrogen reduction of the immobilized rhodium compound produced a catalyst that was active in the butane hydrogenolysis reaction. In comparison with the conventional samples, such catalyst was more active and provided a higher ethane yield.

A number of publications by Ushiki *et al.*[29,55–57] represent a detailed study of the mechanisms of metal acetylacetonate deposition on mesoporous supports. The authors proposed a thermodynamic model of $Me(AcAc)_n$ solubility in sc-$CO_2$.[29] Another study[55] provides adsorption (deposition) equilibria of $[Rh(AcAc)_2]_2$ on mesoporous supports of several types (MCM-41, MSU-H, and HMS). The results of

measurement and simulation of $Co(AcAc)_2$ equilibrium adsorption on MCM-41 in sc-$CO_2$ with methanol as the cosolvent was reported.[56]

Among reactions with other metals, worth mentioning is the synthesis of supported catalysts based on nickel, copper, and cobalt. In these cases, cosolvents were used in addition to sc-$CO_2$. For example, Charoenchaitrakool *et al.*[58] obtained a Ni/SBA-15 catalyst, active in methane cracking to give hydrogen using ethanol as the cosolvent. The CuO/SBA-15 nanocomposite was prepared by deposition of an inorganic copper salt in sc-$CO_2$ with a variety of cosolvents such as ethanol, 1,3-propylene glycol, or n-butanol.[59] Cobalt nanoparticles were deposited on a mesoporous silica gel using methanol as the cosolvent.[60]

Preparation of nanocomposites by metal precursor deposition in sc-$CO_2$ makes it possible to fabricate bimetallic catalytic systems. Yen *et al.*[61] obtained bimetallic nanoparticles by deposition of Ru, Rh, and Pd acetylacetonates on SBA-15 in sc-$CO_2$. The particle size was 2–8 nm, according to the TEM, X-ray diffraction, and energy-dispersive X-ray spectroscopy (EDS) data. The samples of these composites demonstrated the ability to act as catalysts in the hydrogenation reaction. Their catalytic activity was almost eight times higher than that of the catalysts obtained by the conventional method. Qiao *et al.*[62] demonstrated that bimetallic compounds including Pt–Pd nanoparticles of 5 nm in size deposited on the SBA-15 silica acted as catalysts in levulinic acid hydrogenation to γ-valerolactone. The substrate conversion was higher in this case than with catalysts obtained in other media.

#### 2.1.3. Carbonaceous supports

Carbonaceous supports for heterogeneous catalysts include activated carbon, graphite, aerogels of various nature, carbon nanotubes (CNTs), carbon black, graphenes, *etc.* Cangül *et al.*[63] used a traditional support, carbon black, to deposit $Pd(AcAc)_2$ or $Pt(COD)Me_2$ complexes or their mixture in sc-$CO_2$. The palladium particles formed after reduction of precursors with hydrogen had a rather broad size distribution (3–100 nm); conversely, for platinum, it was rather narrow (2–6 nm). In the case of the bimetallic composite, the Pd particle size was 10 nm, that of the Pt particles was 4 nm. The $Pt(COD)Me_2$ platinum complex was also deposited in sc-$CO_2$ on another traditional support, namely, graphite. The heating and subsequent hydrogen treatment led to the formation of a composite with 4.5 nm platinum particles.[64]

A lot of studies address catalyst deposition on modern synthetic carbonaceous materials, the advantage of which is that they enable preparation of carbon nanostructures with desired porosity and a large surface area. Besides, such supports can be easily modified by various methods (ozonolysis, plasma treatment, doping with heteroatoms, or acid of alkali treatment). A very interesting type of carbonaceous supports are nanotubes. They have a large surface area, unique morphology and physical properties (such as high electric conductivity), a specific size and hollow structure that are not found in other types. Figure 2 shows clear images of ruthenium nanoparticles dispersed in carbon nanotube channels as an example.[65]

To study the catalytic properties of this type of supports, Pan *et al.*[66] synthesized a palladium-containing composite based on carbon nanotubes in sc-$CO_2$. The composite was active in Suzuki coupling reactions. The authors noted that this catalyst could be regenerated and used six times without losing activity. In the above-mentioned study,[20] Pd, Rh, and Ru as metal β-diketonate precursors were also deposited on nanotubes. The reduction of these compounds with hydrogen resulted in the formation of metal nanoparticles that had a narrow size distribution and acted as catalysts in alkene oxidation to $CO_2$ and electrocatalytic oxidation reactions. Lin *et al.*[67] reported a supported platinum catalyst formed by $Pt(AcAc)_2$ deposition on carbon nanotubes. The platinum nanoparticles of 5–10 nm in size were active in methanol oxidation and oxygen reduction reactions, which made it possible to use them for electrocatalysis in low-temperature fuel cells.

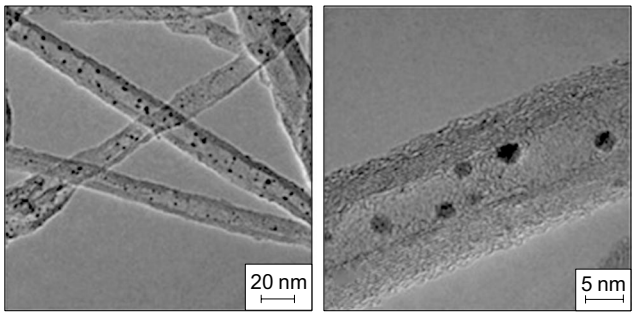



**Figure 2.** TEM images (on different scales) of Ru nanoparticles on carbon nanotubes.[65] Reproduced with the permission of the Royal Society of Chemistry.

The use of nanotubes as supports was described by Yen *et al.*[68,69] They reported[68] the synthesis of a platinum catalyst by $Pt(AcAc)_2$ deposition on carbon nanotubes in sc-$CO_2$ with methanol as the cosolvent. The Pt particles of 5–15 nm in size exhibited activity towards benzene hydrogenation, electrochemical oxidation of methanol, and electrocatalytic oxygen reduction, which opens up the way for using such catalysts in proton-exchange membranes of fuel cells. The other study[69] considered the preparation of bimetallic catalysts based on mixtures of Pt–Ru, Pt–Cu, Pt–Au, Pt–Pd, and Pt–Ni compounds with acetylacetonate ligands or their hexafluoro derivatives deposited on multiwalled carbon nanotubes. The bimetallic nanoparticles (2.8–9.3 nm) turned out to be active in electrocatalytic oxidation of methanol to carbon dioxide (in fuel cells). Their activity was six times higher than that of the monometallic platinum catalyst.[68]

In some of the works, the authors used graphene as a modern carbonaceous support of a regular structure. For example, Zhao *et al.*[70] reported deposition of a platinum compound on graphene prepared by thermal treatment of graphene oxide. The subsequent reduction resulted in the formation of 3.3 nm Pt particles. This composite proved to be active in the electrocatalytic methanol oxidation reaction, with its activity being 3.5 times higher than that of the conventional catalyst — Pt deposited on carbon black (Vulcan XC-72). In another study,[71] the nanocatalysts were obtained by deposition of platinum, ruthenium, and nickel compounds in sc-$CO_2$ on graphene with subsequent hydrogen reduction. The particle size ranged from 2 to 15 nm depending on the metal nature and deposition conditions. The Pt- or Ru-based composites were active in selective limonene hydrogenation to *p*-menth-1-ene.

In addition to the supports discussed above, quite common types of supports for heterogeneous catalysts include aerogels of various nature, including those based

on silica, and also carbon and organic aerogels. They possess unique properties (low viscosity, hardness, transparency, heat resistance, and very low heat conductivity) and have 2 to 5 nm nanoparticle clusters, pores up to 100 nm in size and huge internal voids taking up to 90%–99% of their volume. It is not surprising that supports of this type were also quite useful for preparing supported catalysts in supercritical media.

In an early publication,[72] palladium nanoparticles of two sizes, $<6$ nm and 15–20 nm, were deposited on silica aerogel in sc-$CO_2$. As a result, the palladium content on the support was 8 mass %. The composite was found to be an effective catalyst of cyclohexene hydrogenation in a flow-through reactor. Caputo *et al.*[73] presented an example of preparation of the Ru/$SiO_2$-aerogel composite by $Ru(AcAc)_3$ deposition in sc-$CO_2$. The authors studied the kinetics of deposition of the ruthenium compound on the aerogel, measured adsorption isotherms, and found that the Ru content on the support equals 5 mass %.

Several studies of deposition of metal-containing compounds on carbon aerogels were reported by Prof. Erkey and co-workers.[74–76] The authors deposited $Pt(COD)Me_2$ in sc-$CO_2$ on such a support, while varying conditions of the subsequent complex reduction (gas medium, time, and temperature).[74, 75] It was shown that thermal treatment of the deposited complex at atmospheric pressure in an inert atmosphere (method *1*) led to the formation of particles with a narrow unimodal size distribution (1–3 nm), with the Pt content on the support being 10 mass %–40 mass %. Thermal treatment in sc-$CO_2$ medium (method *2*) increased the content of Pt to 73 mass %. The reduction of the complex with hydrogen (method *3*) resulted in twice larger particles compared to those produced by method *1*, but the unimodal particle distribution and Pt content in the support remained unchanged. In another study,[76] $Ru(AcAc)_3$ and $Ru(COD)(tmhd)_2$ ruthenium complexes were deposited on carbon aerogels of two types (with pore diameters of 4 and 21 nm) in sc-$CO_2$ (tmhd stands for 2,2,6,6-tetramethylheptane-3,5-dionate). The reduction of the complexes was followed by thermal treatment at 300–1000 °C to obtain Ru nanoparticles with a size of 1.7–3.8 nm.

In a comparatively small number of studies, the composites were synthesized with organic aerogels formed from organic compounds, including polymers. For example, the $Pt(COD)Me_2$ platinum complex was deposited on the aerogel prepared from a resorcinol–formaldehyde mixture.[77] The complex reduction at 200 °C in a hydrogen flow led to the formation of platinum nanoparticles with a narrow size distribution (2.0–3.3 nm).

#### 2.1.4. Polymer supports

Less attention has been paid to nanocatalyst preparation by deposition of metal compounds on polymer supports in sc-$CO_2$ than to catalysts based on inorganic porous materials. In the first paper[30] addressing the synthesis of supported nanoparticles in sc-$CO_2$, particularly polymers, poly(4-methylpent-1-ene) or polytetrafluoroethylene, were used as supports for deposition of the $Pt(COD)Me_2$ complex. Another early work[78] also reported the preparation of silver nanoparticles by deposition of the $Ag(F_6AcAc)L$ precursor (L stands for tetraethylene glycol dimethyl ether) on poly(styrene-divinylbenzene) in sc-$CO_2$. The reduction to metal was performed with hydrogen at 60 °C and took 48 h, leading to the formation of 10–100 nm Ag nanoparticles.

Ge *et al.*[79] used polydimethylsiloxane (PDMS) as a polymer support to deposit ruthenium complex $Ru(COD)(tmhd)_2$ in sc-$CO_2$. The authors measured the deposition isotherms of the complex and determined the equilibrium coefficients for the complex distribution between the sc-$CO_2$ and PDMS phases based on the linear section of the curves. The synthesis of hydrogenation catalysts was described by Miao *et al.*,[80] who deposited Pd, Rh, and Pt precursors on hollow polymers in sc-$CO_2$. The reduction of complex with hydrogen afforded $\sim$5 nm metal nanoparticles uniformly distributed over polymer spheres. The composites were active in the allyl alcohol hydrogenation and Heck reactions.

The application of natural nontoxic and cheap polymers (cellulose and chitosan) as supports for heterogeneous catalysts was first described by Baran *et al.*[81] The authors deposited a palladium precursor on these polysaccharides in sc-$CO_2$. The precursor reduction led to the formation of spherical Pd nanoparticles with a size of 26–30 nm that could act as catalysts in the Suzuki–Miyaura coupling reaction.

Another type of polymer materials that could potentially be used as supports for metal nanoparticles is dendrimers — polymers with a tree-like and symmetrical architecture and regular branching. One of the first reviews[82] summarizing the results of studies of dendrimer-based composites and their use in catalysis was published in 2001. The works that followed[83–90] described examples of catalytic reactions, mainly hydrogenation, catalyzed by nanoparticles of the platinum group metals deposited on dendrimers. Among these publications, it is worth mentioning the series of works of Prof. E.A.Karakhanov and co-workers.[85–92] In the last-mentioned study,[92] the authors deposited metal-containing precursors on dendrimers in sc-$CO_2$ and then reduced them with hydrogen. Polypropyleneimine (PPI) and polyamidoamine (PAMAM) dendrimers cross-linked with various diisocyanates were used as such polymers. The precursors were $Rh(AcAc)_3$ and several palladium compounds, including $Pd(O_2CCF_3)_2$ and $Pd(F_6AcAc)_2$, which are quite readily soluble in sc-$CO_2$. According to the TEM data, the reduction yielded small Rh and Pd nanoparticles with a narrow unimodal size distribution in the dendrimer matrix (Fig. 3).

The obtained composites were tested in processes of liquid-phase hydrogenation of unsaturated hydrocarbons (alkenes, conjugated dienes, and alkynes).[92] The rhodium-based catalysts proved to be extremely active in hydrogenation of model alkenes, oct-1-ene and styrene. Their turnover frequency (TOF) ranged from 50 to 100 $s^{-1}$. The palladium catalysts, in addition to very high turnover frequency in diene and alkyne hydrogenation reactions (in some cases their TOF reached 100–200 $s^{-1}$), exhibited high selectivity to alkenes, with a 95%–99% product yield and virtually complete substrate conversion.

Thus, the methods of metal nanoparticle formation on the surface of supports of different nature using supercritical carbon dioxide as the reaction medium are quite effective and have good prospects for the development of catalytic systems for a number of processes of organic chemistry and petrochemistry. The possibility to choose from a wide range of metal-containing precursors and

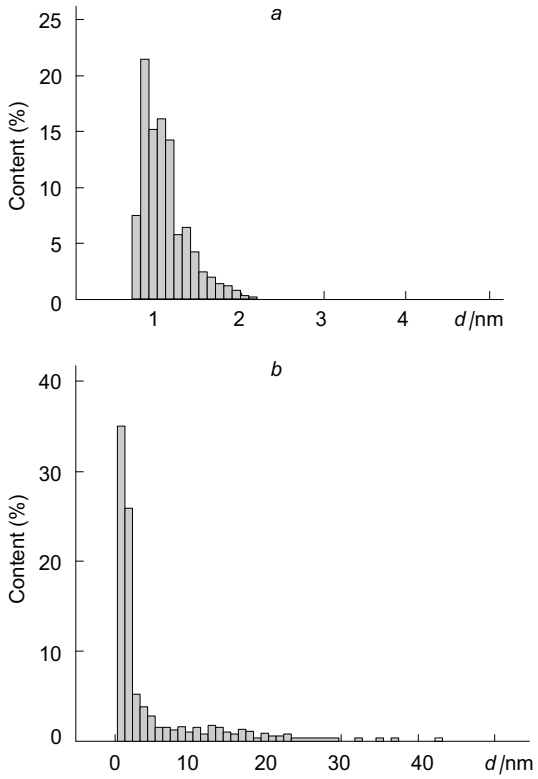



**Figure 3.** Rh particle size distribution in dendrimers based on PPI (*a*) and PAMAM (*b*).[92] Reproduced with the permission of Elsevier.

supports and to change the conditions of deposition of the metal compounds on the surface and methods of their reduction offers great opportunities for targeted synthesis of highly active and selective catalysts. Quite an interesting group of supports is represented by various types of polymer materials that get swollen in sc-$CO_2$. Such polymers can be used to generate active sites of different structure and morphology. The catalytic properties of nanosized composites obtained in supercritical carbon dioxide have not been studied in sufficient detail, since their use in catalysis is still limited to a comparatively small number of chemical reactions. Such composites were mainly tested in processes of hydrogenation of various substrates and in Suzuki–Miyaura coupling reactions. This means that there is still a lot to do in the field of studying these systems in other catalytic processes.

## 2.2. Supercritical solvents in the synthesis of heterogeneous catalysts and in chemical reduction processes

In the design of new catalysts and processes based on them, it is necessary to pay due attention to environmental issues. However, the methods used to prepare heterogeneous catalysts often do not comply with green chemistry principles. In particular, impregnation and deposition procedures generate a lot of liquid waste, which requires the subsequent treatment, neutralization, or processing. Scientists are now developing a new approach to the synthesis of heterogeneous catalysts based on SCFs. The unique properties of such media (low viscosity, fast diffusion, the absence of surface tension, *etc.*) make it possible to create highly active catalysts that are difficult, and sometimes impossible, to obtain by traditional methods.

### 2.2.1. Precipitation and drying in supercritical conditions as a promising method of synthesizing heterogeneous catalysts, adsorbents and supports

The most important stages of synthesis of many heterogeneous catalysts are resource- and energy-consuming precipitation and drying processes. The use of supercritical $CO_2$ at these stages significantly reduces the application of conventional organic solvents and minimizes the amount of waste requiring additional disposal, which makes such approaches environmentally advantageous in comparison with the conventional methods of catalyst synthesis.

#### 2.2.1.1. Synthesis of catalyst supports and accompanying functional materials by precipitation in a supercritical antisolvent

It took researchers quite a lot of time to come to the conclusion about the prospects of using precipitation methods in supercritical media for heterogeneous catalyst synthesis. The first compound to be subjected to dispersion in sc-$CO_2$ as the antisolvent was cyclotrimethylenetrinitramine (RDX).[93] Due to the mild conditions of the dispersion process, the authors were able to obtain the dispersion phase of this explosive and to study the effect of various experimental parameters on the structure of the RDX particles formed. The particle size ranged from 10 to 300 μm.

Some of the first examples of synthesis of precursors for various functional materials are described in several publications[93–96] devoted to the preparation of metal acetate powders, with the average particle size being about 100 nm. Such systems can be used for making superconductors.[97]

Micronization of $C_{60}$ fullerene by supercritical antisolvent (SAS) process results in the formation of particles of the average size from 29 nm to 40 μm.[98] After such modification, fullerene is particularly interesting for pharmaceutics and can be used as a lubricating material, in membrane technologies, *etc.* The SAS process has been also employed to obtain spherical particles of magnesium acetate of 300–700 nm in size.[99] The particles prepared in this way were used as precursors of highly effective hydrogen storage systems based on magnesium hydride. The method of precipitation in a supercritical antisolvent has been also applied to obtain different oxide nanoparticles. For example, thermal decomposition of zinc acetate dispersed by the SAS process led to the formation of poorly crystallized ZnO particles with an average particle size of 17–21 nm.[100]

The SAS process has an original modification for handling aqueous solutions. To improve the miscibility of the water–$CO_2$ system, it is common to add a third component, a cosolvent, *e.g.*, an alcohol. Such approach employing cosolvents was quite successfully implemented to micronize lysozyme,[96] lactose,[101] and yittrium acetate.[102]

Another SAS modification, in which inverse aqueous emulsions of precursor compounds in an organic solvent are used as the spraying solution, was applied to synthesize $SiO_2$, $WO_3$, and $MoO_3$ particles.[103] This method allows one to obtain spherical oxide particles of several tens of nanometres in size with a narrow size distribution.[103]

Two SCF-based approaches were applied to synthesize silica microparticles:[104]

— hydrolysis of $SiO_2$ precursors in a supercritical ethanol medium;

— precipitation of $SiO_2$ precursors in sc-$CO_2$ (SAS process).

The specific surface area of $SiO_2$ prepared by the second method was about 50 $m^2\ g^{-1}$, whereas in $SiO_2$ synthesized by precursor hydrolysis in supercritical ethanol, this value exceeded 500 $m^2\ g^{-1}$ (Ref. 104).

Only in the second half of the 2010s, did researchers begin to use the SAS process for obtaining oxide supports for heterogeneous catalysts. For example, it was shown that $TiO_2$ and $CeO_2$ oxides obtained by precipitation in supercritical $CO_2$ could be used as effective supports for Au-containing catalysts for gas-phase low-temperature CO oxidation[105,106] and Au–Pd-containing catalysts of liquid-phase benzyl alcohol oxidation.[107] The good performance of catalysts with oxide supports obtained by precipitation in sc-$CO_2$ was attributed by the authors to the high dispersion ability of the metal particles deposited on the support surface. For example, the Au particles deposited on the oxides prepared by the traditional method are 2 to 40 nm in size, whereas when the SAS method is used, the support is uniformly coated with subnanometre gold particle clusters.[106] This fact is probably the result of the formation of numerous defects stabilizing the finely dispersed gold particles on the oxide phase surface.

A similar situation is observed in case of deposition of bimetallic heterogeneous Au–Pd catalysts. The Au–Pd particles were found to be more evenly distributed over the surface of the oxide support when deposition in sc-$CO_2$ was used for the synthesis than in the case when the oxide was synthesized by the conventional method.[107] Besides, in the latter case, the metal particles were larger.

The effect of numerous parameters, such as temperature, pressure, solvent flow rate, concentration of the dissolved salt, nozzle diameter, and ratio of the $CO_2$ feed rate to the solvent flow rate, on the size and morphology of the obtained solid particles was analyzed in detail by studying $TiO(OAc)_2$ micronization.[108] It was shown that variation of temperature within the 25–55 °C range and $CO_2$ density within the 0.63–0.84 g $cm^{-3}$ range did not lead to significant changes in the average particle size. However, the most pronounced effect on the $TiO(OAc)_2$ particle size was produced by changes in dispersion parameters, such as solvent flow rate, nozzle diameter, and oxoacetate concentration. By changing these parameters, it is possible to vary the average size of particles from 27 nm to >100 nm.[108]

Titania-based systems can be successfully synthesized by the SAS process from various alkoxide precursors.[109] These oxide systems were tested as supports for Au–Pd-containing heterogeneous catalysts intended for benzyl alcohol oxidation and direct synthesis of hydrogen peroxide. It was shown that $TiO_2$ synthesized from titanium isopropoxide had the highest resistance to agglomeration and was practically the optimal support for catalysts of these reactions. The SAS process was also used to obtain poorly crystallized titania ($TiO_2$) with a large specific surface area (418 $m^2\ g^{-1}$).[110] The formation of solid solutions without phase separation into single oxides was observed during preparation of mixed Zr–Ti-containing systems through their deposition in sc-$CO_2$.[111]

In most of the above-mentioned examples of synthesis of heterogeneous catalyst supports by the SAS process, the oxide phase precursors were acetates or acetylacetonates of metals, which, after dispersion in sc-$CO_2$, were subjected to thermal decomposition. Such technique may not always be very effective because co-precipitation of precursors can lead to the formation of new compounds, which, after their thermal decomposition, can give catalytically inactive phases. To avoid these problems, we proposed a new, original approach consisting in using the SAS process for precipitation of oxides or hydroxides prepared in advance in the form of a stable particle sol.[112] As a result, we were able to synthesize aluminosilicates with different Al : Si ratios and sinle aluminium oxide. A study of the resistance of the obtained systems to agglomeration showed that the aluminosilicate with the molar ratio Al : Si = 9 : 1 had high thermal stability, did not form the corundum phase ($\alpha$-$Al_2O_3$) up to a temperature of 1200 °C, and retained a large specific surface area (98 $m^2\ g^{-1}$).

#### 2.2.1.2. Synthesis of heterogeneous catalysts by precipitation in a supercritical antisolvent

One of the first attempts to use the SAS process for obtaining catalysts[113] consisted in the preparation of the $Sm_2O_3$ catalyst for oxidative dehydrogenation of ethane to ethylene. The obtained catalyst had higher ethylene selectivity than the $Sm_2O_3$ catalyst prepared by direct acetate decomposition.

A similar method of precipitation with sc-$CO_2$ was used to obtain heterogeneous vanadyl phosphate catalysts for n-butane oxidation to maleic anhydride.[114–116] The authors showed that the active phase of these catalysts was the amorphous phase of vanadyl phosphate, which was successfully and selectively obtained by deposition in sc-$CO_2$.

The SAS process was employed to prepare precursors of Cu–Mn oxide catalysts for CO oxidation.[117] The process gave the $CuMn_2O_4$ mixed oxide phase with a hopcalite structure without impurities of single copper or manganese oxide. Additionally, the effect of water concentration in copper and manganese acetate solutions on the catalytic activity of the final catalysts was investigated.[118,119] It was demonstrated that a water content of 10 vol.% resulted in the most active catalysts.

Later, precipitation in sc-$CO_2$ was used to synthesize NiO, $Fe_3O_4$, CuO, and $Co_3O_4$ oxide catalysts,[120] which were tested in complete propane oxidation reactions. It was found that among the synthesized oxides, $Co_3O_4$ was the most active catalyst of complete oxidation.

Marin *et al.*[121] compared the characteristics of Co containing catalytic systems obtained by the SAS process and then used in the Fischer–Tropsch reaction with characteristics of the catalyst prepared by the conventional co-precipitation method. It was noted that in the CO conversion reaction, the catalyst obtained by sc-$CO_2$ precipitation demonstrated higher activity at lower temperatures.

The high rates of diffusion and supersaturation attained in the precipitation in supercritical media can lead to the formation of phases that cannot be synthesized by conventional methods. For example, precipitation in sc-$CO_2$ makes it possible to prepare a mixed copper and zinc hydroxycarbonate with a structure of georgeite, a rare mineral.[122,123] It is shown that the catalysts with such structure are much more active in reactions of methanol synthesis and low-temperature steam reforming of carbon monixide than commercial catalysts.

SAS process can be applied to the synthesis of mixed 3 to 10 nm $MnO_x$–$CeO_2$ oxide particles with a solid solution structure forming spherical agglomerates.[124] Hollow $MnO_x$–$CeO_2$ agglomerates prepared by this method and containing different Mn amounts were studied for their oxygen capacity.[125] During this study, it was established that the increase in the Mn content to 44 at.% led to higher oxygen capacity of the system.[125] These mixed oxide sys-

tems were used as heterogeneous catalysts for reduction of nitrogen oxides $NO_x$ to $N_2$ and $H_2O$.[126] The highest activity of the $MnO_x-CeO_2$ catalysts in the $NO_x$ reduction was observed at Mn : Ce = 1 : 1.[126, 127] Different surfactant additives (polyvinylpyrrolidone, polyethylene glycol, *etc.*) can affect the performance of such systems. For example, it was shown that the above-mentioned surfactant additives can reduce the degree of particle agglomeration and increase the specific surface area of the synthesized systems.[128]

Another example of applying the method of precipitation in sc-$CO_2$ to prepare systems with high oxygen capacity is the synthesis of mixed $Ce_{1-x}Zr_xO_2$.[129] The maximum oxygen capacity was found for the mixed oxide with the Ce : Zr atomic ratio of 3 : 1. The addition of copper to the $Ce_{1-x}Zr_xO_2$ systems obtained by the SAS process had a considerable effect on their oxygen capacity and catalytic activity in the low-temperature CO oxidation reaction.[130] It was noted that the highest oxygen capacity and catalytic activity are reached when the Cu content is 2.63 mol.%.

Jiang *et al.*[131] described mixed $MnO_x-FeO_y$ oxides, which were also synthesized by the SAS process. A study of their catalytic properties in the selective reduction of nitrogen oxides showed that at the Mn : Fe atomic ratioof 1 : 1, the $NO_x$ conversion was maximized.

A similar technique was used to obtain zinc oxide catalysts for photooxidation;[132] the catalysts were tested in the decomposition of the crystal violet dye. It was shown that at the annealing temperature of 500 °C, a regular nanosized oxide structure was formed. The structure had the highest photocatalytic activity and an average particle size of 65 nm. The SAS process is also applicable to the preparation of titania-based photocatalysts.[133] It was shown that this method produces highly active catalysts with the optimal phase composition (93 mass % anatase and 7 mass % rutile). These catalysts have higher photocatalytic activity values than those of the P25 commercial catalyst.[133]

Almost all of the above processes are examples of obtaining bulk catalysts. However, SAS process can also be used to synthesize multicomponent metal catalysts. For example, Nesterov *et al.*[134] proposed the first original approach In which an $SiO_2$ sol prepared in advance is added to a precursor salt solution ready for dispersion by the SAS process. This combination results, for example, in high dispersion of Ni–Cu metallic particles.[134] The use of $SiO_2$ as a stabilizing matrix reduces the size of the metal particles in the samples and increases the metal particle surface accessibility (Fig. 4).

A detailed study of the water effect on the structural characteristics of these Ni–Cu metallic systems was reported.[135] It was found that no phase separation was observed in the original methanol solution of acetate precursors when the water content is >7 vol.%, and $Ni_{1-x}Cu_x$ solid solution was formed as the only product.

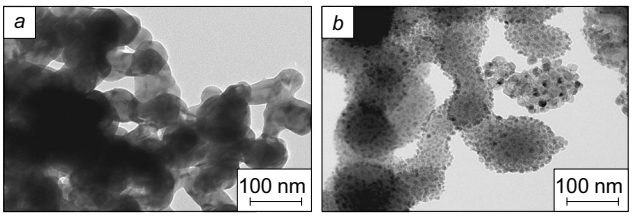



**Figure 4.** TEM images of metal Ni–Cu-containing systems obtained by the SAS method, with the silica content of 0 mass % (*a*) and 50 mass % (*b*).[134] Reproduced with the permission of Elsevier.

Later, similar approaches to obtaining $TiO_2$ nanoparticles confined inside various stabilizing matrices ($SiO_2$, $Al_2O_3$, *etc.*) were patented by the Haldor Topsøe company,[136] which proved their good prospects in the field of synthesis of various functional materials, first of all, effective heterogeneous catalysts.

#### 2.2.1.3. Development of approaches to the preparation of aerogel-based catalysts

Above we summarized as fully as possible the approaches to the synthesis of heterogeneous catalysts by precipitation in a supercritical antisolvent described in open sources. This Section considers the design of functional materials based on aerogels, but since the amount of published information on this subject is enormous, the review mainly focuses on the approaches to the synthesis of composite catalysts that have been applied in real catalytic processes.

Aerogel is a classical nano-structured material consisting of nanometre-scale particles linked into chains and forming a random structure with the pore sizes from several to several hundred nanometres. Aerogels have a number of unique properties: extremely low heat conductivity and resistance to high temperatures, low density, high porosity and a large specific surface area, a low refractive index and high transparency, unique acoustic properties (the lowest speed of sound in a solid body), *etc.*[137] This set of characteristics holds great promise for using aerogels as catalysts and adsorbents.

Since Kistler's¶ first publication on the aerogel synthesis in 1931, scientists have been tirelessly looking for possible ways to use aerogels in catalysis.[138] It is well known that in the 1930s, processes of conversion of acetic, phenylacetic, and propionic acids into acetone, benzyl ethyl ketone, and diethyl ketone, respectively, were of interest for industry. Kistler demonstrated that the selectivity and long-term stability of thorium oxide obtained as aerogel exceeded those of all Th catalysts in the form of xerogels known at that time, with the degree of conversion being the same. Swann *et al.*† extended this approach to the ketonization reaction of aliphatic esters in the presence of Th aerogels. Using numerous simple and mixed aerogels ($SiO_2$, $Pt/SiO_2$, $Ni/SiO_2$, $Cr_2O_3/SiO_2$ and $Fe_2O_3/SiO_2$), they investigated selective oxidation of acetaldehyde to acetic acid by atmospheric oxygen.

The 1990s saw a lot of attempts to make catalysts out of aerogels based on $SiO_2$, $Al_2O_3$, $TiO_2$, and $ZrO_2$ oxides, binary aerogels based on NiO, CuO, $ThO_2$, $Cr_2O_3$, PbO, and $Fe_2O_3$ bound to $Al_2O_3$, $SiO_2$, $ZrO_2$ and MgO, mixed tertiary oxide aerogels and metals deposited on oxide aerogels (Pt, Pd, Cu, Ni on $SiO_2$, $Al_2O_3$, MgO, and $ZrO_2$). The methods of preparation of such aerogels and also numerous targeted reactions involving them (complete and partial oxidation of organic substrates; oxidative dimerization; alkene epoxidation; hydrogenation of cyclopentadiene, toluene, benzene, and nitrobenzene to aniline; ethylene polymerization; syngas reactions in the Fischer–Tropsch process and methanol synthesis; reduction of nitrogen oxides to ammonia; hydrogenolysis; isomerization; and

¶ See S.S.Kistler. *Nature (London)*, **127**, 741 (1931).
† See S.Swann Jr., E.G.Appel, S.S.Kistler. *Ind. Eng. Chem.*, **26**, 1014 (1934).

other reactions) are surveyed in detail.[139–141] In all cases, catalysts based on aerogels did not differ in their chemical composition from the catalysts prepared by conventional methods. The authors of these works focused only on the advantages of high specific surface area and well-developed porous texture of the aerogels, and, in particular, on the possibility to add a larger amount of the active component.[142]

In 2001, it was proposed to use simple organic epoxy compounds of transition and main group metal oxides in the synthesis of metal oxide aerogels.[143] This method considerably broadened the range of chemical elements that could be used for synthesizing oxide catalysts based on aerogels and made it possible to replace inconvenient metal alkoxides with inexpensive salts. For example, aerogels synthesized by the epoxide method from $Fe_2O_3$ were successfully tested in the Fischer–Tropsch‡ reaction and water gas shift reaction (WGS).[144]

Discussions of the prospects for using carbon-based aerogels as sorbents and catalysts[141] have been underway for quite a long time now. Such carbon aerogels can be obtained by thermal carbonization of organic aerogels. The latter, as a rule, are synthesized by the sol–gel method upon polycondensation of various organic monomers. Presumably, the best-studied organic aerogels are those obtained from resorcinol and formaldehyde in aqueous solutions in the presence of a base[145] or acid catalyst.[146]

The first description of carbon aerogel preparation was reported in 1989,§ while the first review[147] about the applications of such carbon aerogels in catalysis appeared in 2005. The fast growth of the research activity in the field of carbon aerogel applications as catalysts and sorbents is associated with the important role played by carbon materials, along with oxide systems, in catalysis, which is reported in numerous reviews of foreign[148, 149] and Russian scientists.[150, 151] Carbon aerogels are quite universal both at the microlevel (due to their porous structure and texture) and at the macrolevel (due to the shape of the macroparticles) and can be obtained as monoliths, granules, powders, or thin films. The possibility to fine-tune the specific surface area, pore volume, and pore size distribution by varying the conditions of synthesis and subsequent treatment opens up opportunities for obtaining a wide range of functional materials with unique properties and provides carbon aerogels with good prospects for the application in catalytic and adsorption processes.

Carbon aerogels were first used as catalyst supports in the late 1990s.[152, 153] There are at least three simple methods for obtaining carbon aerogels with metal particles deposited on them:

— addition of a metal precursor to the initial mixture;

— ion exchange;

— metal precursor deposition on an organic or carbon aerogel.

For example, Pt-PAN, a Pt-containing composite aerogel, was synthesized by mixing platinum precursors ($K_2PtCl_6$, platinum acetylacetonate) with a polyacrylonitrile (PAN) solution in *N*,*N*-dimethylformamide. Then platinum was reduced with $NaBH_4$, and the obtained colloidal solution was turned into a gel and dried in sc-$CO_2$.[152] The prepared organic Pt-PAN aerogel was carbonized in an argon atmosphere at a temperature of 900 °C and later used as an electrocatalyst. A similar method was employed to prepare Fe–Co-PAN composite aerogels,[154] which were also tested in electrocatalytic oxygen reduction reactions (ORR).

The catalytic activity of carbon aerogels with Cr, Mo, and W oxides deposited on them was studied in but-1-ene skeletal isomerization.[153] These aerogels were prepared by mixing chromium nitrate, ammonium heptamolybdate, and ammonium tungstate with an aqueous solution of resorcinol and formaldehyde. After the polymerization and gelation, the obtained composite was dried in sc-$CO_2$ and then subjected to pyrolysis in a nitrogen flow at 1000 °C. An analogous technique was employed to prepare carbon aerogels with deposited Pt particles, which were used in the catalytically assisted combustion of toluene[155] and as an electrode of fuel cells.[156]

The use of a carbon aerogel as a support allows synthesizing highly filled Pt-based catalysts with the metal particle content of up to 40 mass % and an average particle size of ~2–3 nm.[157] Keggin-type heteropolyacids immobilized in the 3D structure of resorcinol–formaldehyde carbon gels proved to be effective catalysts in the synthesis of *tert*-butyl methyl ether from methyl and *tert*-butyl alcohols.[158]

The next step in the development of carbon aerogel applications in catalysis was made in the field of synthesis of graphene aerogels and aerogels based on carbon nanotubes. For example, a graphene aerogel was synthesized by pyrolysis of the resorcinol–formaldehyde aerogel filled with graphene oxide.[159] To synthesize an aerogel based on carbon nanotubes, the nanotubes were first suspended in a resorcinol–formaldehyde solution, then the suspension was gelated and freeze-dried.[160] Later, catalytic carbon deposition was proposed as a method of synthesizing aerogels with carbon nanotubes.[161] Now graphene aerogels are among the most popular objects of study. They are applied as catalysts[162] or supports for active components of electro-[163] and photocatalysts.[164]

A relatively new class of aerogels is represented by composites consisting exclusively of metal chalcogenide frameworks containing $S^{-2}$, $Se^{-2}$, and $Te^{-2}$ ions.[165] Such chalcogenide aerogels are soft Lewis bases, and the interconnected pore volume is responsible for the unique sorption properties, which can be useful for gas separation processes. The large specific surface area of the framework makes these aerogels promising materials to be employed in environmentally important photoinduced processes (for example, in solar cells, photocatalysis, probing, *etc.*), catalytic removal of sulfur impurities from fossil fuels (hydrodesulfurization), heavy metal reduction and gas separation processes. Aerogels can be synthesized from chalcogenides in three different ways:

— thiolysis of metal alkoxides;[166]

— controlled aggregation of chalcogenide nanoparticles;[165]

— metathesis reaction between soluble clusters of chalcogenides and binding metal ions.[167]

The catalytic activity of the aerogels based on Ni–Mo–S, Co–Mo–S, Co–Ni–Mo–S, and Co–Mo–W–S compositions in the thiophene hydrodesulfurization is twice as high as that of conventional sulfidized Co–Mo/$Al_2O_3$;[168] $CoMoS_x$ aerogels proved to

‡ See S.Bali, F.Huggins, G.Huffman, R.Ernst, R.Pugmire, E.Eyring. *Energy Fuels*, **23**, 14 (2009).
§ See US Patent 4873218A (1989).

be reliable electrocatalysts in the hydrogen evolution reaction.[169]

A rather interesting and rapidly developing line of research of the last decade is the synthesis of metal aerogels, *i.e.*, aerogels consisting solely of metal nanoparticles. For example, in 2009–2010, metal aerogels based on Fe, Co, Ni, Cu, *etc.* were for the first time obtained by the carbothermal method.[170,171] The method is based on pyrolysis of a composite metal oxide ($MeO_x$) and a resorcinol–formaldehyde aerogel, which results in the metal oxide reduction by organic carbon to pure metal retaining the aerogel structure. Another method of synthesizing mono- and bimetallic aerogels of noble metals (Pt, Ag, and Au) is based on gelation of sols of particles of these metals to a 'metallic' gel.[172] Metal aerogels have a larger specific surface area than platinum black and may have better prospects for electrocatalytic applications.[173,174]

Aerogels are used as the basis for the fabrication of various composites for catalysis and adsorption. For instance, there is a large group of metal complexes that can act as the active phase in catalytic processes or separation and purification of gases and liquids. This group consists of metal-organic frameworks (MOF). The main drawback of industrially produced MOFs is their usual form of a finely ground crystalline powder that can hardly be compacted or moulded, which is a serious limitation on their application in industrially important flow-through catalytic processes. The use of traditional binding agents for the fabrication of granules reduces the MOF specific surface area and accessibility of catalytically active sites for reactants, which cancels out their main advantages in targeted processes and limits their scope of application

A possible solution to this problem is the inclusion of MOF particles into an aerogel matrix. For example, in 2009, a MOF aerogel involving Fe-BTC (BTC stands for benzene-1,3,5-tricarboxylate) was first synthesized by the sol–gel method.[175] Such MOF aerogel composites catalyze $CO_2$ cycloaddition to epoxides and intramolecular C–H amination of vinyl azides.[176] The MOF@$SiO_2$ aerogel composite was synthesized[177] using the Cu-BTC (HKUST-1) commercial powder, which was mixed with a solution of tetraethoxysilane (TEOS), which was followed by TEOS hydrolysis and sol polycondensation into a gel. Unfortunately, the cited authors[177] were unable to demonstrate the invariability of the state of HKUST-1 active sites upon incorporation into the $SiO_2$ aerogel.

Another original method of synthesizing the HKUST-1@$SiO_2$ aerogel composite was proposed by Nuzhdin *et al.*;[178] according to this method, the commercial HKUST-1 powder was added to a colloidal solution of presynthesized $SiO_2$ sol after the addition of aqueous ammonia for gelation. As a result, the synthesis procedure required the minimum amount of ammonia, which made it possible to completely preserve the structure of the HKUST-1 active sites. In addition, a technique for preparing HKUST-1@$SiO_2$ aerogel granules by the emulsion method was proposed.[179] The HKUST-1@$SiO_2$ aerogel composite is a mesoporous $SiO_2$ aerogel with HKUST-1 microcrystals uniformly distributed in its bulk. The composite synthesized by this method in the form of a monolith and granules was successfully used as a heterogeneous catalyst[179] and a stationary phase for liquid column chromatography in the flow mode under normal conditions.[178]

By now, scientists have developed methods of synthesizing composites based on $SiO_2$, $TiO_2$, AlOOH, carbon, graphene (graphene oxide), cellulose, and other aerogels. The cutting-edge trends in the field of preparation and application of MOF@aerogel composites are described in a review[180] published in 2018.

A new interesting line of research is the synthesis of aerogels that consist of crystalline, including anisotropic, particles of various shapes (plates, sheets, needles, tubes, *etc.*). Such aerogels not only have high porosity, a large specific surface area, and low density, but also possess peculiar properties characteristic of their single building blocks such as superparamagnetism, ferroelectricity, electrical conductivity, luminescence, electro- and photocatalytic activity.

The methods of synthesis of such aerogels can be divided into two groups for convenience:

— preparation of gels from pre-synthesized microcrystalline anisotropic particles (plates, rods, sheets, and tubes);

— formation of these structures *via* hydrothermal treatment and supercritical drying processes.

So far, such aerogels have been synthesized based on AlOOH and $Al_2O_3$, $MnO_2$,[181] $MoS_2$ and $WS_2$ on graphene,[182] boron nitrate,[183] $WO_x$,[184] $Y_2O_3$,[185] $SnO_2$,[186] and $BaTiO_3$[187] substrates. For example, the 3D aerogel synthesized from $MnO_2$ and consisting of ultra-thin nanosheets demonstrates much higher discharge capacity in lithium air batteries than its powdered analogue.[188] Tin oxide aerogels consisting of microcrystalline particles were successfully used as catalyst supports to replace carbon in fuel cells[189] and in photocatalysts for hydrogen production.[190]

It was shown that minor variations in the synthesis conditions and relative Al content in aluminosilicate mixed-oxide aerogels make it possible to change the structure and morphology of the obtained oxide support, which, as a result, affects the mechanical strength and activity of the catalysts. In particular, Al–Si aerogels with the silicon content ranging from 0 mass % to 20 mass % obtained by the sol–gel method from aluminium and silicon alkoxides with subsequent supercritical drying in isopropyl alcohol consist of specific nanostructures: loosely packed ultrathin 2D crystallites. The addition of silica significantly increases the crystallite anisotropy. The aerogel with the Al : Si atomic ratio of 9 : 1 consists of one unit cell-thick pseudoboehmite nanosheets (with the average size of $14.0 \times 1.2 \times 14.5$ nm).[191] After the annealing of the Si containing AlOOH aerogel, the morphology of the ultrathin 2D crystallites is preserved during the phase transition to $\gamma$-$Al_2O_3$.[192] Figure 5 shows TEM images of the Al–Si aerogels with various aluminium contents. An increase in the aluminium content leads to the formation of the AlOOH phase in the form of thin films (50 mol.% aluminium content) and plates of an average size of $20.0 \times 6.5 \times 25.0$ nm (100 mol.% aluminium content).[193]

A group of scientists at the Boreskov Institute of Catalysis, Russian Academy of Sciences, showed that a composite with the optimal combination of mechanical strength and activity can be obtained by preparing a support based on boehmite microcrystallites of about $150 \times 8 \times 8$ nm in size for diesel fuel hydrotreating catalysts.[194] This means that targeted synthesis of microcrystallites with a specified anisotropy can afford catalyst supports with a desired structure and morphology, which can be used for preparation of effective catalysts with enhanced characteristics. It should be noted that aerogel synthesis is almost always associated with the use of SCF in supercritical

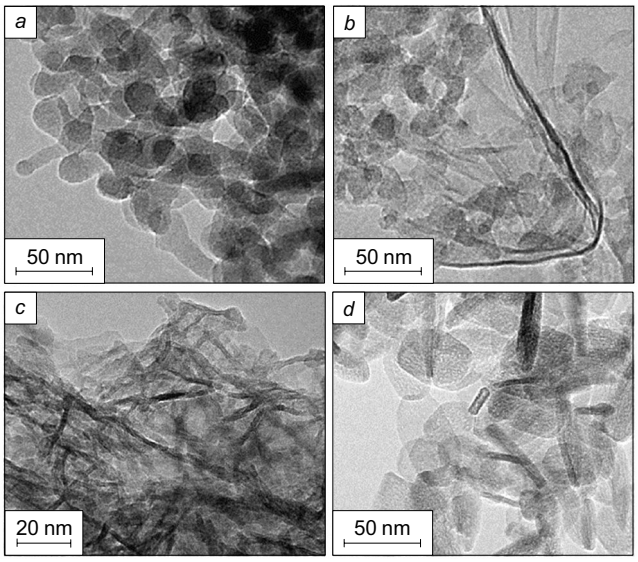



**Figure 5.** TEM-image of Al–Si aerogels with the aluminium content of 0 mass % (*a*), 50 mass % (*b*), 90 mass % (*c*), and 100 mass % (*d*).[193] Reproduced with the permission of Elsevier.

drying processes. The attempts to use other gel drying method such as freeze-drying did not meet with success.

The examples analyzed above show that the technologies employing the supercritical state of matter actually hold great promise for the synthesis of various functional materials including complex systems, such as heterogeneous catalysts, the structure and properties of which are responsible for their good performance in a number of chemical processes. The catalysts, supports, and adsorbents prepared using SCF technologies have unique properties that are not found in similar systems obtained by conventional methods.

Despite the relatively high cost of equipment for conducting synthesis in supercritical conditions, the rapid development of technologies, appearance of new materials and improvement of engineering solutions are gradually making the methods implemented elevated temperatures and pressures more available and economically feasible. The number of works on the synthesis of heterogeneous catalysts using supercritical state of matter is growing extremely fast since such catalysts demonstrate unprecedented selectivity and activity in a number of chemical processes, which can serve as a perfect example of effective application of supercritical media in the synthesis of functional materials with desired properties.

### 2.2.2. Reducing properties of supercritical alcohols as a fundamental basis for innovative chemical processes

Lower alcohols, along with supercritical $CO_2$ and $H_2O$, are the most popular SCFs used for solving applied and fundamental problems. Apart from other important properties making supercritical alcohols multifunctional, their reducing ability remains one of the most promising but rarely used features that have a great application potential. Lower aliphatic alcohols are permanently among the most demanded reagents and solvents in fine organic synthesis and in chemical industry. Diverse reactivity described in numerous publications, a unique combination of physicochemical properties (high dielectric permittivity and dipole moment, hydrogen bonding ability, extraordinary solvation properties, elevated boiling points, *etc.*), together with availability of thermochemical, kinetic, and thermodynamic characteristics of alcohols and processes involving them, ensure persistent interest in lower alcohols for both fundamental and practical purposes.

Surprisingly, numerous scientific reviews analyzing the chemical reactivity of lower alcohols (according to the Scopus database, about 100 publications appeared only in 2015–2019) do not address their reducing or H-donor properties. Meanwhile, transition of lower alcohols to the supercritical fluid state significantly enhances their reducing, H-donor, alkylating, and some other chemical properties.

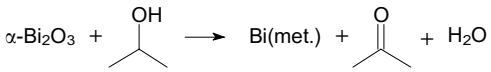
This Section considers the reducing properties of sc-alcohols, with primary attention being paid to the results of research of the last decade. Besides, a prediction is made of the most important lines of research that are expected to rapidly develop in the nearest future and that would make use of the reducing properties of these compounds.

#### 2.2.2.1. Reduction of metal oxides and salts

The reducing properties of alcohols were, evidently, first demonstrated in the classical Meerwein–Ponndorf–Verley (MPV) reaction. It is known that this reaction was studied for ketones and was always catalyzed by aluminium alkoxide. Chemists thought to be unikely that alcohols would reduce inorganic compounds without any catalysts (including aluminium alkoxide) or other auxiliary reagents.

In 2001, Prof. S.P.Gubin's research group[195] published the results of their pioneering study of the reduction of inorganic oxide $\alpha$-$Bi_2O_3$ with propan-2-ol under supercritical conditions. The only Bi-containing product was metallic bismuth (Scheme 1).

**Scheme 1**




This nontrivial result at the border of inorganic and organic chemistry laid the fundamental basis for the later large-scale studies of the reactions of simple metal oxides with sc-Pr$^i$OH, which were summarized by Kargin *et al.*[196] The list of metals whose monoxides have been so far involved in these reactions includes at least 40 elements of the Periodic Table, which is a solid ground for predicting the ability of other element oxides to participate in this reaction.

It was shown that the studied metal monoxides can be divided into four groups in terms of their reactivity in sc-Pr$^i$OH. The first group includes monoxides that, like $\alpha$-$Bi_2O_3$, are completely reduced to metals: $Ag_2O$, $Au_xO_y$, CdO, $Co_xO_y$, CuO, HgO, $Pb_xO_y$, $PtO_2$, $Re_xO_y$, $Sb_2O_3$ and $TeO_2$.[196] Group 2 consists of oxides in which the metal is reduced to an intermediate oxidation state: $Fe_2O_3$, $Mn_xO_y$, $MoO_3$ and $V_xO_y$.[196] For example, iron(III) oxide is reduced to $Fe_3O_4$, after which the reaction stops. Group 3 contains oxides of trivalent rare earth elements, which are converted under the specified conditions to hydroxides without changes in the metal oxidation state: $Dy_2O_3$, $Eu_2O_3$, $Gd_2O_3$, $La_2O_3$, $Nd_2O_3$, $Pr_2O_3$, $Sm_2O_3$, $Tb_2O_3$ and $Yb_2O_3$.[196] It is evident that hydration of these oxides occurs by the water released upon dehydration of the initial alcohol under the reaction conditions. A special place in this group is occupied by $MnO_2$, which is reduced stepwise to $Mn^{2+}$ (like oxides of the second group) and then finally turns into

hydroxide: $MnO_2 \rightarrow Mn_2O_3 \rightarrow Mn_3O_4 \rightarrow [MnO] \rightarrow \rightarrow Mn(OH)_2$. And, finally, group 4 includes inert oxides that remain virtually unchanged when occur in contact with sc-Pr$^i$OH for several hours at temperatures of up to 300 °C: BaO, $CeO_2$, $Cr_2O_3$, $Ga_2O_3$, $GeO_2$, $HfO_2$, $In_2O_3$, NiO, $SiO_2$, $SnO_2$, $UO_2$, $WO_3$, ZnO and $ZrO_2$.[196]

An important consequence of the obtained experimental data is the possibility to reduce not only oxides but also salts of these metals, present as single compounds, parts of complex compositions, or compounds immobilized in organic and inorganic matrices. For example, the formation of nickel, copper, and silver metal particles from solutions of the metal nitrates in alcohols proceeds quite efficiently at 400 °C both in sc-MeOH and in sc-EtOH.[197] In contrast to solutions, $Au^+$, $Bi^{3+}$, $Co^{2+}$, $Cu^{2+}$, $Hg^{2+}$, $Ni^{2+}$, $Pb^{2+}$, $Sb^{3+}$ and $Te^{4+}$ salts immobilized in a polyethylene or opal matrix can be reduced to nano-scale metal particles due to the sc-Pr$^i$OH ability to penetrate into the matrix.[198] For the minerals of the sillenite family with the general structural formula $Bi_{24}M_2O_{40}$, where M = $Al^{3+}$, $Cr^{6+}$, $Cu^{2+}$, $Fe^{3+}$, $Ga^{3+}$, $Ge^{4+}$, $Mn^{4+/5+}$, $Ni^{3+}$, $P^{5+}$, $Si^{4+}$, $Ti^{4+}$, $V^{5+}$ and $Zn^{2+}$, it is possible to achieve a similar result of reduction of doping metals when their content ranges from 0.007 mass % to 0.40 mass %.[198–200] The depth of the surface layer of the reduced metal in the crystalline state is usually 0.1–0.2 mm or more, depending on the properties of the sc-alcohol and the contact duration.[198]

According to the reactivity studies of some metal salts in sc-alcohols, the salts of the elements whose oxides belong to group 4 can be considered as a separate subgroup. The reaction with sc-alcohols does not include reduction of cations of these metals, but the final reaction product is the metal oxide in the form of nanoparticles, which is the case for $Zn(NO_3)_2$ (Ref. 201) and $Ce(NO_3)_4$ (Ref. 202) in sc-MeOH at 400 °C. It is not clear from the reported data whether metal oxide formation is due to thermal decomposition of the corresponding nitrate alone, or the redox reaction involving the $NO_3^-$ anion and sc-alcohol also takes place. If it is the result of thermal decomposition of the metal salt, then all oxygen-containing metal salts that can thermally decompose are potential participants in such transformations in sc-alcohols (Ref. 203, p. 280).

Interestingly, the use of sc-Pr$^i$OH for reduction of complex oxides of two or more metals seems to have good prospects for the preparation of various composites. In particular, it was shown that the reduction of binary metal oxides can lead to at least four different results:[198, 200]

— complete reduction of both metals and formation of an eutectic alloy ($Bi_2CdO_4$);

— complete reduction of both metals and formation of an intermetallic compound ($Bi_2O_3 + TeO_2$);

— complete selective reduction of the oxide of one of the two metals with no changes in the state of the second metal oxide ($Bi_2O_3 + M_xO_y$, where M = Co, Cr, Mn, Mo, V, W);

— partial reduction of one or both metal oxides causing changes in the original oxygen stoichiometry of the complex oxide ($Bi_2O_3 + M_xO_y$, where M = Co, Ge, Mo, Si, Ti, $PbMoO_4$).

The above data provide the conclusion about the prospects of using sc-alcohols, first of all, for fabrication of new metal-containing composite heterogeneous catalysts and other nanostructured functional materials. Evidently, the ability of metal oxides and salts to be completely or partially reduced by sc-Pr$^i$OH or another sc-alcohol makes it possible to sharply change or significantly modify the conventional methods for the preparation of supported catalysts. In particular, using sc-alcohols, it is possible to optimize methods of deposition and(or) reduction of the active component *via* increasing its degree of dispersion, fine tuning the average size and structure of the particles (*e.g.*, they can be formed in the X-ray amorphous state), particular, particles of eutectic alloys and intermetallic compounds. Equally important is the fact that the most demanded oxide catalyst supports, such as $Al_2O_3$, $SiO_2$, $TiO_2$, $ZrO_2$ and $CeO_2$, cannot be reduced by sc-isopropyl alcohol.[196, 198] Supercritical EtOH at the temperatures of 275–350 °C and reaction time of 0.5–5 h cannot reduce popular aluminosilicate supports (HZSM-5, MCM-41 and SBA-15) or $Ag_2O$, $Al_2O_3$, CaO, CuO, $Co_xO_y$, $Fe_xO_y$, MgO, $Mo_xO_y$, NiO and $ZrO_2$ oxides.[204–207] Supercritical methanol is chemically inert towards montmorillonite consisting of $SiO_2$, $Al_2O_3$, MgO, $Fe_2O_3$, $Na_2O$, CaO and $K_2O$ oxides.[208]

Since the above-mentioned groups were formed considering the compounds' reactivity under supercritical conditions, there may be minor variations within the group members if the alcohol nature, temperature, or duration of the reduction reaction change. Gubin and co-workers[195] performed most of their research at temperatures of 280–300 °C using only sc-Pr$^i$OH, as it has higher reducing ability than primary alcohols. It was found that variation of the reaction conditions can lead to changes in the reactivity of some oxides. For example, the reducing ability of lower sc-alcohols does not always obey the simple and seemingly apparent rule: a secondary alcohol is more reactive than a primary one.[209] Another example of this kind is related to an increase in the reaction time and temperature rise to above 300 °C, or replacement of one sc-alcohol with another. For example, reduction of copper(II) salts in sc-methanol at $\leqslant$250 °C produces a mixture of metallic copper and $CuO-Cu_2O$ oxides, whereas at 300 °C and above, only metallic copper is formed.[210] An interesting result was obtained by using various supercritical alcohols (MeOH, EtOH, Pr$^n$OH, Pr$^i$OH, Bu$^n$OH, n-$C_5H_{11}$OH and n-$C_6H_{13}$OH) at 300 °C in the flow mode in the conversion of $(NH_4)_2Ce(NO_3)_6$ to $CeO_2$.[211] It was found that in $C_1-C_6$ primary alcohols, the size of nanocrystallites of newly formed cerium oxide increases ~2-fold with increasing molecular weight of the reducing alcohol. A similar ~1.5-fold increase in the particle size is observed when going from primary (n-propyl) to secondary (isopropyl) alcohol.[211]

The temperature effects can be illustrated in relation to reduction of uranyl nitrate with sc-ethanol. This process consists of two stages: $UO_2^{2+} \rightarrow U_3O_8 \rightarrow UO_2$.[212] The first stage occurs at 180–270 °C. When the temperature is raised to 290 °C, a $U_3O_8-UO_2$ oxide mixture is formed, while when the temperature is above 300–310 °C, only the $UO_2$ phase is observed. A markedly better result of using sc-alcohols is achieved in the reduction of only cobalt oxide in spinel composition $Co_{3-x}Al_xO_4$ ($0 < x < 2$), a catalyst for the Fischer–Tropsch synthesis. In the conventional method of catalyst reductive activation, *i.e.*, in a flow of gaseous $H_2$ at a temperature of 600–700 °C, it takes 2 hours to complete the reaction.[213] However, when sc-Pr$^i$OH is used for reduction at ~250 °C, the reaction takes 20 min.[214] And in this case, superparamagnetic nanoparticles (~2 nm) of metallic cobalt with a narrow size distribution are formed on alumina.

Upon the changes in the reduction conditions, some metal oxides and salts assigned to group 4 (inert compounds) can move to another (reactive) group. For example, $Ni^{2+}$ compounds can be reduced to the metallic state by sc-Pr$^i$OH at 300 °C,[196,198] whereas in the presence of sc-methanol, they are reduced only at 400 °C.[210] A similar result is obtained in the reaction of sc-MeOH with $WO_3$ (an oxide from inert group 4). Partial reduction of this oxide to $WO_2$ proved to be possible at 300 °C, resulting in the formation of the so-called *blue tungsten oxide* with the general formula $WO_{3-x}$ and a low oxygen content ($0 < x < 1$).[215] The increased practical interest in this oxide is the result of its unusual photocatalytic,[216,217] semiconductor and electrochromic[218,219] properties. The preparation of $WO_{3-x}$ *via* the reduction with sc-alcohols can become a very promising scalable alternative method.

#### 2.2.2.2. Reduction of graphene oxide and compounds deposited thereon

Some of the described studies of reduction with sc-alcohols employed metal compounds deposited on graphene oxide (GO).[220,221] The choice of GO as the support for deposition instead of chemically untreated graphene is explained by the fact that oxidized graphene adsorbs much more metal and oxide species than untreated graphene. That is why the most popular method of preparation of metal composite materials based on graphene is deposition of a metal precursor (salt or oxide) on the GO surface followed by reduction. In this case, GO is also reduced forming the so-called *reduced graphene oxide* (RGO), which much closely resembles graphene than GO. In 2011, it was first proposed to use sc-alcohols for GO reduction. Nursanto *et al.*[222] showed that at 400 °C, sc-MeOH and sc-EtOH do it quite well both in an autoclave and in a flow reactor. The oxygen content can be lowered from 34 at.% in the initial GO to 8 at.% in RGO. The process also causes a simultaneous sharp increase in the specific electrical conductivity of the reduced material. To demonstrate the advantages of the new GO reduction method, the obtained RGO was used as an anodic material in the second-generation Li ion batteries, where it showed excellent results in the battery discharge capacity tests.[222] Of certain interest are also comparative data on the elemental composition, C-to-O atomic ratio, and specific conductivity of graphite, the precursor of graphene oxide, which is obtained by oxidation of this graphite, and numerous (al least 25) RGO samples. The samples were prepared using other reduction methods that had been tested earlier and become routine (see the Electronic Supplementary Material in Ref. 222). Analysis of these data clearly shows that there is a correlation between the selected GO reduction method and characteristics of the resulting RGO.

The results of this pioneering study inspired a series of new studies,[223,224] in particular, Russian scientists[225,226] investigated the effect of the reaction conditions on the ability of sc-alcohols to reduce GO and/or on the properties of the resulting RGO (electrochemical properties, electrical and thermal conductivity, and other characteristics), mainly when RGO was used in lithium ion batteries.[227–229] The researchers who studied the properties of RGO prepared by the reduction with sc-alcohols were mainly interested in the effects produced on these characteristics by the particles of metal oxides or salts such as $SnO_2$, SnS, $MoO_2$, $MoS_2$, $TiO_2$ and $Fe_3O_4$ deposited on RGO.[230–236]

The most important, in our opinion, results of the chemical reduction of GO with sc-alcohols were reported by Seo *et al.*,[237] who employed five lower alcohols, MeOH, EtOH, Pr$^n$OH, Pr$^i$OH, and Bu$^n$OH, under supercritical conditions to prepare RGO (the reaction took 2 hours at 400 °C) To identify individual differences in the chemical effect of the sc-alcohols, the authors conducted a detailed study of the morphology, chemical composition, and thermal and textural parametres of RGO obtained after each reaction. The most pronounceed differences were found in the elemental composition and in the specific surface area of RGO. For example, analysis of the C-to-O ratio in the RGO samples showed that there was a 5–6-fold decrease in the relative oxygen content in comparison with the initial GO, while the RGO specific surface area increased 4–25-fold.

The best characteristics were found for the RGO sample reduced with sc-EtOH, in which the C-to-O ratio was 14.4 (6.5 times higher than that in the initial GO), and the specific surface area was 203 $m^2\ g^{-1}$ (25.7 times larger than that of the initial GO).[237] Having indicated a general decrease in the content of oxygen functions in the RGO samples, considering the reaction with sc-EtOH as an example, the authors came to the conclusion that the reduction induces the following changes:

— the number of C—O bonds (ether and epoxide groups, which are most abundant in the initial GO) decreases 8–9-fold;

— the number of carboxyl groups (COOR) decreases 5-fold;

— the concentration of the carbonyl groups (C=O) decreases 2–2.5-fold.

The only parameter that somewhat increases is the concentration of the alcohol hydroxyl groups.

Another important result achieved in this work is associated with alkylation of the reconstructed (recovered) polyaromatic core of graphene with sc-alcohols: the authors identified the dependence of the interplanar distances in the RGO samples on the type of the sc-alcohol used. Another work describes other examples of application of supercritical fluids, including sc-alcohols, for obtaining modified graphene.[238]

Thus, the results presented above show the advantages of using alcohols in the supercritical state for reduction of metal oxides or salts and graphene oxide compared to traditional conditions for similar processes.

#### 2.2.2.3. Reductive transformations of organic compounds

The ability of alcohols to reduce organic substrates can be implemented in two main types of chemical transformations:

— hydrogenation of multiple bonds: C=C, C≡C, C=O, C = N, C≡N, N=N, and N=O, *etc.*;

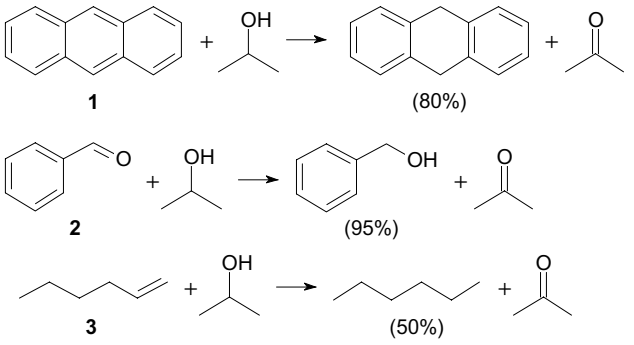
— hydrogenolysis of single bonds: C—X where X = O (hydrodeoxygenation), N (hydrodenitrogenation), S (hydrodesulfurization or hydrodesulfidation), or Hal (hydrodehalogenation); N—X (X = O, N); and S—X (X = O, S).

Reactions of this type are usually termed as 'transfer hydrogenation' (TH) or 'hydrogen transfer reactions' (HTR), although these terms are more general and cover some other types of reactions as well.

Despite the fact that the final result is similar to that of the conventional hydrogenation process, the main distinguishing feature and advantage of the TH and HTR is the absence of molecular hydrogen, complex metal hydrides, or other strong reductants (such as Na metal in alcohol), which makes HTR close to green chemistry processes. Alcohols

under supercritical conditions were first used in TH only in 1983,[239] although the above-mentioned MPV reaction, which is a classical example of the catalytic TH, had been known since 1925.[240] Gubin *et al.*[239] reported the first study of uncatalyzed transfer hydrogenation of anthracene (**1**), benzaldehyde (**2**) and hex-1-ene (**3**) in sc-Pr$^i$OH at 410 °C (Scheme 2).

**Scheme 2**




In fact, this work pointed out several important aspects that have not lost their relevance in the field of sc-alcohol application for organic substrate reduction. First, it is now evident that different classes of unsaturated organic compounds, including aromatic hydrocarbons, aldehydes (perhaps, ketones) and other unsaturated compounds (alkenes and perhaps alkynes) can take part in TH with sc-alcohols. Second, the use of catalysts is not an essential condition for TH in sc-alcohols, in contrast to MPV or HTR reactions under conventional conditions. Third, the obtained experimental data on the comparative reactivity of different types of organic compounds do not always agree with their reactivities under usual reaction conditions. Since lower alcohols reach the supercritical fluid state at elevated temperatures ( > 236 °C), it becomes possible to use poorly reactive substrates stable at these temperatures in such processes.

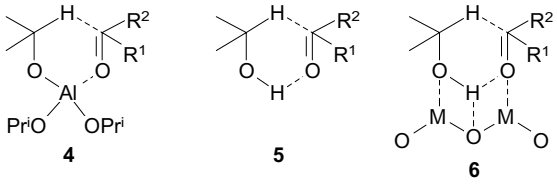
#### 2.2.2.3.1. Transfer hydrogenation of multiple bonds

The last 15 years have seen rapid growth in the number of works devoted to the use of sc-alcohols for reduction of compounds with various functional groups (C=O,[241–243] $NO_2$,[244,245] C=C[246] and C≡N[247]) and reductive dearomatization accompanied by transfer hydrogenation of the aromatic rings.[248]

Transfer hydrogenation of ketones and aldehydes with sc-alcohols is a kind of the MPV reaction and has been studied most intensively. As is known, the classical MPV reaction is carried out in Pr$^i$OH in the presence of a homogeneous catalyst, namely, aluminium isopropoxide or another strong base (*e.g.*, alkali). In some cases, co-catalysts are added. Other alcohols can also be involved as H-donors but it is done much less frequently. The use of sc-alcohols as such donors made it possible to perform this reaction with heterogeneous catalysts or without a catalyst (without a base or an alkali).[241,243] The structure of the activated six-membered complexes is similar for all the three types of the MPV reaction: classical (structure **4**), uncatalyzed (**5**), and metal oxide-catalyzed (**6**) reactions.

For example, the studied mechanism of the uncatalyzed MPV reaction with deuterated sc-Pr$^i$OH also assumes the formation of six-membered transition state **5**.[241,242] The use

**Structures 4 – 6**




$R^1$, $R^2$ = H, Alk; M is metal

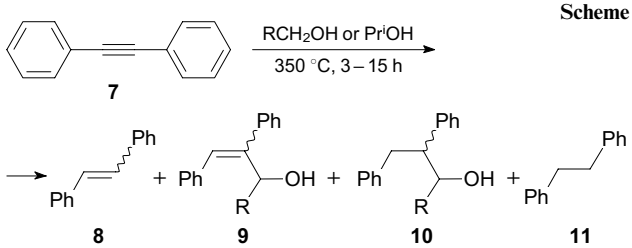
of metal oxides does not exclude the formation of a similar activated complex (**6**) bound to the oxide catalyst surface.[243] The TH of carbonyl compounds with sc-alcohols are known to be reversible,[249,250] like the classical MPV reaction. This enables implementation of the reverse reaction, namely, catalyzed or uncatalyzed transfer dehydrogenation of the alcohol by a suitable ketone or aldehyde under supercritical conditions. Depending on the reaction conditions, the reverse reaction of model alcohol dehydrogenation with sc-acetone may proceed more slowly or more quickly than the forward transfer hydrogenation of the corresponding ketone with sc-Pr$^i$OH.[250]

The MPV reaction is very sensitive to steric hindrance (structural factor).[251] This is the reason why poorly reactive substrates, such as menthone,[209] are the best candidates for TH in sc-alcohols.

The reduction of substituted acetylenes in sc-alcohols remains virtually unexplored, which makes it even more interesting to analyze the results of non-catalytic reaction of 1,2-diphenylacetylene (**7**) with three alcohols, sc-MeOH, sc-EtOH, and sc-Pr$^i$OH (Scheme 3).[246] The authors showed that at temperatures of up to 300 °C, the reaction is very slows, while at 350 °C, the conversion of acetylene **7** sharply increases. For example, 10 h after the reaction started, the substrate conversion in sc-methanol reached ~60% – 65%. However, reduction was not the only process under these conditions. As expected, stilbene **8** was formed as the major product (24%), but the mixture also contained alcohols **9** and **10** (R = H), each being formed in 10% – 15%.[246] Their formation was the result of the competing methanol addition to the C≡C bond (C-alkylation). Similar products are formed in reactions with sc-EtOH and sc-Pr$^i$OH. The yield of the completely reduced 1,2-diphenylethane (**11**) was low in all the cases. This result is at variance with the trends of HTR in sc-alcohols determined earlier, as the ratio of the major products is weakly dependent on the particular alcohol selected as the H-donor.

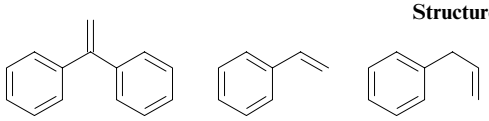
Structurally similar alkenes, 1,1-diphenylethylene (**12**), styrene (**13**), and allylbenzene (**14**), proved to be more reactive under these conditions.[246] The qualitative composition of the products fully corresponds to the expected transformations and is determined by the competing reac-

**Scheme 3**




R = H, Me

**Structures 12 – 14**



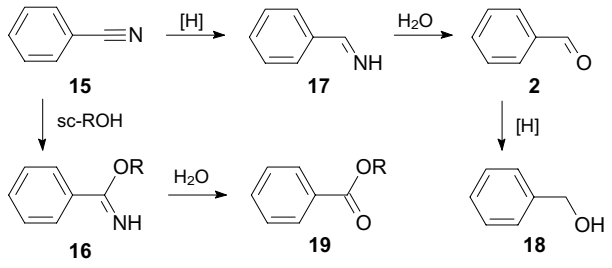
**12** **13** **14**

tions of transfer hydrogenation and C-alkylation of the nonaromatic C=C bond in sc-alcohol. However, in this case, too, the main transformation was C-alkylation yielding a product similar to compound **10**, rather than transfer hydrogenation product. The reactivity of the specified alkenes decreased as follows: **12** > **13** > **14**.

A study of the noncatalytic transformations of unsaturated mono- and bicyclic $C_{10}$ monoterpene hydrocarbons in sc-MeOH, sc-EtOH, and sc-Pr$^i$OH in the flow mode showed that the TH carried out at 300 °C and with short contact times (no more than 5 min) did not result in noticeable transfer hydrogenation of the monoterpene alkenes.[252, 253] Under these reaction conditions, the specified hydrocarbons undergo active thermal skeletal isomerization.

In another work, sc-MeOH, sc-EtOH, and sc-Pr$^i$OH were used in the reaction with benzonitrile (**15**) (Scheme 4) at 350 °C.[247] It turned out that a significant contribution is made by the alcohol addition to the cyano group (C≡N) producing *O*-alkyl imidate **16**. In the reaction with sc-MeOH, this was the main process. The reaction in sc-Pr$^i$OH leads to the expected partial hydrogenation of benzonitrile to intermediate benzaldimine **17**, which is reduced, after hydrolysis, to benzyl alcohol (**18**), representing the major product of the reaction. The reactivity of sc-EtOH towards benzonitrile intermediate between those of sc-MeOH and sc-Pr$^i$OH: among the products of this reaction, the yield of alcohol **18** is higher than that of ethyl benzoate (**19**).

**Scheme 4**

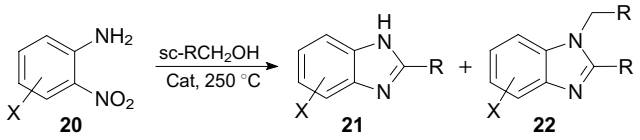



R = Me, Et, Pr$^i$

Development of modern methods for nitro group reduction[254 – 257] remains an extremely relevant and promising trend of organic chemistry. Since sc-alcohols possess reducing properties, HTR may provide an alternative for this purpose.[258] For example, sc-MeOH, sc-EtOH, and sc-Pr$^n$OH were successfully used not only as reducing agents for 2-nitroaniline **20** but also as the source of the $C_1$ moieties incorporated into the heterocyclic systems of the resulting benzimidazole **21** and **22** molecules (Scheme 5).[245] This is a heterogeneously catalyzed reaction, in which copper-doped porous metal oxides supported on hydrotalcite, a magnesium aluminium mineral, act as the catalysts.

The examples of reduction of nitro compounds by sc-Pr$^i$OH reported in a series of publication[244, 259, 260] seem

**Scheme 5**

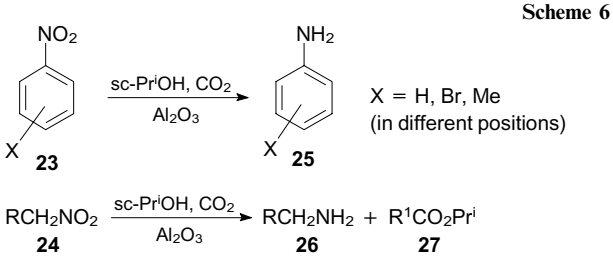



Cat is catalyst; X = H, Alk, Hal

| R (X = H) | Yield of **21** (%) | Yield of **22** (%) |
|---|---|---|
| H | 79 | 16 |
| Me | 77 | 16 |
| Et | 62 | 27 |

rather unusual in the experimental design. The authors used a mixture of an alcohol and $CO_2$, which was passed, together with a nitro compound, through a fixed bed of the $Al_2O_3$ catalyst in the flow. The reaction temperature was varied within the range of 240 – 360 °C to increase the conversion. Both aromatic (**23**) and aliphatic (**24**) nitro compounds (Scheme 6) were used, but their reactivities were significantly different.

**Scheme 6**




R = H, Me, Et, n-Alk; R$^1$ = n-Alk with the chain length < R

In the case of aromatic substrates, anilines **25** were formed as the major products. Among side products, there were *N*- and *C*- isopropyl derivatives resulting from alkylation with sc-Pr$^i$OH.[244, 261] The results of the reductive transformations of the aliphatic nitro compounds were more unpredictable: the reaction products included not only the expected amine **26**, but also ester **27** with a shortened carbon skeleton.[259, 260] The reaction was accompanied by complete loss of the nitrogen functionality, *i.e.*, denitrogenation took place.

#### 2.2.2.3.2. Transfer hydrogenolysis of C – O, C – S, C – N and C – Hal bonds

Hydrogenolysis of the carbon – heteroatom bonds in sc-alcohols has important practical applications, whether it targets a particular bond or is nonselective. It has long been used in transformations that mimic processing of plant biomass,[262 – 264] including lignin[265 – 267] and cellulose,[268, 269] heavy oil fractions,[270, 271] and biofuel obtained upon biomass pyrolysis.[266, 272 – 274] The most common sc-alcohols in this case are sc-MeOH and sc-EtOH. Such processing of plant biomass and its components is always accompanied by depolymerization of natural biopolymers such as lignin, cellulose, and hemicellulose.[275] In addition to depolymerization, the main process of lignin processing under TH conditions is hydrodeoxygenation.[275, 276]

Kim *et al.*[277] also studied the effect of addition of hydrogen gas in the reductive cleavage of lignin. It was

shown that the yield of substituted phenols in the presence of $H_2$ was much higher in sc-alcohols than under subcritical conditions. It was recommended to use supported metal catalysts such as Pt/C, Pd/C, Ru/C, and Ni/C to avoid undesirable side reactions and increase the 'hydrogen release' from sc-alcohols.[275,276,278] Higher hydrogen donating activity of sc-alcohols in the presence of metals promotes effective oxygen removal, which is an advantage of HTR over uncatalyzed pyrolysis in sc-alcohols.[279,280] The main advantage of such metal catalysts in HTR consists in reducing the contribution of dearomatization of the phenol monomers of lignin in comparison with the same reaction carried out in the presence of hydrogen gas.[281]

Desulfurization is quite useful for utilization of lignosulfonates, a large-scale waste of wood pulp and paper industry. Methods based on sc-alcohols can be successfully applied for these purposes. An example of effective reduction of lignosulfonates by sc-ethanol at 310 °C in the presence of a Ni – Mo catalyst supported by $Al_2O_3$ has been reported.[282] The authors pumped some additional amount of hydrogen gas into the reaction mixture to improve the reductive properties of sc-EtOH. The described reaction system produced an excellent result: an almost 97% decrease in the sulfur content in the products of lignosulfonate liquefaction.[282]

The H-donor activity of sc-alcohols can be used for processing of heavy oil fractions. The key features of sc-alcohols in this case are the transfer hydrogenolysis of the C – O, C – S, and C – N bonds, a higher H-to-C atomic ratio, and reductive demetallization.[270,271,283–285] For example, processing of asphaltenes with alcohols (MeOH, EtOH, $Pr^nOH$ and $Pr^iOH$) under supercritical conditions results in a 20% decrease in the sulfur content, a 30% drop in the content of nitrogen, and a 5% – 10% decrease in the amount of oxygen.[283] The chemical transformation of asphaltenes in sc-alcohols increases the H-to-C ratio in the reaction products because of their H-donor activity. Under similar reaction conditions, sc-$H_2O$ induces more intense destruction of asphaltene molecules,[286] and the reaction mixture in this case does not contain any products of partial hydrogenation caused by water gas shift reaction.[287,288]

An interesting example of processing a vacuum residue of petroleum refining in sc-methanol has been reported.[271] Nickel(II) dimethylglyoximate used as a catalyst intensified sc-methanol dehydrogenation, while the generated $H_2$ ensured almost complete desulfurization, denitrogenation, and demetallization of the vacuum residue components and simultaneosly prevented the coke deposition.

The example described above explains why the H-donor activity of alcohols should not be equalled to their reducing properties. It is evident that if the reaction mixture does not contain a hydrogen acceptor (an 'oxidant'), the alcohol can only release $H_2$, *i.e.*, it can behave only as an H-donor, or be dehydrogenated. These processes and their importance can be illustrated by hydrogen production *via* catalytic decomposition of alcohols. Wu *et al.*[289] described MeOH dehydrogenation catalyzed by $Cu/SiO_2$, which started only at 200 – 210 °C, but proceeds much faster on passing to supercritical conditions (240 °C, 4 h). If dehydrogenation of sc-MeOH is carried out at 240 °C for 4 h, 0.88 moles of $H_2$ is released per mole of the alcohol used, and its purity exceeds 95%.[289] This reaction proceeds in accordance with Eqn (1). The authors showed that under these reaction conditions, reaction (2) was the second most significant, but not reaction (3) or (4), which are typical of gas-phase methanol decomposition.

$$MeOH \longrightarrow CH_2O + H_2 \quad (1)$$

$$CH_2O + 2\,MeOH \longrightarrow MeOCH_2OMe + H_2O \quad (2)$$

$$MeOH \longrightarrow 2\,H_2 + CO \quad (3)$$

$$CO + 3\,H_2 \longrightarrow CH_4 + H_2O \quad (4)$$

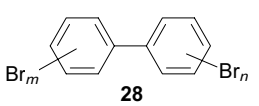
Depending on the structure of alcohols, their ability to undergo catalytic dehydrogenation can vary a lot. For example, a comparative analysis of decomposition of primary alcohols (sc-MeOH, sc-EtOH, sc-$Bu^nOH$ and sc-$C_6H_{13}OH$) at 340 °C in the presence of a Mg – Ni – Mo catalyst deposited on activated carbon shows that the largest amount of hydrogen is formed from methanol, while the smallest amount is produced from from n-butanol.[290]

Transfer hydrogenolysis of the C – O, C – N, and C – S bonds is the only significant side process of biodiesel production in sc-alcohols from microalgae or other whole-plant biomass. There are lots of heterogeneous catalysts that can be used for these purposes. For example, Lewis acids $SnCl_2$, $FeCl_3$, $ZnCl_2$, $AlCl_3$ and $NbCl_5$ were applied for processing of the *Chlorella pyrenoidosa* algae biomass.[291] The best result was achieved with $ZnCl_2$ at 270 °C in sc-EtOH: the amount of sulfur in the products decreased 3.3-fold, the nitrogen content halved, and the oxygen content decreased by 30%.[291]

No research has been done so far to study selective transfer hydrogenolysis of the C – Hal bonds in sc-alcohols. However, it seems quite possible that this reaction has great prospects and will become the basis for new industrial processes in the near future. Its real potential can be evaluated considering the experimental data on liquefaction of waste plastic housings of electronic devices.[292,293] In addition to plastic degradation, sc-alcohols have an important environmental function in this process, namely, extraction of brominated flame retardant additives from the plastic and their simultaneous debromination. The flame retardant additives in these plastics are usually represented by polybrominated biphenyls **28**, diphenyl ethers **29**, and tetrabromobisphenol A (**30**). For example, the degree of flame retardant debromination at 400 °C in sc-$Pr^iOH$ reaches more than 95% at a 60% yield of the liquefied oil product.[292,293]

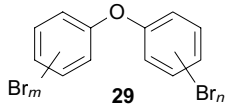
It is worth paying attention to another feature of sc-alcohols, which accompanies the reduction processes. An important role in processing of complex organic materials (biopolymers and plastics) is played by the alcohol penetrability and the strength of interaction with the substrate molecules,[275,283,294] for example, through hydrogen bond-

**Structures 28 – 30**



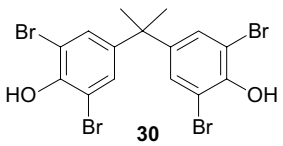

**28**

$m + n = 4 – 10$




**29**

$m + n = 4 – 10$




**30**

ing or dipole – dipole interactions. This leads to the destruction (or erosion) of the initial polymer bulk, facilitating the subsequent reduction and other transformations. This is the reason why sc-MeOH often shows the best outcome in the reactions of lignin and cellulose containing numerous oxygen-containing polar groups.[275, 294] Conversely, in reactions with asphaltenes, which have lower polarity than lignin or cellulose, the best outcome in terms of sulfur, nitrogen, and oxygen removal are achieved with sc-EtOH and sc-Pr$^{i}$OH.[283] The combination of unique physicochemical properties and H-donor activity of sc-alcohols is responsible for the high potential of their application in various reductive transformations of both single organic compounds and complex mixtures.

The prospects for using sc-alcohols in processing of substrates, such as lignocellulosic biomass, heavy oil fractions, and bio-oil, seem quite real, as these processes can be easily scaled up for industry. The high dissolving and wetting capability, fast diffusion, and good mass transfer characteristics of sc-alcohols accelerate the destruction of the native structure of high-molecular-weight compounds, while the reducing properties of sc-alcohols are good enough to perform catalytic and noncatalytic transfer hydrogenolysis of single C – O, C – S, C – N, and C – Hal bonds and for transfer hydrogenation of multiple bonds.

## 2.3. Heterogeneous catalytic reactions in supercritical fluids

Theoretical and applied studies of supercritical fluids show the advantages of conducting heterogeneous catalytic reactions in supercritical substrates over those performed under traditional conditions. This Section addresses the kinetic characteristics focusing on the evolution of the catalytic system as a whole, and, in particular, on the activity and selectivity changes in catalysts in chemical reactions of isomerization, alkylation and condensation, complete and partial oxidation in supercritical water, and also in $C_1$ chemistry. Original data on the transformation of components of renewable raw materials in sub- and supercritical water are presented. A new approach is described to estimation of the ability of monomeric phenol fragments of lignin to react with water depending on the structure of their aqueous solutions under standard conditions with extrapolation to sub- and supercritical conditions based on the molecular dynamics method.

### 2.3.1. Reactions with solid acid and base catalysts

#### 2.3.1.1. Isomerization of alkenes and alkanes. Hydrocarbon cracking

One of the first reactions studied in supercritical conditions was double bond isomerization (positional and *cis – trans* isomerization) of alkenes on $Al_2O_3$. Isomerization of hex-1-ene proved to be a suitable model, as the critical parametres of the substrate ($T_c$ = 231 °C and $P_c$ = 31.1 atm) were virtually identical to the those of the products. Therefore, this reaction can be carried out in supercritical conditions at any conversion of hexene. At pressures up to 30 atm in the liquid and gaseous phases, the ratio of *cis*/*trans*-isomers in the resulting internal alkenes is in the range of 1.2 – 1.3, whereas a pressure increase at temperatures below 230 °C in the liquid phase results in the predominant formation of the thermodynamically more stable *trans*-isomer. When $T > T_c$ and $P > P_c$, the *cis*-isomer is mainly formed because of steric hindrances at the catalyst interface and kinetic effect produced by its higher desorption by the supercritical medium.

Hexene isomerization at 220 – 250 °C in sc-$CO_2$ on the Pt/γ-$Al_2O_3$ catalyst has been investigated for many years by Saim and Subrumaniam.[295, 296] The authors performed a comprehensive study of the thermodynamic behaviour of the system and phase and reaction equilibria; they analyzed the process kinetics and modelled the coke formation and coke removal by the supercritical solvent. It was found that in subcritical conditions, catalyst poisoning results from the deposition of oligomerization products. They also studied the effect of peroxide impurities in hexene on the overall rate of the isomerization catalyst deactivation. The stable activity of the catalytic system in sc-conditions was explained by the high dissolving capacity of sc-$CO_2$ preventing coke deposition in the catalyst pores.

Skeletal isomerization of alkanes is one of the methods of obtaining high-octane fuels. A highly efficient bifunctional industrial catalyst of isomerization is platinum supported on chlorinated alumina. To ensure the catalyst stability, the reaction must be carried out in an excessive amount of hydrogen with addition of a chlorinating agent to the initial mixture of the reactants.

A conceptually new approach to increasing the lifetime of a catalyst with only the acid function was used in isomerization of n-butane at the critical parametres on sulfated zirconium ($SO_4/ZrO_2$) in the absence of hydrogen or noble metals.[297] A considerable increase in the catalyst lifetime in the n-butane isomerization ($T_c$ = 152.2 °C, $P_c$ = 37.5 atm) was observed in supercritical conditions (160 °C, 100 atm) using the Fe – Mn catalyst supported on sulfated zirconium.[298] The kinetics of the supercritical n-butane conversion to isobutane in a flow reactor was studied in detail using a number of solid acid catalysts — sulfated zirconium, titania-supported Keggin heteropoly-acid $H_4[Si(W_3O_{10})_4]\cdot x\,H_2O/TiO_2$, and H-mordenite — at temperatures of 190, 260, and 300 °C and pressures of 65, 110, and 138 atm, respectively.[299] It was shown that n-butane isomerization in supercritical conditions considerably increased the lifetime of all the catalysts studied, compared to the gas phase reaction. The phenomenon of partial or complete regeneration of solid acid catalysts of n-butane isomerization was for the first time observed *in situ* in supercritical conditions after the catalysts were deactivated in the gas phase.

The degree of supercritical conversion of n-pentane on the H-form mordenite in the skeletal isomerization reaction performed at a temperature of 260 °C, pressure of 130 atm, and liquid n-pentane space velocity of 30 $h^{-1}$ was found to be 30% – 35% and the selectivity to isopentane was 90%.[300 – 302] The skeletal isomerization of $C_6 - C_7$ n-hydrocarbons has been studied in supercritical conditions (260 – 450 °C, 80 – 130 atm) on the zeolite H-forms: mordenite, Beta, and ZSM-5. The selectivity to branched hexane and heptane isomers did not exceed 70% and 30%, respectively, since the isomerization of these long-chain hydrocarbons was accompanied by side reactions of dehydrogenation, oligomerization, and cracking.[303]

Cracking of n-heptane was studied on the Y-type commercial zeolite (P-Octacat) at 475 °C in sub- and supercritical conditions at a pressure up to 41.6 atm.[304] The changes in the number of accessible active sites were monitored *in situ* during the reaction by IR-spectroscopy. In the subcritical conditions, the concentration of the Brønsted acid sites sharply decreased, which was attributed by the authors to irreversible adsorption of the hydrocarbons on the catalyst surface. However, in supercritical

conditions, the coke precursors dissolved preventing the blockage of the zeolite channels.

#### 2.3.1.2. Hydrocarbon aromatization on zeolites

The most interesting problem in catalysis is the involvement of the so-called wet gas into the synthetic chemistry of light $C_3-C_5$ alkanes through their oligomerization and aromatization. The most detailed review of the studies of the gas-phase aromatization of light alkanes catalyzed by hydrogen and modified forms of zeolites such as pentasil was reported by Minachev and Dergachev.[305] The UOP company, a leader in the chemical industry, developed a process of $C_3-C_4$ gas dehydrocyclodimerization on high-silica zeolites modified with zinc and gallium (known by the commercial name Cyclar) at temperatures $> 425$ °C with the yield of aromatic compounds up to 60%–65%.[306] The disadvantages of this process in terms of its practical application include low space velocities of 100–500 $h^{-1}$ under standard conditions (STP) and fast catalyst deactivation.

The company was also the first to carry out a reaction of model aromatization of n-butane in supercritical conditions on high-silica zeolites HZSM-5 ($SiO_2/Al_2O_3$ molar ratio of 30–70) and S-115 silicalite ($SiO_2/Al_2O_3$ molar ratio of 500) modified with gallium, zinc, and platinum. The aromatization of gaseous n-butane at a temperature of 530 °C and a pressure of 1 atm leads to fast deactivation of the catalysts, with the benzene–toluene–xylene selectivity $> 50\%$. It was established that the catalyst productivity increases 20–50-fold in supercritical conditions at a temperature of 430–560 °C and a pressure of 100–200 atm. The catalysts retain their activity (almost 100%) for several days.[307]

#### 2.3.1.3. Solid acid alkylation

Isobutane alkylation with butenes in industry has long been catalyzed by concentrated sulfuric and hydrofluoric acids. Alkylation in the presence of mineral acids is an extremely environmentally hazardous chemical process. An alternative is solid acid alkylation. However, the industrial application of solid acid alkylation is limited by the fast catalyst deactivation, low content of alkylated products in the reaction products, and low thermal stability of the catalyst. The major disadvantage of solid acid alkylation is the fast deactivation of catalysts caused by butene oligomerization that accompanies the alkylation and formation of heavy products adsorbed on the catalyst surface and leading to catalyst poisoning.[308] The critical parametres of $C_4$ mixtures are technically suitable for alkylation in supercritical conditions. This fact explains the great attention of researchers to both fundamental and practical aspects of this catalytic reaction and the large amount of literature data on isobutane alkylation with butenes in supercritical conditions with a number of catalysts [Nafion®, sulfated zirconium ($SO_4/ZrO_2$), USY, Pt/USY, *etc.*] in reactions with and without additional hydrocarbon solvents ($CH_4$, $C_2H_6$, $C_3H_8$, $CO_2$, and $CHF_3$).[308–320]

The effect of supercritical conditions on isobutane and isopentane alkylation with isobutene on the USY zeolite was studied by Fan *et al.*[309] Isoalkanes were used as both a reactant and the supercritical solvent (in a 50-fold excess in comparison with the alkene). The alkylate yield reached 70% in both supercritical and liquid phases. However, the catalyst lifetime in the liquid and gas phases was much shorter than that in supercritical conditions. Salinas *et al.*[310] showed that the zeolite structural type has a considerable effect on the activity and deactivation of the zeolite catalyst when the $C_4$ alkane alkylation is carried out in supercritical conditions. The H-beta zeolite is superior to H-USY in its stability of action and quality of the alkylated product, which mainly consists of isoparaffins in the case of H-beta zeolite. The fast H-USY deactivation is explained by the fact that the processes inside the zeolite channels are predominantly butene oligomerization rather than alkylation. It was shown that smaller crystallites are more efficient for the removal of compaction products from the external surface and zeolite channels in a supercritical medium, which decreases the catalyst deactivation rate.

A process of isobutane alkylation with butenes on sulfated zirconium oxide (SZ and Fe-Mn/SZ) in supercritical ethane at the isobutane : alkene ratios of 0.4 and 8 was reported by Chellappa *et al.*[311] It was found that the $C_8$ products mainly consisted of alkenes, with dimethylhexenes prevailing over the other products. The catalyst deactivation was attributed by the authors to oligomerization and subsequent cracking processes. In the absence of isobutane, alkene dimerization took place to give $C_{5+}$ products in $> 90\%$ yield at the dimethylhexene selectivity of $\sim 75\%$. It was established that the catalyst poisoning was less pronounced than in the alkylation reaction.

The alkylation of the butane–butene ($C_4$) fraction was carried out with a series of catalysts based on potassium salt of phosphotungstic heteropolyacid ($K_3PW_{12}O_4$) in the liquid and supercritical phases in a batch reactor.[312,313] It was found that the transition from the liquid phase (40 °C, 7–9 atm) to supercritical conditions (145 °C, 42–48 atm) increases the amount of the cracking products and $C_{9+}$ fraction in the $C_{5+}$ alkylate. When the pressure rises from 40 to 90 atm, the butene conversion increases from 77 % to 100% and the alkylate quality improves. Clark and Subramaniam[314] showed that when sc-$CO_2$ is used as the solvent, the reaction can proceed in the supercritical medium at a comparatively lower temperature ($< 135$°C). The alkylate yield at a temperature of 50°C and pressure of 155 atm was 5%–10%, with 20% alkene conversion (the $CO_2$ : isobutane : but-1-ene ratio in the feed was 86 : 8 : 1). Despite the low output in comparison with traditional alkylation, an important result in this case is that the reaction proceeds for several days with a stable conversion degree. Alkylation in the supercritical substrate requires a higher temperature ($> 135$ °C), at which the cracking and coke formation reactions prevail.

A study of the effect of the sc-$CO_2$ pressure on the Nafion®/$SiO_2$ catalyst activity in the alkylation showed that the alkene conversion does not change when the pressure rises from 80 to 167 atm and equals 80 %, whereas $C_8$ selectivity goes down from 30% to 7%.[315,316] The yield of heavy products increases in parallel. The changes in the selectivity following pressure increase were attributed to the higher density of the medium and deterioration of transport properties, affecting the desorption of $C_8$ products, which are removed from the catalyst pores before being converted to heavier products. From the obtained results, the authors made a conclusion about good prospects of low-temperature alkylation in a supercritical $CO_2$ medium.

Opposite results were reported Ginosar *et al.*,[317] who studied the effect of an inert solvent (methane, ethane, propane, carbon dioxide, and trifluoromethane) on solid acid alkylation of isobutane with *trans*-but-2-ene (isobutane : alkene = 25) at 60 °C and 111 atm with a number of catalysts (Nafion®, S/$ZrO_2$, USY, and Pt/USY). The results indicate that supercritical conditions have no bene-

ficial effect on the process in comparison with the reaction in the liquid phase: they do not increase the catalyst lifetime, while the $C_{5+}$, $C_8$, and trimethylpentane yields become lower. The difference in the results may stem from the fact that in the studies of Subrumaniam and co-workers,[315, 316] butene dimerization rather than alkylation was the predominant reaction. This assumption is indirectly confirmed by the low selectivity to trimethylpentane and the higher content of alkenes in the products, as it was mentioned by the authros.

A series of publications [316 – 320] describe a detailed study of solid acid alkylation of isobutane with butenes on sulfated zirconia (SZ) and a number of zeolites, such as the H-form of the ultrastable Y-type zeolite (H-USY) with the $SiO_2$ to $Al_2O_3$ ratio of 5.5, 10.5, and 32.7; H-mordenite ($SiO_2 : Al_2O_3 = 32$); H-Beta (Si/Al = 37.5), and H-ZSM-5 ($SiO_2/Al_2O_3 = 30$), in the temperature range of 80 – 150°C and a pressure range of 20 – 120 atm. The highest-quality alkylate was formed in the presence of H-USY. In all the cases where the solid acid alkylation was conducted in supercritical conditions, the catalyst lifetime was longer than in traditional liquid and gas phase conditions.

The possibility of Friedel – Crafts alkylation of mesitylene ($1,3,5\text{-}Me_3C_6H_3$) and anisole (PhOMe) with propene and propanol in a continuous flow reactor in the pesence of solid acid catalysts (Nafion® and Deloxan®) in sc-$CO_2$ and propane was demonstrated by Hitzler *et al.*[321] Benzene alkylation with propene in supercritical and traditional conditions on the H-Beta zeolite was studied by Tian *et al.*[322]

#### 2.3.1.4. Aldol condensation of acetone on solid acid catalysts

The benefits for conducting substrate condensation reactions in the sc-state were demonstrated by Koklin *et al.*[323] The authors performed for the first time the aldol condensation of acetone with the $CaO - SnO_2$ solid base catalyst in a temperature range of 300 – 450 °C and pressure range of 15 – 75 atm. The products of acetone dimerization are isomeric isomesityl and mesityl oxides, while acetone trimerization gives isophorone. Stable performance of the $CaO - SnO_2$ catalyst, with the maximum conversion of supercritical acetone of 40% at 400 °C, 75 atm, and an unusually high flow rate of liquid acetone (8.1 g $h^{-1}$ per gram of the catalyst).

### 2.3.2. Hydrogenation and dehydrogenation

Liquid phase hydrogenation of organic compounds is faced with some problems, in particular, extremely low solubility of hydrogen in a liquid substrate and, as a result, diffusion limitations for virtually all processes. Meanwhile, the hydrogen concentration is an order of magnitude higher in a supercritical solution than in a traditional solvent. Consequently, the amount of the reaction gas adsorbed on the catalyst surface can be increased severalfold, leading to sharp increase in the reaction rate and catalyst performance. Supercritical fluids (carbon dioxide, ethane, propane, and alcohols) are successfully used as solvents for hydrogenation of natural fats and oils, for obtaining products in pharmaceutical and fine chemistry, and in asymmetric and Fischer – Tropsch syntheses.[324]

The problem of fat and vegetable oil hydrogenation stems from the fact that natural products with several double bonds are the *cis*-forms, while hydrogenation of one double bond turns them into *trans*-isomers. This *cis* – *trans* rearrangement is facilitated by the low hydrogen concentration on the catalyst surface, which is a drawback of the classical autoclave process. Hydrogenation in supercritical propane in a continuous flow reactor improves the hydrogen solubility and its transport towards the Pd catalyst surface. The rate of hydrogen saturation of fatty acid methyl ester is 400 times higher than that of the liquid phase process. The *cis*- to *trans*-isomer ratio also significantly increases. However, during the hydrogenation, the catalyst activity is noticeably reduced.[325]

Supercritical $CO_2$ was used for hydrogenation of fats and oils, fatty acids and their esters. The catalyst activity in this solvent was 6 times higher than that of Pd/C in the flow gas phase mode, and the catalyst lifetime increased. The importance of appropriate choice of the solvent for reactions in supercritical conditions was demonstrated by the synthesis of fatty alcohols from oleates. Hydrogenation in sc-$CO_2$ leads to higher conversion, while that in supercritical propane improves the catalyst performance, although it also increases the yield of the side products, that is $C_{16}$ and $C_{18}$ n-alkanes.

Hydrogenation of the functional groups of some organic molecules in SCF solvents has been reported;[326, 327] for example, Pd-catalyzed hyrogenation of unsaturated ketones in sc-$CO_2$ was carried out in a gradientless cyclic reactor. Piqueras *et al.*[325] hydrogenated cyclohexene, acetophenone, and nitrobenzenes on Pd/C in sc-$CO_2$ and propane. They also studied the Pd- and Pt-catalyzed conversion of a variety of compounds (alkenes, alkynes, aliphatic and aromatic ketones, aldehydes, epoxides, phenols, nitro compounds, and nitriles). Supercritical $CO_2$ was used as a solvent for aliphatic and aromatic hydrocarbons, while supercritical propane was employed for nitrogen-containing organic compounds, because hydrogenation in $CO_2$ results in the formation of insoluble carbamide salts as by-products. The large temperature gradients observed in the hydrogenation in adiabatic conditions are smoothed out even when a small amount of sc-$CO_2$ is added to the system. Noted that this SCF is also used as the medium and a reagents in alkene hydroformylation catalyzed by heterogenized Rh- and Ru-catalysts, Fischer – Tropsch synthesis in supercritical n-hexane with Co catalyst and in supercritical propane on the Fe contact, and in supercritical n-hexane with the Fe – Cu – K – Si catalyst manufactured by Ruhrchemie.

Dehydrogenation of a number of normal alkanes ($C_{10} - C_{14}$) to the corresponding normal alkenes was performed [328] at 400 – 450 °C, a liquid feed space velocity of 32 $h^{-1}$ and pressures of 17 – 44 atm in supercritical solvents on the $Pt - Sn/\gamma\text{-}Al_2O_3$ catalyst. The alkane conversion increased 2 – 3-fold when the subcritical conditions changed to supercritical ones, while the selectivity and conversion remained invariable for 100 h. Besides, in contrast to the gas phase, the reaction conducted in supercritical conditions produced almost no dialkenes or aromatic compounds. When hydrogen was added to the system, the alkane conversion decreased, which could be explained by changes in the supercritical medium density.

#### 2.3.2.1. Hydrogenation of $CO_x$. Fischer – Tropsch synthesis

Of interest is the application of SCF in the Fischer – Tropsch synthesis (preparation of hydrocarbons from the synthesis gas $CO + H_2$), which is mainly associated with the problem of hampered heat and mass transfer of the substrate and products in traditional gas phase conditions. Pentane, hexane, and mixtures of higher hydrocarbons are

used as supercritical solvents in these reactions. Yokota and Fujimoto[329] showed that, although the reaction rate becomes slightly lower, the heat and product withdrawal from the catalyst surface is more effective in the supercritical medium (240 °C, 20–65 atm, $H_2:CO = 2$) than in the gas phase. Besides, in the supercritical solvent, the amount of heavier products is higher than in the gas and liquid phases.

#### 2.3.2.2. Hydrogenation of supercritical $CO_2$

Heterogeneously catalyzed reduction of $CO_2$ is the most promising route for its utilization. Hydrogenation of $CO_2$ on metal-supported catalysts makes it possible to obtain a variety of valuable chemical products: carbon monoxide, methane, hydrocarbon mixtures, $C_{2+}^{=}$ alkenes, methanol, and other oxygenates. (Scheme 7).

**Scheme 7**

$$CH_4 + H_2O \longleftarrow CO_2 + H_2 \rightleftharpoons CO + H_2O \xrightarrow{H_2} C_xH_yO_z + H_2O$$

The variability the products of carbon dioxide reduction is the equilibrium water gas shift reaction:

$$CO + H_2O \rightleftharpoons CO_2 + H_2, \quad (5)$$
$$\Delta_R H_{573\,K} = -38 \text{ kJ mol}^{-1}$$

For the reverse water gas shift reaction, hydrogenation of carbon dioxide, high catalytic activity is inherent in Cu-, Ni-, and Fe-containing catalysts and their bimetallic compositions such as Cu–Ni, Cu–Zn, and Cu–Fe,[329,330] which are more stable during $CO_2$ conversion to CO. For example, $CO_2$ conversion at a temperature of 600 °C and pressure of 1 atm is 14%–16% (depending on the iron content) and was invariable for 120 h on the $CuFe/SiO_2$ catalyst.[330]

Iron-based catalysts are also active in the reverse water gas shift reaction. The $CO_2$ reduction to CO at the atmospheric pressure occurs at higher temperatures of 450C–470°C with a productivity of 50 mmol $(h\ g_{Cat})^{-1}$ and with selectivity of 99% on $Fe/\gamma\text{-}Al_2O_3$ and $Fe–K/\gamma\text{-}Al_2O_3$ systems.[331,332] Potassium promotion triples the reaction rate, but the catalyst deactivation rate is doubled.[331] The bimetallic $Co–Fe/Al_2O_3$ catalyst remains stable for up to 40 h; the yield of CO with this catalyst is 48% at a pressure of 1 atm and temperature of 650 °C.[332]

The 100% CO selectivity in the $CO_2$ hydrogenation reaction is reached on the Fe–K and Fe–Cu–K catalysts at 350–400 °C at a pressure of 1 atm; the substrate conversion is 24% and 21%, respectively. The catalysts are stable in the selected reaction conditions.[333] In the reverse water gas shift reaction, high activity is observed for metallic catalysts supported on cerium oxide. Dai *et al.*[334] considered the transformation of $CO_2$ to CO on a number of $Me/CeO_2$ catalysts (Me = Fe, Cu, Ni, Co, and Mn). $Ni/CeO_2$ proved to be the most active catalyst, but it was least selective to CO (the maximum selectivity was 28% at a temperature of 320 °C and a pressure of 1 atm). The drawback of the catalysts based on cerium oxide is their deactivation in the presence of carbon particles on the surface.

The reverse water gas shift reaction in supercritical conditions was also studied by Bogdan *et al.*,[335] who used a series of Au- and Au–Ni-containing catalysts on oxide supports. The catalysts were stable in the reverse water gas shift reaction, with the CO selectivity being up to 96%–98%. Despite the fact that the system contained nickel, the methanation barely took place on the Au–Ni catalyst. $Au–Ni/ZrO_2$ and $Au–Ni/TiO_2$ appeared to be the most selective catalysts (the CO selectivity was 95%–100%) throughout the given temperature range (180–450 °C). The main advantage of conducting this process in supercritical conditions is the increase in the product volume yield due to the use of a denser (in comparison with the gas) medium. The productivity reached 1.54 g $(h\ g_{Cat})^{-1}$, which was 7–8 times higher than the values obtained for $CO_2$ hydrogenation in the gas phase.

Direct generation of methane through carbon dioxide hydrogenation [reaction (6)] in the presence of a nickel catalyst was discovered by Paul Sabatier, a French chemist, in 1902. In the methanation reaction, in addition to Ni and Co, high catalytic activity was found for catalysts based on noble metals: Ru, Ir, and Rh.[336–338]

$$CO_2 + 4\,H_2 \longrightarrow CH_4 + 2\,H_2O, \quad (6)$$
$$\Delta_R H_{573\,K} = -164.7 \text{ kJ mol}^{-1}$$

From the standpoint of thermodynamics, high pressures and low temperatures are favourable for this reaction. Methanation reaction (6) underlies a method for harvesting and storage of energy from renewable sources, that is, power-to-gas (PTG) technology. Carbon dioxide reacts with hydrogen, obtained by water electrolysis using wind or solar energy, to give methane. Between 2009 and 2013, Germany implemented five pilot projects based on the PTG technology with the power capacity from 25 to 6300 kW.[339] Catalytic methanation is also a part of tandem reactions of water regeneration on board of space vehicles.

A wide range of methanation catalysts based on Ni, Rh, and Pd deposited on $Al_2O_3$, $CeO_2$, $SiO_2$, and MCM-41 oxides were studied by Martin *et al.*[336] The highest conversion of carbon dioxide (44 %) was reached on $Rh/CeO_2$ at a temperature of 350 C and atmospheric pressure. The high activity, selecivity ($S_{CH_4}$ = 99%). and stability of operation for 150 h at 75% conversion of $CO_2$ were observed for the 10 mass % $Ni/Ce_{0.72}Zr_{0.28}O_2$ catalyst at 350 °C and 1 atm.[337]

The activity and selectivity of methanation catalysts depend on not only the nature of the active component and the support, but also on the metal particle size. We *et al.*[338] studied the hydrogenation of carbon dioxide on a series of $Ni/SiO_2$ catalysts with various nickel contents (from 0.5 mass % to 10 mass %) at a temperature of 350 °C and atmospheric pressure. The metal particle size depended on the metal content on the catalyst surface. When the nickel content in the catalyst was 0.5%, the particles were rather small (and were not detected on the powder X-ray diffraction patterns), and the reaction mainly gave CO, whereas the reaction with 10% nickel content in the catalyst (and particle size of 9 nm) proceeded as methanation.

The conversion of $CO_2$ under hydrogen in the presence of catalysts of the water gas shift reaction leads to the formation of hydrocarbon mixtures and oxygenates [reaction (7)].

$$2x\,CO_2 + (2y + 1)\,H_2 \longrightarrow 2\,(C_xH_y)O_z + H_2O \quad (7)$$

One of the new reactions of $CO_2$ hydrogenation is heterogeneously catalyzed reduction in the supercritical state, which is beneficial for the catalytic properties: activity, selectivity, and lifetime.[333,335,340–342] Carbon dioxide

hydrogenation in supercritical conditions was studieds[340, 341] using carbon-supported Ru, Rh, and Ir catalysts over a wide temperature range of 50 – 450 °C at a pressure of 80 atm. The Ru/C and Rh/C catalysts demonstrated almost 100% selectivity to methane. The major process on the Ir/C catalyst was the reverse water gas shift reaction. The authors were able to achieve 50% carbon dioxide conversion on the Ru/C catalyst at $H_2 : CO_2 = 2 : 1$. The catalyst was active at relatively low temperatures (120 – 200 °C). In the presence of Rh/C, the reaction required higher temperatures (360 – 400 °C), with the methane selectivity reaching ~80%. The CO selectivity on Ir/C at 350 °C was 80%.

Hydrogenation of carbon dioxide into methane in supercritical conditions was studied with Co and Ni catalysts supported on multiwalled carbon nanotubes.[342] The methane selectivity on the cobalt catalyst was 100%, while the selectivity to ethane and CO was 0.1%. The ethane selectivity on the $Co/Al_2O_3$ catalyst studied for comparison reached several percent. The Ni/YHT catalyst was active in the reaction with 100% methane selectivity. The cobalt particles were 3 – 6 mm in size, while the nickel particle size was 5 – 8 mm. The most active catalyst was 10 % Co/YHT at 200 °C. Carbon dioxide hydrogenation in supercritical conditions resulted in a 5 – 7-fold higher methane yield in comparison with the gas phase.

Hydrocarbons and $C_{2+}^{=}$alkenes are prepared on iron-containing catalysts.[343] Promotion of Fe-catalysts by the first group metals increases their activity selectivity to hydrocarbons. Boreriboon *et al.*[344] illustrated the effect of promotion of the $FeCu/TiO_2$ catalyst by potassium and lanthanum. The experiments were conducted at a temperature of 300 °C and a pressure of 1.1 MPa. The system reached a steady-state regime after 15 – 16 h, with the $CO_2$ conversion being ~20%, the chain growth factor being up to ~0.5, and the CO selectivity ranging from 50% to 35%. The optimal K : Fe ratio in the system was 0.1. The promoters increased the catalyst activity and $C_{5+}$ hydrocarbon selectivity. According to the data of thermoprogrammed desorption (TPD) and diffuse reflectance infrared Fourier transform spectroscopy (DRIFTS), the presence of potassium considerably inhibited $H_2$ adsorption, thus slowing down the $CH_4$ formation.

Pokusaeva *et al.*[333] performed a comparative study of th hydrocarbon synthesis using promoted iron-containing catalysts supported on the Sibunit carbon material in supercritical conditions (80 atm) and in the gas phase (1 atm). The pressure was shown to have a great effect on the distribution of reaction products. Carbon monoxide was formed as the only product in the case of Fe – K/C and Fe – Cu – K/C catalysts at 1 atm and 350 – 450 °C. At 80 atm in supercritical conditions, the hydrocarbon selectivity could reach 50%, and the staable operation of the catalysts was observed for 8 hours. Among the hydrocarbon products, there were $C_1 - C_{12}$ alkanes and alkenes, with both unbranched and branched molecules, with their amounts being in line with the Anderson – Schulz – Flory distribution law.

Transition from the gas phase to supercritical conditions[345] in the carbon dioxide hydrogenation catalyzed by Fe – K/C resulted in increasing $CO_2$ conversion and increasing the hydrocarbon selectivity. A further pressure increase in the supercritical region (from 6.5 to 8.5 MPa) did not have any effect on the distribution of reaction products.

**2.3.3. Oxidation**

Oxidation reactions carried out either in sub- or in supercritical conditions can be divided into two main groups:

— partial oxidation of organic compounds;
— complete oxidation in supercritical water.

**2.3.3.1. Partial oxidation of organic compounds**

The main products of partial oxidation of methane under the action of sc-$H_2O$ are methanol, carbon monoxide, and carbon dioxide. None of the studies conducted so far have reported considerable methanol yields in methane oxidation reactions in supercritical water. Lee and Foster[346] noted that the methanol selectivity at a temperature of 400 – 450 °C and pressure up to 250 atm is 35%, while the methane conversion is extremely low: 1% – 3%. Similar results were obtained in another study,[347] where the methanol yield did not exceed 0.7% at 350 – 480 °C. Armbruster *et al.*[348] also employed supercritical water as a medium for partial propane oxidation; the reaction was carried out at 360 – 420 °C and 167 – 280 atm using a series of oxide catalysts. The catalyst nature was found to have a minor effect. The total selectivity to oxygenates (mainly methanol) was 15%, with the propane conversion being 90%. The main reaction type involved was complete oxidation.

Supercritical $CO_2$ is the most common solvent for hydrocarbon partial oxidation reactions. In sc-$CO_2$, oxidation of propane proceeds at lower temperatures and pressures.[349] For example, at a temperature of 300 °C and pressure of 100 atm, the selectivity to oxygenates is 59% and the propane conversion is 12%. The preparation of *tert*-butyl alcohol *via* isobutane oxidation was studied by Fan *et al.*[350] Despite the fact that the selectivity and conversion in supercritical conditions are higher than in the gas and liquid phases, the *tert*-butyl alcohol yield does not exceed 5%. In the partial oxidation of aromatic compounds by oxygen in sc-$CO_2$ studied by Sato *et al.*,[351] increasing oxygen concentrations in the reaction mixture promoted complete oxidation. Kustov *et al.*[352, 353] reported the first selective oxidation of benzene and alkylbenzenes into the corresponding phenols by $N_2O$ on H-ZSM-5-type hydroxylated zeolites. The maximum toluene conversion in the presence of the H-ZSM-5 zeolite into the correspondinge products (cresols and phenol) in the 370 – 420 °C temperature range and 70 – 160 atm pressure range was 35%. The amount of cresols formed decreased in the following series: *m*-cresol > *o*-cresol > *p*-cresol. The partial oxidation of toluene was accompanied by disproportionation and formation of biphenyls at any reaction conditions.

Bogdan *et al.*[354] pioneered the oxidative condensation of supercritical dimethyl ether and its mixtures with sc-$CO_2$ into mono- and diglymes with atmospheric oxygen in a temperature range of 250 – 300 °C, at a pressure of 100 atm using $CaSnO_3$, a new solid base catalyst. The maximum conversion in the $Et_2O$ partial oxidation was 40% and the monoglyme and diglyme selectivities were 55% and 45%, respectively, in the reaction carried out at 250 °C and 100 atm in a 5% ether mixture with $CO_2$.

Another pioneering study[355] focusing on the oxidative dehydrogenation of supercritical ethane (ODE) by oxygen using the $MoVNbTeO_x$ catalyst and pressures up to 100 atm. It was found that high pressure reduces the process temperature from 360 °C at 1 atm to 280 °C at 100 atm and increases the ethylene production rate from 205 to 290 g $(h\ kg_{Cat})^{-1}$. The ethylene selectivity remains high

(~90%), and the catalyst performance does not decrease for 40 hours. At the atmospheric pressure, the activity of the ODE catalyst becomes lower due to its irreversible deactivation.

#### 2.3.3.2. Oxidation of components of renewable raw materials by supercritical water

The last few years have seen a growing interest in the alternatives to fossil fuels as energy sources. The study and development of energy-efficient and energy-saving technologies of processing renewable raw materials are primary goals of research programmes both in Russia and in the developed countries all over the world. These studies mainly focus on aqueous phase reforming of lignocellulosic materials.[356] Conducting aqueous phase reforming in supercritical water (SCW) has certain advantages over the steam method traditionally used in industrial processes. All chemical processes accompanying gasification of biomass and its components in SCW can be represented as an overall endothermic reaction (8), in which SCW acts not only as the reaction medium but also as a reactant and a hydrogen atom source.

$$C_xH_yO_z + (2x-z)\,H_2O \longrightarrow x\,CO_2 + (2x-z)\,H_2 \qquad (8)$$

Resende and Savage[357] studied the cellulose and lignin conversion kinetics in SCW without a catalyst. The kinetic model included 11 reactions, such as hydrolysis, thermal degradation, steam reforming, water gas shift reaction, and methanation. The water gas shift reaction is exothermic and predominates when the reaction time is long. A low temperature (350–500 °C) facilitates the formation of $CH_4$, while temperature rise (400–600 °C) enhances the formation of hydrogen.

Man *et al.*[358] assumed that lignin depolymerization in SCW proceeds *via* hydrolysis and dealkylation, with generation of reactive low-molecular-weight fragments. However, it was shown[359] that the decomposition of ligno-*p*-cresol follows two pathways: hydrolysis and pyrolysis. At lower hydrothermal temperatures, hydrolysis prevails over the formation of low-molecular-weight compounds. However, at higher temperatures and longer reaction times, the main reactions are pyrolysis and condensation of aromatic compounds with subsequent carbonization and transformation into coal.

Among the plant biomass components, lignin is a type of waste that is most difficult to recycle. Since lignin has a complex polymer structure, an important step towards understanding of the mechanisms and ways of natural lignin transformation in SCW consists in studying the conversion of model monomers such as phenol and guaiacol (*o*-methoxyphenol).[360–364] A study of guaiacol and phenol transformation at 400–700 °C after their 8–60 min residence in a vacuum-sealed quartz reactor showed that the main products of the guaiacol gasification were $H_2$, CO, $CO_2$, and $CH_4$.[361] The rest of guaiacol decomposed into phenol and *o*-cresol or turned into coal. The presence of a Ni catalyst did not affect guaiacol conversion, but significantly changed the ratio of the gaseous products. It should be said that the yields of the conversion products and rate of phenol gasification in homogeneous conditions were rather low,[362] but increased in the presence of the Ni catalyst. On the basis of experimental data, Huelsman and Savage[363] proposed a methanism for phenol conversion in SCW in a closed system at 500–700 °C. The kinetic model consisted of 13 reactions responsible both for the gasification and the formation of liquid and solid phase products.

The kinetics of phenol and cyclohexanol conversion in SCW was studied at temperatures of 500–750 °C, a pressure of 300 atm, and a space velocity of 1.2–2.0 $h^{-1}$ in the flow mode.[364] The conversion of phenol in SCW at 500–600 °C resulted only in the formation of pyrolysis products such as benzene, toluene, and naphthalene and a number of fused aromatic compounds. Almost complete phenol conversion was achieved at 750 °C, with the selectivity to gaseous hydrogen-containing light hydrocarbons being 30%. In contrast to phenol, the gasification of cyclohexanol in SCW already starts at a temperature of 600 °C, with the selectivity of 35%, and complete cyclohexanol conversion is achieved at 700 °C. The yield of gaseous products in this case is 70%, with the methane–ethane mixture accounting for 40%. It was established that the presence of an aromatic ring in the molecule of an organic substrate is the main cause for the lower rate of substrate reaction with the supercritical water: the conversion and the selectivity to gaseous products were lower for phenol than for cyclohexanol.

In order to explain the low reactivity of phenols in reactions conducted in supercritical conditions and the tendency towards the formation of phenol condensation products, Alekseev and Bogdan[365] performed a classical molecular dynamics simulation of the structure of aqueous solutions containing 2 mass % molecules with alcohol groups (ethanol, phenol, and guaiacol) under standard consitions (STP) ($T$ = 298 K, $P$ = 1 atm) and under supercritical conditions ($T$ = 673 K, $P$ = 230 atm) using the $NVT$ ensemble [a canonical ensemble with constant number of particles ($N$), volume ($V$), and temperature ($T$)]. The computational cell contained 10 000 molecules. The MD trajectories showing the behaviour of the computational systems were 10 ns long. The agglomeration of alcohol molecules was analyzed and the diffusion coefficients ($D$) were calculated. The simulation results showed that the diffusion coefficients are lower for molecules containing aromatic moieties both at STP and under sc-conditions. The errors in the calculation of the diffusion coefficients were rather high, which can be attributed to the existence of different types of agglomeration of water and alcohol molecules (water, phenol, alcohol, water–phenol, and water–alcohol clusters of various sizes) and single molecules. The diffusion coefficients of ethanol at STP, as opposed to those of phenols, resemble most closely the diffusion coefficient of water, which indicates that ethanol molecules are likely to be incorporated in water clusters. This result is in line with the experimental data about the chemical reaction of water and ethanol at 673 K and allows the assumption that the chemical reaction is preceded by the formation of water–ethanol clusters.

The low $D$ value for phenol and guaiacol compared with ethanol, first, can be explained by lower mobility of heavier molecules. Second, since the diffusion coefficients of the water molecules are three times higher than those of the phenol molecules, the solvation shells become unstable in sc-conditions. Consequently, phenols are less solvated than ethanol, which, along with the lower velocity of molecular motion (compared to that in water), correlates with the low reactivity of aromatic alcohols under simulated conditions.

An analysis of agglomeration of alcohol molecules shows that phenol molecules are more prone to agglomeration than ethanol molecules. The agglomerates are

dynamic entities that tend to be destroyed with time and form again. The role of hydrogen bonds in the overall agglomeration of phenol is low, evidently, due to hydrophobic effects. When the number of molecules in the alcohol agglomerate was calculated from geometric considerations, atoms of different molecules were found to be located at a distance of 0.35 nm from one another. Although the solution mainly consisted of single alcohol molecules due to the low concentration of the solute, a detailed, step-by-step analysis of the molecular dynamics trajectories made it possible to identify some characteristic features of the agglomeration. At some steps of the trajectory, the agglomerate size can reach 6 or 7 ethanol molecules and 5 or 6 phenol molecules at STP, whereas in the supercritical region where single molecules prevail, dimers were also detected. A study of guaiacol at STP showed that with increasing the observation time, the number of single molecules decreases and the agglomerate becomes larger. In phenol and ethanol solutions, no tendency towards agglomerate growth was observed. An analysis of guaiacol solutions in supercritical conditions revealed the formation of an agglomerate of two molecules, which existed for 3 ns.

A comparison of the obtained results with the experimental data on the chemical transformation of ethanol and phenol in supercritical conditions [366] shows that the most complete ethanol conversion can be attributed to the fact that ethanol molecules are mainly surrounded by water and become accessible to the oxidant on going to the supercritical region. This results in the formation of gaseous products of ethanol reactions with water: hydrogen, methane, and carbon dioxide. The properties of dilute aqueous solutions of phenol and guaiacol indicate that the molecules of aromatic alcohols tend to form agglomerates, which explains the easy condensation of aromatic benzene rings at higher temperatures and pressures and the low yields of gaseous products of reactions between aromatic compounds and water in supercritical conditions.

## 2.4. Enantioselective catalytic reactions in supercritical fluids

The last few years have seen a growing demand for possible applications of alternative solvent types,[367] including liquid or supercritical carbon dioxide,[368] ionic liquids (ILs),[369] and water [370, 371] in chemical processes. Such solvents produce a lower adverse effect on the environment than conventional organic solvents (chlorohydrocarbons, aromatic compounds, *etc.*). Liquid and sc-$CO_2$ forms are thought to be the most promising solvents due to their availability, low cost, non-toxicity, non-combustibility, tolerance to a wide range of chemicals, and ability to dissolve (extract) a lot of nonpolar chemical compounds.[372, 373] The critical point parametres of this fluid [$T_c$ = 31 °C, $P_c$ = 7.4 MPa ≈ 74 atm (bar)] can be easily generated both in laboratory and under industrial conditions. At the same time, the physical properties of $CO_2$ (density, viscosity, dielectric constant, *etc.*) can be adjusted within a wide range of values (especially in the vicinity of the critical point) by changing pressure and temperature to achieve the maximum efficiency of a chemical reaction.[374, 375]

Carbon dioxide in liquid or supercritical state is especially attractive for enantioselective synthesis of complex organic compounds, in particular, pharmaceutical agents, where it helps to completely get rid of undesirable toxic organic solvents. The asymmetric synthesis of drugs is usually carried out in the presence of chiral catalysts.[376, 377] Chemical reaction of $CO_2$ with some functional groups of a catalyst and(or) substrate (for example, with a hydroxyl or amino group) can be used to control a catalyzed process (temporary protecting group).[378, 379] The phase composition of the system is also important for successful application of sc-$CO_2$ in asymmetric catalysis.[380] Being a poor solvating agent for polar chemical compounds, sc-$CO_2$ readily dissolves lipophilic catalysts and ligands containing fluoroaryl [381, 382] or fluoroalkyl [383 – 388] groups, which considerably accelerates reactions in the presence of these catalysts and ligands.[389] In some cases, reactions efficiently proceed in two-phase $CO_2/H_2O$ (Ref. 390) or $CO_2$/IL system.[391, 392]

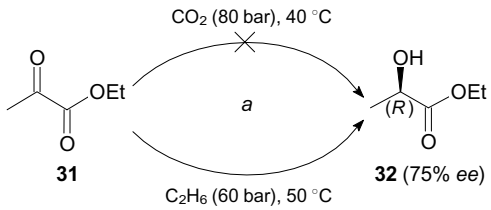
This Section summarizes the results of studies published before 2019 concerning the application of liquid and supercritical $CO_2$, and also some other SCFs, as a reaction medium in enantioselective catalytic transformations accompanied by reduction of multiple bonds or formation of new carbon – carbon and carbon – heteroatom bonds. Among these reactions are hydrogenation, hydroformylation, alkylation, allylation, cycloaddition, hydrovinylation, cyclopropanation, epoxidation, aldol and Michael reactions, and some other processes that can be used to build a carbon skeleton and functionalize organic molecules. A separate part of the Section is devoted to asymmetric tandem and domino reactions in sc-$CO_2$. The material is classified by types of transformations. Since the size of the review is limited, reactions involving enzymes [393 – 396] and asymmetric catalytic reactions in which carbon dioxide acts as a reagent (synthesis of carbonates, polycarbonates, *etc.*) [397, 398] are beyond the consideration.

### 2.4.1. Asymmetric hydrogenation

Catalytic asymmetric hydrogenation is widely used for enantioselective synthesis of biologically active chiral substances. Gaseous $H_2$ is infinitely miscible with $CO_2$ in sc-conditions;[399] hence, high hydrogen concentrations in the reaction mixture are possible, which accelerates the reaction. However, this process may be accompanied by a side reaction of $CO_2$ reduction to CO. This was the case when ethyl pyruvate (**31**) was treated with $H_2$ in the presence of 5 mass % $Pt/Al_2O_3$/cinchonidine catalytic system in sc-$CO_2$ (40 °C, 80 bar) [400] (Scheme 8). Hydrogenation product **32** is not formed in this reaction, which was attributed by the authors to catalyst poisoning with $CO_2$ reduction products on the Pt surface. This hypothesis was confirmed by Fourier transform infrared spectroscopy (FTIR) and enantioselective synthesis of lactate **32** by a similar reaction conducted in sc-ethane with ~100% substrate conversion.

The undesirable $CO_2$ reduction was prevented by using Ru or Rh complexes with chiral phosphinic, phosphite, or phosphoramide ligands as catalysts. Using this approarch,

**Scheme 8**

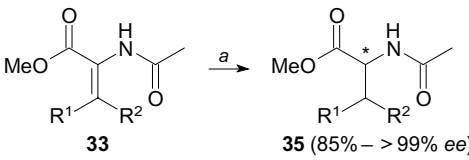



(*a*) $H_2$ (70 bar), $Pt/Al_2O_3$/cinchonidine (5 mass %);
*ee* is enantiomeric excess

hydrogenation of various compounds containing C=C, C=O, or C=N bonds was carried out in liquid and sc-$CO_2$ with fairly high chemo- and enantioselectivity. However, the poor solubility of the polar substrates in sc-$CO_2$ usually necessitates the addition of an organic cosolvent (see p. 351 in monograph [401] and Refs 402 – 404), an excess of a liquid reactant,[405 – 407] or an ionic liquid to the system.[408]

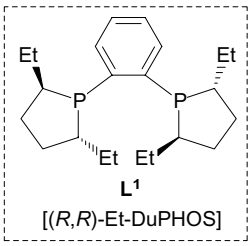
The first successful use of sc-$CO_2$ without a cosolvent was evidently asymmetric hydrogenation of prochiral α-enamides **33** in the presence of rhodium cationic complexes [Rh(COD)(**L**$^1$)$_2$]An (**34a**,**b**) containing a chiral bidentate ligand, (*R*,*R*)-Et-DuPHOS (**L**$^1$) (Scheme 9).[382] Products **35** are formed in sc-conditions with enantioselectivity comparable with or even exceeding that attaiined in conventional organic solvents (MeOH or n-hexane). The reactions proceed in homogeneous conditions, as the solubility of complexes **34a**,**b** in sc-$CO_2$ is rather high, because they contain lipophilic fluorine-containing anions (BARF or OTf). This method can be considered a promising green approach to obtaining enantiopure α-amino acid derivatives.

**Scheme 9**




**33** **35** (85% – > 99% *ee*)

(*a*) $H_2$ (14 bar), [Rh(COD)(**L**$^1$)$_2$]An (**34a**,**b**), sc-$CO_2$, 40 °C, 345 bar; An = BARF (**a**), OTf (**b**); $R^1 = R^2$ = H, Me; $R^1$ = H: $R^2$ = Me, Et, Ph, 3,5-$(F_3C)_2C_6H_3$; $R^1 - R^2 = (CH_2)_5$; BARF is tetrakis[3,5-bis-(trifluoromethyl)phenyl]borate, Tf is trifluoromethanesulfonyl (triflyl)

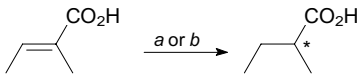



**L**$^1$
[(*R*,*R*)-Et-DuPHOS]

Ruthenium complexes with bidentate bisphosphine ligands were also found to selectively catalyze asymmetric hydrogenation in sc-$CO_2$. Hydrogenation of tiglic acid (**36**) in the presence of 0.7 mol.% Ru(OAc)$_2$[(*S*)-H$_8$-BINAP] [(*S*)-**37a**] [BINAP is 2,2′-bis(diphenylphosphino)-1,1′-binaphthyl] led to the formation of (*S*)-2-methylbutanoic acid [(*S*)-**38**] in up to 99% yield and with up to 81% *ee* (Scheme 10, conditions *a*).[399] Interestingly, the components do not react in liquid $CO_2$ (20 °C), which, in the authors' opinion, is explained by different solubilities of the catalyst in liquid and supercritical phases (in sc-conditions, the system is completely homogeneous). The asymmetric hydrogenation of acid **36** in the presence of ruthenium complex (*R*)-**37b** containing a BINAP ligand modified with trifluoromethoxy groups in sc-$CO_2$ (conditions *b*) was less selective (35% *ee*).[409] However, when a cosolvent (MeOH) was added, *ee* increased to 62%.

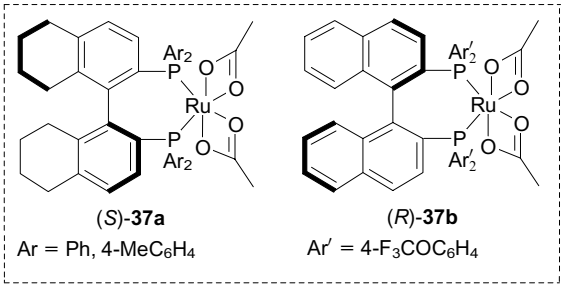
As a rule, inclusion of polyfluorinated structural moieties significantly increases the affinity of polar organic compounds for carbon dioxide,[410 – 413] thus suppressing their ability to self-association [414] and(or) reducing their polarity.[415] However, asymmetric hydrogenation of dimethyl itaconate (**39**) in the presence of RuL complexes,

**Scheme 10**




**36** (*S*)-**38** (81% *ee*) or (*R*)-**38** (up to 62% *ee*)

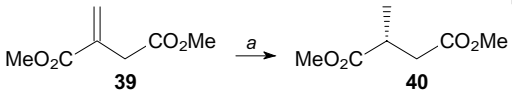
(*a*) $H_2$ (25 – 35 bar), (*S*)-**37a**, sc-$CO_2$ (177 bar), 50 °C; (*b*) $H_2$ (30 bar), (*R*)-**37b**, sc-$CO_2$ (166 bar), 25 °C, 12 h




(*S*)-**37a** Ar = Ph, 4-$MeC_6H_4$ (*R*)-**37b** Ar′ = 4-$F_3COC_6H_4$

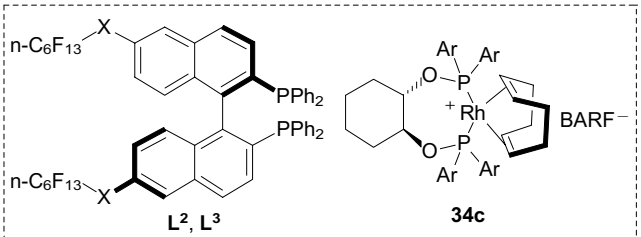
obtained from [$RuCl_2$(PhH)]$_2$ and fluorine-containing chiral phosphine ligands (**L**$^2$ and **L**$^3$) based on BINAP,[416] was less selective in sc-$CO_2$ than in MeOH, evidently, because of the low SCF polarity (Scheme 11). When the reaction was catalyzed by fluorine-containing '$CO_2$-philic' rhodium diphosphinite complex **34c**, the stereoinduction in sc-$CO_2$ (30 bar $H_2$, 150 bar $CO_2$, 45 °C) was also quite moderate (up to 72% *ee*).[417] The substrate conversion ranged from 75% to 100%.

**Scheme 11**




**39** **40**

(*a*) $H_2$ (30 – 50 bar), Ru(**L**$^2$ or **L**$^3$) or **34c** (0.05 mol.% – 0.1 mol.%), sc-$CO_2$ (100 – 150 bar), 45 – 80 °C (72% – 76% *ee*) or MeOH, 22 °C ( > 95% *ee*)



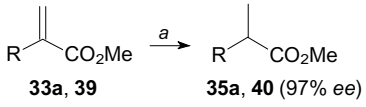

**L**$^2$, **L**$^3$ **34c**

X is absent (**L**$^2$), $(CH_2)_5$ (**L**$^3$) Ar = 4-[n-$F_{15}C_7(CH_2)_2$]$C_6H_4$

Rhodium complexes with bifunctional phosphino phosphite ligands based on 1,1′-binaphthyl-2,2′-diol (BINOL) turned out to be more efficient in the stereoinduction in the hydrogenation of activated alkenes in $CO_2$. For example, excellent results were achieved in asymmetric hydrogenation of methyl 2-acetamidoacrylate (**33a**) and dimethyl itaconate (**39**) in sc-$CO_2$ with the complex [Rh(COD)$_2$]$BF_4$ and the ligand **L**$^4$ [(*R*,*S*)-3-$H_2F_6$-BINAPHOS, X = $(CH_2)_2C_6F_{13}$-n] containing perfluoroalkyl substituents in the aryl moieties.[386] The products (*R*)-**35a** and (*S*)-**40** were obtained in these reactions in high yields and 97% *ee* (Scheme 12).

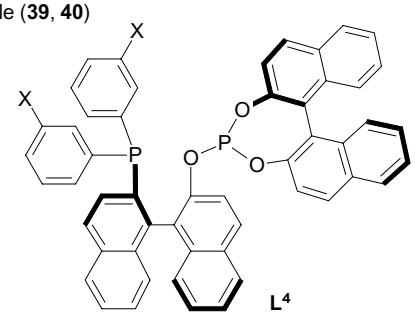
Later, the same research team [387, 388] suggested carrying out Rh-catalyzed asymmetric hydrogenation of polar

**Scheme 12**




**33a**, **39** **35a**, **40** (97% *ee*)

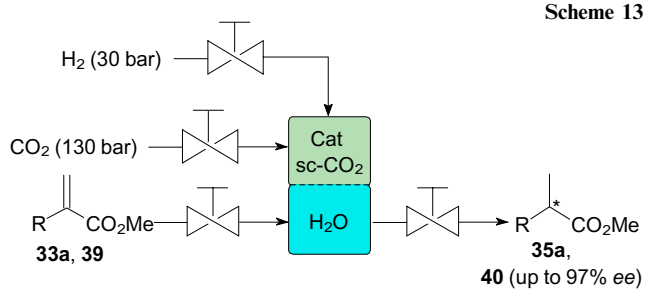
(*a*) $H_2$ (30 bar), $[Rh(COD)_2]BF_4$, **L**$^4$ [X = $(CH_2)_2C_6F_{13}$-n], sc-$CO_2$ (130 bar), 40 °C; R = NHC(O)Me (**33a**, **35a**), $CH_2CO_2Me$ (**39**, **40**)




**L**$^4$

alkenes in an inverse sc-$CO_2$/water two-phase system. The '$CO_2$-philic' Rh catalyst obtained from $[Rh(COD)_2]$BARF and fluorinated (*R*,*S*)-3-$H_2F_6$-BINAPHOS (**L**$^4$) was localized, in this case, in sc-$CO_2$ (the upper phase), whereas polar substrate **33a** or **39** was in the aqueous medium (Scheme 13). By vigorous stirring (1000 rpm), these two phases were converted to an emulsion. After the reaction was completed (> 99% conversion) and the emulsion was broken, the aqueous phase was removed through the needle valve on the reactor bottom without significant pressure drop to obtain products (*R*)-**35a** or (*S*)-**40** (87% and 97% *ee*, respectively). The Rh catalyst retained its activity and stereoinduction level over five catalytic cycles. The rhodium and phosphorus contents in the aqueous phase did not exceed 1.4 and 5.2 ppm, respectively, which indicates that the method is environmentally safe.

**Scheme 13**

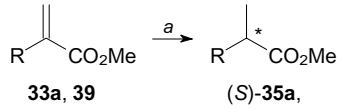



Cat = $[Rh(COD)_2]BF_4$ + **L**$^4$ (X = $(CH_2)_2C_6F_{13}$-n)

In some cases, available phosphite or phosphoramidite ligands derived from BINOL provided efficient stereoinduction in the asymmetric hydrogenation of alkenes.[418] A two-fold excess of these ligands was successfully used to perform hydrogenation of compounds **33a** and **39** catalyzed by $[Rh(COD)_2]BF_4$ in sc-$CO_2$ (Scheme 14).

The hydrogenation of itaconate **39** in sc-$CO_2$ in the presence of phosphites **L**$^5$ – **L**$^7$ containing carborane moieties was faster (1 – 2 h) than this reaction in $CH_2Cl_2$ (16 h), but the enantioselectivity was lower (76% – 93% *ee versus* ~99% *ee* in $CH_2Cl_2$).[419 – 421] By employing phosphoramidite ligands **L**$^8$ and **L**$^9$, the researchers were able to increase the stereoinduction in sc-$CO_2$ for both substrates to

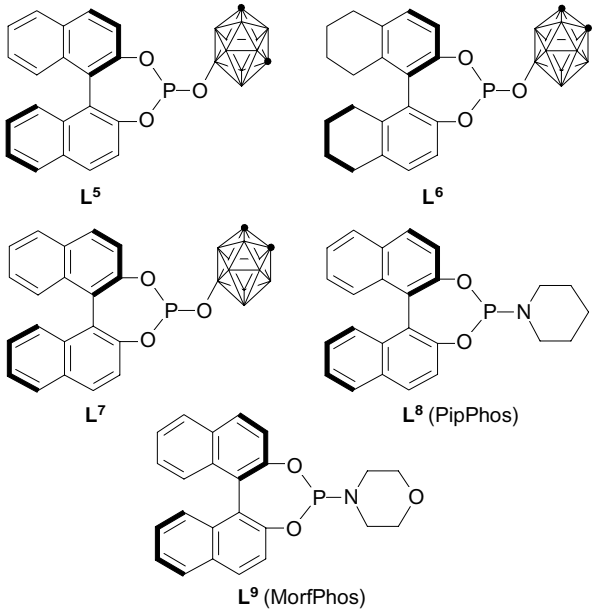
**Scheme 14**




**33a**, **39** (*S*)-**35a**, (*R*)-**40** (76% – 99% *ee*)

(*a*) $H_2$ (100 bar), $[Rh(COD)_2]BF_4$, **L**$^5$ – **L**$^9$, sc-$CO_2$ (100 bar), 35 °C, 0.5 – 132 h; R = NHC(O)Me (**33a**, **35a**), $CH_2CO_2Me$ (**39**, **40**)

**Structures L$^5$ – L$^9$**

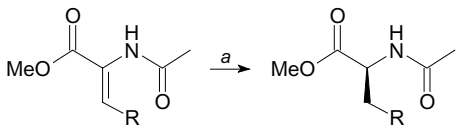



97% – 99% *ee*, without lowering the high productivity of the catalytic system (the reaction time was 35 – 50 min).[422]

β-Aryl-substituted acrylates **33b** – **f** also appeared to be suitable substrates for asymmetric hydrogenation catalyzed by the Rh(**L**$^8$) complex in sc-$CO_2$. The resulting α-amino acid derivatives **35b** – **f** were obtained in high yields and enantiopurity of up to 97% *ee* in these reactions (Scheme 15).[423] The optimal reaction conditions (14 – 27 bar $H_2$, 140 – 250 bar $CO_2$, 40 – 70 °C) and catalyst activity depended on the solubility of the starting compounds in $CO_2$, but in all cases, it took no longer than 3 h to achieve complete substrate conversion. The use of phosphite ligands containing carborane groups lowered the enantioselectivity (37% – 52% *ee*).[424]

The reduction of β-amidoacrylates **41a** – **d** in the presence of the rhodium complexes obtained *in situ* from $[Rh(COD)_2]BF_4$ and phosphoramidite **L**$^{10}$ (Ref. 425) or

**Scheme 15**

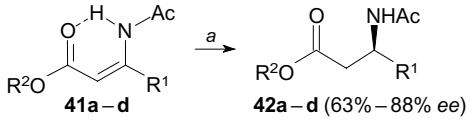



**33b** – **f** **35b** – **f** (up to 97% *ee*)

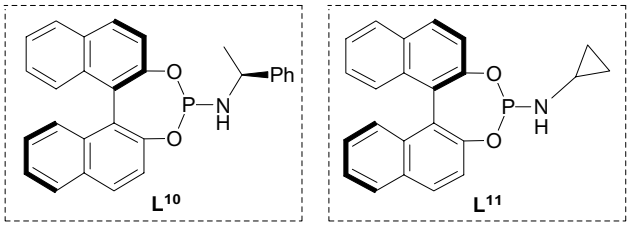
(*a*) $H_2$, $[Rh(COD)_2]BF_4$, **L**$^8$, sc-$CO_2$, 40 – 70 °C, 1.5 – 3 h; R = Ph (**b**), 4-$ClC_6H_4$ (**c**), 4-$FC_6H_4$ (**d**), 2-Naph (**e**), cymantrenyl (**f**); Naph is naphthyl

**L[11]** (Ref. 426) was carried out in a sc-$CO_2$/protic cosolvent system [hexafluoropropan-2-ol (HFIP) or AcOH]. This led to complete substrate conversion, yielding chiral β-amino-esters **42a – d** with the enantiomeric purity up to 88% (Scheme 16). The added acid evidently activated the catalyst and substrate **41**, promoting the cleavage of the strong hydrogen bond between the proton at the nitrogen atom and the oxygen atoms of the carboxyl group. If nonfluorinated alcohols (Pr$^i$OH or Bu$^t$OH) with weaker H-donor properties were used as cosolvents, the conversion ( < 13%) and enantioselectivity (36% – 50% *ee*) values were lower.

**Scheme 16**

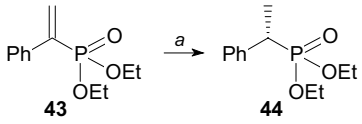



(*a*) $H_2$ (40 bar), $[Rh(COD)_2]BF_4$, 2 **L[10]**(**L[11]**), sc-$CO_2$, HFIP or AcOH, 100 bar, 50 °C, 3 h; $R^1$ = Me: $R^2$ = Et (**a**), Me (**b**); $R^2$ = Et: $R^1$ = Pr$^i$ (**c**), Ph (**d**)

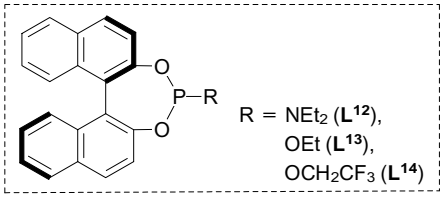



Available phosphite and phosphoramidite ligands (**L[12]** – **L[14]**) based on BINOL were used in combination with the $[Ir(COD)_2]$BARF complex in asymmetric hydrogenation of prochiral vinylphosphonate **43** in sc-$CO_2$ (with 38% substrate conversion). The highest enantiopurity of chiral product (*S*)-**44** (62% *ee*) exceeding that obtained upon the reaction in $CH_2Cl_2$ (54% *ee*) was achieved in the presence of phosphoramidite **L[12]** (Scheme 17).[427] Metal nature plays the key role in this process: the replacement of Ir with Rh leads to the formation of racemic product **44**.

**Scheme 17**



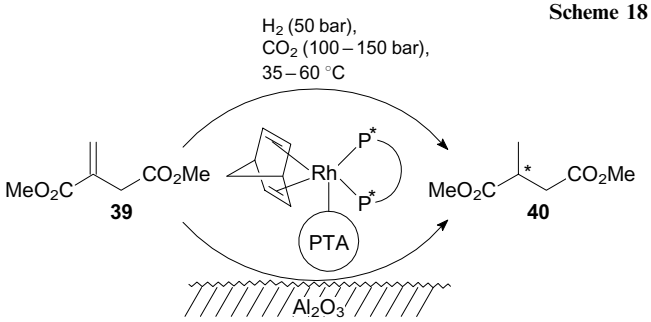

(*a*) $H_2$ (50 bar), $[Ir(COD)_2]$BARF, 2 **L[12]**, sc-$CO_2$, 250 bar, 60 °C;

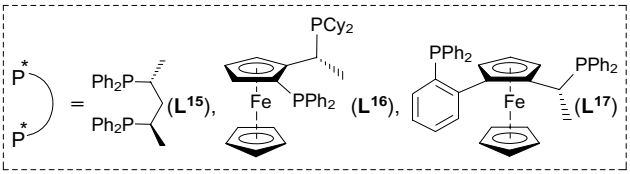



All the hydrogenation reactions considered above were carried out in batch reactors. The main drawbacks of such processes are that they require large solvent amounts, have low productivity, and, in many cases, it is difficult to reuse the valuable chiral catalysts.[428] Effective continuous flow systems based on $CO_2$ are viewed as an environmentally friendly alternative to batch reactors.[429] They may be more advantageous in terms of possible process automation, higher product yield, and lower catalyst loss. However, implementing such concept requires reliable immobilization of chiral catalysts,[430] without destroying the geometry of the ligand system and structure of the catalyst active sites.

These requirements are partially satisfied by the rhodium complex with norbornadiene (nbd) and bisphosphine ligand **L[15]** attached to γ-alumina with a linker based on phosphotungstic acid, $H_3O_{40}PW_{12}$ (PTA) (Scheme 18). This complex was employed to catalyze the asymmetric hydrogenation of dimethyl itaconate (**39**) in a $CO_2$ flow (at the hydrogen : substrate ratio of 4 : 1 and flow rate of 0.25 mL min$^{-1}$), ensuring the formation of (*R*)-**40** with 63% *ee* and moderate conversion (66%).[431] Later, the same research team[432] immobilized rhodium complexes with ferrocene-containing bisphosphine ligands **L[16]** and **L[17]** on alumina in a similar way. In the presence of **L[16]**, the enantioselectivity of the flow hydrogenation of compound **39** in sc-$CO_2$ reached 83%, exceeding the respective value (72% *ee*) achieved in homogeneous conditions with chiral rhodium complex **34**c (see Scheme 11).[417]

**Scheme 18**



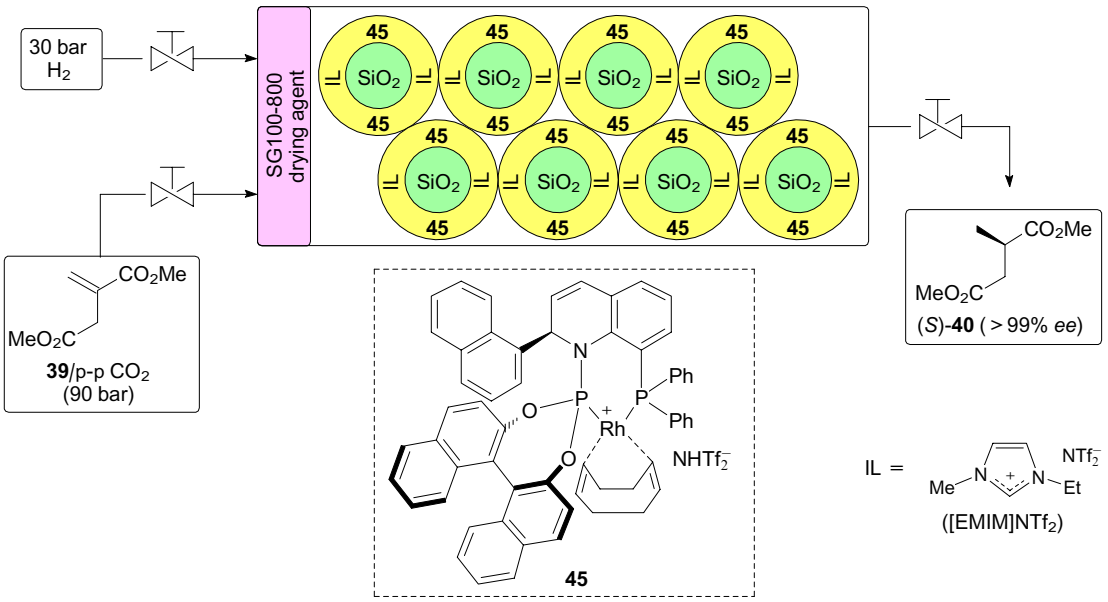




| Ligand | Conversion (%) | *ee* (%) |
|---|---|---|
| **L[15]** | 66 | 63 |
| **L[16]** | 35 | 83 |
| **L[17]** | 59 | 57 |

Cy is cyclohexyl

Another promising method of immobilization of asymmetric reaction catalysts in a $CO_2$ flow is based on catalyst dissolution in a small amount of ionic liquid immobilized on the surface of porous inorganic oxides, such as silica or alumina. This approach was applied by Leitner's group[433] for asymmetric hydrogenation of dimethyl itaconate (**39**). The active component of the catalyst was the Rh cationic complex **45** with a chiral bidentate phosphine-phosphoramidite ligand [($S_a$,$R_C$)-1-Naph-QUINAPHOS], introduced into the thin layer of the $[EMIM]NTf_2$ ionic liquid (EMIM is 1-ethyl-3-methylimidazolium) deposited on the surface of silica particles (Scheme 19). The **45**/IL system exhibited high catalytic activity in the reaction: the IL, which is poorly soluble in sc-$CO_2$,[434] kept the catalyst on the $SiO_2$ surface, while hydrogenation product (*S*)-**40** was continuously extracted by the sc-$CO_2$ flow. However, the high initial enantiopurity of (*S*)-**40** (99%) decreased to ~70%

**Scheme 19**

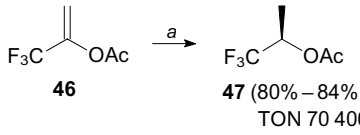



after 5 – 10 h of the reactor operation, because the active cationic $Rh^{III}$ dihydride decomposed on contact with water accumulated in the IL during the catalytic process.[435] The problem was solved by placing dehydroxylated silica sorbent SG100-800, in front of each cartridge with catalyst **45**. As a result, the stereoinduction level remained high (> 98% *ee*) for 30 h of continuous hydrogenation process, which corresponded to the catalyst turnover number (TON) of 70 000. Thus, 14 g of enantiomerically pure product (*S*)-**40** was obtained using only 1.6 mg of catalyst **45**, with the conversion of substrate **39** exceeding 99%.

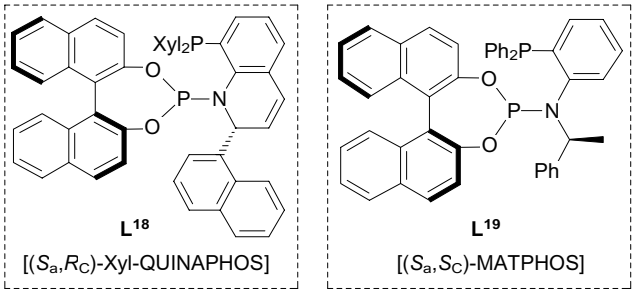
In 2015, Leitner's research team[436] carried out asymmetric hydrogenation of 1-trifluoromethylvinyl acetate (**46**) in the presence of Rh complexes with chiral phosphinic-phosphoramidite ligands **L**$^{18}$ [($S_a$,$R_C$)-Xyl-QUINAPHOS, Xyl stands for 3,5-xylyl] or **L**$^{19}$ [($S_a$,$S_C$)-MATPHOS] in sc-$CO_2$ flow using [EMIM]$NTf_2$ or [EMIM]$NTf_2$/$SiO_2$ supported ionic liquid phase (SILP) as the stationary phases (Scheme 20). The [Rh(COD)$_2$]$BF_4$ – **L**$^{18}$/SILP catalytic system turned out to be more efficient (with the substrate conversion reaching 70% – 90% per cycle). The TON value (70 400 over 233 h) was 6 times higher than that obtained in the sc-$CO_2$/IL system with the same catalyst. The enantiomeric purity of the hydrogenation product **47** (80% – 84%) even increased a little as the reactor continued to operate. This method is quite practical: the reactor metal etching had only a small effect on the process performance.

The use of Ru complexes containing bidentate phosphine ligands enabled the enantioselective ketone hydrogenation to chiral alcohols, which are used to prepare flavouring substances and pharmaceutical agents. For example, the enantioselective hydrogenation of β-ketoester **48** catalyzed by chiral complex the $RuCl_2$(**L**$^{20}$) in sc-$CO_2$ afforded enantiomerically enriched (> 98% *ee*) β-hydroxy ester **49**, an intermediate for the preparation of Xenical (Orlistat), a gastrointestinal lipase inhibitor, which blocks lipolysis (Scheme 21).[437] The reaction rate increased upon hydrogen partial pressure rise up to 60 bar. Unfortunately, the authors used the MeOH cosolvent without specifying its amount, which may complicate reproducing the obtained results.

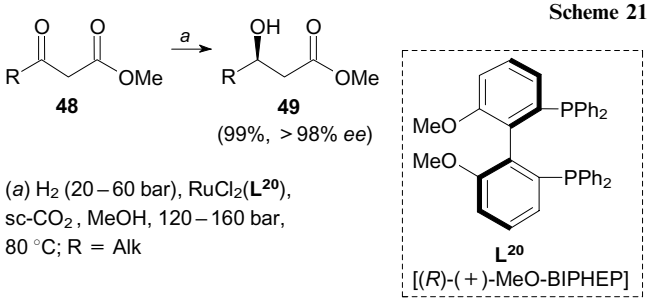
**Scheme 20**




(*a*) [Rh(COD)$_2$]$BF_4$ – **L**$^{18}$ (0.1 mol.%)/[EMIM]$NTf_2$ or [Rh(COD)$_2$]$BF_4$ – **L**$^{18}$ (0.1 mol.%)/SILP, $H_2$ – sc-$CO_2$ (flow system), 120 bar, 60 °C, 233 h



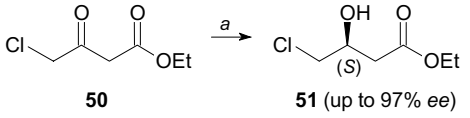

**Scheme 21**




(*a*) $H_2$ (20 – 60 bar), $RuCl_2$(**L**$^{20}$), sc-$CO_2$, MeOH, 120 – 160 bar, 80 °C; R = Alk

Chlorine-substituted β-hydroxy ester **50** can be enantioselectively reduced in sc-$CO_2$ in the presence of the chiral ruthenium complex $[RuCl_2(PhH)]_2$ and the ligand (*R*)-BINAP.[438] Since the active complex cannot be formed in the nonpolar sc-$CO_2$ medium, it was presynthesized in an organic solvent or formed *in situ* in the sc-$CO_2$/IL two-phase system, where [BMIM]$BF_4$ served as an IL (BMIM is for 1-n-butyl-3-methylimidazolium). In the optimal conditions (Scheme 22), the reaction led to the formation of ethyl

**Scheme 22**

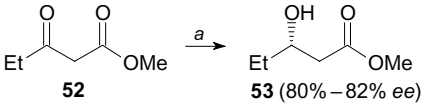



(*a*) $H_2$ (27 bar), $[RuCl_2(PhH)]_2$, (*R*)-BINAP, sc-$CO_2$, $[BMIM]BF_4$, 110 bar, 75 °C, 13 h

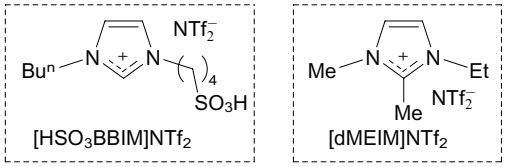
(*S*)-3-hydroxy-4-chlorobutyrate (**51**), a carnitine (vitamin $B_T$) precursor.[439]

The asymmetric hydrogenation of β-ketoesters, in particular methyl 3-oxopentanoate (**52**), can also be carried out in a continuous flow reactor[440] using the $[RuCl_2(PhH)]_2$–(*S*)-BINAP catalyst, the molten imidazolium salt $[dMEIM]NTf_2$ as the stationary phase, and sc-$CO_2$ as the mobile phase (Scheme 23). Product **53** was formed in 180 g $L^{-1}$ $h^{-1}$ yield and had enantiopurity of 80% – 82% *ee*, with substrate conversion being almost complete after one pass, in the presence of an acidic IL — $[HSO_3BBIM]NTf_2$. Although the conversion gradually decreased as the catalyst continued to operate (down to 91% within 100 h and to 69% within 150 h), evidently because of water accumulation in the system, the continuous process was more efficient than the batch one. It allowed obtaining the same product quantities in a much smaller reactor using a three time smaller amount of the catalyst. Product **53** did not have any IL or catalyst impurities.

**Scheme 23**



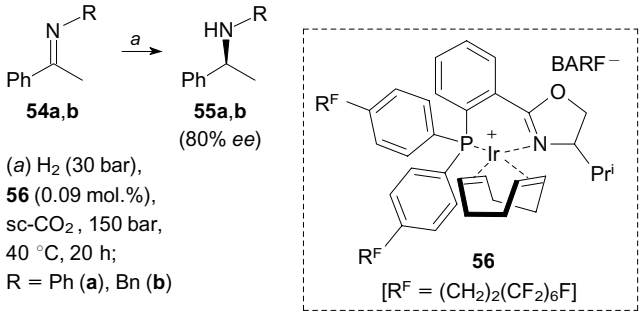

(*a*) $H_2$, $[RuCl_2(PhH)]_2$, (*S*)-BINAP (0.2 mol.%), $[HSO_3BBIM]NTf_2$ (5 equiv.), [dMEIM]$NTf_2$/sc-$CO_2$, 250 bar, 60 °C, 150 h (flow reactor)




Asymmetric hydrogenation of the C=N bond catalyzed by the chiral Rh, Ir, Ru, and Ti,[441 – 443] complexes is a convenient method for preparing chiral amines. This approach was used by the Ciba-Geigy company[444, 445] for the industrial production of (*S*)-metolachlor, a chiral herbicide. This reaction can also be of use for manufacturing levofloxacin (an antibiotic), sertraline (an antidepressant), stepholidine (an antipsychotic agent), anstruurine and calicotomine alkaloids, and a number of other biologically active compounds in enantiomerically enriched form.[446]

Leitner and co-workers[447] were the first to carry out catalytic asymmetric hydrogenation of acetophenone phenylimine **54a** to chiral amine **55a** in sc-$CO_2$ (Scheme 24). Quantitative conversion and 80% *ee* enantioselectivity were achieved in the presence of iridium complex **56** containing lipophilic perfluoroalkyl groups in the cation and BARF-anion. After the reaction was completed, product **55a** was extracted with sc-$CO_2$ (40 °C, 110 bar) and collected in a cooled trap. The catalyst remaining in the reactor was reused in the next batch reaction. Thus, organic solvents

**Scheme 24**

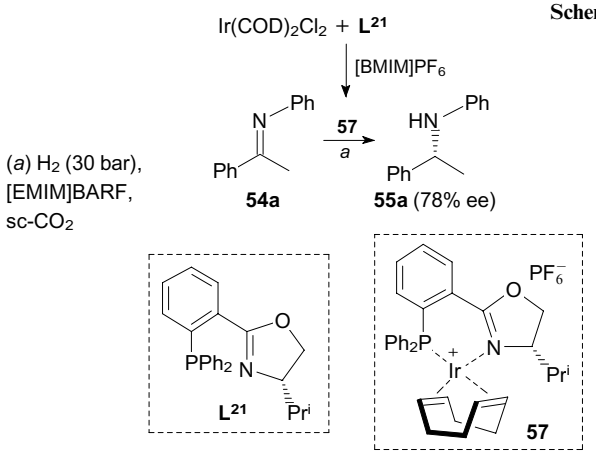



(*a*) $H_2$ (30 bar), **56** (0.09 mol.%), sc-$CO_2$, 150 bar, 40 °C, 20 h; R = Ph (**a**), Bn (**b**)

were excluded from all the process stages. However, benzylimine **54b** was a less active substrate in the proposed conditions (15% conversion), evidently, because of the formation of a strong coordination bond between the nucleophilic nitrogen atom and $CO_2$.

Later Leitner's research team[448] applied the sc-$CO_2$/IL system for the catalytic hydrogenation of imine **54a** (Scheme 25). The best results (>99% conversion, 78% *ee*) were achieved by using iridium complex **57** in combination with the [EMIM]BARF salt. Complex **57** could be generated *in situ* from $Ir(COD)_2Cl_2$ and the ligand $\mathbf{L^{21}}$ in $[BMIM]PF_6$, a commercially available ionic liquid. In the authors' opinion, [EMIM]BARF activates complex **57** by replacing the $PF_6$ anion with more '$CO_2$-philic' BARF anion. Product **55a** was extracted using sc-$CO_2$, and the remaining Ir catalyst could be reused in the reaction.

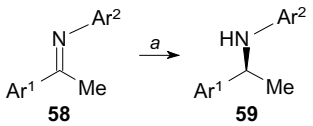
**Scheme 25**




(*a*) $H_2$ (30 bar), [EMIM]BARF, sc-$CO_2$

Good results were achieved in similar reactions by the use of an iridium catalyst formed *in situ* from $[Ir(COD)_2]$BARF (0.5 mol.%) and the monodentate phosphoramidite $\mathbf{L^8}$ (1 mol.%).[449] In the optimal conditions (40 bar $H_2$, sc-$CO_2$, total pressure of 250 bar, 45 °C, 2 h), imines **58** containing aryl and hetaryl substituents were transformed into respective chiral amines **59** with quantitative conversion and enantioselectivity of up to 95% (Scheme 26).

**Scheme 26**




(*a*) $H_2$ (40 bar), $[Ir(COD)_2]$BARF (0.5 mol.%), $\mathbf{L^8}$ (1 mol.%), sc-$CO_2$, 250 bar, 45 °C, 2 h; $Ar^1$, $Ar^2$ = Ph, 2-Naph, cymantrenyl

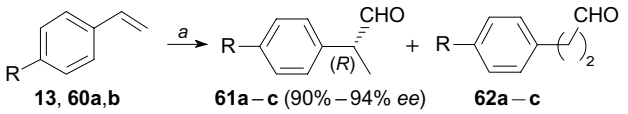
### 2.4.2. Enantioselective reactions accompanied by the formation of a carbon – carbon bond

Liquid and supercritical $CO_2$ can also be used for carrying out asymmetric catalytic reactions accompanied by enantioselective formation of carbon – carbon bonds, including hydroformylation, allylation, hydrovinylation, aldol condensation, Michael reaction, cyclopropanation, and some other. These well-known reactions are widely used to obtain complex organic compounds occurring in nature and exhibiting various types of biological activity.

#### 2.4.2.1. Hydroformylation reactions

Catalytic hydroformylation of alkenes with syngas is one of the most efficient methods of preparing enantiomerically enriched aldehydes used in perfume, food and pharmaceutical industries.[450] The possibility to carry out this reaction in sc-$CO_2$ was first demonstrated [451] by hydroformylation of styrene (**13**). Initially, a rhodium complex with a bifunctional phosphine phosphite ligand (*R*,*S*)-BINAPHOS (**L**$^4$, X = H) was used as the catalyst (see Scheme 12). The reaction was regioselective (the **61a** : **62a** product ratio was > 93 : 7). However, the enantiomeric purity of branched aldehyde **61a** obtained by this method was low (5% – 35% *ee*), evidently, because of poor solubility of **L**$^4$(X = H) in sc-$CO_2$. The level of stereoinduction was raised by applying the (*R*,*S*)-3-$H_2F_6$-BINAPHOS ligand [**L**$^4$, X = $(CH_2)_2C_6F_{13}$-n] with lipophilic perfluoroalkyl groups. In the presence of the complex obtained *in situ* from $(CO)_2$Rh(AcAc) and **L**$^4$ [X = $(CH_2)_2C_6F_{13}$-n], alkenes **13** and **60a**,**b** were regioselectively transformed into branched aldehydes **61a** – **c** with almost quantitative conversion (> 98%) and 90% – 94% *ee* (Scheme 27).[452]

**Scheme 27**

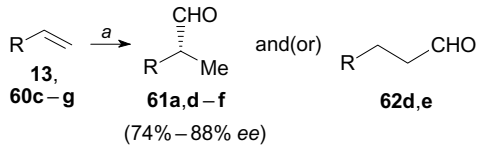



**13**, **60a**,**b** **61a** – **c** (90% – 94% *ee*) **62a** – **c**

(*a*) $H_2$/CO, [$(CO)_2$Rh(AcAc)], **L**$^4$ (X = $(CH_2)_2C_6F_{13}$-n), liq-$CO_2$ or sc-$CO_2$, 115 – 240 bar, 30 – 60 °C; R = H (**13**, **61a**, **62a**), Cl (**60a**, **61b**, **62b**), Bu$^i$ (**60b**, **61c**, **62c**)

In some cases, good results in alkene hydroformylation reaction are achieved by application of immobilized bifunctional phosphine phosphite ligands. For example, asymmetric hydroformylation of a number of terminal alkenes **13** and **60c** – **g** was successfully conducted in sc-$CO_2$ flow in the presence of Rh$^I$ complex **63** covalently attached to the cross-linked polystyrene and containing the (*R*,*S*)-BINAPHOS phosphine phosphite ligand (**L**$^4$, X = H).[453] Depending on the type of substituent R, most of the products were either branched [**61a**,**d** – **f**, regioisomeric ratio (*rr*) ranging from 7 : 3 to 9 : 1] or linear (**62d**,**e**, *rr* = 8 : 2) aldehydes. The *ee* values were somewhat lower than those in homogeneous conditions (Scheme 28). The authors believe that this method can be used in combinatorial synthesis of enantiomerically enriched aldehyde libraries for pharmacological screening.

**Scheme 28**




**13**, **60c** – **g** **61a**,**d** – **f** (74% – 88% *ee*) **62d**,**e**

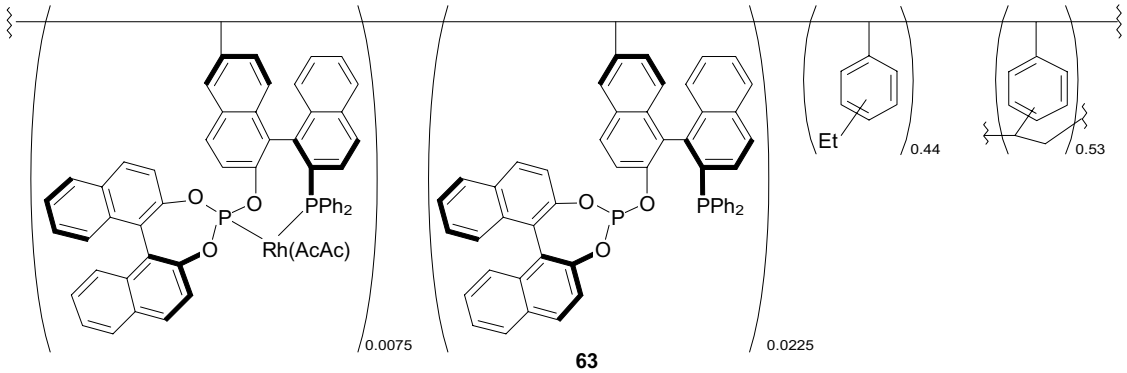
(*a*) $H_2$ + CO (1 : 1), **63**, sc-$CO_2$, 120 bar, flow (40%–54% conversion); R = Ph (**13**, **61a**), $C_6F_5$ (**60c**, **61d**), OAc (**60d**, **61e**), n-$C_6F_{13}$ (**60e**, **61f**), Bu$^n$ (**60f**, **62d**), n-$C_6H_{13}$ (**60g**, **62e**)

#### 2.4.2.2. Alkylation and allylation reactions

Supercritical fluids are successfully used in the asymmetric alkylation of aromatic aldehydes producing enantiomerically enriched benzyl alcohols, which are valuable for pharmacology. For example, benzaldehyde (**2**) reacts with diethylzinc in the presence of (2*S*)-(−)- or (2*R*)-(+)-3-*exo*-(dimethylamino)isoborneolate (Hdaib) in sc-$CHF_3$, sc-$C_2H_6$, or sc-$CO_2$ forming chiral adducts transformed into α-ethylbenzyl alcohol (**64**) *via* hydrolysis (Scheme 29).[454] Good stereochemical outcome was obtained when this reaction was carried out in sc-$CHF_3$ or sc-$C_2H_6$, whereas the reaction in sc-$CO_2$ was less selective.

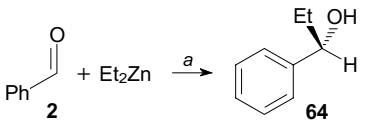
The asymmetric allylation reactions of carbon acids (the Tsuji – Trost reaction), which is quite common in enantioselective synthesis of complex polyfunctional compounds,[455 – 457] can also be carried out in sc-$CO_2$. In this medium, dimethyl malonate reacts with (*E*)-1,3-diphenylallyl acetate (**65**) in the presence of cationic and neutral palladium complexes **I** – **IV** with phosphorodiamidite ligands **L**$^{22}$ and **L**$^{23}$, obtained from (*S*)-proline, within a wide range of pressures (170 – 240 bar) and temperatures (40 – 75 °C). The product of the reaction is (*S*)-**66**, an enantiomerically enriched unsaturated diester (Scheme 30).[458] Caesium carbonate served as a soft base. The complete substrate conversion was achieved by appli-

**Structure 63**



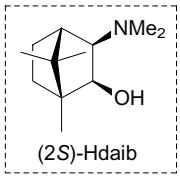

**63**

**Scheme 29**

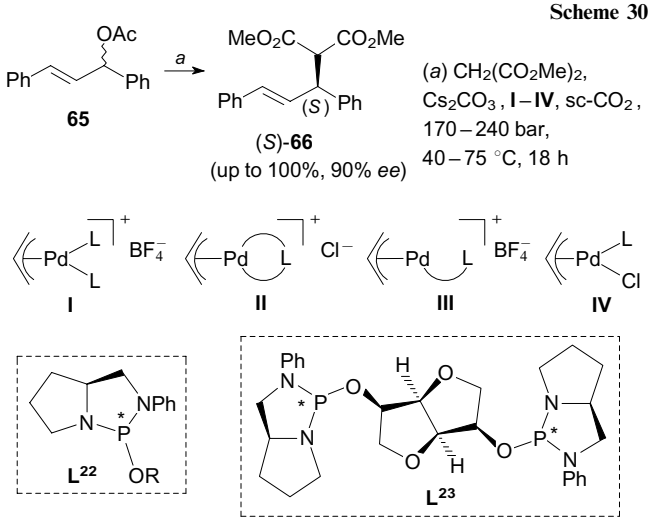



(*a*) 1) (2*S*)-Hdaib, SCF; 2) $H_2O$

| SCF | *P*/bar | *T*/°C | *ee* (%) |
|---|---|---|---|
| sc-$C_2H_6$ | 240 | 36 | 98 |
| sc-$CHF_3$ | 60 | 31 | 89 |
| sc-$CO_2$ | 150 | 36 | 25 |




**Scheme 30**



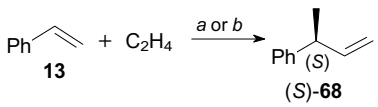

cation of cationic complex **II** with the bidentate ligand $\mathbf{L^{23}}$ and a chloride anion, although the reaction enantioselectivity in sc-$CO_2$ was somewhat lower than in the organic solvents.

### 2.4.2.3. Hydrovinylation and cycloaddition reactions

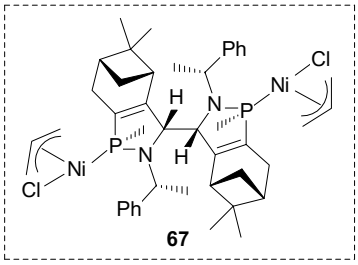
The reaction of alkenes with ethylene catalyzed by transition metals and producing 3-substituted but-1-enes (hydrovinylation) has a great potential in terms of practical application. An important result in this field was implementation of continuous hydrovinylation of styrene (**13**) in an IL/liq-$CO_2$ two-phase system.[459] The best outcome, that is, complete substrate conversion and 89% *ee*, were achieved for product **68** in the presence of Ni complex **67** dissolved in the IL with a voluminous BARF anion at 25 °C, 80 bar, and $CO_2$ flow rate of 30 mL $min^{-1}$ (Scheme 31, conditions *a*). The $CO_2$ flow considerably reduced the viscosity of the stationary phase (**67**/IL), improved the mass transfer, and stabilized the active catalyst particles by removing the hydrovinylation product from the catalyst surface. In the optimal conditions, complex **67** retained its activity and stereoinduction level for 60 h.

Later it was shown that hydrovinylation in sc-$CO_2$ can be catalyzed by palladium carbosilane dendrimers **69** (Ref. 460) and **70**,[461] containing P-centred stereogenic centres combined with the NaBARF tetraarylborate (see Scheme 31, conditions *b*).

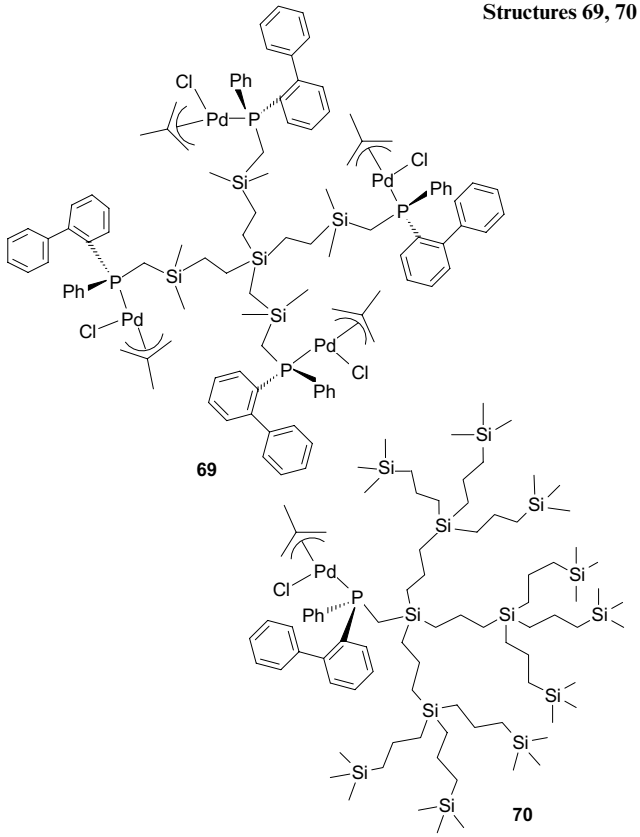
**Scheme 31**




(*a*) **67**, [EMIM]BARF, $CO_2$ (30 mL $min^{-1}$), 80 bar, 25 °C (100% conversion, 89% *ee*); (*b*) **69** or **70**, NaBARF, $CO_2$ (285 bar), 35–45 °C (60% conversion, 76% *ee*)



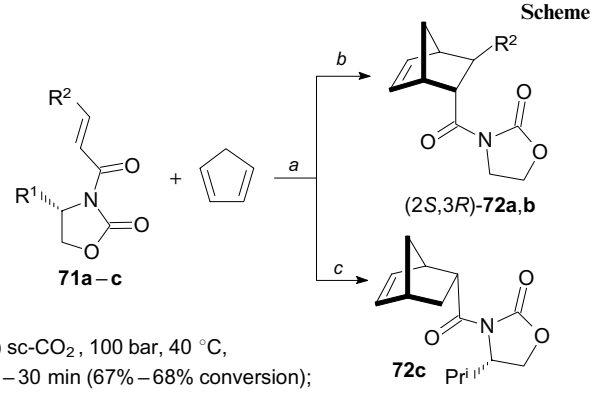

**Structures 69, 70**



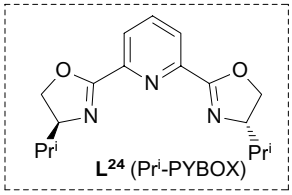

However, the conversion and enantioselectivity were lower in this batch-reaction than in the continuous flow process with Ni complex **67**, despite better solubility of the palladium dendrons with $CO_2$-philic alkylsilyl groups. Nevertheless, the results achieved in both case were better than those obtained in the organic solvent ($CH_2Cl_2$).

Supercritical $CO_2$ can be used as the medium for extremely important cycloaddition reactions, which are normally accelerated by a pressure increase.[462] For example, 3-acryloyl- and 3-crotonoyl-1,3-oxazolidin-2-ones (**71a**,**b**) add to cyclopentadiene much faster in the presence of the scandium(III) triflate chiral complex with $Pr^i$-PYBOX ($\mathbf{L^{24}}$) in sc-$CO_2$ (15–30 min) than in $CH_2Cl_2$ (up to 18 h), although the enantiopurity of products **72a**,**b** becomes lower (63%–65% *vs.* 78%–82%) (Scheme 32).[463] The addition of alkene **71c** with the stereocentre in the heterocycle to cyclopentadiene proceeds enantioselectively when catalyzed by $La(OTf)_3$, an achiral Lewis acid. Cycloadduct **72c** is formed with a higher diastereomeric excess (*de*) in sc-$CO_2$ than in $CH_2Cl_2$ (69% and 42% respectively).

**Scheme 32**



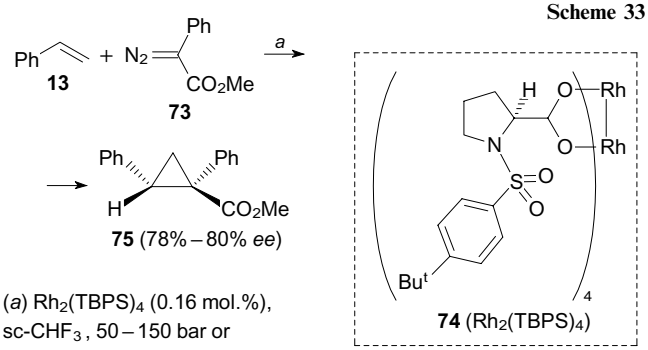

(*a*) sc-$CO_2$, 100 bar, 40 °C,
15 – 30 min (67% – 68% conversion);
(*b*) for $R^1$ = H:
$Sc(OTf)_3$ – **L**$^{24}$ (10 mol.%)
(*endo* : *exo* ≈ 9 : 1);
(*c*) for $R^1$ = $Pr^i$, $R^2$ = H:
$La(OTf)_3$ (10 mol.%)
(*endo* : *exo* ≈ 8 : 2);
$R^2$ = H (**a**), Me (**b**)




### 2.4.2.4. Cyclopropanation reactions

Asymmetric cyclopropanation of alkenes by diazo compounds can also be efficiently implemented in SCF.[464] For example, cyclopropane derivative **75** was successfully obtained by the reaction of styrene (**13**) with methyl-1-phenyl diazoacetate (**73**) in the presence of the $[Rh_2(TBPS)_4]$ complex (**74**) (TBPS stands for 4-*tert*-butylbenzenesulfonyl) in sc-$CHF_3$ or sc-$CO_2$ (Scheme 33). In contrast to the reaction in sc-$CHF_3$, in which the stereochemical outcome depends on pressure (78% *ee* at 50 bar, 40% *ee* at 100 bar), pressure has almost no effect on the enantioselectivity in sc-$CO_2$ (~80% *ee*), obviously, because pressure does not significantly affect the dielectric permittivity of $CO_2$.

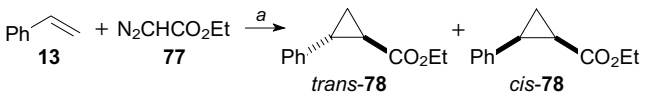
**Scheme 33**




(*a*) $Rh_2(TBPS)_4$ (0.16 mol.%),
sc-$CHF_3$, 50 – 150 bar or
sc-$CO_2$, 80 bar, 30 – 35 °C

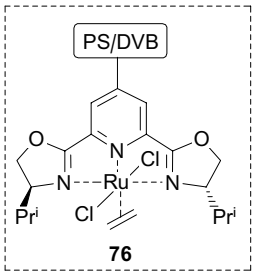
The use of heterogeneous Ru complex **76** with a PYBOX ligand immobilized on a polystyrene – polydivinylbenzene support (PS/DVB) enabled cyclopropanation of styrene (**13**) by ethyl diazoacetate (EDA, **77**) in sc-$CO_2$ flow (Scheme 34).[465] As a result, the productivity increased 8-fold and product **78** had higher enantiomeric purity (83% – 89% *ee* for the major *trans*-isomer) than that in this reaction carried out in $CH_2Cl_2$. Less toxic copper complexes **79** (Ref. 466) and **80** (Ref. 467) immobilized on cross-linked polystyrene are thought to be even more promising catalysts for the cyclopropanation reaction, according to the green chemistry concept. These catalysts were used to synthesize functionally substituted cyclopropane **78** in a sc-$CO_2$ flow (80 bar, 40 °C, 1 mL $min^{-1}$) with a much higher productivity than in $CH_2Cl_2$ (1402 g $L^{-1}$ in 2.7 h *vs.* 836 g $L^{-1}$ in 9 h), which indicates utility of the method. However, copper complexes **79** and **80** have a lower stereoinduction level than Ru complex **76**.

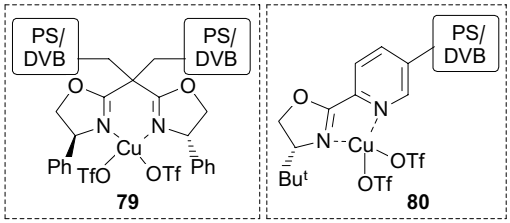
**Scheme 34**




(*a*) **76**, or **79**, or **80** (5 mol.%), sc-$CO_2$ (0.5 – 1.0 mL $min^{-1}$), 80 bar, 40 °C (~100% conversion)

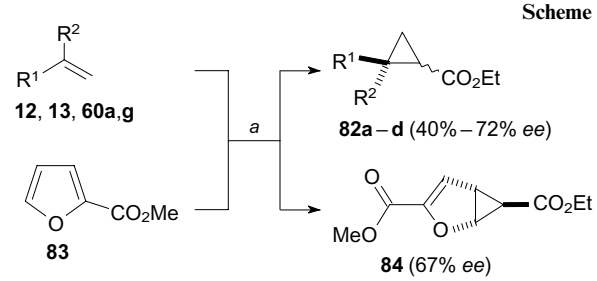
| Cat | **76** | **79** or **80** |
|---|---|---|
| *trans* : *cis* | ~ 9 : 1 | ~ 1 : 1 |
| *ee* (*trans*) (%) | 83 – 89 | 55 – 59 |
| *ee* (*cis*) (%) | 56 – 59 | 44 – 57 |



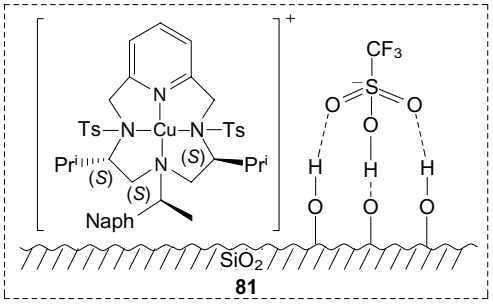




Ionic copper complex **81** obtained later,[468] which has a pyridine-containing tetraazamacrocyclic ligand attached to the silicate support by hydrogen bonds formed by the triflate counter-ion, expanded the range of substrates suitable for this reaction. In the presence of complex **81**, styrene derivatives **12**, **13**, and **60a**, and oct-1-ene (**60g**) yielded

**Scheme 35**




(*a*) EDA (**77**), **81**, sc-$CO_2$ (0.5 mL $min^{-1}$), 130 bar, 40 °C, up to 25 h (> 99% conversion); $R^1$ = H: $R^2$ = Ph (**13**, **82a**), 4-$ClC_6H_4$ (**60a**, **82b**), n-$C_6H_{13}$ (**60g**, **82c**);
$R^1$ = $R^2$ = Ph (**12**, **82d**); Ts is *p*-toluenesulfonyl

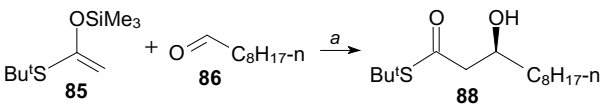


cycloadducts **82a – d** with good conversion (> 99%) and enantioselectivity (up to 72%), which remained high during 24 h of continuous operation of the reactor (TON of up to 440) (Scheme 35). The diastereoselectivity of the cyclopropanation of the specified alkenes was rather low (the *trans* : *cis* ratio ranged from 1 : 1 to 2 : 1). However, methyl 2-furoate (**83**) was exclusively converted under the same conditions to *trans*-cyclopropane **84** (*trans* : *cis* = > 99 : 1), a precursor to rocellaric acid.[469]

#### 2.4.2.5. Aldol reactions

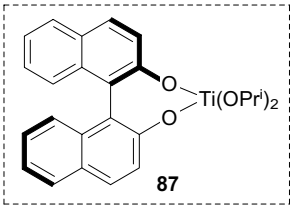
Ikariya and co-workers[470] applied supercritical fluids ($CO_2$ and $CHF_3$) as the media for a catalytic asymmetric aldol reaction of silyl enolates with aldehydes (the Mukaiyama method) used to form C – C bonds in carboxylic acid derivatives. Thioacetal **85** enantioselectively reacted with aldehyde **86** in the presence of titatum(IV) binaphthol complex **87** yielding aldol **88** (Scheme 36). The enantiomeric excess of the product in the sc-$CO_2$ medium was not lower than that in toluene, and in sc-$CHF_3$ it was even higher. However, the yield of compound **88** in sc-$CO_2$ was only 8%, evidently, because of the low catalyst solubility.

**Scheme 36**




(*a*) **87** (5 mol.%), sc-$CHF_3$ (100 bar) or sc-$CO_2$ (200 bar), 34 °C

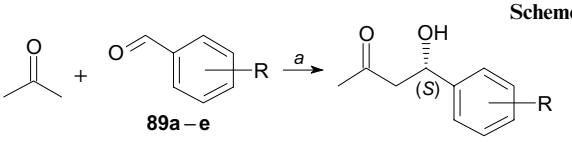
| Medium | Yield of **88** (%) | *ee* (%) |
|---|---|---|
| sc-$CHF_3$ | 46 | 88 |
| sc-$CO_2$ | 8 | 72 |
| MePh | 49 | 72 |




Metal-free asymmetric aldol reactions catalyzed by chiral amines (organocatalysts) have become quite popular recently and can also be carried out in SCFs such as $CO_2$ or 1,1,1,2-tetrafluoroethane (Freon R134a). When catalyzed by natural (*S*)-proline, acetone reacts with benzaldehyde derivatives **89a – e** to give *S*-enantiomers of aldols **90a – e** in up to 62% yields and up to 80% *ee* (Scheme 37).[471] The yield of aldol **90a** in the optimal conditions (200 bar, 40 °C) was somewhat higher in R134a (62%) than in sc-$CO_2$ (47%), but in the latter case, the reaction was more selective (60% and 74% *ee*, respectively).

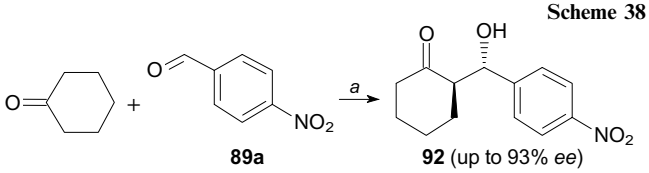
The $CO_2$/water system is an efficient medium for asymmetric aldol reactions in some cases.[472] For example, proline-containing dipeptide **91**, which can hardly catalyze the reaction of cyclohexanone with 4-nitrobenzaldehyde (**89a**) in water, appeared an efficient catalyst for the reaction of $CO_2$-saturated (50 bar) aqueous brine, producing *anti*-aldol **92** in a quantitative yield (99%) with high diastereo- (*anti* : *syn* = 84 : 16) and enantioselectivity (up to 93% *ee*) (Scheme 38). Evidently, $CO_2$ converts dipeptide **91** into water-soluble bicarbonate, which can form enamine intermediates, required for this reaction, in an aqueous medium. In this case, product **92** precipitates and the catalyst that remains in the solution can be reused four more times, with catalyst activity and reaction enantioselectivity being preserved. Interestingly, (*S*)-proline cannot catalyze this reaction in the proposed conditions.

**Scheme 37**

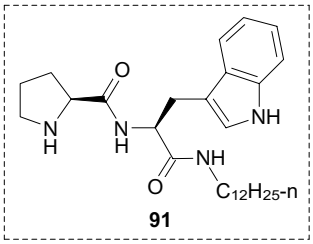



(*a*) (*S*)-proline (30 mol.%), sc-$CO_2$ or R 134a, 200 bar, 40 °C, 24 h (acetones : aldehyde = 20 : 1);
R = 4-$NO_2$ (**a**), 3-$NO_2$ (**b**), 2-$NO_2$ (**c**), 4-Cl (**d**), 4-OMe (**e**)

**Scheme 38**



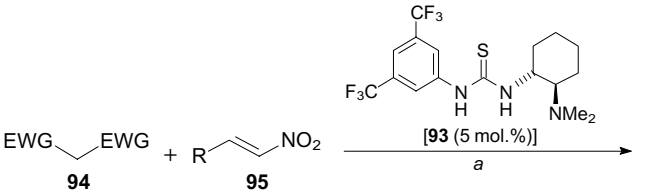

(*a*) **91** (5 mol.%), NaCl (aq.), $CO_2$ (50 bar), 25 °C, 15 h




#### 2.4.2.6. Conjugate addition to multiple bonds

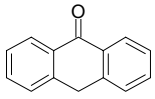
Liquid $CO_2$ is a promising medium for organocatalytic asymmetric Michael reactions.[473] In the presence of bifunctional chiral tertiary amine **93** containing a thiourea group, various carbon acids **94** (malonates, malononitrile, and anthranone) enantioselectively react with nitroalkenes **95** in liquid $CO_2$ to form Michael adducts **96** (Scheme 39). As a rule, the yields and enantiomeric purity of products **96** obtained in a $CO_2$ medium are comparable to the yields in toluene or are even higher (up to 95%). Besides, the reaction proceeds faster in liquid $CO_2$ than in organic solvents with a smaller amount of the catalyst (5 mol.% instead of 10 mol.%). γ-Nitro esters **96** (EWG = $CO_2$Me, R = 4-$ClC_6H_4$, Bu$^i$) are precursors to the most active

**Scheme 39**




(*a*) liq-$CO_2$, 100 bar, 20 °C;
EWG is electron-withdrawing group = $CO_2$Me, CN;

EWG – $CH_2$ – EWG =



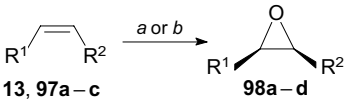
enantiomers of Baclofen,[474] a $GABA_B$ receptor agonist, and Pregabalin,[475] an anticonvulsant medication. The reaction is scalable and the products can be isolated by mere decompression.

### 2.4.3. Enantioselective reactions accompanied by the formation of a carbon – heteroatom bond

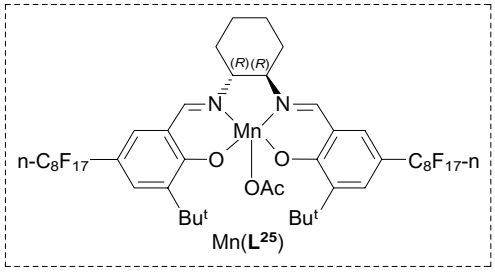
There are examples of asymmetric catalytic epoxidation and phosphorylation of alkenes in a compressed $CO_2$ medium. The $Mn^{III}(\mathbf{L^{25}})$ complex containing a chiral salen ligand with linear perfluoroalkyl groups catalyzes oxidation of *cis*-alkenes **13**, **97a – c** on treatment with iodosobenzene in sc-$CO_2$. The resulting *cis*-epoxides (**98a – d**) are formed in the optimal conditions (250 bar, 35 °C) in a high yield with 100% conversion of the reactant, but with modest enantioselectivity (21% – 47% *ee*) (Scheme 40, conditions *a*).[476] The optical purity of epoxide **98a** was raised to 76% *ee* (although the conversion decreased to 51%) by using di(*tert*-butyl) peroxide as the oxidant and $Mn^{III}(\mathbf{L^{26}})$ complex, readily soluble in sc-$CO_2$, with the salen ligand containing a fluoroalkylated binaphthyl moiety as the catalyst (conditions *b*).[477] Both methods are environmentally friendly, and the resulting epoxides (**98**) are stable in sc-conditions.

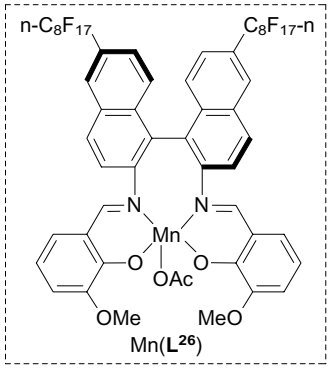
It has been recently reported that the reaction of triphenyl phosphite with nitroalkenes **95** in sc-$CO_2$ (110 bar, 35 °C) catalyzed by pseudo-enantiomeric bifunctional tertiary amines **99a** and **100** containing a squaramid moiety affords β-nitro phosphonates **101** in high yields (57% – 97%) with good enantioselectivity (68% – 94% *ee*) (scheme 41).[478] By changing the catalyst, it is possible to synthesize both enantiomers of the products (**101** and *ent*-**101**), which are direct precursors of biologically active[479] β-(aminoalkyl)phosphonic acids, including those of natural origin.[480] Fractional extraction of products with sc-$CO_2$ completely excluded organic solvents from the process, which is of great importance according to the green chemistry principles.

**Scheme 40**

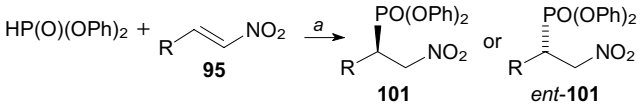



(*a*) PhIO, $Mn^{III}(\mathbf{L^{25}})$ (5 mol.%), sc-$CO_2$, 250 bar, 35 °C;
(*b*) $(Bu^tO)_2$, $Mn^{III}(\mathbf{L^{26}})$ (2 mol.%), sc-$CO_2$, 150 bar, 40 °C;
$R^1$ = Ph: $R^2$ = H (**13**, **98a**), Me (**97a**, **98b**);
$R^1CH{=}CHR^2$ is 1,2-dihydronaphthalene (**97b**, **98c**), indene (**97c**, **98d**)

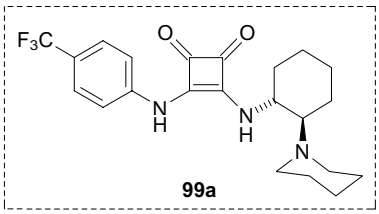


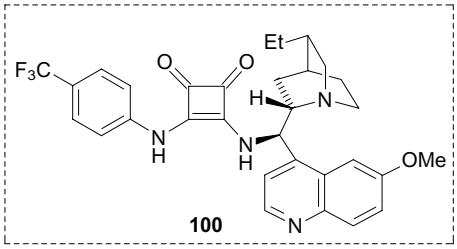




**Scheme 41**




(*a*) **99a** or **100** (5 mol.%), sc-$CO_2$, 100 bar, 35 °C;
R = $Bu^i$, aryl, 2-furyl, 2-thienyl



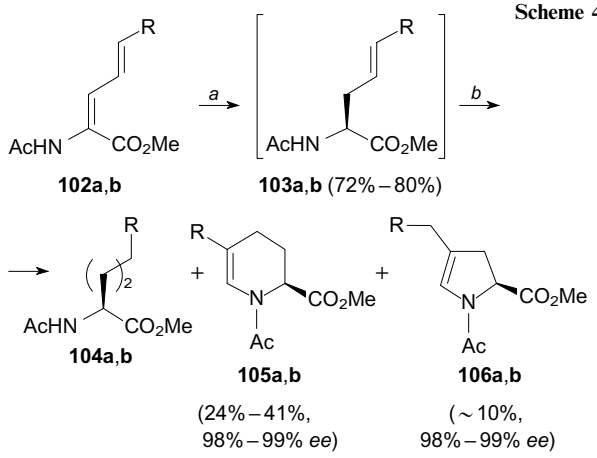




### 2.4.4. Asymmetric tandem and domino reactions

Tandem one-pot reactions, in which several transformations are performed in one reactor without isolation or purification of intermediate compounds, are far less labour- and resource-consuming than sequences of these reactions carried out separately.[481] Tandem reactions in environmentally safe solvents, such as liquid or supercritical $CO_2$, are especially attractive, since they reduce the amount of waste hazardous formed.

The first example of an asymmetric catalytic tandem reaction in sc-$CO_2$ is, evidently, the transformation of available prochiral dienamides **102a**,**b** into tetrahydropyridine and dihydropyrrole derivatives by one-pot sequence including asymmetric hydrogenation, hydroformylation, and intramolecular amination (Scheme 42).[482] The first two of them are catalyzed by a Rh complex with the phosphine ligand *ent*-$\mathbf{L^1}$ [(*S*,*S*)-Et-DuPHOS] (see Scheme 9). With this catalyst, hydrogenation of compounds **102a**,**b** in sc-$CO_2$ chemoselectively affords allylglycine derivatives **103a**,**b** as the major products. An important role in this process is played by hydrogen pressure: when it is not high enough, the conversion is incomplete, while excess $H_2$ leads to the formation of undesirable exhaustive hydrogenation products **104a**,**b**. Then, $H_2$ and $CO_2$ are removed by decompression, and the reactor containing intermediate compound **103a**,**b** and the catalyst is filled with syngas ($CO : H_2 = 1 : 1$) and sc-$CO_2$. The hydroformylation of intermediates **103a**,**b** is accompanied by sponta-

**Scheme 42**

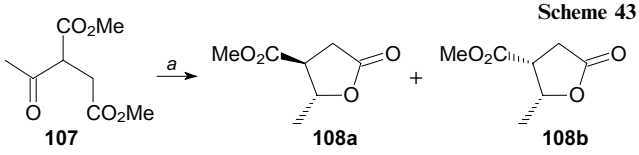



(*a*) $H_2$ (14–21 bar), [Rh(COD)(*ent*-**L**[1])]OTf (2 mol.%), sc-$CO_2$ (83 bar), 40 °C, 18 h; (*b*) $H_2$ + CO (1 : 1) (28 bar), sc-$CO_2$ (83 bar), 60 °C, 48 h; R = H (**a**), Me (**b**)

neous intramolecular amination of isomeric aldehydes and affords cyclic products **105a**,**b** and **106a**,**b** in moderate yields with 98%–99% *ee*. Unfortunately, the dihydropyrrole derivatives **106** contain impurities of compound **104**, which were hard to separate.

Other, even more promising green chemistry tools are the domino reactions, in which, like in the tandem processes, several bonds are formed, but each subsequent step is spontaneously triggered by the previous one without adding new reagents and(or) catalysts.[483, 484] An example of such reaction is the transformation of dimethyl acetylsuccinate **107** into diastereomeric paraconic acid derivatives **108a**,**b**, which includes enantioselective reduction of the carbonyl group and diastereoselective lactonization. This reaction was carried out in sc-$CO_2$ in the presence of the ruthenium complex $[RuCl_2(PhH)]_2$–(*R*)-BINAP in combination with acidic additive (HCl) (Scheme 43).[438] As a result, the required diastereomers **108a**,**b** (3 : 1 ratio) were obtained with 85% and 28% *ee*, respectively. The enantioselectivity was raised to 90% and 83% *ee* by conducting this reaction in a two-phase sc-$CO_2$/IL system (20 : 1). This means, evidently, that the hydrogenation proceeds in the sc-$CO_2$-saturated IL phase (CXL-phase) containing the catalyst. The better selectivity in this case can be attributed to lower viscosity of the CXL phase and higher solubility of $H_2$ induced by the SCF.

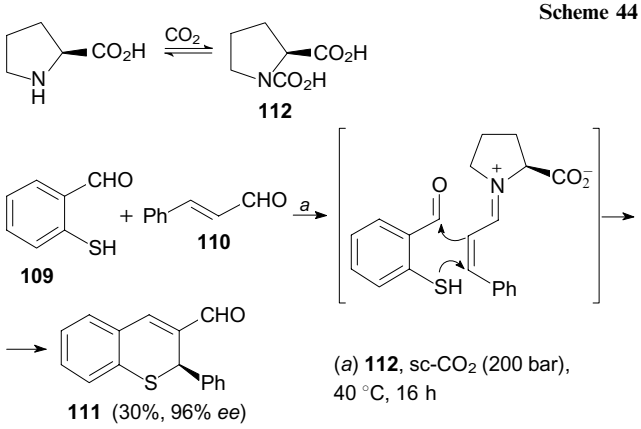
**Scheme 43**




(*a*) $H_2$ (27 bar), $[RuCl_2(PhH)]_2$–(*R*)-BINAP, HCl, sc-$CO_2$ or sc-$CO_2$/[BMIM]$BF_4$, 110 bar, 75 °C (95% conversion)

Supercritical $CO_2$ can also be used as a medium for organocatalytic domino reactions. For example, 2-sulfonylbenzaldehyde (**109**) reacts with cinnamic aldehyde (**110**) in the presence of (*S*)-proline (10 mol%) to give thiochromone-3-carbaldehyde **111**.[485] The reaction includes enantioselective addition of the SH group of aldehyde **109** to the double bond of α,β-enal **110** and intramolecular aldolization of the adduct releasing the catalyst (Scheme 44). The reaction outcome depends on the time, pressure, and temperature; this may be related to reversible formation of proline carbamate (**112**) affecting the phase composition of the system and process performance. In the optimal conditions (200 bar, 40 °C), product **111** is formed in 30% yield and with 96% *ee*. However, there are no data about the reaction scope.

**Scheme 44**

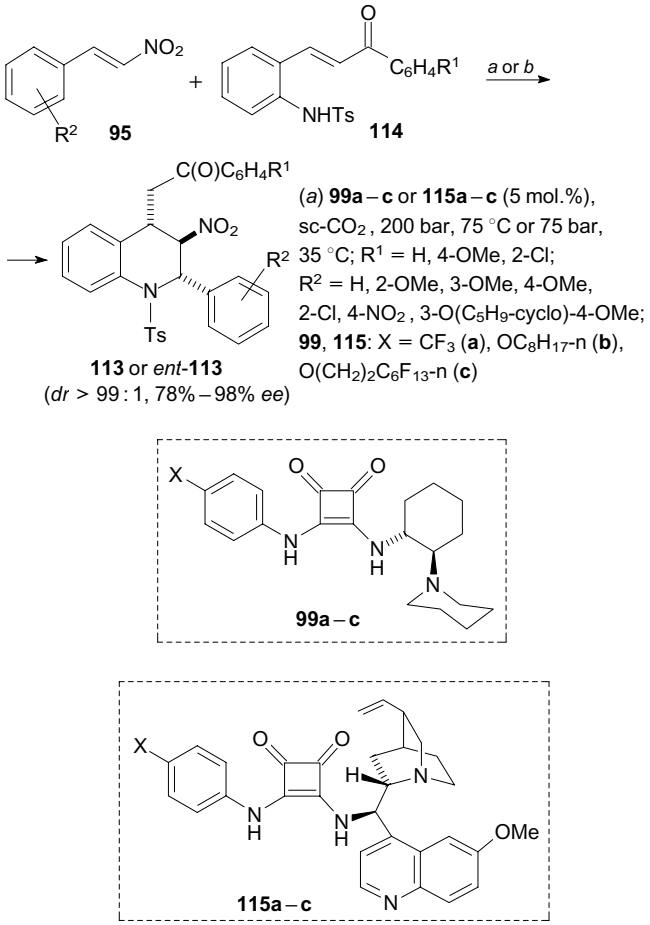



Another example is domino synthesis of tetrahydroquinolines **113** bearing a structural moiety of angustureine[486] and martinelline[487] alkaloids in sc-$CO_2$. The process includes asymmetric Michael addition of nitroolefins **95** to *o*-tosylaminochalcone **114** catalyzed by pseudo-enantiomeric bifunctional chiral tertiary amines **99a**–**c** and **115a**–**c** and spontaneous diastereoselective cyclization of the resulting adducts (Scheme 45). By replacing the catalyst, it is possible to enantioselectively (78%–98% *ee*) obtain the enaniomers of heterocycles **113** as a single diastereomer in 99% yield. The conditions of the domino reaction depend on the catalyst solubility in sc-$CO_2$. Amines **99a** and **115a** containing a $CF_3$ group in their aromatic ring produce high yields of products at a pressure of 200 bar and temperature of 75 °C.[488] However, more $CO_2$-philic catalysts **99b**,**c** and **115b**,**c** with long-chain alkoxyl or fluoroalkoxyl groups are effective in milder conditions (75 bar and 35 °C)[489] that are easy to achieve in industry.

Thus, the data given in this Section show that the use of compressed gases, especially carbon dioxide in liquid and supercritical states, as a medium for catalytic asymmetric reactions offers great opportunities. For example, $CO_2$ was used as the medium for enantioselective hydrogenation of the C=C, C=O, and C=N multiple bonds in the presence of transition metal complexes. Various hydroformylation, alkylation, cycloaddition, allylation, hydrovinylation, cyclopropanation, epoxidation, aldol, Diels–Alder and Michael reactions accompanied by the formation of carbon–carbon and carbon–heteroatom bonds can be enantioselectively performed in this medium. Supercritical $CO_2$ can be employed in asymmetric tandem and domino reactions, which are believed to be promising green chemistry methods due to their efficiency and environmental safety.

Carbon dioxide allows minimizing or even avoiding the use of toxic and flammable organic solvents in reactions and makes catalyst regeneration easier. Some continuous flow processes in $CO_2$ are promising for industrial application.

**Scheme 45**




Only a few organocatalytic reactions have been implemented so far in sub- and supercritical fluids. They do not require the activation of reactants with metals; this is important for the synthesis of medications that must not contain even residual amounts of toxic heavy metals. Besides, many organocatalytic reactions are characterized by high stereo- and enantioselectivity and a minimum amount of waste (the atom economy principle). Further studies of organocatalytic processes in sub- and supercritical fluids can pave the way to creating efficient green processes for enantioselective production of most active and safe drug enantiomers.

## 3. Supercritical fluids in the chemistry of polymers

Supecritical $CO_2$ as an environmentally friendly and nonflammable substance has excellent prospects for application in the chemistry and engineering of macromolecular compounds. Carbon dioxide can be used as a medium for obtaining polymers and new composite or functional materials. Unlike conventional organic solvents, SCFs can be easily removed from the polymer by decompression. Besides, sc-$CO_2$ can be applied to purify polymers from low-molecular-weight compounds through supercritical extraction.

The use of sc-$CO_2$ has so far been described in relation to the preparation of a wide range of new polymers, aerogels, foams, composites, and porous and nanoporous coatings (see ¶).[368, 372, 490] This Section of the review considers the progress of synthesis and chemical modification of polymers in sc-$CO_2$, preparation of aerogels and polymer foams by supercritical processes, pore formation during $CO_2$ desorption from glassy polymers, physical modification of polymeric gas-separation membranes on treatment with sc-$CO_2$, and impregnation of polymers with photoactive compounds.

### 3.1. Preparation of advanced polymer materials in supercritical fluids

A lot of attention is now being paid to the development of more environmentally friendly and economically viable processes for the polymer industry. Many traditional methods of polymer production require large amounts of organic solvents for the polymerization stage or as processing media for moulding, extraction, impregnation or for decreasing the viscosity of polymer materials. However, for environmental protection and for safety and economic issues, it is extremely desirable to develop alternative approaches to obtaining polymers that would reduce the application of organic solvents. One of the ways to solve this problem is the replacement of conventional organic solvents by 'volatile' sc-$CO_2$, which considerably simplifies the solvent removal stage and excludes the energy-intensive polymer drying stage (Fig. 6).[490] Polymerization reactions in sc-$CO_2$ also ensure fast monomer conversion and give high-molecular-weight polymers.

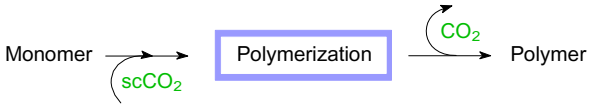



**Figure 6.** Diagram of polymer synthesis in sc-$CO_2$.[490]

#### 3.1.1. Synthesis of polymers in supercritical carbon dioxide

A lot of polymers, including commercially available ones have been synthesized in sc-$CO_2$. In terms of mechanism, polymerization reactions are divided into step-growth and chain-growth polymerization. Chain polymerization is typical of radical and ionic polymerization reactions. Supercritical $CO_2$ is most frequently used for chain radical polymerization reactions. In the case of the ionic mechanism, the dominant reaction type is cationic polymerization since $CO_2$ is inert towards cations. In the case of anionic polymerization, chain termination can take place, because of the anion reaction with the electrophilic carbon dioxide molecule.

In terms of the process, polymerization reactions in sc-$CO_2$ are divided into homogeneous and heterogeneous types, including suspension, emulsion, precipitation, and dispersion polymerization. In this Section, we address the reactions of polymer preparation depending on the mechanism and nature of the active site and polymerization

¶ See monograph *Aerogels Handbook* (Eds M.A.Aegerter, N.Leventis, M.M.Koebel) (New York: Springer, 2011) and the following publications: E.Di Maio, E.Kiran. *J. Supercrit. Fluids*, **134**, 157 (2018); E.Aram, S.Mehdipour-Ataei. *Int. J. Polym. Mater. Polym. Biomater.*, **65**, 358 (2016); C.Forest, P.Chaumont, P.Cassagnau, B.Swoboda, P.Sonntag. *Prog. Polym. Sci.*, **41**, 122 (2015); I.Tsivintzelis, G.Sanxaridou, E.Pavlidou, C.Panayiotou. *J. Supercrit. Fluids*, **110**, 240 (2016).

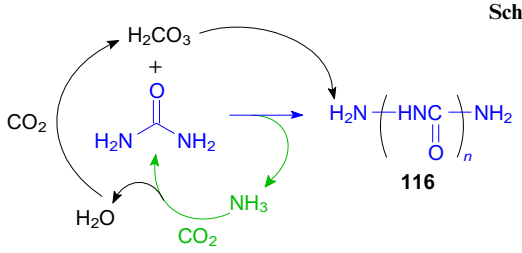
conditions. A separate part is devoted to controlled living radical polymerization in sc-$CO_2$.

#### 3.1.1.1. Step-growth polymerization (polycondensation) in sc-$CO_2$

Step-growth polymerization is a process of polymer formation through step-by-step macromolecule assembly. Monomer molecules react with each other forming *n*-mers, which then react with each other, thus increasing the polymer molecular weight. The increase in the viscosity of the medium following the increase in the molecular weight prevents the removal of side products, while high vacuum can hardly be used industrially. Side products of polycondensation in sc-$CO_2$ are extracted in rather mild conditions, which allows for the synthesis of polyesters,[491] polyamides (nylons),[492, 493] polyurethanes,[494] and polyester-carbonates.[495]

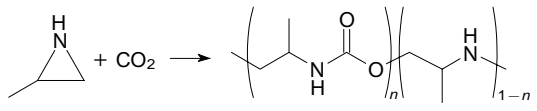
For example, high-molecular weight nylon 46 with the maximum molecular weight of 48,200 Da was successfully obtained in sc-$CO_2$. The whole polymerization process took ~5 – 6 h.[492] Yuan *et al.*[493] showed that sc-$CO_2$ takes part in urea polycondensation by binding the released ammonia and shifting the equilibrium towards the formation of polymer **116** (Scheme 46).

**Scheme 46**




The aziridine copolymerization with $CO_2$ resulted in the synthesis of polyurethanes **117** consisting of urethane and amine units (Scheme 47). The use of sc-$CO_2$ as both the reaction medium and a reactant makes it possible to control the polymer structure by changing the system pressure and temperature. The polymers obtained in this way have a high content of urethane units and are temperature-sensitive, which can be used in targeted drug delivery systems, tissue engineering, mixture separation and catalysis.[494] Supercritical $CO_2$ has great prospects in the field of preparation of polycarbonates by reaction with epoxides.[496]

**Scheme 47**




Thus, sc-$CO_2$ can act as a solvent or a reactant (or both) in stepwise polymerization. It can also facilitate the removal of low-molecular-weight compounds released in these reactions.

#### 3.1.1.2. Chain-growth polymerization in sc-$CO_2$

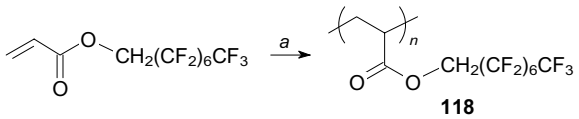
In the case of chain-growth polymerization, polymer macromolecules are formed as a result of opening of multiple bonds or rings of monomers under the action of the active sites at the ends of the growing polymer chains. The polymer molecular weight quickly increases. The choice of the polymerization method depends on the solubility of the polymerization products in sc-$CO_2$. For example, amorphous fluoropolymers are synthesized by homogeneous polymerization, but most polymerization reactions are performed in heterogeneous conditions because of the low solubility of most polymers in sc-$CO_2$.

##### 3.1.1.2.1. Homogeneous polymerization in sc-$CO_2$

Fluorine-containing polymers, insoluble in conventional organic solvents, used to be synthesized by homogeneous polymerization in chlorofluorocarbons (freons), which destroy the Earth's ozone layer. The properties of sc-$CO_2$ as a solvent are similar to those of fluorocarbons, but sc-$CO_2$ is environmentally safe. This SCF is the most suitable solvent for homogeneous synthesis of fluoropolymers by cationic or free-radical polymerization.

DeSimone *et al.*[497] were the first to show that amorphous fluoropolymers **118** could be obtained by thermally initiated homogeneous radical polymerization of fluorine-containing acrylates in sc-$CO_2$ (Scheme 48).

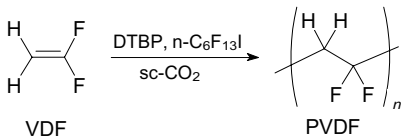
**Scheme 48**




(*a*) AIBN, sc-$CO_2$, 60 °C, 207 bar, 48 h;
AIBN is azobis(isobutyronitrile)

The best studied example of homogeneous polymerization in sc-$CO_2$ is polymerization of vinylidene fluoride (VDF).[498 – 500] Polyvinylidene fluoride (PVDF) was synthesized in the homogeneous phase in sc-$CO_2$ an at 120 °C and 1500 atm, with di-*tert*-butyl peroxide (DTBP) acting as the reaction initiator and perfluorohexyl iodide used to control the molecular weight (Scheme 49). An analysis of the molecular weight showed that the polydispersity index of the obtained PVDF samples was low and ranged from 1.2 to 1.5.[498]

**Scheme 49**




Materials similar to commercially available Teflon AF were also synthesized by copolymerization of tetrafluoroethylene and 2,2-bis(trifluoromethyl)-4,5-difluoro-1,3-dioxole in sc-$CO_2$.[501] The low reaction temperature and use of a perfluorinated initiator led to the formation of copolymers with properties comparable to those of the commercial product. However, owing to the use of sc-$CO_2$, the products can be isolated in a pure state directly from the reactor, which makes this solvent a promising green alternative to Freons.

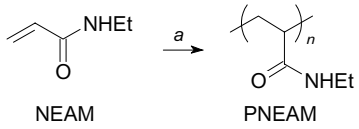
##### 3.1.1.2.2. Heterogeneous polymerization in sc-$CO_2$

The most common high-molecular-weight polymers are slightly soluble in sc-$CO_2$; often, this makes it possible to obtain high-purity products in good yields by heterogeneous polymerization methods.

#### 3.1.1.2.2.1. Emulsion and suspension polymerization

Emulsion and suspension polymerization processes, in which the monomer and the polymer have extremely low solubility in the continuous phase, are applied to synthesize polymers based on hydrophobic vinyl monomers in water. Adamsky and Beckman [502] studied the 'inverse' emulsion polymerization of acrylamide in water in sc-$CO_2$ (AIBN, 60 °C, 345 atm, 1 h), with polyhexafluoropropylene oxide with amide end groups being used as a surfactant. Recent publications [503 – 506] present a few examples of emulsion and suspension polymerization of acrylamide and acrylic acid in $CO_2$. For example, emulsion polymerization of *N*-ethylacrylamide (NEAM) in sc-$CO_2$ in the presence of the PMAGlc-b-PFOMA hydrophilic-$CO_2$-philic diblock copolymer as a surfactant led to the generation of water-soluble poly(*N*-ethylacrylamide) (PNEAM) in the form of a stable colloid in >90% yield (Scheme 50). It was shown that the particle diameter and size distribution depend on various reaction parameters, including $CO_2$ pressure.[505]

**Scheme 50**




NEAM PNEAM

(*a*) AIBN, sc-$CO_2$ (352 bar), PMAGlc-b-PFOMA, 65 °C, 20 h; PMAGlc-b-PFOMA is poly(3-*O*-methacryloyl-D-glucopyranose)-block-poly(1,1-dihydroperfluorooctyl methacrylate)

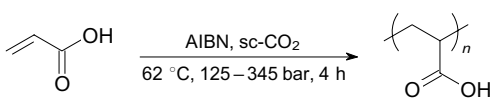
Another green process was described by Kamrupi *et al.*[507] as a method for obtaining macroporous polystyrene particles by suspension polymerization in a mixture of water and sc-$CO_2$ at a pressure of 70 – 320 atm with polyvinyl alcohol used as the stabilizer, divinylbenzene as the cross-linking agent, and AIBN as the initiator. Supercritical $CO_2$ in this case acted as a pressure-controlled foaming agent. Besides, pressure also affects the polymer molecular weight characteristics: its increase leads to particle diameter growth (up to 8 – 22 μm).

#### 3.1.1.2.2.2. Precipitation polymerization

In the general case, a monomer, a solvent, and an initiator form a homogeneous solution, but polymerization may lead to polymer precipitation. Unlike emulsion and suspension polymerization, in this case, no surfactants are needed for stabilization. The method of precipitation polymerization in sc-$CO_2$ has been used to synthesize various polymers, first of all, acrylates.[508 – 513] The products were extracted as dry powders directly from the reactor after decompression. It should be said that suspension or inverse emulsion polymerization in hydrocarbons is often faced with the problems of removal of residual surfactants and stabilizers. When the process is carried out in sc-$CO_2$, there are no such problems. Polymers based on styrene [511] and polylactide-co-glycolide (PLGA), a copolymer of lactic and glycolic acids,[514] were obtained under similar conditions.

DeSimone and co-workers [508] described precipitation polymerization of acrylic acid (AA) in sc-$CO_2$ with AIBN as the initiator. The reaction gave a linear polymer with a high molecular weight (Scheme 51). The researchers also determined the effect of pressure on the molecular weight of polyacrylic acid (PAA), molecular weight distribution, size and morphology of particles.

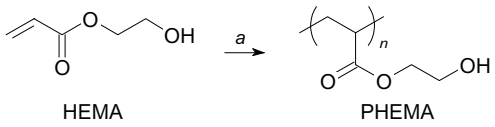
**Scheme 51**




AA PAA

Wang *et al.*[512] obtained poly(2-hydroxyethyl methacrylate) (PHEMA) based on 2-hydroxyethyl methacrylate (HEMA) in sc-$CO_2$. The authors studied the effect of pressure, initiator and monomer concentrations, temperature and time of the reaction on the polymerization (Scheme 52).

**Scheme 52**

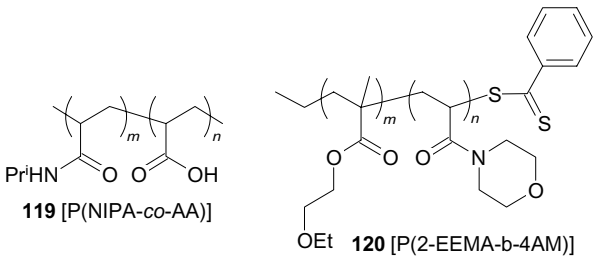



HEMA PHEMA

(*a*) AIBN (2 mol.% – 12 mol.%), sc-$CO_2$, 60 – 80 °C, 150 – 270 bar, 2 – 10 h

Precipitation polymerization in sc-$CO_2$ without stabilizers allowed chemists to prepare pure block copolymers that can be potentially used in various fields of biomedicine, for example, for targeted drug delivery. Also, this method makes it possible to combine different initial monomers in various ratios to synthesize copolymers with desired properties, for example, copolymers of *N*-isopropylacrylamide and acrylic acid [P(NIPA-co-AA) **119**] [510] or 2-ethoxyethyl methacrylate and 4-acryloylmorpholine [P(2-EEMA-b-4AM), **120**].[513]

**Structures 119, 120**



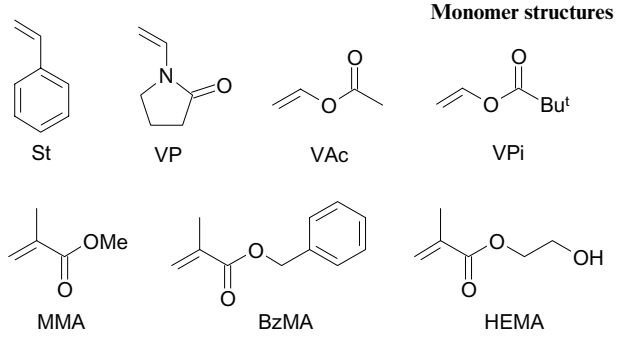

**119** [P(NIPA-*co*-AA)] **120** [P(2-EEMA-b-4AM)]

Precipitation polymerization in a sc-$CO_2$ medium can be viewed as a method of synthesis of high purity polymers.

#### 3.1.1.2.2.3. Dispersion polymerization

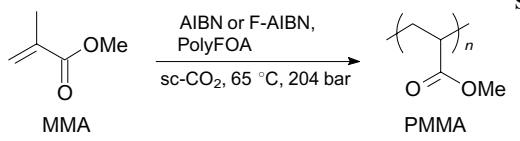
In contrast to emulsion and suspension polymerization processes, in which the monomer solubility in the continuous phase is very low, in the case of dispersion polymerization, the initial conditions are homogeneous. Hence, dispersion polymerization can be considered a type of precipitation polymerization that employs stabilizers to prevent aggregation of the particles formed. This method was applied to obtain various polymers based on methyl methacrylate (MMA),[515 – 519] 2-hydroxyethyl methacrylate,[520 – 522] 1-vinyl-2-pyrrolidone (VP),[523] and styrene (St),[524, 525] and copolymers of methyl methacrylate with styrene [526, 527] or with benzyl methacrylate (BzMA) [526] and coppolymers of vinyl pivalate (VPi) and vinyl acetate (VAc).[528]

**Monomer structures**




An example of dispersion polymerization in sc-$CO_2$ is methyl methacrylate polymerization.[529] When the process is carried out without stabilizers, it results in the formation of polymethyl methacrylate (PMMA) with low molecular weight (80 – 150 kDa) and low monomer conversion (10% – 40%). However, when 2 mass % – 4 mass % poly(1,1-dihydroperfluorooctyl acrylate) (PolyFOA) as a polymeric surfactant stabilizer is added to the reaction mixture, the product molecular weight reaches 190 – 325 kDa, and the monomer conversion exceeds 90% (Scheme 53). The product consists of homogeneous spherical particles with the average diameter of 1.2 – 2.5 mm, according to the scanning electron microscopy (SEM) data.

**Scheme 53**



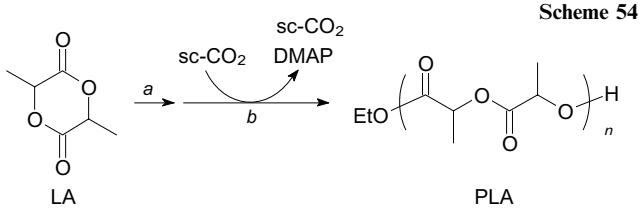

F-AIBN is a highly fluorinated initiator obtained by treatment of 4,4′- azobis(4-cyanopentanoyl chloride) with 1,1,2,2-tetrahydroperfluorodecanol

#### 3.1.1.2.3. Ring-opening polymerization

There are two types of ring-opening polymerization (ROP) in sc-$CO_2$: dispersion and precipitation polymerization. This method is used to prepare polymers based on lactides,[514, 530 – 534] glycolides,[535] and caprolactone[536, 537] and various block copolymers.[538 – 540] One example of ROP was described above (preparation of polyurethane **117** from aziridine and $CO_2$, see Scheme 47).[494] Another example is the synthesis of polylactide (PLA) from lactide (LA) in sc-$CO_2$ in the presence of the 4-dimethylaminopyridine (DMAP) – ethanol catalytic system.[534] The process results in high monomer conversion (> 95%) and formation of a polymer of low dispersity (the polydispersity index is 1.10). In order to obtain high-purity PLA, the remaining catalyst was extracted with sc-$CO_2$. The extraction was more efficient at a low temperature and high pressure (Scheme 54).

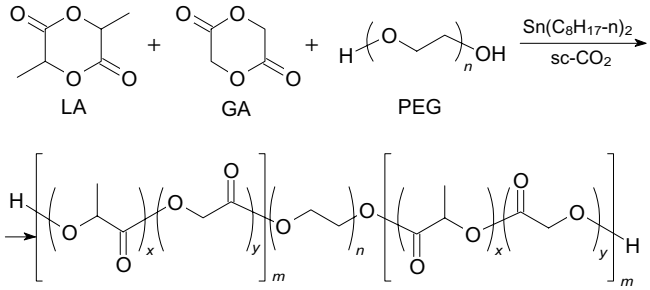
Polymerization of hydrophobic dimers of lactic (LA) and glycolic acids (glycolide, GA), together with hydrophilic polyethylene glycol (PEG) led to the formation of a gel-forming and temperature-sensitive triblock copolymer (PLGA-PEG-PLGA) (Scheme 55). This product has good prospects as a drug delivery agent since it possesses the following benefits: biodegradability, biocompatibility, and simplicity of preparation.[539]

**Scheme 54**




(*a*) DMAP (6.6 mol.%), EtOH (3.3 mol.%), sc-$CO_2$, 60 °C, 100 bar, 2 h; (*b*) sc-$CO_2$, 40 °C, 200 bar, 5 h

**Scheme 55**

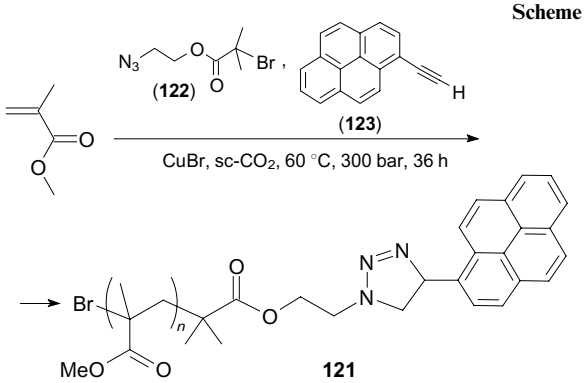



#### 3.1.1.2.4. Controlled living radical polymerization

The most common methods of controlled living radical polymerization (CLRP), which has recently become popular, include nitroxide-mediated radical polymerization (NMP), atom transfer radical polymerization (ATRP), and reversible addition – fragmentation chain transfer (RAFT). These methods were implemented in heterogeneous conditions in sc-$CO_2$. For example, NMP in the presence of alkoxyamine initiators in sc-$CO_2$ made it possible to synthesize polyacrylates[504, 511, 516] and polystyrenes[504, 524, 525, 541] with a narrow molecular weight distribution, predictable molecular weight and composition, and a clearly defined architecture. The ATRP method of MMA polymerization in the presence of CuBr and sc-$CO_2$ was used to prepare polymethyl methacrylates.[515, 542, 543] For example, polymethyl methacrylate **121**, a functional copolymer, was prepared by one-pot synthesis involving a combination of the click-reaction (involving azide **122** and alkyne **123**) and ATRP in sc-$CO_2$ (Scheme 56).[542]

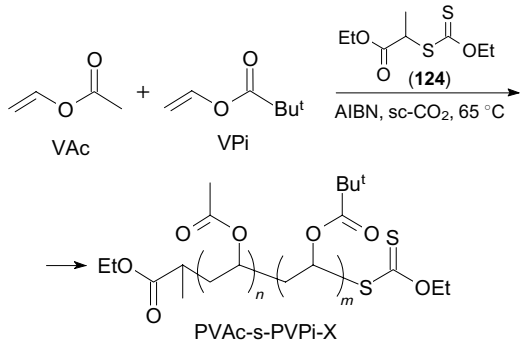
The most popular method is RAFT providing a lot of opportunities for controlling the polymer molecular weight and molecular weight distribution. This method allows for the synthesis of polymers with a clearly defined architecture, including star-shaped, block, brush-shaped, comb-shaped,

**Scheme 56**



and gradient copolymers, and polymers with predictable functionality. This method was employed to synthesize various polyacrylates [544, 545] and polystyrenes with a rather high polydispersity index,[546, 547] and also their copolymers, *e.g.*, PVAc-s-PVPi-X, a copolymer of vinyl acetate and vinyl pivalate was prepared using compound **124** in a sc-$CO_2$ medium (Scheme 57).[513, 526, 528, 548, 549]

**Scheme 57**




Thus, the methods of polymer synthesis in sc-$CO_2$ have good prospects as they possess a number of economic, environmental, and chemical advantages. The advantages include: accessibility of $CO_2$ supercritical conditions, absence of expensive processes of drying and extraction of the polymerization side products, use of $CO_2$ as both a solvent and a reactant, and the possibility of varying the $CO_2$ temperature and pressure in order to control the polymer molecular weight characteristics.

### 3.1.2. Chemical modification of polymers in sc-$CO_2$. Preparation of cross-linked polymers

Modification of polymers in SCF is a good alternative to traditional methods, which allows avoiding the possible side reactions due to very mild conditions. Most of the studies are devoted to reactions with polyimide end groups (modifications with succinic anhydride, 1,2-epoxybutane, and various ketenes) [550 – 552] and carboxyl end groups [553] or to acrylate grafting to polypropylene films.[554 – 556] The use of sc-$CO_2$ ensures higher dispersion of the reagents in the polymer matrix at low temperatures.

Some of the practically important examples of polymer modification in SCF include dyeing and chemical treatment of textile materials in order to endow them with the desired properties. For example, cotton treatment with functional polysiloxanes in sc-$CO_2$ leads to a considerable improvement of the hydrophobic properties of this material.[557] Dyeing of various polar polymers with spirooxazine photochromes in the same medium yields promising materials for optical, biomedical, and electronic devices.[558]

Another promising trend in the chemistry of macromolecular compounds is the use of SCFs in the synthesis of cross-linked polymers. In some cases, for example, when they are prepared in high-dilution conditions, such materials are similar in their properties to aerogels, although there are some differences, namely, they have a small specific surface area. It was shown that hydrosilylation [559, 560] and hydrothiolation [561] reactions involving organosilicon substrates enable the preparation of hydrophobic polysiloxane aerogels in a one-stage process (Fig. 7).

Radical polymerization in sc-$CO_2$ is a rather common method of synthesizing cross-linked polymers. Examples of

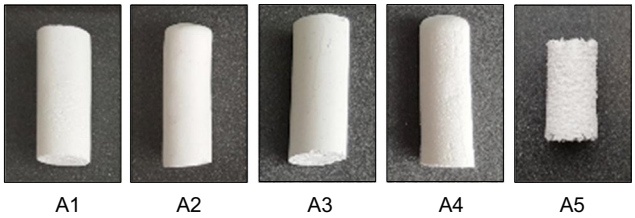



**Figure 7.** Organosilicon polysiloxane aerogels prepared by hydrothiolation in sc-$CO_2$.[561]
A1 – A5 are the sample codes. Reproduced with the permission of Elsevier.

the use of this method include the processes of preparation of pH-sensitive materials that sorb metal ions by treatment of poly(4-vinylpyridine) [562 – 564] and the copolymer of hydroxymethyl acrylamide and acrylic acid using *N*,*N*-methylenebis(acrylamide) as the cross-linking agent.[565] The monodispersed cross-linked polymer synthesized from divinylbenzene by radical polymerization in sc-$CO_2$ consists of microspheres with a 2-μm diameter.[566, 567] Reactions of this type were also carried out with methyl methacrylate,[568 – 570] acrylic acid, [503] and the styrene – divinylbenzene system.[571] In the conditions of photoinduced radical polymerization in sc-$CO_2$, the process afforded cross-linked spherical polymer microparticles.[572] Supercritical $CO_2$ is also a suitable medium for synthesis of porous coordination polymers.[573]

### 3.1.3. Preparation of aerogels by traditional and alternative methods

A promising application of sc-$CO_2$ is the preparation of aerogels and polymer foams. Aerogels are gels, in which the liquid phase is completely replaced by the gas phase, most often, by using the supercritical drying technique.[574, 575] Such mesoporous materials have a large surface area, low density, high porosity, and very low heat conductivity. An example would be the aerogel prepared from carbon with the density of only 0.16 mg $cm^{-3}$ (Ref. 576) and the aerogels based on silica with extremely low heat conductivity and thermal stability up to 1000 °C, which makes them unique heat-insulating materials.

As mentioned above, aerogels were first obtained by Kistler in 1931 on the basis of silica by replacing the liquid component in the gel with air by a special drying technique. Among the great variety of the aerogels that have been so far described, the most widely used types are silica aerogels,[577 – 580] non-silica inorganic aerogels [581 – 585] and carbon aerogels;[586 – 591] polymeric aerogels based on polysiloxanes,[559, 592 – 595] polyurethanes,[596 – 599] polyurea,[600 – 604] polyvinyl alcohol,[605, 606] polydicyclopentadiene,[607] polyamides,[608] polyimides,[609 – 617] polystyrene,[618, 619] polyether ketones,[620] resorcinol – formaldehyde [621, 622] and cellulose;[623 – 635] and organometallic aerogels.[636] Aerogels have been considered in a large number of reviews [575, 578 – 580, 587 – 590, 637 – 646] and monographs,[574, 647, 648] which give a detailed description of the preparation and properties of these materials.

The classic method for aerogel preparation consists of several (mainly rather long) stages of obtaining a gel (sol – gel process) and supercritical drying at the end (Fig. 8).[590, 639] At the first stage, the initial reactants and the catalyst are mixed in a suitable solvent. Some time later, it leads to the formation of a sol that transforms into a gel.

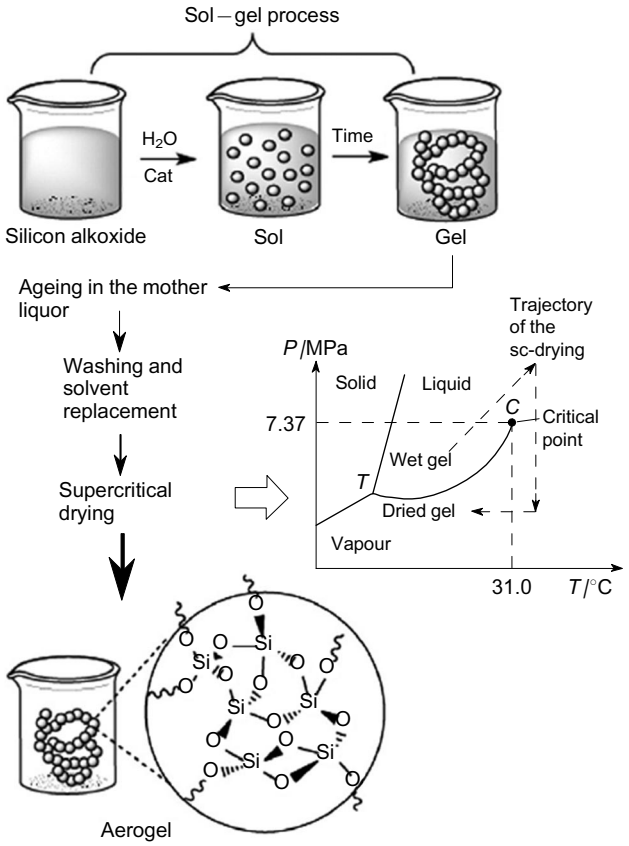



**Figure 8.** Diagram of aerogel preparation by the classical method.[580] Reproduced with the permission of Elsevier.

The next stage is a long-time process of gel ageing in the mother liquor. Then the solvent in the gel is replaced by another solvent more suitable for effective supercritical drying (as a rule, acetone or methanol). At the final stage, the solvent is removed but the volume and shape of the gel are preserved due to replacement of the solvent by sc-$CO_2$ followed by $CO_2$ decompression. The last stage is the most energy-intensive, which limits the practical application of aerogels. Besides, there are problems with scaling-up of the process.

The last few years have witnessed the development of new, more efficient and less energy-intensive methods of aerogel preparation (Fig. 9). Most of them also include stages of sol and gel preparation and gel ageing, but differ from the traditional methods in the drying process.

Among the main alternative methods of obtaining aerogels, the following are worth mentioning:

1. The FD (freeze drying) method includes removing the solvent from the frozen gel.[604, 649 – 652] Before the solvent is removed, it is replaced by a more suitable one, mainly using benzene ($T_{melt}$ = 5.5 °C), *p*-xylene ($T_{melt}$ = 13.3 °C), and *tert*-butanol ($T_{melt}$ = 25.5 °C). The main disadvantage of this method is the lower aerogel quality because of partial destruction of the gel because of solvent crystallization in the pores.

2. The OSSD (organic solvent sublimation drying) method is similar to the one described above and is very efficient in the case of aerogels based on inorganic oxides.[584]

3. The VD (vacuum drying) method consists in removing the solvent from the gel by evacuation of the sample.[576, 653, 654]

4. The APD (ambient pressure drying) method is the most common alternative technique but it includes the

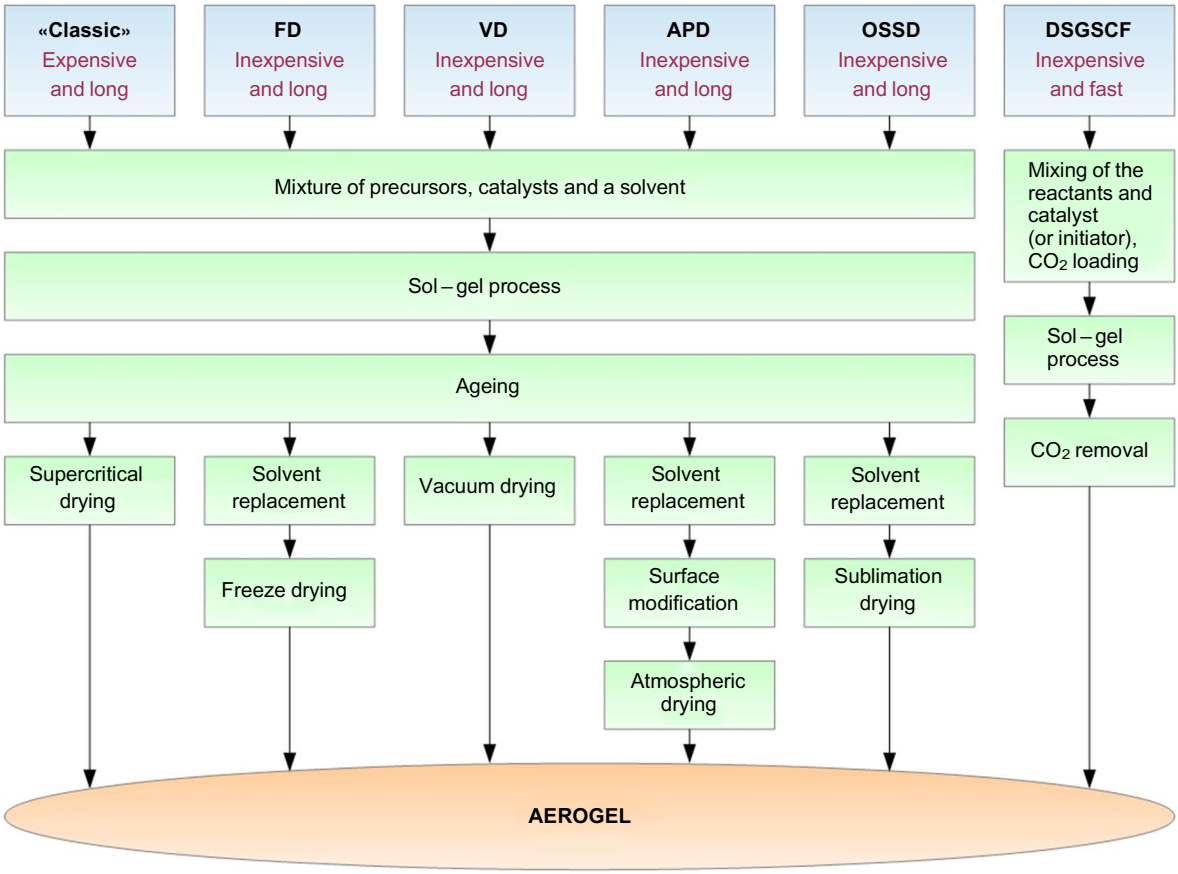



**Figure 9.** Methods of aerogel preparation (see the text).

greatest number of stages and takes the most time.[577, 585, 622, 655 – 664]

5. The DSGSCF (direct sol – gel process in supercritical fluid) method is considerably different from all the methods described above and consists in carrying out the sol – gel process directly in a supercritical solvent. The advantages of this method consist in the fact that the process does not include a supercritical drying stage, has only a small number of stages, and is fast, which considerably reduces the cost of aerogel preparation. The limiting factor is again the complexity of the control over the process under pressure. There are only several examples in the literature, in which aerogels are obtained by polycondensation,[665] hydrosilylation [559, 560] and hydrothiolation [561] using the DSGSCF method.

It should be said that the listed methods are not always universal and are suitable, as a rule, for preparing aerogels of a certain type. The main disadvantage of these methods is increase in the aerogel density due to the pore collapse in comparison with the aerogels obtained by the classic method.

Since aerogels are highly efficient heat insulators, it is relevant to study their properties.[637, 656, 666 – 668] The extremely low heat conductivity of aerogels, the high transparency and mechanical strength make them promising composite materials for glazing of buildings.[669, 670] Besides, aerogels are used for preparation of catalysts,[581, 638, 652, 671 – 673] sensors,[674, 675] optical devices,[676 – 679] adsorbents [577, 627, 680 – 683] and electrochemical devices,[586, 684 – 686] for separation of oil – water mixtures, [627, 654, 687 – 689] and as materials for space technologies.[690 – 693]

### 3.1.4. Polymer foam materials obtained by supercritical methods

The attraction of synthetic porous materials for various branches of industry (construction, machine building, medicine, and electronics; aerospace, chemical, and food industries; *etc.*) is associated with the fact that mechanical, heat- and sound-insulating properties, permeability, specific surface area, density, and sorption capacity of these materials can be adjusted, within a wide range of values, by changing the morphology, density, size, and type of pores. For example, good sound insulation is achieved when the pores are connected with one another, whereas good heat insulation requires pores isolated from one another.[694] The choice of a polymer for foam production is also determined by the application field. For example, polystyrene foam is used for protection from mechanical damage, while foams based on biodegradable polylactide are employed as tissue regeneration scaffolds in medicine.

There are two main ways of foam preparation. The first one consists in adding a chemical foaming agent (CFA), such as metal carbonate, to a polymer melt. The gas released during thermal decomposition of the carbonate foams the polymer melt. The disadvantages of this rather simple method are that it requires high temperatures for foaming agent decomposition, it is difficult to control the foam morphology, and the final product contains residual solvent and foaming agent. The second method consists in using a physical foaming agent (PFA), first of all, sc-$CO_2$, $N_2$, $H_2O$, or their combinations.[695 – 703] This approach is characterized by milder conditions and higher environmental safety. It also allows controlling the morphology of the obtained foams by changing the foaming parameters.

The process of PFA foaming consists of two main stages: the first stage represents $CO_2$ sorption into a polymer or a polymer mixture; the second stage includes the bubble nucleation and growth (Fig. 10). At the first stage, $CO_2$ plays the role of a plasticizer. The glass transition temperature ($T_g$) of its melt with the polymer under pressure is lower than that of the initial polymer. The better the $CO_2$ solubility in the polymer, the lower the melt $T_g$. This makes it possible to process such melts at a lower temperature, which is important for using thermally unstable polymers such as natural ones.[704] After polymer swelling in $CO_2$, the system is gradually depressurized, which leads to $CO_2$ and polymer phase separation. The generated $CO_2$ bubbles start growing, and the glass transition temperature of the melt increases. If the temperature and decompression rate are selected correctly, the polymer undergoes a glass transition, and the pores formed after $CO_2$ removal are fixed in the polymer structure. It is worth noting the use of sc-$CO_2$ as the PFA guarantees the absence of residual amounts of toxic compounds and organic solvents.

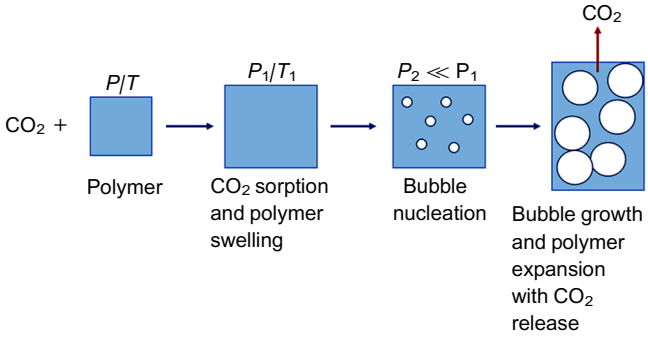



**Figure 10.** Stages of polymer foaming with a physical foaming agent.[694] Reproduced with the permission of Elsevier.

As a rule, amorphous polymers, especially polystyrene, polycarbonate, and PMMA, with a glass transition temperature above the room temperature are used for foaming. Polylactide also has good prospects as a substrate, which is bioinert and biodegradable and, hence, applicable for making porous scaffolds for healing damaged tissues. Another promising trend is the preparation of foams from semicrystalline polymers and rubbers.[694]

The principles of foaming of polymers, copolymers, and their melts are described in reviews.[694, 704 – 707] Key processes of obtaining foamed materials for various purposes using SCF and their benefits are discussed below.

#### 3.1.4.1. Preparation of foamed materials under the action of sc-$CO_2$

There are three main approaches to obtaining foams using sc-$CO_2$ as a PFA:[694]

— periodic approach consisting in polymer saturation with carbon dioxide in a high-pressure reactor and subsequent decompression at a certain rate and temperature;

— injection moulding, in which a melt of a polymer and sc-$CO_2$ is injected into a die where a pressure reduction or a temperature increase leads to foaming;

— extrusion in an extruder equipped with a PFA injection system, in which foaming is achieved by a pressure reduction at the extruder outlet nozzle.

The periodic approach is mainly applied for research purposes. A polymer is placed into a small autoclave and is saturated with $CO_2$ at certain pressure and temperature values. The saturation is followed by either a one-stage process, in which the $CO_2$ decompression leading to the

formation of a porous structure is carried out in the same reactor,[701, 703, 708 – 719] or a two-stage process, in which foaming of the saturated $CO_2$ melt is conducted in another chamber. In the second case, the saturated melt is cooled, and after the decompression, the solid polymer containing $CO_2$ is foamed by various methods, for example, in an oil bath [720, 721] or by injection moulding.[722, 723] Such equipment is easy to use in laboratory for studying the effect of saturation conditions and sc-$CO_2$ melt decompression conditions on the product morphology and kinetics of pore formation.[724]

The simplicity of the periodic method makes it easy to modify. For example, Kiran and co-workers [725] designed an autoclave with temperature gradient along the length, allowing the preparation of foamed materials with varying physico-mechanical properties. However, scaling-up of this method is problematic. Besides, the product shape depends on the preliminary stage of polymer sample processing (for example, extrusion or press moulding).

Injection moulding can be used to obtain foams in one stage, and the shape of the final product depends on the shape of the cell in which the foaming is conducted. A homogeneous polymer solution in $CO_2$ prepared in advance is injected into a chamber of a certain geometry. Chamber expansion leads to a pressure decrease and $CO_2$ bubble nucleation (Fig. 11). This is an industrially important process as it allows production of parts of required geometry, which is essential for the manufacture of sports goods and for automobile and aerospace industries.[705] Three companies have already implemented this method commercially. These are: the MuCell process developed by Trexel (USA), Optifoam developed by Sulzer Chemtech AG (Switzerland), and ErgoCell developed by Demag (Germany).[726]

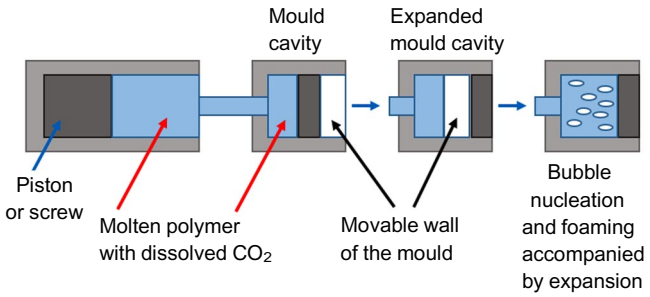



**Figure 11.** Schematic of polymer foaming by injection moulding.[694] Reproduced with the permission of Elsevier.

Tromm *et al.*[699] established that pressure and time of injection into a die have a considerable effect on the size and structure of the resulting pores. The process visualization showed that the correct choice of conditions allows preventing the formation of primary bubbles and ensures the homogeneous structure of the melt before the die is opened. There is a theoretical model of injection moulding, which agrees with the experimental data.[727]

However, industrial application of injection moulding is still limited by the high equipment costs. One of the possible solutions to this problem is preliminary preparation of polymer granules in $CO_2$, as was demonstrated by Sun and Turng.[702] The authors showed that polymer saturation with $CO_2$ can be performed in an extruder, and the obtained gas-saturated granules can be then introduced into a mould (Fig. 12). Since the extruder operates in the continuous

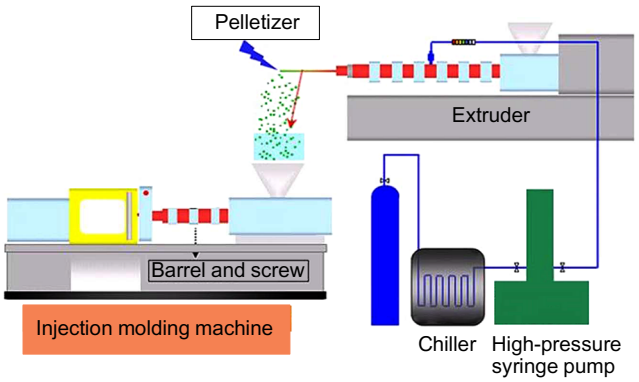



**Figure 12.** Schematic of polymer saturation with $CO_2$ in an extruder and injection into a mould.[702] Reproduced with the permission of John Wiley and Sons.

mode, it can be used to fill several moulds. The production costs in this case are considerably reduced.

An upgrade of the injection moulding technique was reported.[697, 728] The specially designed feeding screw and gas injector allowed the authors to feed the gas directly from the cylinders without PFA ($CO_2$, $N_2$) transition to the supercritical state.

The advantage of the extrusion method is its continuous mode of operation (see reviews [694, 704, 729 – 731]). In combination with sc-$CO_2$, this technology becomes even more attractive. Carbon dioxide lowers the polymer glass transition temperature and viscosity, which then reduces the melt processing temperature. As a result, it becomes possible to process polymers with a low degradation temperature, and the energy expenditure is reduced. Finally, an important thing is that polymer foaming by the extrusion method does not require preliminary preparation of samples. This is especially important for foaming of polymer mixtures and fabrication of filled composites.

An extruder (Fig. 13) consists of several parts. The temperature and pressure in each of the parts can be controlled. The key parameters affecting foaming are temperature, pressure, and die geometry, but the melt flow rate, pressure in the extruder, and screw rotation speed also make

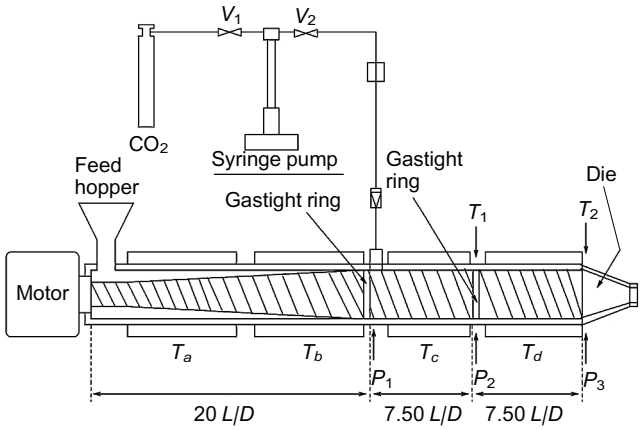



**Figure 13.** Schematic of an extruder for preparing foam with a physical foaming agent.[732] Reproduced with the permission of Elsevier publishing.

their contributions. This makes the nucleation process and further foaming rather unpredictable because nucleation in a continuous process can be caused by the flow, shear stress, or cavitation.[729]

Thus, among the three main methods of polymer foam preparation using sc-PFA, the periodic process in a high pressure reactor is the method of choice for studying foaming of new polymer systems (mixtures of polymers, nanocomposites, and copolymers) in laboratory, whereas the other methods are more appropriate in industrial implementation. Injection moulding can be used to fabricate materials of certain geometry, while extrusion has high performance and can be easily scaled-up. Of great interest is also the development of hybrid methods that would combine the advantages of several approaches.

#### 3.1.4.2. Application of foamed materials obtained using sc-$CO_2$

One of the main fields of application of foamed materials is heat insulation.[733] The cell structure of foams makes them good heat insulators. Since it is possible to obtain foams with various cell parameters in sc-$CO_2$, the heat conductivity and mechanical properties of these materials can be controlled.[734] An important trend is production of foams with heat conductivity lower than that of air.

Antunes *et al.*[735] compared two methods of obtaining heat-insulating foams based on polypropylene, one using a physical foaming agent (sc-$CO_2$) and one using a chemical foaming agent (azodicarbonamide). The morphology of the foams prepared by these methods was different (Fig. 14). In the system with PFA, the pores had an oblong shape, and when CFA was used, the pores were spherical. A possible explanation is that in the former case, the gas ($CO_2$) was released in a particular direction during decompression, while in the latter case, the gas ($N_2$) was released in all directions. The oblong cells caused heat conductivity anisotropy of the foam: the ratio of the heat conductivity in the axial and radial directions ($\lambda_{ax}:\lambda_{rad}$) was 14.9. The $\lambda_{rad} = 0.0179$ W m$^{-1}$ K$^{-1}$ value of the foam was comparable with that of silica aerogels and was lower than that of air (0.022 W m$^{-1}$ K$^{-1}$).

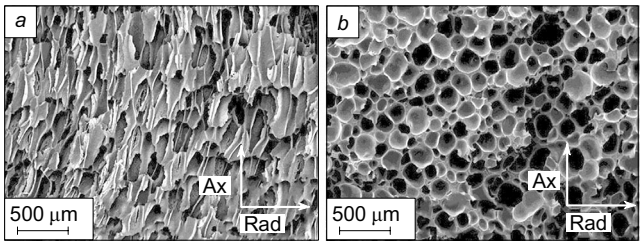



**Figure 14.** Micrographs of foams obtained by using a physical (*a*) and a chemical (*b*) foaming agent.[735] Reproduced with the permission of Elsevier.

Composite foams based on a polymer matrix and a conducting nanofiller can be used for protection of electronic devices and people from electromagnetic radiation. In addition to the required electromagnetic radiation shielding ($\geqslant 20$ dB), such materials must be lightweight (to be used in portable devices, aircrafts, and space vehicles) and have certain mechanical characteristics (flexibility and hardness), which can be achieved by using sc-$CO_2$ for foaming of an electrically conducting composition.

Xiao *et al.*[736] described PS/graphene composites. After foaming, the specific weight of the compositions decreased by 30% – 40% and the electric conductivity improved: the percolation threshold was lowered from 0.34 vol.% to 0.16 vol.%. The electric conductivity of the material could be controlled by changing the $CO_2$ temperature and pressure.

The composite based on a silicone matrix and containing nanotubes and $Fe_3O_4$ had high electromagnetic radiation shielding capacity (up to $\sim$27 dB), which was retained even after 1000 bending – relaxation cycles.[737] Finally, Chen *et al.*[717] were able to obtain a composite foam from polystyrene and carbon nanotubes, which provided the required shielding value of 23.2 dB with only 1.88 vol.% filling. It is evident that with acceleratiion of technological progress, studies in this field will become even more relevant.

Foams are widely used in medicine as bioinert and biodegradable scaffolds for tissue regeneration. They must have certain mechanical characteristics and a network of interconnected pores, improve cell adhesion, and accelerate tissue growth;[738] this can be achieved by using $CO_2$ as a PFA. In fact, $CO_2$ is readily soluble in PLA and PLGA, polymers that serve as materials for tissue scaffolds, and the use of $CO_2$ excludes the presence of residual toxic compounds and organic solvents in the final product. The pore morphology can be rcontrolled by changing foaming conditions.[739 – 743]

An important problem is drug encapsulation into foams.[744] Milovanovic *et al.*[745] impregnated PLA and PLGA polymers with thymol, a biologically active substance, in sc-$CO_2$. Subsequent decompression of $CO_2$ led to the formation of a foam, the morphology of which depended on the decompression parameters and affected the rate of release of the biologically active compound.

Another application of foams is environment protection. Some compounds with high sorption capacity towards organic solvents combined with hydrophobicity can be used for collecting oils, such as crude oil spills, from the water surface.[746] For example, low-density foams (up to 0.05 g cm$^{-3}$) with high oil sorption capacity (17 g of oil per g of foam) were obtained.[747] An important feature of these foams is that they remain superhydrophobic even after being subjected to mechanical impact.

Thus, the use of SCFTs is promising for preparing foamed materials. By changing the foaming parameters (pressure, temperature, saturation – decompression time, *etc.*), it is possible to adjust, within a wide range of values, the porous structure morphology determining the set of mechanical and physicochemical properties of a material and its potential applications.

### 3.2. Modification of glassy polymers and polymeric membranes by supercritical carbon dioxide

Modification of functional properties of polymeric materials [694, 706, 734, 748, 749] is one of the most important trends of polymer chemistry and engineering. For example, obtaining polymeric foams, packaging materials, or coatings with low dielectric permittivity and thermal conductivity [560, 750] requires materials with a certain porous structure, density and morphology and, consequently, with adjustable functional characteristics.[751, 752] Preparation of membranes for separation processes also requires an asymmetric porous structure with specified separation characteristics.[753, 754]

In modern industrial processes, sc-$CO_2$ is used as a solvent in the synthesis [755] and supercritical extraction of low-molecular-weight compounds,[756] including polymer purification from monomers, oligomers, and residual solvents. Many of the recent promising discoveries are concerned with the synthesis of porous materials *via* polymerization in sc-$CO_2$.[757, 758] The discoveries made it possible to obtain pure materials without residual solvents and to change the pore size within a wide range. The application areas of sc-$CO_2$ have been rapidly expanding in the last few years. It was used as an active foaming agent,[748, 759] in particular, with different polymeric [760] and inorganic [761] additives, and also in some exotic processes such as formation of a nanoporous structure by delocalized crazing.[762] The use of foaming agents that are liquid or gaseous [760, 763] under ambient conditions, together with sc-$CO_2$ provides an additional tool for controlling and optimizing the morphology of the obtained porous structure.[764, 765]

Carbon dioxide at elevated pressures is actively sorbed by polymers up to the their transition temperature from the glassy to highly elastic state. Desorption of $CO_2$ induces polymer transition back to the non-equilibrium glassy state, with the desorption rate affecting the morphology and porosity of the polymeric product.[766] The rate and quantitative characteristics of sc-$CO_2$ diffusion into polymers can be fine-tuned by changing the pressure and/or temperature in the reaction bulk. By varying the sc-$CO_2$ pressure and/or temperature during the exposure, exposure time, and decompression rate, it is possible to shape the morphology of the polymeric product.[767–769] Therefore, studies of changes in the properties of glassy polymers during swelling in sc-$CO_2$ and subsequent decompression have gained importance in the last few years.[770] As a rule, these studies develop along two lines. The first and the key line of research is concerned with pore formation in $CO_2$ desorption processes for the design of polymer foams and coatings with low dielectric permittivity and heat conductivity,[748–750, 771] and for fabrication of polymeric membranes with controlled open porosity [772] for ultrafiltration and electromembrane processes.[773] The second line of research deals with modification of polymeric coatings and nonporous polymeric membranes used for gas separation or for supercritical extraction. Below, the theoretical fundamentals of the former line of reseach and results obtained aling this line are described in brief. The problems and prospects of sc-$CO_2$ application for production of polymeric gas separation membranes are considered in more detail.

#### 3.2.1. Pore formation in $CO_2$ desorption processes

The simplest practical method of preparing closed-pore polymer foams is the use of sc-$CO_2$ as the foaming agent. The structure and pressure of such foams depend, to a large extent, on the temperature, pressure, and exosure and decompression times.[694, 706, 748, 749, 774] The physical causes of this dependence can be illustrated by pore formation in polystyrene (PS) as a model amorphous glassy polymer.[768] Exposure of PS to sc-$CO_2$ lowers $T_g$ through plastification.[775] A part of the volume of the PS sample that is exposed to sc-$CO_2$ in concentration exceeding the critical value required for the frcrease in $T_g$ is in the highly elastic state, which facilitates pore formation.

According to the diffusion theory, the concentration depth profile of sc-$CO_2$ in the sample increases exponentially at the initial time instants [776]

$$\frac{C(t)}{C_\infty} = 1 = \frac{512}{\pi^6}\sum_{i=0}^{\infty}\frac{\exp(-\pi^2(2i+1)^2Dt)/l_x^2}{(2i+1)^2}\cdot \cdot\sum_{j=0}^{\infty}\frac{\exp(-\pi^2(2j+1)^2Dt)/l_y^2}{(2j+1)^2}\sum_{k=0}^{\infty}\frac{\exp(-\pi^2(2k+1)^2Dt)/l_z^2}{(2k+1)^2} \quad (9)$$

where $C(t)$ is the sorbate concentration at time point $t$; $C_\infty$ is the equilibrium sorbate concentration; $D$ is the diffusion coefficient; $l_x$, $l_y$ and $l_z$ are the linear dimensions of the sample; $i$, $j$ and $k$ are the summation indices.

Equation (9) holds until the equilibrium degree of swelling is reached in the sample, and the sc-$CO_2$ concentration becomes constant throughout the sample volume. Fast decompression of the sample, along with diffusion relaxation (*i.e.*, slow gas release without pore formation) in the experiments with PS was accompanied by active pore formation. According to the classical theory of homogeneous nucleation, the most intensive pore formation must be observed in the areas with the highest sorbate concentrations (supersaturation areas):[777]

$$J_p = NB\exp(-G) \quad (10)$$

where $J_p$ is the rate of increase in the number of pores per unit volume of the polymer; $N$ is the concentration of potential nucleation sites over the polymer bulk (concentration of $CO_2$ molecule clusters); $B$ is the kinetic factor of nucleation determined by the rate of transfer of $CO_2$ molecules from the polymer to the nucleus or by the rate of increase in the nucleus size; $G$ is the Gibbs free energy calculated by the formula:

$$G = \frac{W}{k_B T} \quad (11)$$

where $W$ is the work of critical nucleus formation; $k_B$ is the Boltzmann constant; $T$ is the temperature. $W$ is calculated from the expression

$$W = \frac{16\pi\sigma}{3(\Delta P)^2} \quad (12)$$

Here $\sigma$ is the surface tension at the pore/PS interface, $\Delta P$ is the pressure difference across this interface. The expression for the radius ($r_0$) of a critical unstable-equilibrium spherical pore is as follows:

$$r_0 = \frac{2\sigma}{\Delta P} \quad (13)$$

The experimental conditions are selected in such a way that the sc-$CO_2$ concentration is non-uniform over the bulk and decreases towards the sample centre [see Eqn (9)]. This means that the porous structure density and pore sizes should decrease from the sample edge towards the centre: the pore diameter decreases as the pressure and sc-$CO_2$ exposure time increase, while the nucleation rate follows a complex dependence on temperature [see Eqns (10) and (11)]. The pore size in the PS near-surface layer non-linearly depend on temperature. Nikolaev *et al.*[769] the authors studied the effect of pressure drop rate on the morphology of the porous structures being formed. The experiments were conducted for a fairly wide range of pressure drop rates (from 5 to 500 kPa $s^{-1}$). Other parameters being

equal, the porous structure morphology changed insignificantly over this range.

The decompression method also affects the porous structure morphology. It was established that when the chamber with the sample was cooled to a temperature that was close to the critical point (31.1 °C) but lower than the PS glass transition temperature ($T_g \approx 100$ °C), no pore formation was observed at any pressure and any PS residence time in sc-$CO_2$ if the pressure was constant. Consequently, by varying the sc-$CO_2$ sorption time, it is possible to change the $CO_2$ concentration depth profile and thus affect the pore formation. In the areas with higher $CO_2$ concentrations, the nucleation process (Fig. 15, path *3*) is more intensive, while at the sample centre with $CO_2$ concentration being too low for pore formation, it is possible to supress the formation of pores. Thus, to promote active pore formation, the polymer must be in the viscoelastic state.

It was shown [768–770, 778] that when polymers are saturated with $CO_2$ at a high pressure (> 2.0 MPa), the kinetics of gas bubble nucleation can be described by mathematical tools (equations) of the stationary homogeneous nucleation model. Neglecting the dependence of the kinetic factor of nucleation $B$ on pressure $P$, one has [769]

$$\left(\frac{\partial G}{\partial P}\right) \cong -\left(\frac{\partial \ln J_P}{\partial P}\right) \tag{13a}$$

With the assumption that the surface tension changes littly with pressure, it is possible to derive a relation for estimating the pressure difference at the pore/polymer interface from Eqns (10) – (13).[769]

$$\Delta P \cong -\frac{2}{\partial \ln G/\partial P} \tag{13b}$$

In the general case, the growth of pore nucleus is associated with fast diffusion of $CO_2$ and its ability to physically push apart the polymer molecules and form gas-saturated areas inside the polymer bulk. Both these processes were shown [769] are relatively slow in the polymers in comparison with the nucleus evolution in low-viscosity single-component liquids, where $B \sim 10^{10}$ s$^{-1}$. In a solid solution, like in the cited publication,[769] $B \approx 10^3$ s$^{-1}$.

For effective growth of a spherical pore, the pressure inside the pore must be higher than the surface tension resisting this growth, *i.e.*, $\Delta P$ must be higher than the $2\sigma/r_0$,

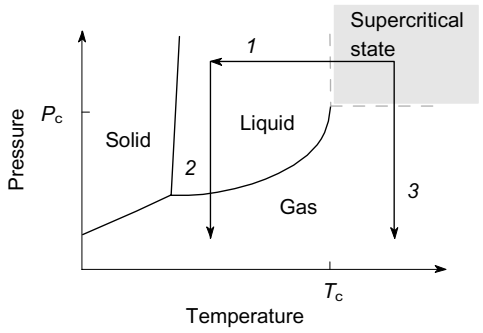



**Figure 15.** Various decompression methods: temperature decrease at a constant pressure (arrow *1*) and pressure drop (arrows *2* and *3*).[768]

and the polymer must have sufficient fluidity for the pore to grow to the required size within the real experimental time. It was assumed [779] that polymer melt viscosity is the only factor restricting the bubble growth under excessive pressure. At higher viscosity, the bubbles may not grow to the required size within the specified time.

On the basis of temperature dependences of the the Gibbs number, it is possible to derive the temperature dependence of polymer integrity on the $CO_2$ concentration (Fig. 16). Region *1* corresponds to uniform $CO_2$ desorption from PS, not accompanied by pore formation. In region *2*, the pore formation process is spontaneous and its intensity depends on the distance from the stability boundary.

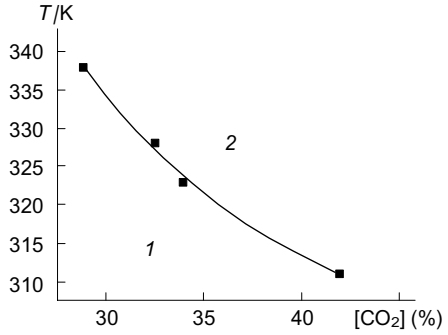



**Figure 16.** Diagram of polystyrene thermal stability during the decompression (for regions *1* and *2*, see the text).[769]

The pore nucleation in polymers during $CO_2$ desorption after the polymer exposure to supercritical carbon dioxide can be quite adequately described by the classical theory of homogeneous nucleation.[780] In addition, the non random hydrogen bonding (NRHB) equation of state [781] can be used to describe the supercritical medium solubility in the polymer matrix and the plastification profile of the polymer – supercritical liquid system. These two approaches can also be used in combination.[749]

Thus, it is possible to quite accurately predict the pore formation and characteristics of closed pore structures by using a variety of mathematical tools [749, 768, 780] for describing the observed processes and by varying temperature, pressure, and exposure and decompression times. It is also possible to find conditions in which pores are not formed, which enables targeted modification of nonporous polymeric coatings, in particular, gas separation membranes.[782]

### 3.2.2. Modification of gas separation properties of nonporous polymer membranes by sc-$CO_2$

#### 3.2.2.1. Gas separation properties and polymer free volume

Most membrane gas separation processes are carried out on nonporous (diffusion) polymeric membranes, representing a thin continuous selective polymer layer (film), with the thickness from several tens to several hundreds of nanometres. The film is deposited on a porous substrate (support), which does not significantly increase the resistance to the flow of the gas mixture to be separated. The separation is due to the concentration gradient between the two surfaces of the membrane (or continuous polymer film) and follows the dissolution – diffusion mechanism described in a lot of monographs and textbooks.[753, 754, 783–785] The penetrating component (gas) is adsorbed on the membrane input surface; the arising concentration gradient causes the

gas to diffuse through the membrane, and then the component is desorbed on the output surface of the membrane.

In this case, the flow ($J$) through the membrane is described by Fick's law of one-dimensional diffusion in an isotropic medium. If the flow is stationary, the temperature is constant, the concentration gradient in the membrane is linear, and the diffusion coefficient does not depend on the concentration of the penetrating component (which is usually the case with gases at low pressures), this law is reduced to the following expression:

$$J = D\frac{\Delta c}{l} \tag{14}$$

where $\Delta c$ is the gas concentration gradient in the membrane, $l$ is the membrane thickness.

Gas concentration in the membrane is a function of pressure $c = f(P)$, according to the equilibrium isotherm of gas sorption in the membrane material. At low gas pressures, all types of isotherms are reduced to the Henry isotherm. In this case, $\Delta c = S\Delta P$, where $S$ is the coefficient of gas solubility in the polymer, $\Delta P$ is the pressure difference across the membrane. Then, the gas flow through the membrane is directly proportional to the pressure difference and inversely proportional to the membrane thickness:

$$J = DS\frac{\Delta P}{l} \tag{15}$$

The permeability coefficient $\tilde{P}$ is the proportionality coefficient $\tilde{P}$.

$$\tilde{P} = DS \tag{16}$$

Equation (15) is the simplest expression for the dissolution – diffusion mechanism.

In membrane literature, the coefficient $\tilde{P}$ is normally given in Barrer, arbitrary units [1 Barrer = $10^{-10}$ cm$^3$ (STP) cm (cm$^2$ s (cm Hg))$^{-1}$], $D$ is expressed in cm$^2$ s$^{-1}$, and $S$ is in cm$^3$ (STP) (cm$^3$ (cm Hg))$^{-1}$. The parameter $S$ determines the driving force of the process and is a thermodynamic characteristic of permeability, whereas $D$ is the kinetic factor responsible for the mobility of the penetrating component in the material. The $p$ values of polymer materials may differ from each other by 3 – 8 orders of magnitude, depending on the polymer and gas natures.[783, 784] For example, for $CO_2$, the $\tilde{P}$ values of the polymers range between $10^{-3}$ and $10^5$ Barrer.

The permeability parameter is used to estimate the gas permeability of the membranes, in which the selective layer thickness is known only approximately.

$$Q = \frac{\tilde{P}}{l} = \frac{J}{\Delta P} \tag{17}$$

An equally important factor determining the efficiency of gas separation is selectivity, or separation factor for gases $i$ and $j$.

$$\alpha_{ij} = \frac{Q_i}{Q_j} = \frac{\tilde{P}_i}{\tilde{P}_j} \tag{18}$$

In the case of experimental measurements of permeability of single gases, this value is an ideal separation factor showing the possible extent to which a gas mixture can be enriched with the $i$th component in relation to the $j$th component in one cycle. The higher the $\alpha_{ij}$, the higher the concentration of the $i$th component that can be reached in a flow that passes through the membrane. In real gas mixtures, the real selectivity value is, as a rule, lower than the ideal one.[753, 754, 783 – 785] It means that the higher the polymer material permeability for the $i$th component ($\tilde{P}_i$) and parameter $\alpha_{ij}$, the more efficient the use of this material for separation of mixtures of gases $i$ and $j$. The $\alpha_{ij}$ selectivity in glassy polymers is usually determined by the diffusion selectivity, $\alpha_{ij}^D = D_i/\mathrm{D_j}$.

The permeability, diffusion, and solubility coefficients, as well as the ideal selectivity (separation factors) and diffusion and solubility selectivities are considered to be parameters of a polymer – gas system at a constant temperature and together are referred to as transport parameters of this system.

The relationship of $D$ and $S$ for nonporous polymer materials with gas properties is well-known and has been theoretically grounded.[783] At the same time, the relationship between the transport parameters and polymer properties, especially for polymers in the non-equilibrium glassy state, is much more complex. One of the theories explaining this relationship is the free volume theory. According to the simplest variant of this theory, the logarithmic dependence of the diffusion coefficient on the inverse free volume is linear:

$$\ln D = A - \frac{B}{\mathrm{FFV}} \tag{19}$$

where $A$ and $B$ are the polymer – gas system parameters; the FFV denotes the fractional free volume of a polymer, which is determined from the polymer density ($\rho$) at a given temperature and the van der Waals volume of monomeric unit $V_w$:[783, 785, 786] $\mathrm{FFV} = 1 - 1.3\,V_w\rho$.

Interestingly, gas solubility in glassy polymers is also dependent on the free volume: the larger the free volume, the higher the solubility. This is caused by the fact that gas sorption at elevated pressure in glassy polymers is subject to the so-called dual-mode sorption model, that is, the sum of the Langmuir and linear components:

$$C = k_\mathrm{D}P + \frac{C'_\mathrm{H}bP}{(1 + bP)} \tag{20}$$

where $k_\mathrm{D}$ is the Henry's law solubility constant; $b$ is the gas and polymer affinity constant; $C'_\mathrm{H}$ is the Langmuir sorption capacity. The $C'_\mathrm{H}$ value increases with increasing free volume, and the correlations given by the following dependence hold for all gases to a greater or lesser extent[787]

$$\ln S = A - \frac{B}{C'_\mathrm{H}} \tag{21}$$

Thus, $C'_\mathrm{H}$ can be considered a parameter characterizing free volume, while the permeability coefficient according to Eqn (16), like the parameter $D$, is linearly related to FFV by Eqn (19).

The modern views on the free volume in glassy polymers and physical methods of its study have been described in detail.[783, 786, 788] According to the authors of these studies, the structure of amorphous glassy polymers is microheterogeneous[783, 786, 788] and consists of microcavities ('holes') surrounded by a more densely packed polymer matrix

('wall'). In this case, the average 'hole' size can be estimated by probe methods;[786, 788, 789] the average 'hole' concentration ($N_h$) in the polymer is approximately constant [786, 788 – 791] [$N_h = 4 – 6 \times 10^{20}$ cm$^{-3}$ (Refs 786, 790)] and, consequently, the $\tilde{P}$ and $D$ values are determined by polymer packing as a whole, *i.e.*, by the characteristic size of the 'holes'. However, according to the microheterogeneous model, these transport parameters depend on the average 'wall' thickness $\lambda$ and the average radius of a spherical 'hole' $R_h$.[785, 790, 791]

$$\lambda = N_h^{-1/3} - 2R_h \quad (22)$$

Since $N_h$ in a polymer does not change significantly, any factors influencing the polymer such as ageing, swelling, thermal annealing, plastification, *etc.*, will change the 'hole' size, 'hole' size distribution, 'wall' thickness, and even chain packing in the 'walls', which will inevitably cause changes in the transport parameters.[786, 788, 790] Moreover, the recent studies indicate that measurement of gas transport parameters in glassy polymers can help to quantitatively estimate changes in the chain packing order in the 'walls'.[792] Such changes can be measured considering the diffusion selectivity ($\alpha^D$).

#### 3.2.2.2. Polymer membrane conditioning at high $CO_2$ pressures

The development of membrane technologies of separation of $CO_2$-containing gas mixtures at high pressure and temperature provided an understanding of the potential and limitations of using polymer membranes in these conditions.

For example, an important problem of supercritical extraction is to ensure the continuity of the process with isolation of the target product from the sc-$CO_2$ solution. One of the approaches to solving this problem was found in membrane separation of a supercritical extract. The first attempts of this kind were made in the early 1990s.[793] In these attempts, scientists used asymmetric Kapton® polyimide membranes because the membrane material had to be resistant to corrosive environments, high pressures, and elevated temperatures. The performance of these membranes was rather low, therefore, they were later replaced by nanofiltration polymer and inorganic membranes.[794 – 796] Moreover, swelling of nonporous membranes in sc-$CO_2$ leads to the formation of a nanoporous structure, which changes the permeation mechanism with increasing pressure in the system. In subcritical conditions, the $CO_2$ ability to penetrate through nonporous polymer membranes grows exponentially, which is in line with the dissolution – diffusion mechanism at high sorbate pressures. On passing through the critical point, the $CO_2$ permeability decreases, according to the viscous flow model, which corresponds, according to Patil *et al.*,[796] to the formation of a nanoporous structure in the membrane.

Polymer membranes have been used for $CO_2$ extraction from associated and natural gas since the mid-1970s.[753, 785] The main materials of the nonporous layer in these membranes are glassy polymers, such as cellulose triacetate or polyimides.[753, 785, 797] Since $CO_2$ is intensively sorbed by the material in the nonporous layer of the membranes, at high $CO_2$ pressures, this leads to polymer plasticization resulting, at a certain pressure (called plasticization pressure), in the segmental mobility, *i.e.*, polymer devitrification.[775, 797, 798] At such pressures, the diffusion selectivity drops sharply, thus reducing the separation selectivity. The reduction in the selectivity upon the $CO_2$-induced plasticization is noticeable even for the most thermally stable and pressure drop resistant polymers such as polyimides.[798] The plasticization is accompanied by slow matrix restructuring and, as steady-state separation conditions are achieved, the membrane properties gradually change. Moreover, these changes are also observed upon great changes in the $CO_2$ pressure, temperature, or concentration in the inlet flow. A large number of studies on this subject focus on $CO_2$-induced plasticization and dependence of membrane properties on the application conditions: pressure, temperature, operation time, and thickness of the selective layer of a membrane or a film.[798 – 801]

Since glassy polymers are in the non-equilibrium state, considerable $CO_2$ pressure drops or cyclic flow drops caused by the membrane module shutdown can significantly change the membrane properties. For example, one of the consequences of $CO_2$-induced plasticization is the so-called conditioning of glassy polymers.[799] A decrease in the $CO_2$ pressure and transition through the plasticization pressure results in polymer glass transition and, consequently, the polymer enters a new steady state, which is retained, due to the chain rigidity, even after complete $CO_2$ desorption from the membrane. Such conditioned films and membranes are characterized by a greater specific volume (lower density) and, hence, by higher gas permeability due to the increase in the diffusion and solubility coefficients. The increase in permeability upon conditioning of membranes, like that upon $CO_2$-induced plasticization, reduces their selectivity.

Another phenomenon related to changes in the chain mobility during $CO_2$ plasticization is faster physical ageing of glassy materials leading to free volume relaxation and decrease [802] and, as a result, to lower permeability and higher selectivity.[803] The intensity of these processes largely depends on the thickness of the selective layer,[80] chemical structure of the polymer units, chain rigidity and free volume.[803 – 808] For example, the larger the polymer free volume, the higher the material ageing rate.[804, 808] All these phenomena affect the processes of gas separation of $CO_2$-containing mixtures, making the properties of the polymer membranes dependent on the operation time and protocol. This means that it is rather difficult to make long-term predictions about the process performance.

Solving the problems related to these phenomena has become a priority trend of membrane materials science. For example, one of the methods reducing polymer plasticization and the consequences of ageing and conditioning is cross-linking of glassy polymers, including polyimides, during membrane preparation.[809, 810] The use of cross-linked polyimides is especially important because in cascade processes of separation of $CO_2$-containing mixtures, it is possible to achieve $CO_2$ transition to supercritical state at high pressures and high $CO_2$ concentrations.[811, 812] Cross-linked polyimide membranes are also necessary for controlling the syngas composition in carbon gasification processes at high (up to 300 °C) temperatures of gas flows.[810] For this reason, not only plasticization and conditioning of the membranes used or recommended for separation of $CO_2$-containing mixtures were studied, but also the consequences of treatment of these materials with sc-$CO_2$. According to Kratochvil *et al.*,[811, 812] such membranes can be more stable, depending on the nature and degree of cross-linking, than membranes made of linear polyimides. The authors studied cross-linked and non-cross-linked copolyimides based on (4,4′-hexafluoroisopropylidene)diphthalic anhydride (6FDA).

In non-cross-linked polyimides, the transition through the critical point was accompanied, as in the case of separation of supercritical extracts, by a permeability decrease. In contrast to conditioning, the reduction of the $CO_2$ pressure in the system lowered the permeability in comparison with the initial membrane. The authors attributed this effect to matrix restructuring and formation of a denser and more equilibrium chain packing, which was also confirmed by an increase in the ideal selectivity of gas separation. However, sorption studies, on the contrary, indicated an increase in $C'_H$ and, consequently, in the free volume and $CO_2$ solubility.

In case of a cross-linked polymer, the situation was radically different.[812] Transition through the critical point did not reduce the permeability. At a lower pressure, the permeability increased and the selectivity decreased. This happened both for single gases and for real mixtures. The authors concluded that conditioning of cross-linked polymers in sc-$CO_2$ loosens their structure.[812] This fact was also confirmed by sorption studies: $C'_H$ and, hence, the solubility increase. This means that conditioning of a cross-linked polymer in sc-$CO_2$ produces an effect similar to that observed in glassy polymers during $CO_2$ plasticization in the subcritical state.

However, the question about the effect of sc-$CO_2$ treatment on the free volume and gas permeability of amorphous glassy polymers has not been adequately studied as yet.

#### 3.2.2.3. Changes in the free volume and gas separation properties of polymer films treated with sc-$CO_2$

The density decrease in nonporous polymer films after their treatment with sc-$CO_2$ attracted particular attention of researchers back in the 2000s when the results of the studies of polystyrene[813,814] and butadiene–styrene rubber were published.[815] In these works, the authors applied optical methods and studied positron annihilation and oxygen permeability to show that after decompression, the free volume and gas permeability of nonporous polymers increased. However, they noticed that such increase is considerably dependent on temperature, swelling pressure, and decompression conditions. The increase in the free volume in the swelling–decompression conditions quite naturally lowers also the dielectric permittivity, as was shown by Ronova *et al.*[816–820] for chemically diverse polymers. The authors noted that the degree of increase in the free volume and decrease in the dielectric permittivity depends not only on the swelling–decompression conditions, but also on the structure of the polymer units, presence of fluorinated substituents, and polymer chain rigidity.

Recent publications[782,821–828] present detailed studies of the sc-$CO_2$ treatment effect on the polymer density, free volume, and gas transport characteristics for a number of gases and on the sorption parameters[827] and dielectric permittivity.[782,822]

The gas permeability of nonporous polymer films after swelling in sc-$CO_2$ and subsequent decompression has been so far studied only for ten polymers (**125**–**134**) (Table 1, for expansion of the abbreviations, see the text). Seven of them belong to the class of polyimides. However, some regularities can be identified even on this small data array. Table 1 shows the changes in the density and FFV value in percent relative to the same parameters of the initial film. The positive deviations are decreasing density and, consequently, increasing FFV; the negative deviations are increasing density and decreasing FFV. The results given in Table 1 were calculated taking into account the density and FFV values provided in the cited works.

**Table 1**. Physical properties of polymers **125**–**134**.

| Polymer (name) | $T_g$/°C | $\Delta\rho$ (%) | ΔFFV (%) | Ref. |
|---|---|---|---|---|
| **125** (PEI-1) | 180 | 4.4 | 50 | 782, 821, 822 |
| **126** (PEI -2) | 181 | 1.2 | 9 | 782, 821, 822 |
| **127** (PEI -3) | 207 | 1.5 | 12 | 782, 821, 822 |
| **128** (PEI -4) | 204 | 2.4 | 18 | 782, 821, 822 |
| **129** (Ultem-1000) | 215 | 0.8–1.7 | 3–9 | 825, 826 |
| **130** (PHFP) | 160 | 2.5–3.5 | 7–10 | 823, 824, 826 |
| **131** (Matrimide-5218) | 305 | −0.2 to 0.4 | −1 to 2 | 827 |
| **132** (AC) | 185 | 0.2–1.2 | 1–6 | 827 |
| **133** (6FDA-TMPDA) | 420 | −0.8 to 0.7 | −4 to 3 | 827 |
| **134** (PIM-1) | >350 | −17 to −3 | −56 to −4 | 828 |

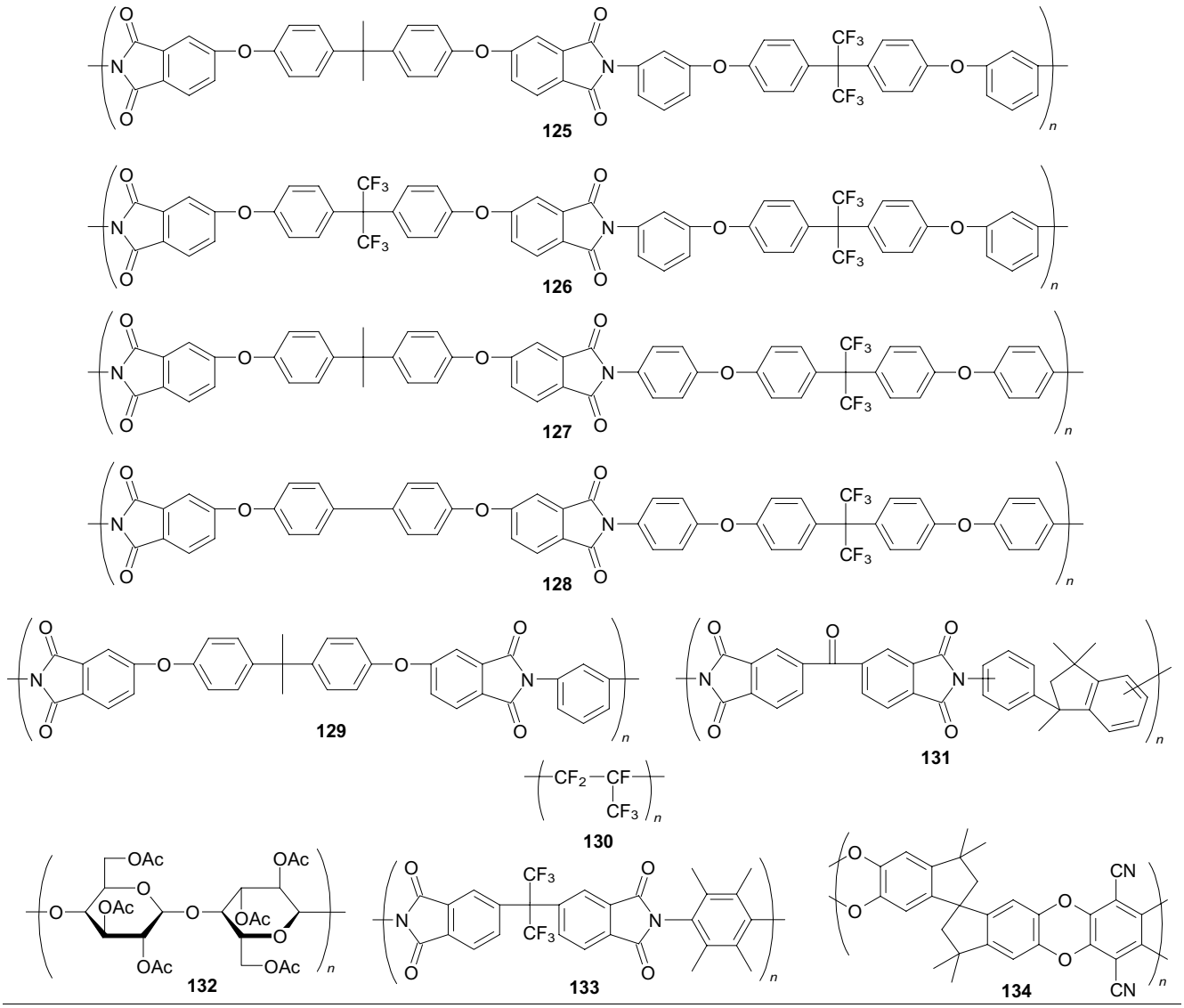
The swelling and decompression conditions for the first six polymers (see structures **125**–**130**) were selected by the procedure used for preparing transparent nonporous films. For five polyether imides (PEI), these conditions were approximately the same: the pressure was 120 atm (12 MPa), the temperature was 40 °C, the swelling lasted for 6 h, the decompression rate was 5–15 atm $h^{-1}$ (0.008–0.025 MPa $min^{-1}$), and the decompression time was 8–24 h[782,821,822,825,826] The conditions for polyhexafluoropropylene (PHFP, **130**) were as follows: pressure of 150 atm (15 MPa), temperature of 40 °C, swelling time of 5 h, decompression rate of 30 atm $h^{-1}$ (0.05 MPa $min.^{-1}$), and decompression time of 5 h.[823,824] For polymers **131**–**133** the following conditions were used: pressure of 25 MPa, temperature of 50 °C, swelling time of 2 and 8 h, decompression rate of 12.0 and 0.17 MPa $min^{-1}$, and decompression time of 2 min and 2.5 h.[827,828]

As can be seen in Table 1, depending on the polymer unit structure and swelling and decompression conditions, treatment with sc-$CO_2$ leads to radically different results. For example, in the case of slow decompression lasting for 5–24 h,[782,821–826] the outcome was same for polyether imides **125**–**129** and for polyhexafluoropropylene (**130**), namely, the free volume increased. The fast decompression lasting for several minutes and the medium-time process (2.5 h) led to either decrease or increase in the free volume.[827,828]

For sc-$CO_2$-treated PHFP films,[823] not only the density and gas transport parameters were determined, but also direct experiments by the positron annihilation and low-temperature gas desorption methods were carried out. According to the positron annihilation data, supercritical $CO_2$ treatment (Table 2) induced an increase in the average free volume element (FVE) size and in the permeability and diffusion coefficients of all the gases. The result did not depend on the initial state of the films, either 'dried' (films cast from solution at room temperature and brought to a constant weight in vacuum) or 'annealed' (films annealed above the glass transition temperature).[823,824,826] The transport parameters for oxygen and nitrogen are also given in Table 2.

The results obtained are quite logical in terms of the microheterogeneous model and free volume theory: an increase in the average FVE size makes the permeability

**Structures 125 – 134**




and diffusion coefficients higher. This, in turn, leads to a decrease in the ideal selectivity due to diffusion selectivity changes.[823, 824, 826] Since diffusion selectivity is also an indicator of chain packing order in the 'walls', sc-$CO_2$ treatment leads to packing disorder.[792] The ageing of the samples swollen after the sc-$CO_2$ treatment is reversed dou to decreasing FVE size. Certain changes in the FVE size distribution after swelling in sc-$CO_2$ and ageing of the swollen samples were also observed by the low-temperature nitrogen desorption method.[823] Thus, the results produced by these methods in the PHFP studies mainly agree with the data on conditioning of cross-linked glassy polymers in subcritical $CO_2$.[797 – 801]

However, the results of sc-$CO_2$ treatment of PEI films are rather unexpected. For example, in polymer **125** (PEI-1), film annealing reduces the $\tilde{P}$, $D$ values and increases $\alpha$ and $\alpha^D$ (Table 3),[829] which is attributed to the removal of the residual solvent.[829, 830] The higher perme-

**Table 2**. Average size of a free volume element ($2R_h$) and gas separation characteristics of PHFP (**130**) before and after treatment with sc-$CO_2$.[823, 824, 826]

| Conditions of film formation | $2R_h$/Å | $\tilde{P}(O_2)$/Barrer | $D(O_2) \times 10^8$/cm$^2$ s$^{-1}$ | $\alpha(O_2/N_2)$ | $\alpha^D(O_2/N_2)$ |
|---|---|---|---|---|---|
| Drying | 10.0 | 79.2 | 56 | 3.4 | 2.5 |
| Drying + sc-$CO_2$ | 12.3 | 291 | 120 | 3.1 | 2.4 |
| Drying + sc-$CO_2$ + 3 week storage | 11.1 | 157 | 72 | 3.4 | 2.5 |
| Annealing | 9.1 | 27.8 | 21 | 4.8 | 3.2 |
| Annealing + sc-$CO_2$ | 11.7 | 165 | 91 | 3.5 | 2.7 |
| Annealing + sc-$CO_2$ + 3 week storage | 10.8 | 117 | 67 | 3.6 | 2.7 |

**Note**. Here and in Tables 3 and 4, gases or gas pairs for which the gas separation characteristics were measured are given in parentheses.

**Table 3**. Gas separation characteristics of PEI-1 (**125**) before and after treatment with sc-$CO_2$.

| Conditions of film formation | $\tilde{P}(O_2)$ /Barrer | $D(O_2) - 10^8$ /cm$^2$ s$^{-1}$ | $\alpha(O_2/N_2)$ | $\alpha^D(O_2/N_2)$ | Ref. |
|---|---|---|---|---|---|
| Drying | 0.81 | 2.3 | 4.7 | 2.8 | 829 |
| Annealing | 0.44 | 1.9 | 7.3 | 3.5 | 829 |
| Drying | 0.50 | 1.2 | 6.0 | 3.7 | 821 |
| Drying + + sc-$CO_2$ | 1.2 | 0.87 | 8.6 | 5.1 | 821 |

ability in films treated with sc-$CO_2$ can also be attributed to the non-equilibrium removal of residual solvent.[821, 829, 830] However, the increase in the coefficient $\tilde{P}$ is accompanied by a decrease in $D$ and considerable growth of $\alpha$ due to higher $\alpha^D$ values.[821] The same effects are also observed fot the other structurally similar PEI,[821] but they are not as strong since the free volume increase is less pronounced (see Table 1), which is explained by higher rigidity of their chains.[821]

The fact that the parameters $\tilde{P}$ and $\alpha$ increase simultaneously is unusual for glassy polymers, although it is quite useful for gas separation processes. However, the behaviour of coefficient $D$ of PEI after sc-$CO_2$ treatment completely contradicts the free volume theory [see Eqn (19)]: an increase in the free volume lowers the $D$ value. Meanwhile, the microheterogeneous model of glassy polymer structure qualitatively explains this effect: the overall growth of the free volume makes the 'holes' bigger and, consequently, increases the permeability coefficient $\tilde{P}$ but the 'walls' become denser, which is manifested in lower diffusion coefficient $D$ and higher $\alpha$ and $\alpha^D$ values.

The results are even more intricate in polymer **129** (Ultem-1000) (Table 4). Annealing of the Ultem-1000 films, like that of PEI-1 films, reduces the $\tilde{P}$ and $D$ values and increases $\alpha$, but $\alpha^D$ becomes noticeably lower.[792, 829, 831] When dried films are treated with sc-$CO_2$, the $\tilde{P}$ and $D$ values decrease for all of the gases and $\alpha$ and $\alpha^D$ increase. This fact is attributable to the removal of the residual solvent and free volume relaxation in the polymer matrix.[86] However, treatment of the annealed films without a residual solvent leads again to a simultaneous increase in the permeability and selectivity, but it also causes a decrease in $D$, which contradicts the free volume theory. As in the case of PEI-1, this can be explained by the microheterogeneous model of glassy polymer structure, namely by increase in the density of the 'walls' following increase in the size of 'holes'. A sharp increase in the $\alpha^D$ value means that the polymer chains in the 'walls' become more ordered.[792]

Thus, sc-$CO_2$ treatment of all PEI and Ultem-1000 films, in contrast to PHFP films, results in a free volume increase and ordering of chain packing in the 'walls', *i.e.*, in the dense part of the polymer matrix. Evidently, the stresses caused by swelling during sc-$CO_2$ treatment of the polymers of this class contribute to the chain packing ordering. During the decompression, the stress relaxation occurs more slowly than the $CO_2$ removal from the polymer. That is why the packing structure in the polymer film remains ordered after $CO_2$ desorption. Chain packing ordering is indirectly confirmed by changes in the mechanical characteristics caused by strain-induced ordering of PEI-1 and Ultem-1000 films.[829, 831] This mechanism of formation of larger 'holes' and ordered 'walls' also explains the contradictions noted by Kratochvil *et al.*,[811] namely the increase in the $C'_H$ values and, consequently, in the free volume with decreasing permeability and increasing selectivity for non-cross-linked fluorine-containing polyimide.

Unlike the authors cited above,[782, 821 – 826] Scholes and Kanehashi[827, 828] used higher temperatures and pressures for swelling in sc-$CO_2$ and higher decompression rates. For similar swelling times (8 h), it is possible to compare some of the obtained results.

For example, fast decompression (12 MPa min$^{-1}$) in polymer **131**, cellulose acetate (**132**), and highly-permeable polyimide **133** (6FDA-TMPDA; TMPDA stands for 2,3,5,6-tetramethylphenylene-1,4-diamine)[827] increases the $C'_H$ value by up to 70%. This means that the free volume must also increase, although the FFV measurements based on film density do not always correspond to the changes in $C'_H$. These changes in $C'_H$ are matched by up to 50% increase in $\tilde{P}$(He) and a 2 – 3-fold increase in $\tilde{P}(N_2)$ and $\tilde{P}(CH_4)$. When the permeability increases, the selectivity decreases by 10% to 60%, depending on the polymer and the pair of gases. Thus, the effect observed in these polymers is similar to that induced by polymer conditioning in subcritical $CO_2$.[797 – 801] At the medium decompression rate (0.17 MPa min$^{-1}$), the same trend holds for polyimide **131**.[827] However, in cellulose acetate, a 14% increase in the $C'_H$ value and insignificant growth of FFV measured by density (< 1%), that is, still an increase in the free volume induce a 10% – 40% decrease in the permeability, depending on the gas nature, and a considerable increase in the selectivity.[827] This case corresponds to sc-$CO_2$ conditioning of highly permeable polyimide **133** based on 6FDA, a fluorine-containing dianhydride.[811] Finally, in highly permeable 6FDA-TMPDA, slow decompression leads to a 15% decrease in $C'_H$ and, consequently, in the free volume; simultaneously, the permeability decreases by 3% – 5% and the selectivity to $CO_2$-containing gas pairs increases.[827] Similar changes are observed in PIM-1, a highly permeable polybenzodioxane (**134**) for both fast and slow decompression.[828] In this case, the most significant changes in FFV measured by density (see Table 1) make the permeability slightly lower (3% – 4%) for all gases, except methane (35% – 40%), increase the selectivity to $CH_4$-containing gas pairs, and reduce the selectivity to other gas pairs.

Thus, depending on the swelling and decompression conditions, all possible consequences of sc-$CO_2$ treatment can be obtained for chemically different polymers: free

**Table 4**. Gas separation parameters of polyetherimide Ultem-1000 (**129**) before and after treatment with sc-$CO_2$.[792, 825, 826, 829, 831]

| Conditions of film formation | $\tilde{P}(O_2)$ /Barrer | $\tilde{P}(CH_4)$ /Barrer | $D(CH_4) \times 10^8$ /cm$^2$ s$^{-1}$ | $\alpha(CO_2/CH_4)$ | $\alpha^D(CO_2/CH_4)$ |
|---|---|---|---|---|---|
| Drying | 0.77 | 0.13 | 0.09 | 33 | 4.3 |
| Drying + sc-$CO_2$ | 0.60 | 0.035 | 0.014 | 83 | 7.6 |
| Annealing | 0.32 | 0.028 | 0.043 | 49 | 2.4 |
| Annealing + sc-$CO_2$ | 0.45 | 0.033 | 0.0087 | 58 | 12.9 |

volume increase[782, 811, 812, 816–827] and decrease,[827, 828] simultaneous increase in the permeability and selectivity,[792, 821, 822, 825, 826] permeability increase and selectivity decrease,[792, 812, 823, 824, 827] permeability decrease and selectivity increase,[811, 827, 828] and simultaneous decrease in both permeability and selectivity for some of the gas pairs.[828] All these features can be explained in terms of the microheterogeneous model of the amorphous glassy polymer structure. However, for some polymers, there are sc-$CO_2$ conditions in which the permeability and selectivity increase due to chain packing ordering in the dense part of the polymer matrix.[792, 821, 822, 825, 826] This effect is especially promising in terms of practical application of polymers in membrane gas separation processes.

It is possible to obtain porous or nonporous materials by changing sc-$CO_2$ treatment conditions (swelling time, pressure, and temperature and decompression rate) of glassy polymers. In this case, it is possible to quite adequately predict the pore formation. For obtaining nonporous glassy polymer films, the polymer free volume can be increased or decreased depending on the sc-$CO_2$ treatment conditions. In this case, gas permeability and selectivity of the polymer membranes do not always increase or decrease in accordance with the changes in the free volume. Swelling in sc-$CO_2$ of a number of polymers leads to ordering of the dense polymer matrix, which results in higher gas separation selectivity. Changing the conditions of treatment of glassy polymers with supercritical $CO_2$ makes it possible to achieve simultaneous improvement of permeability and selectivity, which is the aim of membrane gas separation.

### 3.3. Impregnation of polymers with photoactive compounds in supercritical $CO_2$

As it has been said above, functionality of high-molecular-weight systems can be achieved by introducing a functional filler (FF) into the polymer matrix. There is a variety of FF introduction methods: solid phase modification during extrusion, introduction into polymer melt or addition from solution in an inert solvent, normally a high polarity one. The solution is either used for impregnation of a swelling polymer matrix or for film casting if the polymers are soluble. The solution methods are most frequently employed for obtaining photosensitive optically transparent compositions used to fabricate optical memory devices; holographic materials; information processing and transfer systems; three-dimensional recording media; goods for human eye protection from undesirable effects of bright light; *etc.*[832, 833] However, these methods, as a rule, cannot ensure uniform distribution of FF particles of different sizes in the matrix bulk.

The last decade has seen a rapid development of the method of obtaining polymeric, in particular photochromic and photoluminescent, materials with a functional filler the surface of which is treated *ex situ* or *in situ*.[834, 835] This is done using amphiphilic solvents compatible both with the compounds being introduced and with the polymer (monomer). These solvents (and, at the same time, dispersion media) include, first of all, pyridine and its alkyl derivatives, which are efficiently adsorbed on the surface of hydrophilic FF nanoparticles, thus promoting their binding to the monomer such as methyl methacrylate.[835] However, even in this case, it is impossible to achieve uniform dispersion of FF micro- and nanoparticles, which requires additional treatment of FF with surfactants to prevent aggregation.[836]

Among the most popular materials are polymer compositions containing photoactive compounds (PAC) that are used in optoelectronic devices, optical memory systems, and information processing and transfer devices.[837–839] The methods for PAC introduction into the polymeric matrix are virtually independent of the nature of photoactive compounds, except the cases when PAC fixing in the polymer matrix can be accompanied by PAC destruction (for example, in the case of sputtering of luminescent mixed-ligand europium β-diketonates).[840] Photoactive compound–polymer systems in which the components are not bound to each other chemically are usually obtained through codissolution of the polymer and PAC with subsequent film casting onto a suitable surface and solvent evaporation or through impregnation of the polymeric film prepared in advance with a PAC solution. In these systems , implementing the adsorptive type of PAC binding to the polymer, quite common are non-uniform distribution and aggregation of photoactive compounds in the matrix, which deteriorates the functional properties of the material.[840, 841] Besides, PAC diffusion into the polymer may change its properties over time.[842] Modification of high-molecular-weight compounds, such as ultrahigh-molecular-weight-polyethylene, in a melt or *via* extrusion is diffucult due to high viscosity of the plasticized polymer.[843] Moreover, materials for medical purposes may be deactivated in the melt.[844]

The use of supercritical fluids, mainly sc-$CO_2$, has provided new opportunities for creation of functional solid phase systems by impregnation of polymer matrices with low-molecular-weight FFs.[845–847] Supercritical carbon dioxide facilitates the diffusion of the target components, has low dynamic viscosity, high dissolving capacity, and low surface tension, and can be easily removed from the final materials. The use of sc-$CO_2$ made it possible to impregnate biocompatible polymers (PMMA and polyvinylpyrrolidone) with drug compounds (nimesulide, estradiol and ketoprofen[848–850]) and create their prolonged-release dosage forms. Impregnation of polyimides and polyethers with organometallic complexes in sc-$CO_2$ with subsequent decomposition of these complexes or metal reduction gave polymers with semiconductor properties. Besides, sc-$CO_2$ was successfully applied for dyeing polymer fibres (in particular, polycaprolactone fibres) with rhodamine dye[851] and for targeted modification of the mechanical characteristics of ultrahigh-molecular-weight polyethylene.[846]

Supercritical $CO_2$ affects the properties of PAC, preserving or changing their functional characteristics in the polymer matrices through specific solvation. At the same time, sc-$CO_2$ affects parts of polymer matrices and determines the possibility of their conformational transformations upon coordination to PAC. The available literature does not provide enough data about effects of this type, which finally determine the functional properties of the obtained composite material.

This Section addresses the role of these factors in polymer impregnation with compounds possessing photochromic, luminescent, and photosensitizing properties. The choice of the study objects is dictated by not only the simplicity of quantitative estimation of their functional state and its variations, but also the relatively high solubility of these PAC in sc-$CO_2$. An important factor in this case is the chemical affinity of sc-$CO_2$ for both polar and nonpolar high- and low-molecular-weight compounds caused by the low quadrupole moment and electronic polarizability of

$CO_2$ molecules in combination with the absence of a permanent dipole moment.[852–854] Moreover, the combination of high self-diffusion coefficients and low dynamic viscosity, which is inherent of SCFs, enables the introduction of both readily soluble and virtually insoluble low-molecular-weight PAC into an sc-$CO_2$ medium.

### 3.3.1. SCF-modification of polymers by compounds that are poorly soluble and insoluble in sc-$CO_2$

Today, there are three types of SCF modification of polymers with compounds insoluble in sc-$CO_2$. The processes differ from each other in the mechanism of introduction of insoluble components:

— introduction of compounds with low sc-$CO_2$ solubility ($< 10^{-4}$ mol $L^{-1}$) into polymers;

— introduction of sc-$CO_2$-insoluble nanosized objects into polymers;

— combining of SCF-based approaches with traditional methods of polymer modification.

The first studies of the potential of SCFT in the fabrication of compositions with poorly soluble compounds focused on searching for new methods of uniform dyeing of fabrics with azo dyes. As is known, traditional methods of dyeing use water as the solvent. Treament of waste water is an expensive and energy-consuming process; dyeing is environmentally hazardous and requires high temperatures. Meanwhile, SCF technologies simplify the process of dye insertion into the matrix, decrease the energy consumption, and makes it possible to reuse the dye that has not entered the matrix. Furthermore, low temperatures of dyeing in this case enable the use of less expensive and less heat-resistant dyes. In several studies,[855–857] it was shown that some dyes have low solubility in sc-$CO_2$.

In one of the first studies[858] dealing with the preparation of coloured matrices in sc-$CO_2$, the authors used polymethyl methacrylate and nitrogen-containing dyes that are traditionally used for fabric dyeing, such as 4-diethylamino-4′-nitroazobenzene (DENAB) and 4-[*N*-(2-hydroxyethyl-*N*-ethyl] amino-4′nitroazobenzene (Disperse Red 1, or DR1). PMMA is known to have a limited ability to swell in sc-$CO_2$. An autoclave equipped with two $BaF_2$ windows was used to record the IR spectra. The spectral data obtained for determining solubility of dyes in sc-$CO_2$ showed that a pressure rise from 7 to 25 MPa entails an increase in the solubility from $10^{-8}$ to $10^{-5}$ mol $L^{-1}$ for DENAB and from $10^{-8}$ to $10^{-6}$ mol $L^{-1}$ for DR1 at a constant temperature of 40 °C. The solubility increased by two orders of magnitude for pressure rise from 7 to 10 MPa, and the solubility maximum was reached at 15 MPa. After that, the solubility remained almost unchanged. The concentration of the dye introduced into the polymer matrix was 3%, *i.e.*, on the average, it was two orders of magnitude higher than the dye solubility in the sc-$CO_2$ medium.

The authors attributed this effect mainly to the high partition coefficient of the dye, defined as the ratio of dye concentrations in PMMA and in sc-$CO_2$. The authors assumed that after the dye dissolved in sc-$CO_2$ started to penetrate into the swollen PMMA, a dye-saturated phase was formed outside the polymer matrix, so that the dye concentration in the solution always remained constant due to dye excess. Thus, an equilibrium concentration of the dye was attained in the polymer. An important result obtained in this study[858] is elucidation of pressure dependence of the dye partition coefficient. It was shown that a pressure increase from 8.6 to 9.2 MPa induces a decrease in this coefficient by two orders of magnitude, which dramatically increased the dye concentration in the polymer upon a minor pressure variation.

PMMA impregnation with a dye can be performed in an electric field.[859] This approach can serve to align the dye molecules in the polymer matrix according to their dipole moment. At a pressure drop, the dye molecules were fixed in the polymer matrix; the resulting composite material had linear optical properties (*i.e.*, generated the second harmonic of laser radiation). It should be noted that this method makes it possible to reduce the Brownian motion of the dye molecules during the polymer glass transition and obtain samples with a more ordered structure.

The results obtained by Li-qiu[860] indicate the possibility of dyeing polypropylene fibres with a variety of dyes, such as DR1 and DY7 {4-[4-(phenylazo)phenylazo]-*o*-cresol}. DR1 and DY7 were also used to dye polyethylene terephthalate films.[861] A steel rod tightly wrapped into a 12-μm thick polymer film (25 layers) was used in the experiments. The polymer impregnation was accompanied by constant rotation of the sample and lasted for 4 h, simulating the industrial process of fabric dyeing. It was shown that temperature rise from 90 to 110°C increased the dye penetration depth more than twofold for both dyes to reach values of 150 and 170 μm for DR1 and DY7, respectively. As the pressure increased from 22 to 25 MPa, the penetration depth did not change. By simulating the technique of fabric dyeing, the authors showed that it was possible, in principle, to employ SCF in this process.

Compounds poorly soluble in sc-$CO_2$ have been used for the fabrication of composite polymers.[860,861] However, it should be noted that convective flows appearing in such a medium determine its unique transport properties and make it possible to introduce nanosized objects that cannot completely dissolve in polymers in this medium. For example, one of the possible approaches to the synthesis of highly stable polymer nanocomposites with definite optical properties is monomer copolymerization accompanied by quantum dot (QD) synthesis in sc-$CO_2$. This method is based on a one-stage process, which makes it simple and efficient. It was used, for example, to obtain copper and silver nanoparticles from solutions of the corresponding organometallic compounds in the initial monomer by dissolution of the precursors in sc-$CO_2$. Then polymerization and metal reduction were induced at elevated temperatures. As a result, the obtained materials possessed surface plasmon resonance.[862]

Structures containing quantum dots can be formed in a similar way. These materials representing nanocrystals of semiconductor elements with characteristic linear dimensions from several to several tens of nanometres have a high quantum yield of photoluminescence in the visible and near UV-regions. The QD fluorescent properties (high total brightness in a narrow spectral range, depending both on the size of QDs and on their environment) make it possible to design new types of photovoltaic devices and promising sensor and telecommunication systems.[863] It is vitally important to stabilize QDs and prevent their aggregation and also to increase their resistance to atmospheric impacts. The introduction of QDs into polymers not only preserves their fluorescent characteristics, but also makes it possible to apply the modified polymers for the design of of optical systems.

Powdered fluorescent polymer nanocomposites were obtained by dispersion copolymerization of methyl meth-

acrylate and styrene in the presence of CdSe/CdS quantum dots in sc-$CO_2$.[863] It was found that QDs were uniformly distributed throughout the bulk of the polymer, which demonstrated stable fluorescence, even after exposure to air. Besides, Xu and Charpentier [864] prepared composite materials based on CdS/CdS – ZnS QDs and polyvinyl acetate and polytetrafluoroethylene. During the QD synthesis, methoxy groups were grafted on the QD surface for subsequent binding to the polymer groups. The resulting QD – polymer systems were used to fabricate nanostructured films with considerable absorption in the UV and visible regions and emission in the red region. Akhmetzyanov *et al.*[865] prepared stable nanocomposites containing CdS/CdSe QDs by the SAS method. It was shown that varying the the process parameters enabled the preparation of polymer particles with sizes from 40 to 500 nm and stable photoluminescence characteristics.

### 3.3.2. Impregnation of polymers with photochromic indoline derivatives in sc-$CO_2$

Spiro indoline compounds (SIC) — spiropyrans and spirooxazines — represent the most important class of photochromic substances. A molecule of a photochromic spiro indoline compound in its initial form **A** consists of two topologically mutually perpendicular parts: indoline and oxazine (or pyran) moieties.[866 – 869] In the compounds of this type, spirocyclic form **A** absorbs in the UV spectral region. Light excitation at a particular wavelength induces cleavage of the C – O spiro bond and subsequent isomerization, resulting in the formation of planar conjugate form **B**, which absorbs visible light. The photochromism of spiro compounds is associated with the UV-induced conversion of the initial colourless form **A** with a nonplanar structure to the coloured merocyanine open form **B** with a developed system of conjugated double bonds and absorption peak in the visible region of the spectrum.[870] The reverse **B** → **A** transition is induced by visible light or proceeds under thermal (dark) conditions. This transformation of a SIC molecule is shown in Scheme 58, where $R^i$ represents various substituents and X is CH (spirobenzopyrans, SBPs) or N (spirooxazines).

The spectra of spiro indoline compounds are characterized by a considerable frequency difference between the absorption bands of the initial and photoinduced forms, high absorption coefficients of the photoinduced form, high efficiency of phototransformations, and high photochemical stability. Besides, the photochromic parameters of a system can be adjusted within a wide range by varying its composition and structure.

Polymer materials with introduced photochromes are used in electronics (magnetic information storage devices), optics (optical memory and molecular switches), biomedicine (bioactivity photocontrol devices and photodynamic chemosensors) and in other areas.[871 – 876] These materials are normally prepared by polymerization or copolymerization of monomers modified with photochromes,[877 – 880] or by chemical modification of a polymer with appropriate groups.[881 – 885] Among the compounds that have been synthesized so far are, for example, polysiloxanes and polysulfones containing spirooxazine side groups [880 884, 886] and polyphosphazenes with spiropyran or azobenzene substituents in the side groups.[887 – 889] The main disadvantage of such systems is the complicated synthesis of monomers with photochromic groups. Photochromes are compounds that have an extended conjugation system and can easily bind to free radicals, while photochromic groups can inhibit polymer chain growth, which results in rather low polymerization and copolymerization rate constants.

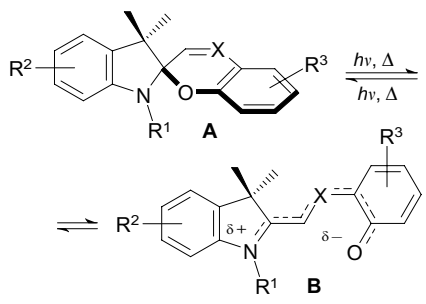
An alternative method of photochrome introduction into polymers consists in codissolution of a polymer and a photochromic compound and subsequent film casting on a suitable surface. If one of the components is a poorly soluble polymer (polyethylene terephthalate or polycarbonate) or a cross-linked system (acrylates or epoxides), the polymer matrix is usually impregnated with a photochrome solution or a photochrome solution is introduced at the stage of polymer curing.[890] When the solvent is removed, the photochromes usually form aggregates of various sizes in the polymer free volume. The aggregates are non-uniformly distributed over the matrix bulk, which lowers the functionality of such materials.[891 – 892]

An interesting and efficient method of modifying high-molecular-weight compounds in order to endow them with new functional properties and to form polymer composites is based on polymer impregnation with functional compounds of different nature in supercritical $CO_2$.[893 – 898] The easy removal of sc-$CO_2$ from the polymer after the process is completed rules out the undesirable effect of the solvent on the optical properties of the composite.

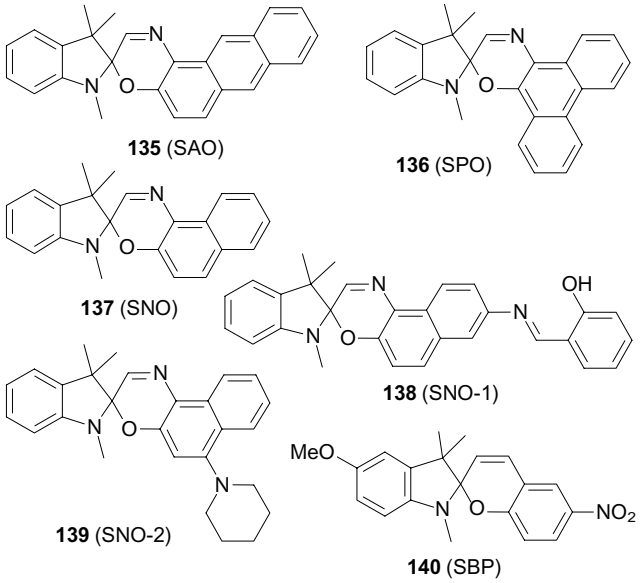
As it has been said before, SCF impregnation can be carried out not only with compounds that are readily soluble in SCFs, but also using agents that do not form true solutions with sc-$CO_2$ and even nanoparticles, which in fact form SCF colloids. It should be emphasized that $CO_2$ molecules are rather poor solvating agents for the introduced components and polar moieties of polymer chains, and this, in contrast to immobilization of low-molecular-weight compounds in organic solvents, creates conditions for direct interaction and coordination of the introduced compounds near the functional groups of the macromolecules.

For example, it was established [899 – 901] that sc-$CO_2$ can be successfully used to introduce spiro-indoline-oxazines (SIO) into thermoplastic polymers (polycarbonate or polymethyl methacrylate) and into 3D cross-linked oligomers based on substituted methacrylates up to the content of 3 mass % – 5 mass %. It was shown that, regardless of the molecule size, low-molecular-weight compounds introduced into the polymer are uniformly distributed over the whole polymer matrix bulk.[902] In this case, the functional properties of SIO introduced into a polymer are strongly affected by the matrix chemical structure.[903, 904] It was found [905, 906] that the introduction of SIO **135** – **139** and spirobenzopyran **140** into polymer matrices [poly(bisphenol A carbonate), F-42 fluoroplastic, and cross-linked oligomethacrylates containing bisphenol moieties) in sc-$CO_2$ leads to the formation of long-lived coloured SIO forms.

**Scheme 58**



**Structures 135 – 140**




SAO is spiroanthroxazine, SPO is spirophenanthroxazine, SNO is spironaphthoxazine

It is worth noting that stable (for ~1 h) coloured SIO forms were earlier obtained by subjecting dry spiroanthroxazine (SAO) and F-42 powders to high pressure (up to 80 000 atm) and shear strain (HP + SS) on Bridgman anvils, *i.e.*, without a solvent.[907]

Spiro compounds were also introduced by SCF impregnation method into various polymer matrices (Table 5).[904] The polymer samples for SCF-impregnation were prepared in the form of 120 – 500-μm thick optically transparent films.

It turned out that the content of a compound in the polymer after the SCF impregnation depends on several factors: solubility of the compound in carbon dioxide and in the polymer, the polymer swelling capacity in sc-$CO_2$, time of impregnation, *etc*. An increase in the size and molecular weight of spiro indoline compounds, other conditions being equal, should lead to a decrease in their solubility both in $CO_2$ and polymer matrices. This explains the experimentally observed reduction in the SIC content in the polymer with increasing molecular weight of the spiro compounds and sizes of their molecules. The spiro indoline compounds can be arranged in accordance with their concentrations in the polymer matrices after the SCF-impregnation as follows: **138** < **139** < **135** ≈ **136** < **140** < **137**, which correlates with their molecular weights/Da: 447, 411, 378, 352, and 328, respectively. The SCF impregnation parameters also considerably affect the amount of a spiro compound introduced into a polymer. In all cases, a pressure and temperature increase leads to monotonic growth of the photochrome content in the polymer matrix. The amount of compound **135** (SAO) that could be introduced into PC and LDPE at 90 °C was approximately the same and was more than 2.5 times higher than the amount of SAO introduced into polypropylene (PP). We believe that this is the result of higher crystallinity degree of PP (63%) in comparison with the crystallinity of LDPE (30%) and PC (30%) as SCF impregnation mostly affects amorphous polymer fragments.

**Table 5**. Characteristics of the polymers used for SCF impregnation.[904]

| Polymer (abbreviated name) | Manufacturer | Parameters | |
|---|---|---|---|
| | | $M_w$/Da | $T_g$/°C |
| Polymethyl methacrylate (PMMA) | Ekotec | $\sim 5 \times 10^5$ | 105 |
| Low-density polyethylene (LDPE) | Sabic | $\sim 4 \times 10^5$ | −80 |
| Polyvinyl chloride (PVC) | Ekotec | $\sim 8 \times 10^4$ | ~82 – 85 |
| Vinylidene fluoride and tetrafluoroethylene copolymer (E-42) [a] | Plastpolymer | $\sim 8 \times 10^4$ | −45 |
| Polycarbonate (PC) | Sabic | $\sim (3-5) \times 10^4$ | 150 |

**Note**. $M_w$ is the weight-average molecular weight, $T_g$ is the glass transition temperature; [a] the molar ratio of the units is 2 : 1.

### 3.3.3. Matrix SCF immobilization of spiro indoline compound – polymer systems

The effect discovered by Glagolev *et al.*,[899] concerning the formation of long-lived coloured forms of spiro-indoline-oxazine molecules during their matrix SCF immobilization in polymers was observed in the following experiment. Samples of PC and photochrome initial form **A** were placed into a high-pressure chamber and kept in sc-$CO_2$ conditions. After decompression and a temperature decrease, the coloured polymer sample containing impregnated spiro compound molecules (partly in form **B**) was taken out of the reactor. This means that a pressure drop leads to stabilization of the planar conformation of coloured form **B** of the photochrome molecule in the PC matrix formed after the introduction of SIC molecules in sc-$CO_2$ conditions followed by relaxational restructuring of the polymer.

We will consider the above-described stabilization the coloured SIC form in the polycarbonate matrix in more detail in relation to the **135**/PC composite system. During the SCF impregnation, some of the SAO **135** molecules in the polycarbonate matrix were transformed into the coloured merocyanine form. This was confirmed by a comparison of the absorption spectra of the PC and PMMA samples containing impregnated compound **135** before and after the photoexcitation (Fig. 17). It can be seen in Fig. 17 *a* that the spectrum of PC samples containing molecules of **135** introduced by the SCF impregnation exhibits a band at 600 nm characteristic of the coloured SAO form both before and after the UV exposure. In the case of PMMA (Fig. 17 *b*), there is no such band in the absorption spectrum of the **135**/PMMA system before the exposure to UV radiation. This means that the coloured form of SAO **135** is formed in the PMMA matrix only on exposure to UV light. It is important to note that the content of the coloured form of compound **135** in the PC matrix increases during relaxation of the PC structure in air and doubles within the next 4 – 5 h after the sample has been removed from the sc reactor.

Figure 18 shows the dependences of changes in the sample mass and the ratio of the number of molecules in form **B** to the number of molecules in form **A** for SAO **135** introduced into the PC matrix on the time that has passed after the SCF impregnation was finished. An analysis of these dependences shows that the decrease in the **135**/PC

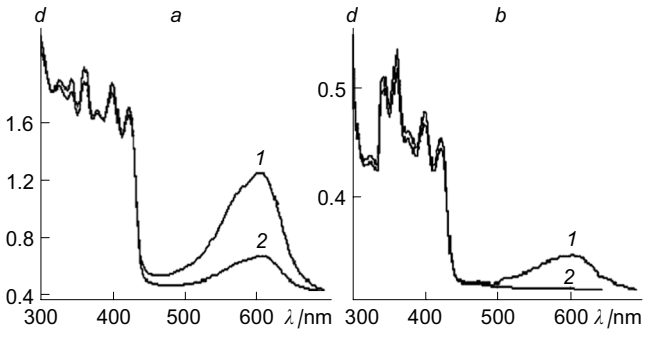



**Figure 17.** Electronic absorption spectra of PC (*a*) and PMMA (*b*) plates with spiroantrooxazine **135** introduced in sc-$CO_2$.[899] (*1*) samples after irradiation at 365 nm, (*2*) initial samples. *d* is absorbance.

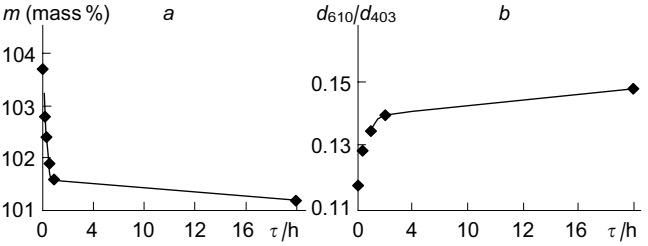



**Figure 18.** Time dependences of sample mass (*a*) and ratio of the numbers of molecules in forms **B** and **A** of spiroantrooxazine **135** introduced into polycarbonate (ratio of the absorbances at 610 and 403 nm) (*b*) after completion of SCF impregnation.[900] Reproduced with the permission of Springer.

sample mass caused by $CO_2$ diffusion from the polymer matrix after the SCF impregnation was accompanied by an increase in the ratio of the absorbance at 610 nm corresponding to coloured form **B** to the absorbance at 403 nm corresponding to colourless form **A**.

It was found that when the **135**/PC system is prepared by solvent evaporation from a solution of PC and SAO, colourless form **A** is not formed in the PC matrix. It is not formed either when SAO is introduced into polymers without aromatic moieties (even if sc-$CO_2$ is used). The studies showed that PC samples prepared by SCF impregnation and containing SAO molecules in form **B** do not change their colour for more than seven years (the maximum observation time), which indicates the exceptional stability of the merocyanine form of SAO after the introduction of this photochrome into the PC matrix with the help of sc-$CO_2$. These results attest to the active role of the polymer matrix in its impregnation with photochromic spirooxazines in sc-$CO_2$ conditions. It was shown that impregnation of polymers containing donor-acceptor groups (polycarbonate, polyvinyl chloride, or fluoroplastic) with spiro indoline oxazine compounds (spiropyrans and spirooxazine) can lead to conformational transitions in the photochromes accompanied by stabilization of the merocyanine forms with a quinoid or bipolar structure.

A.B.Solovieva and co-workers [902 – 904, 908] discovered and studied the intense photoluminescence of the coloured forms of spiro compounds introduced into halogenated matrices by matrix SCF impregnation. The role of the matrix was most obvious in the SCF impregnation of the F-42 fluoroplastic with SAO molecules. As it was shown, the conformational transitions of the molecules introduced into the F-42 matrix in sc-$CO_2$ and fixed in their metastable form $B'$ with an absorption band at 610 nm led to the formation of coloured form $X$ unknown before with an absorption band at 535 nm. The subsequent matrix restructuring resulted in the formation and final stabilization of form $Y$ with an absorption band at 475 nm in the matrix. Understanding the mechanism of such transformations requires taking into account the amorphous crystalline structure of fluoroplastic with a rather low crystallinity degree ($\sim 10\% - 15\%$). Besides, the SCF impregnation temperature is higher than the fluoroplastic glass transition point, *i.e.*, the polymer is in the high-elasticity (relaxation) state. This structurally non-equilibrium system possesses a 'structural energy' (or strain energy) $G'$,[909] which is defined as excess free energy over the free energy of an equilibrium crystalline system of an equivalent composition. Since there is no data about $G'$ for such systems, the value of $G' \approx 2$ kJ mol$^{-1}$ (Ref. 909) obtained by measuring the latent heat of the organic glass – crystal transition can be taken as the reference value for estimating this parameter. The possibility to make use of the stored structural energy during the relaxation restructuring of the metastable system composed of SAO molecules as form $B'$ and F-42 fragments solvating them is due to the viscoelastic state of the polymer matrix and the plasticization effect of the carbon dioxide introduced into the matrix (at least into its near-surface layers) on the polymer chain fragment mobility. These factors are responsible for the mutual restructuring of the matrix and photochrome molecules and for conformational transitions of their non-coplanar structure containing $\delta^+ - \delta^-$ charge pairs into energetically more favourable form $Y$ stabilized in the matrix bulk.

Thus, at a temperature above $T_g$, the amorphous fragments of the polymer matrix become not only an inert space for the introduced compounds in the accessible free volume, but an active system making use, within the thermodynamic limits, of the stored structural energy of the non-equilibrium fragments. This is manifested as the formation of metastable coloured forms of the initial photochrome and subsequent immobilization of the thermodynamically favourable coloured form in the matrix.

This local restructuring of the polymer matrix can lead to a sorbent – substrate multiple-site correspondence, with polymer fragments composed of up to a hundred atoms being able to simultaneously move from their initial positions.[909] This concerted [910] local restructuring of the polymer and the introduced SAO molecule induced by impregnation in sc-$CO_2$ makes it possible to minimize the system free energy following a decrease in the polymer matrix strain energy and formation of a planar structure of coloured spiroantrooxazine forms.

This energy contribution was also found to be necessary for the formation of coloured forms of the SIC/polymer system upon mechanochemical activation [911] of the reactions in such systems at a high pressure and shear strain.[907] It can be assumed, according to the data reported by Timashev,[909] that the conditions created in this case are favourable for reaction of compounds that do not normally react with each other because of steric hindrances or low reactivity. The elimination of the obstacle inherent in impregnation of polymer matrices in organic solvents, particularly, solvation by the solvent molecules, enables

the direct donor-acceptor interaction of spiro compounds with polar polycarbonate fragments and halogen-containing polymers and formation of strong intermolecular charge transfer complexes.[909] This is one of the most important advantages of carrying out impregnation in sc-$CO_2$.

## 4. Supercritical fluids for medicine

The relatively simple transition of environmentally friendly media, such as carbon dioxide and water, to supercritical state bodes well for SCFT application in medicinal chemistry and pharmaceutics. The most promising fluid for pharmaceutical industry is sc-$CO_2$ due to its availability, low cost, and low critical point parameters. There are several fields in pharmaceutics in which SCF application is especially advantageous. First of all, they concern the increase in the activity and bioavailability of poorly soluble drug substances for oral, pulmonary, and transdermal administration. SCF treatment of drug substances significantly changes their morphology and polymorphism and makes it possible to produce substances with a high degree of purity unattainable by other methods.

Another field where the SCF advantages are also evident is the production of prolonged-release drugs. In particular, impregnation of block copolymers with an active pharmaceutical ingredient in an sc-$CO_2$ medium makes it possible to prepare high-purity dosage forms with controlled polymorphism of the active ingredient. Besides, SCF application in this case allows controlling the phase state of a substance and, hence, its bioavailability.

One more trend is SCF-assisted preparation of biocompatible polymers for implant design. In this case, SCF produces a sterilizing effect on the compounds, which can be used to fabricate sterile hypoallergenic matrices of organic polymer materials preventing the development of infections in implants.

This Section of the review looks in detail at SCF-assisted preparation of low-antigenic biomaterials for reconstructive surgery and active polymorphic forms of drugs.

### 4.1. Formation of decellularized biological tissues in sc-$CO_2$: chemical aspects

Development of biocompatible materials is an urgent problem of reconstructive surgery. There are a number of requirements for such materials, including wear resistance, mechanical strength, and hemodynamic load and proteoclastic degradation resistance. There is a group of biomaterials, allogeneic and xenogeneic tissue grafts (allografts and xenografts), which reproduce most accurately the characteristics of tissues to be reconstructed. The undeniable advantages of tissue grafts over their artificial analogues are: natural hemodynamic resistance, no need for lifelong anticoagulant treatment, reduced risks of thromboembolic complications and hemorrhagic events after anticoagulant therapy, *etc.*[912] However, their use in clinical practice is limited for a number of reasons. The problem with the application of allografts is the lack of donor material, and the use of xenografts is significantly limited by the immune reaction of recipient's body. The development of tissue implants requires new methods of forming biocompatible materials for surgical treatment of patients that need reconstruction of damaged organs or tissues.

There are two main approaches aimed at increasing the service life of implanted biotissues and eliminating their immunogenicity. The approach that was first widely used in clinical practice is based on the application of cross-linkers fixing the tissue and masking the antigens.[913] The most popular crosslinkers are: glutaraldehyde[914] and ethylene glycol diglycidyl ether, an epoxy compound.[915] It is rather difficult to integrate such biomaterials into a recipient's body because they become cytotoxic and dense, which prevents cell infiltration and creates the risk of calcification.[915,916] An alternative method eliminating the immunogenicity and reducing the risk of tissue rejection is the decellularization–devitalization process based on removing the cell component.[917] The composition of such cell-free extracellular matrix (ECM) is very close to that of the natural environment of the cells, and ECM can stimulate regeneration of damaged tissues.[918] In the last few decades, the application of the supercritical fluid extraction method has improved the biotissue decellularization and sterilization technologies.[919]

#### 4.1.1. Decellularization of biological tissues in sc-$CO_2$ in combination with chemical agents

Traditional approaches to decellularization are based on chemical or enzymatic effects on tissues[920] and include their treatment with nonionic detergents such as Triton X-100[921,922] and 3-[(3-chloroamidopropyl)dimethylammonio]propane-1-sulfonate (CHAPS);[923] ionic detergents including sodium dodecyl sulfate (SDS)[924,925] and sodium deoxycholate;[926] alkalis;[927] and enzymes, *e.g.*, a mixture of trypsin with ethylene diamine tetraacetate (EDTA).[928,929]

Despite the large variety of decellularization protocols, for a number of reasons, it is important to carefully select the process conditions. On the one hand, this procedure is aimed at removing the donor cell residues, antigens, and potential pathogens. On the other hand, it is necessary to preserve the structural arrangement of the ECM and its characteristic functions.[930,931] However, the use of detergents often increases the cytotoxicity of an implant and requires long and careful washing, which increases the risk of degradation and bacterial contamination.[932] Enzymatic hydrolysis is less effective and destroys the structural arrangement of the ECM fibrils.[923,929]

One sort of methods of physical decellularization is extraction in sc-$CO_2$, which can be used as an independent technique or in combination with the classical methods.[933–935] The application of sc-$CO_2$ considerably increases the process efficiency, reduces the contamination risk, and shortens the procedure. The resulting biomaterials can become a personalized tool for treating patients with a variety of systemic pathologies.

The principle of tissue decellularization in sc-$CO_2$ is based on the destruction of cell membranes consisting of a double lipid layer with nonpolar moieties. It is common practice to use cosolvents for extraction of polar phospho- and glycolipids (such as ethanol) and(or) nonpolar lipids (aqueous solutions of detergents) and for denaturing structural proteins.[935,936] The dissolving capacity depends on the cosolvent concentration in the reaction mixture and pressure inside the chamber. The increase in the sc-$CO_2$ pressure and density leads to increasing cosolvent content in the SCF, while the increase in the cosolvent concentration results in higher dissolving capacity of the system.

Supecritical $CO_2$ inside the reactor diffuses through the cosolvent causing its partial transition to the gas phase. The result is a decrease in the cosolvent dissolving capacity and release of the biomolecules extracted by the cosolvent from the tissue, due to the high mass transfer potential of sc-$CO_2$.

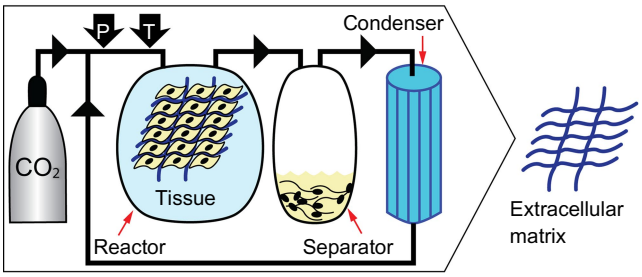



**Figure 19.** Scheme of the apparatus for biotissue decellularization in a supercritical carbon dioxide medium.

Thus, sc-$CO_2$ can act independently or as an antisolvent for separating the extracted cellular material from the cosolvent and ECM. The cell debris is accumulated in the separator and sc-$CO_2$ can be condensed and reused (Fig. 19). After the process is completed, the reactor contains the cell-free ECM.

The extracellular matrix mainly consists of collagen molecules hierarchically arranged into fibrils, fibres, fibre bundles and laminates.[937] The structural unit of a collagen fibril represents a triple helix of tropocollagen.[938] The quantitative ratio of the collagen types is determined by the tissue type. ECM proteins include: elastin, fibronectin, fibrillin, integrins, laminin, tenascin C, *etc*.[939] The collagen, fibronectin, and tenascin C molecules include a sequence of L-arginine, glycine, and L-aspartic acid (RGD tripeptide), meant for providing integrin-mediated cell adhesion.[940] The ECM protein fibres are immersed in a supporting amorphous matrix consisting of glycosaminoglycans and proteoglycans.[924, 937]

The first report about the use of sc-$CO_2$ as the medium for decellularization of mammalian tissues was published by Sawada *et al*.[933] The authors incubated porcine aorta fragments in sc-$CO_2$ at 15 MPa and 37 °C for 1 h. Complete decellularization was achieved when ethanol was added on the reactor bottom (Fig. 20). The procedure did not have any effect on the material mechanical properties. The tissue

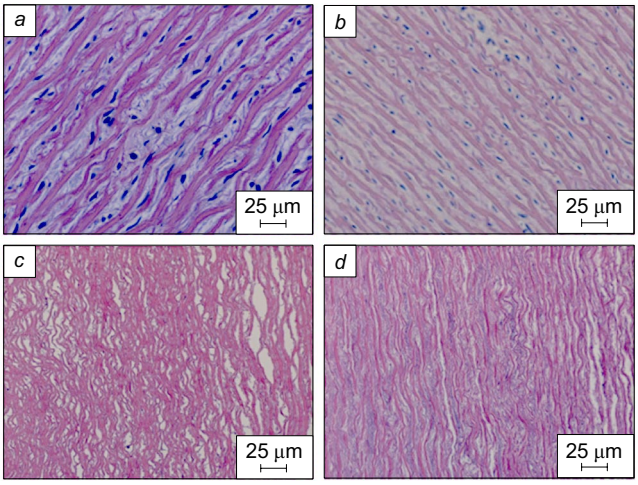



**Figure 20.** Hematoxylin and eosin staining of the porcine aorta tissue before decellularization (*a*) and after decellularization in sc-$CO_2$ without a cosolvent (*b*) and with ethanol as a cosolvent for 60 min (*c*) and 15 min (*d*).[933] Reproduced with the permission of John Wiley and Sons.

became more rigid as the exposure time increased. This was associated with the tissue dehydration, as ethanol is hygroscopic and sc-$CO_2$ dissolves up to 0.5% water.[941] However, the changes occurred within the physiologically relevant range.

Later, Guler *et al*.,[934] who experimented with the ovine aorta, showed that a twofold pressure increase destroyed the structural arrangement of the ECM and could cause embolism and aneurysm upon the subsequent implantation. This is related to increasing rate of solvent mass transfer. The pressure in the chamber must ensure the uniform penetration of the solvent into the tissue.

A modification of this method is decellularization of the porcine aorta by treatment with sc-$CO_2$ and one of four cosolvents: water, a solution of Ls-54 detergent (Dehypon®, Germany), ethanol, or a water–ethanol mixture.[935] The authors noted that it is necessary to avoid tissue dehydration. Therefore, sc-$CO_2$ was first saturated with water, which kept the matrix in the hydrated state even in the presence of other cosolvents, and addition of a polar cosolvent (ethanol) did not lead to a considerable increase in the decellularization degree. The use of sc-$CO_2$ reduced the time of experiment, with complete decellularization being attained 24 h earlier than in the standard decellularization protocol using an SDS solution, although the residual detergent concentrations were comparable. In this case, the structure of the matrix proteins and mechanical properties of the native aorta were preserved.

Zambon *et al*.[942] adjusted this method to decellularization of the digestive tract walls. The authors selected fragments of porcine esophagus and subjected them to detergent enzymatic treatment by placing the tissue into deionized water at 4 °C for 24 h and then into a 4% SDS solution for 4 h and into a 1 M NaCl solution containing DNase I for 3 h at room temperature. The sc-$CO_2$ was then applied at a temperature of 35 °C and a pressure of 10 MPa for 60 or 120 min without pretreatment or for 15 and 30 min after a 80-min pretreatment with ethanol. The hematoxylin and eosin staining confirmed that there were no intact nuclei in the biomaterial. The authors noticed that the structure had become porous, but a closer examination showed that qualitatively, the composition and integrity of the ECM were preserved. A more accurate determination of the mechanical properties, such as strength and maximum strain, did not reveal any significant differences between the samples before and after the treatment. A cytotoxicity study showed that the material was highly cytocompatible.

Huang *et al*.[943] reported the results of implanting a porcine cornea decellularized by sc-$CO_2$. The implant was first subjected to osmotic shock produced by successive treatment with a 2 M solution of NaCl and deionized water. The sc-$CO_2$ treatment was carried out with an addition of 60% ethanol at a pressure of 35 MPa and a temperature of 45 °C and lasted for 80 min. This resulted in removal of the cornea cellular elements without worsening the optical properties of the materials. However, the decrease in the amount of glycosaminoglycans and structural proteins during treatment with sc-$CO_2$ destroyed the structural organization of the corneal ECM. The treatment with a 0.2% Triton X-100 solution carried out in accordance with the traditional protocol for 6 h resulted in a less pronounced effect. A histological study showed that the cells were completely lysed and the cell fragments were removed from the implant. The sc-$CO_2$-treated cornea tissue samples consisted of ECM with numerous perfora-

tions and threefold decreased Young modulus. Nevertheless, corneal grafting in rabbits did induce an immune response, implant rejection or degradation within two months. The regeneration of the cornea was confirmed by the migration of the corneal keratocytes and epithelial cells into the implant. There were no complications during the recovery of the animals after the experimental implantation of the decellularized cornea. For a certain time after the surgery, the implants were opaque but two weeks later they became transparent. Complete re-epithelization of the implanted corneal ECM was observed four weeks after the grafting, while 6 months after the surgery, the cornea contained cells typical of a healthy tissue. These results suggest that sc-$CO_2$ treatment could be successfully used for fabrication a cornea bioequivalent. The physical method of cornea decellularization developed earlier consists in destroying cells at high pressure (up to 100 MPa);[944–946] however, this requires sophisticated and expensive equipment.

One of the most popular sources of biomaterials for reconstructive surgery is the bovine pericardium.[947] It is often decellularized by alkali treatment, which ensures that the biomaterial is biologically safe. Halfwerk *et al.*[948] described a method of decellularization of the bovine and porcine pericardia in sc-$CO_2$ (10 MPa, 35 °C) for 1 h after pretreatment with 1.25 M NaOH. Supercritical $CO_2$ facilitated fast removal of the cellular elements from the pericardium fragments, and its effect on the mechanical and structural properties of biomaterials was insignificant.

Tovar *et al.*[949] evaluated the effect of sc-$CO_2$ treatment of a decellularized porcine pericardium on the efficiency of periodontal tissue defect regeneration. For this purpose, the authors used a model of class III furcation defect at the maxillary premolar regions of beagle dogs. The experimental defects were covered with the decellularized porcine pericardium. The sc-$CO_2$-pretreated pericardium reconstructed the damaged bone with the same efficiency as the untreated decellularized pericardium. Twelve weeks later, the regeneration of the periodontal ligament began. At the 24-th week after the implantation, the authors observed almost complete resorption of the implants. However, the native periodontium was not regenerated in the defects that had not been covered. Scanning electron microscopy did not reveal any differences between the samples either; however, the pericardium thickness had significantly increased after the sc-$CO_2$ treatment ($366 \pm 54$ μm) in comparison with the initial value ($265 \pm 75$ μm).

Supercritical $CO_2$ is also applicable to decellularization of dense articular cartilage, tendon, and skin tissues.[950] Decellularization of human skin and equine superficial digital flexor tendon by treatment first with a 2% solution of LS-54 detergent (Dehypon®, Germany) and then with sc-$CO_2$ (25 MPa, 31–37 °C) for 1 h significantly lowered the content of cellular elements. However, the ECM still contained fibronectin and laminin, which promoted cell adhesion. The tendon elastic modulus changed only slightly: from $126.35 \pm 9.79$ MPa to $113.48 \pm 8.48$ MPa. Full-scale cartilage decellularization requires a multi-stage pretreatment of the cartilage tissue. The authors subjected a bovine articular cartilage to six freezing–thawing cycles, treatment with a 0.05% trypsin–EDTA solution for 24 h, and then osmotic shock. As a result, the cartilage modulus of elasticity decreased from $12.06 \pm 2.14$ MPa to $1.17 \pm 0.34$ MPa.

Chang *et al.*[951] studied the biocompatibility of bone-filler materials processed in sc-$CO_2$ . They made a powder of human femoral shaft and then delipidation and sterilization were carried out by placing the samples into a sc-$CO_2$ extractor at a temperature of 45 °C and pressure of 40 MPa. Acording to SEM examination, the size of the remaining adipose tissue particles in the biomaterial ranged from 100 to 400 nm. There was no bacterial contamination in the processed samples. The cytotoxicity tests confirmed that the biomaterial was not toxic. The intradermal administration of experimental extracts in laboratory animals (rabbits and Guinea pigs) induced a mild inflammatory response comparable with that in the reference group. Then the obtained bone tissue powder was transplanted to five patients aged 50 to 75 (three males and two females) to treat fractures common among elderly people. In the six months following the transplantation, no signs of inflammation or implant rejection were observed.

Wang *et al.*[936] used sc-$CO_2$ for adipose tissue decellularization. The adipose tissue was treated for 3 h at 18 MPa and 37 °C in the presence of ethanol as a cosolvent. The obtained material consisted of ECM components and did not contain any adipose cells. The proposed decellularization method differs from the existing ones by its high process rate and low cost. The development of an inexpensive and environmentally friendly method of obtaining ECM from adipose tissues will improve the tissue engineering methods employing autologous materials.

It should be said that the described biomaterials based on decellularized biotissues and prepared by sc-$CO_2$ extraction are new-generation products and hold great promise for the application of tissue engineered constructs in the therapy of various pathological processes.

#### 4.1.2. Sterilization of biological tissue implants in sc-$CO_2$

In addition to the numerous advantages of sc-$CO_2$ application for decellularization of biological tissues, this SCF is known to produce a sterilizing effect, which is confirmed by the studies of decellularization of cornea, aorta, and other tissues. An essential condition for successful sterilization is the correct choice of the method of microorganism inactivation. An optimally selected method ensures biological safety and the absence of ECM structure degradation. There is a great variety of sterilization methods. One of them consists in developing a high pressure and a high temperature (120–134 °C) in an autoclave chamber, which provides effective sterilization of medical instruments and laboratory equipment with steam. However, these conditions are unsuitable for sterilization of biological tissues as they damage the ECM due to protein denaturation. Hot air sterilization in heating and drying ovens at 160–200 °C also damages ECM. UV radiation neutralizes bacteria and viruses, but has poor penetrability. It is used, most often, for surface and air sterilization, but is inappropriate for porous non-transparent materials. Ethanol (70%) is widely applied as a desinfectant, because of low toxicity, but it is not sufficiently effective against fungi, endospores, and some viruses and causes protein denaturation in ECM. One more chemical sterilization technique, treatment with ethylene oxide, ensures high sterility of treated items, but requires long degassing (airing) of the samples, because of the high toxicity of the agent, and expensive specialized equipment and supplements. Sterilization by γ-radiation effectively kills microorganisms, but it is expensive and difficult to implement. Meanwhile, biological tissue sterili-

zation in sc-$CO_2$ has advantages over all the above methods in terms of the ECM structural integrity and commercial availability.[952]

In 2016 Baldini *et al.*[953] presented the results of their study of the sc-$CO_2$ sterilization effect on the biomechanical properties of soft tissues. As the object, the authors used the human anterior and posterior tibials tendons. The experimental samples were divided into three groups: intact samples, samples sterilized by γ-radiation (20–28 kGy), and samples sterilized by supercritical $CO_2$. The authors did not notice any significant difference between the samples in the three groups when they measured the failure stress, but the samples of group 3 showed a 27%–36% lower stiffness. This result agrees with the data reported earlier. For example, Yanke *et al.*[954] showed that sterilization of a human patellar tendon with γ-radiation in a 1.0–1.2 mrad dose (0.01–0.012 Gy) leads to a 20% reduction in the material stiffness. Interestingly, HIV inactivation requires a dose of 1.5–4.0 mrad (0.015–0.04 Gy).

Supercritical $CO_2$ is often used for sterilization of biomaterials in combination with acids and oxidants.[955,956] For example, Balestrini *et al.*[957] suggested treatment in sc-$CO_2$ with 0.018% peracetic acid (as the cosolvent) for lung ECM sterilization at a pressure of 10 MPA and a temperature of 35 °C. The method was tested on a murine lung tissue contaminated with *Bacillus atrophaeus* spores (Mesa Labs). It turned out to be ineffective in the absence of peracetic acid. However, when the acid was used, its concentration was an order of magnitude lower than the value required for sterilization under usual conditions, which made it possible to preserve the qualitative composition of the connective tissue (elastin, desmosine, and collagen), and the structural integrity of the ECM. The biomechanical properties of the latter also remained close to the native parameters. It is shown that sc-$CO_2$ treatment increases the tissue stiffness, but this increase does not affect the functional properties.

Van de Pol *et al.*[956] reported sc-$CO_2$ sterilization of biomaterials produced from bone allograft, which were used for filling femoral and tibial tunnels for anterior cruciate ligament reconstruction. The authors implanted bone grafts (manufactured by Australian Biotechnologies) sterilized in sc-$CO_2$ into the femoral and tibial tunnels of twelve patients. Biopsy samples were taken at the second stage of the surgery, on average, 8.8 months after the implantation. In all of the samples, the graft tissues were remodelled because of the creeping substitution (creeping of the recipient surrounding tissues). Two of the samples had endochondral ossification foci, while in three samples, the bone tissue was remodelled due to the effect produced by the combination of osteoclastic and osteoblastic activities. The average implant volumes in the samples with long periods between the surgery stages (>10 months) did not differ from each other.

The retention of mechanical properties by bone tissue biomaterials is also of primary importance. In 2013, Russel *et al.*[958] demonstrated the differences between the mechanical properties of the cortical bone tissue sterilized by supercritical sc-$CO_2$ and γ-radiation. The authors sterilized paired (right and left) fragments of the rabbit humeri bone. The paired samples (60 pairs) were randomly divided into four groups and were sterilized by different methods: with 10 and 25 kGy doses of γ-radiation, sc-$CO_2$ ($P$ = 10 MPa, $T$ = 37 °C) without additives or with peracetic acid (14.1%) or hydrogen peroxide (4.9%). The sc-$CO_2$ sterilization without a cosolvent did not significantly change the mechanical properties of the samples. In particular, it led to a minor decrease in the maximum load (by 5%) and in the energy to failure according to the three-point bending test (by 7%), while stiffness increased by 5%. When peracetic acid or hydrogen peroxide were added, the results were similar. At the same time, γ-radiation produced a noticeable dose-dependent adverse effect on the mechanical properties, namely: the maximum load decreased by 12% and 18% and the energy to failure according to the three-point bending test decreased by 26% and 44% for 10 and 25 kGy doses, respectively.[958,959]

In 2015 Wehmeyer *et al.*[960] developed a biomaterial from an amniotic membrane sterilized in sc-$CO_2$. The material was obtained after a caesarean section with informed consent of the parturient women. The amniotic membrane was separated from the placenta by blunt dissection in sterile conditions and rinsed in physiological saline to remove the remaining chorion, blood clots, and dead cells. Then the membrane was placed with its epithelial side up on nitrocellulose paper and frozen at a temperature of −80 °C. To follow the sterilization protocol, each of the samples was first contaminated with *Staphylococcus epidermidis* or *Clostridium sporogenes* cultures with $10^6$ CFU (colony-forming units) per g. The sterilization was carried out in sc-$CO_2$ ($P$ = 9.9 MPa, $T$ = 35 °C) for 10–30 min. with 0–2 mL of peracetic acid. After the sterilization, the samples were stored for 14 days in a nutrient broth at 37 °C. The samples contaminated with bacteria but not sterilized were used as the reference.

The sterilization was incomplete in the absence of the acid, but only 2 mL of peracetic acid were enough to inactivate both types of bacteria in the shortest possible time (10 min). The sterilization did not affect the tissue architecture of the biomaterial: the paraffin sections of the sterilized samples demonstrated uniform type I collagen staining without lipid inclusions. According to the biochemical analysis data, the samples also had identical contents of ECM components (hydroxyproline, type IV collagen, elastin, and glycosaminoglycans). The structure of the amniotic epithelium was studied by the SEM and fluorescence microscopy methods. After the sterilization, the epithelium flattened and had less distinct cell boundaries. The sample cytotoxicity was investigated by using mesenchymal stem cells of the human adipose tissue. By the fourth day of cell culturing on the allograft surface, the cell population increased more than two times.

Biological tissue sterilization in sc-$CO_2$ is also applicable to structures with a complex organization, including the aortic valve.[961,962] This technique has a milder effect on the mechanical and structural properties of ECM than traditional sterilization (by γ-radiation, in a mixture of ethanol with peracetic acid, by electrolyzed water, or a hydrogen peroxide solution) (Fig. 21).

Hennessy *et al.*[962] used porcine aortic valves decellularized by 1% SDS and sterilized in sc-$CO_2$ for implanting into the ovine right ventricular outflow tract for further evaluation of their recellularization potential in the next 5 months. After the implantation, the authors did not observe any signs of post-surgery complications or infections in the animals. The results of the transthoracic echocardiography showed that the implantation did not lead to either thickening of the valve cusp or vegetations on its surface. The Doppler continuous wave and colour flow mapping methods revealed moderate valve insufficiency. The histological

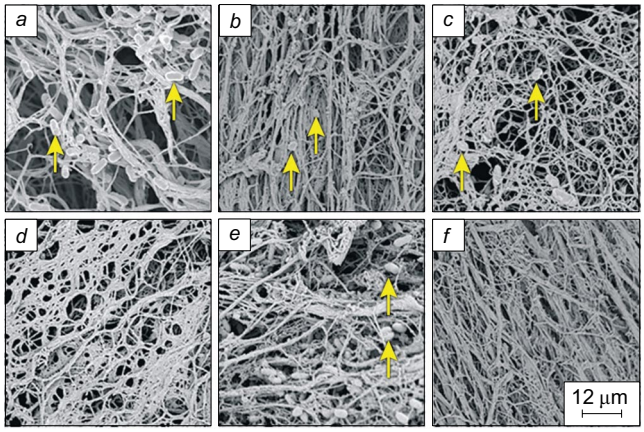



**Figure 21.** SEM images of decellularized tissues of aortic valves before (*a*) and after sterilization by electrolyzed water (*b*), γ-radiation (*c*), a mixture of 96% ethyl alcohol with 2% peracetic acid (*d*), 6% $H_2O_2$ (*e*), and in sc-$CO_2$ (*f*). The arrows show microbial inclusions.[961] Reproduced with the permission of Elsevier Science and Technology.

studies of the explants indicated recellularization by the recipient cells and epithelization of the implant surface layers without lymphoplasmacytic infiltration. The Gram staining did not reveal any bacterial contamination. The uniaxial tensile testing of the cusps showed that the valve was stiffer, which could be explained by collagen synthesis. These results indicate that the implantation of a decellularized porcine aortic valve sterilized in sc-$CO_2$ into the ovine right ventricular outflow tract led to recellularization of the biomaterial and sufficient restoration of the hemodynamic function.

Thus, sc-$CO_2$ treatment is an effective method of sterilizing biotissues of different origin. The low surface tension and high density enable sc-$CO_2$ to effectively penetrate into solid matrices and extract microorganisms, whereas the low temperature of the process and absence of toxic chemicals make this method advantageous for most grafts, including complex three-dimensional structures.

## 4.2. Polymorphism screening of biologically active substances in a supercritical fluid medium

The term 'polymorphism' means the ability of one compound to form several crystal structures. Polymorphs possess different physicochemical properties (melting temperature, density, enthalpy of formation, heat conductivity, colour, *etc.*). In some cases, polymorphism determines the field of material application such as pharmaceutical, pigment, or agrochemical industry and some other branches of small-scale chemical industries.[963] Polymorphism plays a special role in the design of new pharmaceuticals. Different polymorphs of an active pharmaceutical ingredient (API) may exhibit different pharmacological behaviours. Besides, the API compressibility and compactibility play an important role for tableting of the final product, and its thermodynamic characteristics are related to the solubility and bioavailability of the dosage form. Hence, the control of polymorphism is an essential requirement for every active pharmaceutical ingredient. This fact has led to a considerable increase in the number of publications about this phenomenon in the last 20 years.[964]

It is known that despite the same chemical formulae, different polymorphs are not identical in their spectral characteristics [vibrational (IR and Raman), NMR, and X-ray diffraction]. Spectral methods provide comprehensive information about the molecular and crystal structures of a compound, intra- and intermolecular interactions, phase transitions, and dynamics of changes in the crystal lattice. In particular, a powerful tool for studying polymorphism of drug compounds is vibrational spectroscopy in combination with molecular dynamics simulation and quantum chemical calculations.

### 4.2.1. Types of polymorphism

There are two main types of polymorphism: conformational and packing polymorphisms. In polymorphs of the former type, the crystal structure differences are the result of dissimilar molecular conformations in the polymorph unit cells.[965,966] One of the representatives of this type is mefenamic acid, which can exist as three polymorphs, one stable and two metastable ones.[967] The differences in the crystal structure of the packing polymorphs, for example, paracetamol polymorphs,[968–970] are caused by dissimilar packing of the molecules in a crystal, with the conformations of these molecules in various polymorphs being almost the same (Fig. 22).

There is a third, less frequent type of polymorphism called synthon polymorphism. The differences in the lattice in this case are caused by the formation of hydrogen-bonded cyclic and linear structures. For example, carbamazepine forms synthon-type polymorphs, in which the crystals contain cyclic hydrogen-bonded dimers or chain structures.

### 4.2.2. Methods of polymorph preparation

The key methods of obtaining different polymorphs include the methods based on thermal conversion or recrystallization from melts,[971–975] crystallization from solutions,[976–980] and mechanochemical treatment.[981,982] However, there are certain problems associated with their use. For example, thermal conversion is usually accompanied by sublimation.[975] In some cases, it is difficult to reproduce the

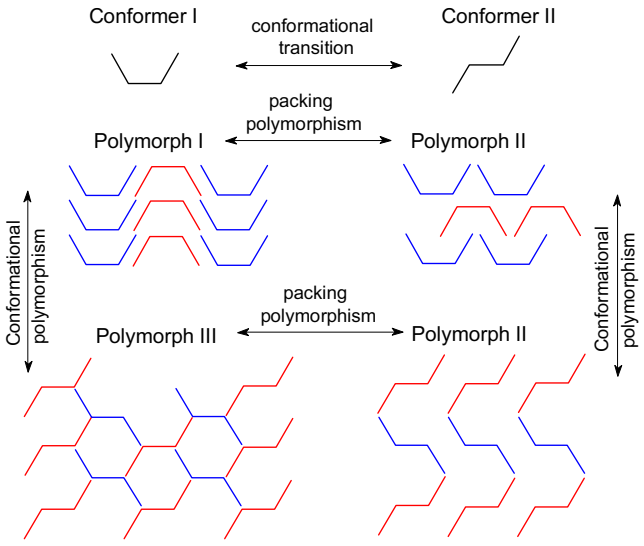



**Figure 22.** Schematic representation of conformational and packing polymorphisms.

obtained results.[973, 980, 983, 984] The biggest problems for pharmaceutical industry are the concomitant polymorphism,[985] meaning preparation of one polymorph contaminated with another one,[980] and disappearing polymorphism.[986 – 988] The latter term denotes an empirical situation where a polymorph that has been obtained earlier cannot be synthesized anymore even when all the necessary conditions are fulfilled.[989, 990] Finally, a compound that is formed may contain residual amounts of the solvent, in which it was dissolved. An effective way to solve some of these problems is application of SCF during the polymorph preparation.

#### 4.2.3. SCF technologies for obtaining crystalline forms of active pharmaceutical ingredients

Preparing crystal modifications of organic compounds with the help of SCF is, in fact, a separate branch of chemistry.[991 – 1001] SCF technologies used for obtaining crystal forms of drug compounds can be divided into two groups depending on the role played by the SCF, whether a solvent or an antisolvent. In the former case, the product crystallizes from an SCF solution and this process is accompanied by rapid SCF expansion, because of a significant reduction in the dissolving capacity and density (rapid expansion of supercritical fluids, RESS).[1002, 1003]

The RESS process consists of two stages: compound dissolution in SCF and subsequent precipitation of the solute particles upon fast decompression, which causes immediate supersaturation of the solution and, as a result, leads to nucleation and formation of micrometre and submicrometre particles.[1004] It was shown [1005, 1006] that the average diameter of the particles and their size distribution can be controlled by varying the process parameters, such as SCF temperature and pressure. Moreover, by varying the size of the nozzle and the expansion rate, it is possible to change the polymorph existing in the crystal phase. However, RESS can only be used when the material in question has relatively good solubility in sc-$CO_2$ ($> 10^{-4}$ mole fractions). The application of RESS to nonpolar and low-polar compounds also has its limitations.[1007, 1008] The dissolving capacity of sc-$CO_2$ can be increased by adding organic cosolvents [1009, 1010] or additives.[1011] Besides, nanosized particles (from 20 to 50 nm) can be formed when the solute precipitates in a liquid that does not dissolve the target compound or in an aqueous solution containing phospholipid particles mixed with a nonionic surfactant.[997]

A good alternative to RESS is the SAS method (see above), in which SCF acts as an antisolvent. In this case, adding sc-$CO_2$ to a solution of the target compound leads to its precipitation.[1012 – 1014] This method is used for micronization of substances that are insoluble or poorly soluble in sc-$CO_2$. If the thermodynamic and hydrodynamic characteristics of the binary solvent – antisolvent system are known, it is possible to control the size and morphology of the resulting particles.[1007, 1015, 1016] The process is usually conducted at temperatures of 308 – 333 K, which makes it possible to micronize thermally labile compounds.[1017] The known modifications of the SAS method have been surveyed.[997]

An important benefit of using sc-$CO_2$ for the formation of particles is product sterilization directly during the synthesis, because a lot of bacteria, fungi, and viruses are inactivated in this medium.[1018] However, the interrelation between the RESS and SAS parameters, on the one hand, and formation of drug compound polymorphs, on the other hand, has not yet been adequately studied.[1019 – 1025] For example, it is unclear whether the mechanism of solvation in SCF depends on the parameters of state. It has been proved that the mechanism of solvation in SCF solvents can vary in different parts of the phase diagram.[1026 – 1037]

The critically important factors for selecting the method of producing a drug compound (RESS or SAS) are the compound solubility in sc-$CO_2$ and the thermodynamic parameters ($P$ and $T$) of its synthesis. The compound solubility in SCF can be quite accurately measured by chromatography,[1038] 'vanishing point' method,[1039 – 1041] static recirculation, and dynamic flow methods,[1040 – 1047] and dynamic saturation technique.[1048] A promising approach to measuring API solubility in SCF is based on IR-spectroscopy, which makes it possible to determine very low concentrations of a solute (less than $10^{-6}$ mole fraction) within a wide range of parameters of state and to study the kinetics of API dissolution.[1049 – 1052] The solubilities of drug compound in sc-$CO_2$ and their dependences on the parameters of state are not the same for different polymorphs.[980, 1053 – 1055] Thus, the development of industrial processes of producing drug compounds using SCF requires comprehensive studies including not only API solubility measurements but also their polymorphism screening.

#### 4.2.4. Polymorphism of drug compounds in sc-$CO_2$

One of the first works in this field addressed polymorphism of a micronized carbamazepine powder obtained by the RESS method.[1056] The authors showed that it was possible to control the polymorphism of carbamazepine by changing the initial parameters of state of its solution in sc-$CO_2$. Later, the same results were obtained for tolbutamide and barbital micronization.[1019] Tuerk and Boltens [1057] found a region of the phase diagram of a tolbutamide solution in sc-$CO_2$ in which the RESS-process led to the formation of a stable second polymorph, whereas the first polymorph was formed beyond this region. But, despite the great progress made in the field of controlled polymorphism, all the results concerning the adiabatic expansion process were obtained empirically.

A similar situation is observed in the SAS processes, but in this case the polymorphism is affected by not only the SCF parameters of state, but also the organic solvent characteristics.[1058] For example, when acetone is replaced with ethanol for sulfathiazole micronization, the polymorph of the final product also changes.[1059] By studying the effect of a wide range of solvents (acetone, acetonitrile, tetrahydrofuran, and acetic acid) on the polymorphism of a micronized powder prepared for the SAS method, Clercq *et al.*[1060] were able to empirically select the optimal combinations of the solvent and process parameters that guaranteed the formation of several polymorphs and their mixtures. Certain achievements have been made along this line, but the major problem of these methods is the lack of correlation between the micronization parameters and polymorphism of the final form.

To look for such correlations, Oparin *et al.*[1061 – 1063] developed a comprehensive approach to studying the polymorphism of drug compounds in SCF. According to this approach, polymorphism screening is based on the analysis of conformational equilibria of molecules in the sc-$CO_2$ phase being in a thermodynamic equilibrium with the crystal phase of the compounds. By studying drug compounds with different types of polymorphism, the authors showed that there is a correlation between the conformational diversity of the compound molecules in the sc-$CO_2$

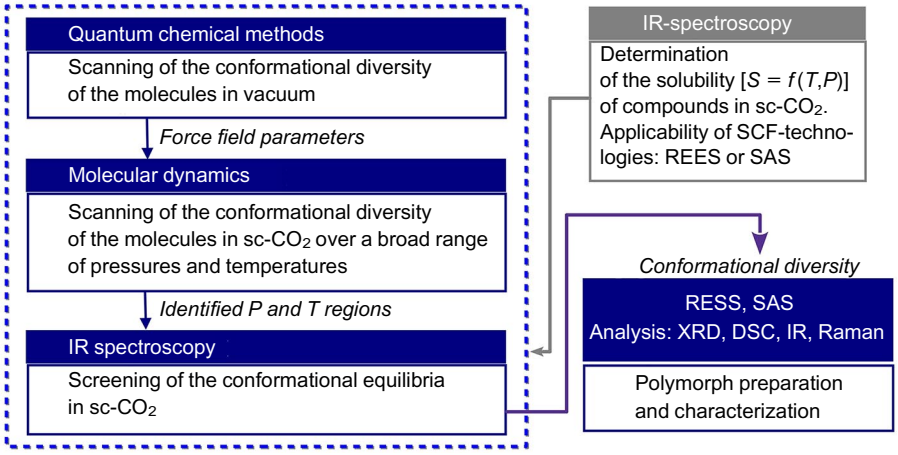



**Figure 23.** Diagram of the integrated approach to studying the polymorphism of drug compounds by SCF-based methods. XRD is X-ray diffraction, DSC is for differential scanning calorimetry.

phase and polymorphism of its crystal phase provided that these phases are in equilibrium.[1061 – 1063] The developed approach is a combination of theoretical [molecular dynamics simulation (MDS) and quantum chemical calculations] and experimental (IR spectroscopy) methods (Fig. 23) and is implemented as the following sequence:

— the first stage includes an IR spectroscopic study of the solubility of drug compounds in SCF within a wide range of parameters of state with the aim to select the more appropriate method (SAS or RESS);

— the next stage includes quantum chemical calculations for surveying the conformational diversity of the drug compound molecules in order to find the most stable conformers, determine their energy characteristics and vibrational frequencies of the functional groups involved in the conformational transitions;

— the third stage implies the use of MDS to select the force field for describing the intermolecular interactions in such a way as to achieve good reproducibility of potential energy curves related to the conformational transitions and obtained by the quantum chemical calculations; then the conformational diversity of the drug compound molecules in the solvent is examined over a wide range of parameters of state in order to identify the phase diagram regions in which particular conformers are formed and to find the energy barriers for the conformational transitions.

— the fourth stage consists in calculation of the API conformer populations in the SCF solution in the phase diagram regions identified by the MDS on the basis of IR spectroscopy data and results of the quantum chemical calculations. This calculation makes it possible to identify the effect of the thermodynamic parameters of state of the fluid solvent on the changes in the API conformational equilibria.

— finally, the target compound is crystallized from SCF at the parameters of state determined at the previous stages, which is followed by analysis of the microcrystalline phase in order to investigate its polymorph by the DSC, X-ray diffraction, and micro-IR and micro-Raman spectroscopy.

It is evident that such spectroscopic studies in a wide range of parameters of state, including supercritical values, require the use of special optical cells for operation at high temperatures and pressures. This imposes certain requirements on the cell material and design. A considerable contribution to the development of the cell design was made by Gorbaty *et al.*,[1064 – 1066] who took part in designing unique, conceptually different optical cells for UV, IR, Raman, and time-resolved IR spectroscopy and a system for sealing their parts.[1067, 1068] Such cells can operate within a wide range of parameters of state. As a result, Oparin *et al.*[1063] designed and manufactured a high-temperature high-pressure cell adjusted to various types of IR spectrometers equipped with a standard port for sample mounting. The optical cell described by Rey[1069] was used as the prototype for this cell. The adjustable coordinate positioning system allowed the authors to optimize the cell location inside the spectrometer for achieving the maximum signal level.

#### 4.2.5. Polymorphism of micronized forms of active pharmaceutical ingredients

In accordance with the developed integrated approach, Oparin *et al.*[1061] performed polymorphism screening of paracetamol obtained by crystallization from sc-$CO_2$ solution under isochoric heating within a wide range of temperature. The experiment consisted of two stages. First, the authors performed a detailed conformational analysis of paracetamol molecules dissolved in sc-$CO_2$ in the considered range of parameters of state based on the IR spectroscopy data and quantum chemical calculations. They found that at each point of the phase diagram, the spectral pattern corresponded to the equilibrium of two conformers, but melting and subsequent cooling in the sc-$CO_2$ phase gave rise to a third conformer.

Then the authors studied the paracetamol crystal structures that had formed during the sc-$CO_2$ treatment in the same thermodynamic conditions. The methods of micro-IR and micro-Raman spectroscopy and DSC showed that the paracetamol samples obtained from the bottom phase after sc-$CO_2$ treatment represented mixtures of two polymorphs. The micronized forms of paracetamol crystallized from the sc-$CO_2$ phase consisted of only the second polymorph. This fact should be taken into account for developing methods of preparation of pure second polymorph of paracetamol possessing better compactibility than the first one,[1070] which plays an important role in the manufacture of tablet dosage forms. These results show that, although paracetamol is characterized by the packing polymorphism, the

polymorphic transitions in the bottom phase correlate with the rearrangement of the conformational diversity of the molecules in the SCF occurring in equilibrium with the bottom phase.

Oparin *et al.*[1063] described the polymorphism screening of mefenamic acid dissolved in sc-$CO_2$ and being in a thermodynamic equilibrium with the bottom phase containing a constant excess of crystalline mefenamic acid in isochoric heating conditions. The experiment is based on the known fact about the thermal conversion of one polymorph of mefenamic acid to the second polymorph.[975] An analysis of the IR spectra of mefenamic acid dissolved in sc-$CO_2$, together with the quantum chemical data, showed that the conformational transition starts at a temperature close to the temperature of the onset of polymorphic transition of mefenamic acid in the solid phase ($\sim$160 °C). The authors also determined the regions of the phase diagram in which complete transition from the first conformational state to the second one was observed (180 – 190 °C). The *in situ* Raman spectroscopy study of the polymorphic transition of crystalline mefenamic acid in the bottom phase being in equilibrium with sc-$CO_2$ within the considered range of parameters of state showed that if the crystalline form of mefenamic acid and its solution in sc-$CO_2$ are in equilibrium, the polymorphic transition also starts at 160 °C and complete polymorphic transition is detected at 180 – 190 °C.

Two crystalline samples of mefenamic acid taken out of the experimental cell after its cooling and carbon dioxide removal were analyzed. The first sample was taken from the bottom part of the cell (sample holder), which contained an excess of mefenamic acid throughout the experiment; the second sample was taken from the upper part of the cell where precipitation of this API from sc-$CO_2$ solution took place. The micro-IR and micro-Raman spectroscopy methods showed that both samples represented pure second polymorph, and key differences between them was in the crystal phase grain size. From these results, it was concluded that there is a correlation between the polymorphism of the crystalline mefenamic acid and the conformational state of its molecules in sc-$CO_2$, if the phases are in a thermodynamic equilibrium with each other. This allows for the control over polymorphs by monitoring the conformational state of the molecules in the SCF solution. Since mefenamic acid has good solubility in sc-$CO_2$, a RESS-based method can be a reliable way of obtaining pure second polymorph.

Another interesting object of study is ibuprofen possessing a number of unique properties, including a considerable difference between the melting temperatures of its polymorphs,[973] and its ability to exist in the amorphous form within a wide range of parameters of state.[1071] Racemic ibuprofen, which is widely used in pharmaceutics, has two stable conformational polymorphs. Oparin *et al.*[1063] reported a study of the conformational equilibria of the molecules of racemic ibuprofen dissolved in sc-$CO_2$ and being in equilibrium with excess ibuprofen under isochoric heating along two isochors corresponding to high- and low-density states of the SCF solution. It was established that within the given range of temperatures, the SCF solution mainly contains conformers of the first type, which, according to the literature data [1072] and quantum chemical claculations, corresponds to the first polymorph. As the temperature becomes higher, the mole fraction of the first, energetically more favourable, conformer grows monotonically, while that of the second one decreases. Hence, taking into account the conformational type of ibuprofen polymorphism, it can be assumed that the RESS process within the studied temperature range must lead to the formation of a mixture of two polymorphs, with the content of the second polymorph being lower. This hypothesis was tested and confirmed by the DSC and X-ray diffraction data for micronized ibuprofen forms obtained by the RESS method from an sc-$CO_2$ solution at various temperatures.[1073] It was established that the micronized ibuprofen form prepared by the RESS method is generally the first polymorph, but its crystal structure is damaged and may contain amorphous phase microinclusions as defects. The content of these defects would decrease with increasing temperature of the initial SCF solution.

Thus, this Section gives a systematic account of the data obtained in the last 20 years about the polymorphism of drug compounds and its important role both for the API synthesis and for the preparation of the final pharmaceutical product. We analyzed the key types of polymorphism and identified the main aspects related to the importance of obtaining dosage forms with a high degree of purity and as the desired polymorph. The Section outlines the major problems faced in implementation of these tasks and the ways of solving these problems based on SCF technologies during the synthesis of drug compounds.

## 5. EPR spectroscopy of supercritical fluids

In some cases, electron paramagnetic resonance (EPR) spectroscopy can be a useful analytical tool for studying SCF and chemical processes conducted in SCF. This method provides information about the microstructure and microdynamics of the test specimens, the intermediates and mechanisms of reactions involving paramagnetic species.[1074] It is also successfully used to investigate diamagnetic media by introducing paramagnetic probes or labels (stable radicals either free or covalently bonded to molecules of the medium).[1075] Nitroxide radicals, organic compounds containing a >NO group bearing an unpaired electron, often act as such labels and probes. The high anisotropy of the hyperfine coupling (HFC) between the electron and the $^{14}N$ nucleus makes the spectra of nitroxides sensitive to rotational mobility (Fig. 24 *a*; TEMPO stands for 2,2,6,6-tetramethylpiperidine-1-oxyl). Besides, the exchange interaction of the electrons caused by their collisions affects the EPR spectral pattern and provides infor-

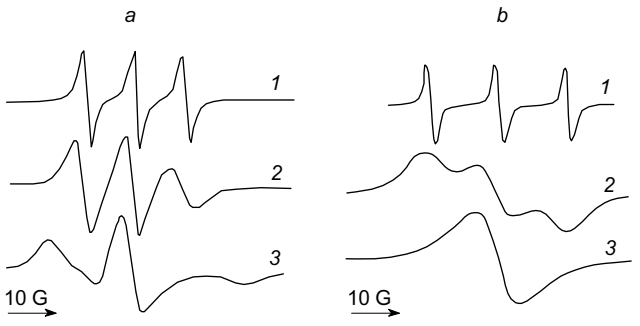



**Figure 24.** Theoretical EPR spectra of the TEMPO radical with the rotational correlation times of $1 \times 10^{-10}$ (*1*), $2 \times 10^{-9}$ (*2*), $2 \times 10^{-8}$ s (*3*) (*a*) and experimental spectra in toluene at the radical concentration of $1 \times 10^{-4}$ (*1*), $4 \times 10^{-2}$ (*2*), $8 \times 10^{-2}$ mol $L^{-1}$ (*3*) (*b*).[1075]

mation about the dynamics of translational motion (see Fig. 24 *b*).

### 5.1. EPR spectroscopy at a high pressure

High-pressure EPR spectroscopy was first applied in 1957.[1076] The numerous high-pressure experiments proposed since that time can be divided into two groups. The first group includes the experiments in which the cavity of the EPR spectrometer is placed into a high-pressure reactor made of a nonmagnetic alloy (beryllium copper or austenitic stainless steel).[1077, 1078] These systems can be used at pressures of up to 1.5 GPa, but they are difficult to operate.[1079] Experiments of the second group are based on the use of special tubes or capillaries, including those developed for high-pressure NMR spectroscopy (some are available commercially), and standard cavities and temperature-control systems. The pressure range is several tens or even several hundreds of megapascals.

High-pressure tubes are normally made of quartz or various grades of glass. In the simplest case, a required amount of a solvent (water, ethane, *etc.*) is placed into a thick-walled capillary, then the capilary is sealed and mounted into a standard cavity of an EPR [1080–1082] or NMR [1083] spectrometer. In 1972, using this approach, Shaulov *et al.*[1080] recorded (apparently, for the first time) an EPR spectrum near the critical point. A quartz tube was connected to the high-pressure system with Teflon-sealed coupling nut [1084, 1085] or with epoxy resin.[1086, 1087] The recommended pressure reached 20 MPa (in the tests, 35 MPa and 900 °C were used). For higher pressures (up to 400 MPa), thin quartz capillaries [with the outer ($d_{out}$) and inner ($d_{in}$) diameters of 0.36 and 0.1 mm, respectively, and volume ($V$) of 7 μL] were used. The capillaries were bent back and forth to fit into a standard tube.[1088–1090] The flow cell can be made of glass fibre [1091] or polyether ether ketone (PEEK).[1092] Besides, quartz tubes can be used for operating at pressures up to 30 MPa.[1093, 1094] The operating pressure range can be increased to 600 MPa by thorough treatment of quartz tubes ($d_{out}$ = 3.7 mm, $d_{in}$ = 1.0 mm) by a variety of techniques, including etching and annealing.[1095] High-pressure tubes can also be manufactured from pyrex,[1096, 1097] sapphire,[1098–1100] and polymer materials: polyvinyl chloride [1101] and PEEK.[1102, 1103] Tubes sealed at one end can be used in combination with a flow reactor.[1104]

### 5.2. EPR spectroscopy of supercritical fluids *in situ*: the main results

#### 5.2.1. Local increase in supercritical fluid density

The spectral parameters of a lot of substances depend on the dielectric permittivity ($\varepsilon$) of solvent; this can be used to estimate the local density ($\rho_{loc}$) of the media,[1105] including SCFs,[1106, 1107] by UV (Refs 1108, 1109), IR (Refs 1110, 1111), NMR (Ref. 1112), and EPR spectroscopy using molecular probes. For example, the dependence of the HFC constants ($a^N$) of nitroxides on the electrostatic interaction with a solvent can be formalized in terms of the Onsager theory.[1113–1115] The deviations from the theoretical dependence of the HFC constant on $\varepsilon$ and the solvent reduced density ($\rho_r$) were detected for stable di-*tert*-butylnitroxide (DTBN) in supercritical ethane,[1116] $CO_2$, and trifluoromethane [1092] and for TEMPO in supercritical $CO_2$ (Fig. 25 *a*).[1117]

The most pronounced (by a factor of 2 to 3) deviations of the solvent local density in the nitroxide solvation shell was observed at temperatures close to $T_c$ and average

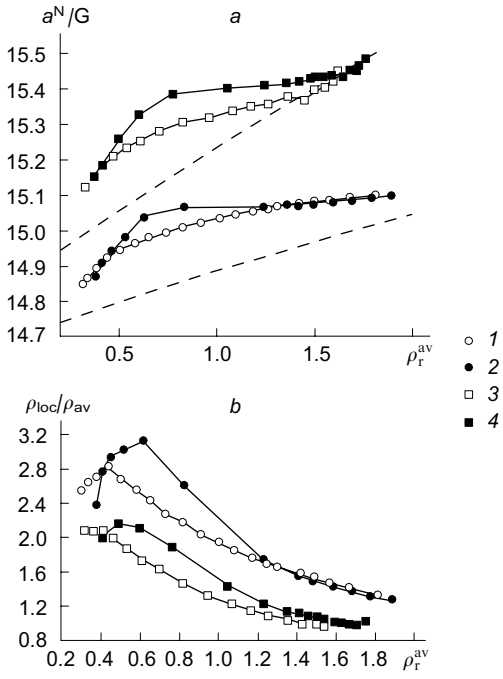



**Figure 25.** (*a*) HFC constants of nitroxides *vs.* average reduced density of the solvent and (*b*) local density to average density ratio *vs.* average reduced density of the solvent for DTBN in ethane (*1*, *2*) [1116] and TEMPO in $CO_2$ (*3*, *4*; Ref. 1117).[1116, 1117] Reduced temperature ($T_r$): 1.09 (*1*), 1.01 (*2*), 1.06 (*3*), 1.03 (*4*). The dashed lines show expected dependences of the HFC constants of the nitroxides on the average reduced density of the solvent at a constant local density. The figure was composed by the authors on the basis of reported data.[1116, 1117]

reduced density of about 0.6 (see Fig. 25 *b*), which is in line with the results obtained by other methods.[1118] As the temperature increased, the deviations diminished.

Solvent clustering can change the EPR spectrum linewidth due to the increase in the local viscosity, decrease in the rotational diffusion coefficients and spin-rotation constants. The contribution of the spin-rotation interaction to the linewidth in the liquid phase can be related to the solvent local viscosity and effective hydrodynamic radius of the probe, for example, by the Debye–Stokes–Einstein equation.[1119] This equation is valid for TEMPO in hexane or ethanol [1087] at pressures significantly exceeding the critical value [the reduced pressure in the experiments ($P_r$) is 2.32 for hexane and 1.63 for ethanol] both at $T < T_c$ and at $T > T_c$. However, in the vicinity of the critical point at $P_r \approx 1$ and $T_r > 1.03$, the rotational diffusion rate is higher than the value predicted by the Debye–Stokes–Einstein equation, but is lower than that in the gas phase. The researchers assumed that this could be the result of switching to the gas phase kinetics, on the one hand, and of increasing higher local density, on the other hand.

The rotational diffusion coefficients can also be estimated by a computer-assisted analysis of the EPR spectral shape. In sub- and supercritical conditions, a rotational diffusion coefficients accessible for EPR measurements are inherent in bulky transition metal chelates. An example of these chelates is copper 2,2,3-trimethyl-6,6,7,7,8,8,8-heptafluorooctane-5,5-dionate (CuFod), for which the rotational diffusion in sc-$CO_2$ with reduced density from 0.6 to 1.8 was found to be slower [1120] than that predicted by the

Debye – Stokes – Einstein equation.[1121] This fact can be explained by both $CO_2$ clustering around the complex and association of the complexes themselves (see below).

**5.2.2. Heisenberg spin exchange. Bimolecular processes**

Spin exchange interactions can be used as model processes for estimating the rate constants of diffusion-controlled chemical reactions. By modelling the EPR spectra, it is possible to measure the spin exchange rate. At high pressures, the spin exchange reaction kinetics in ethane,[1091] hexane, ethanol,[1087] and $CO_2$ (Ref. 112) can be adequately described by the Smoluchowski and Stokes – Einstein equations (Fig. 26 *a*).

However, at low pressures, the experimental spin exchange rate constants are much higher than those predicted by the Stokes – Einstein equation (see the dashed line in Fig. 26 *b*). Brownian dynamics modelling reproduces the spin exchange rate constants for high solvent densities, but if the density is below the critical value, the calculated rate constants are much lower than the values measured experimentally.[1092] This fact agrees with the above-mentioned assumption about the CuFod association at low $CO_2$ density.[1120] The higher spin exchange rate constants can be explained by the fact that collisions give rise to pairs that require collision with a solvent molecule to be broken[1087] (see Fig. 26 *a*).

Thus, in the region of high SCF densities, the standard equations of liquid-phase kinetics can adequately describe the kinetics of diffusion-controlled reactions in supercritical solvents, whereas in the region of low temperatures and low pressures ($< 1.5\,P_c$), the calculations must also take into account the formation of labile associates of the solute.

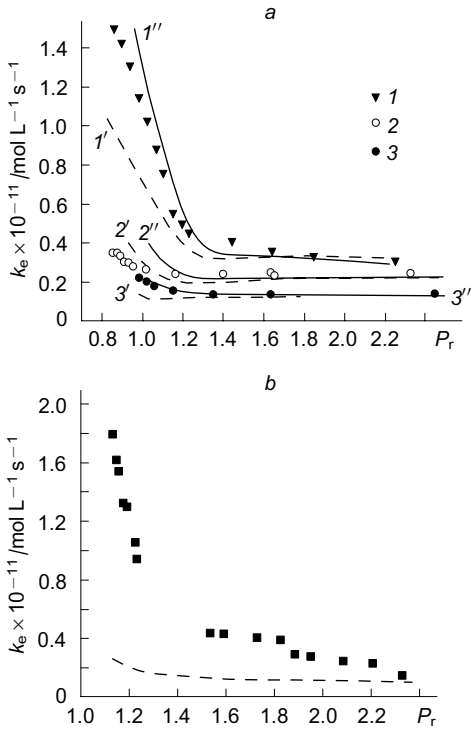



**Figure 26.** Spin exchange rate constants *vs.* reduced pressure for DTBN in ethane (*1*) at $T_r = 1.03$,[1091] TEMPO in hexane (*2*)[1087] and ethanol (*3*) at $T_r = 1.02$ (*a*),[1087] and for CuFod in $CO_2$ (*b*).[1120] Curves *1′ 2′* and *3′* show the calculation results by the Stokes – Einstein equation; curves *1″*, *2″*, and *3″* show the calculation results taking into account the association. The figure was composed by the authors on the basis of reported data.[1087, 1091, 1120]

**5.2.3. Clustering of substances dissolved in supercritical fluids**

Molecules of a substance dissolved in sub- and supercritical fluids can also participate in clustering.[1106] In a number of works, EPR spectroscopy was used for studying aggregation of spin-labelled cholesterol in sc-$CO_2$.[1122, 1123] Some of the measurements were made in the presence of immobilized spin-labelled cholesterol oxidase.[1094, 1124] The EPR spectra of nitroxides in standard solvents at concentrations about $10^{-3}$ mol L$^{-1}$ and lower consist of three narrow lines of approximately the same intensity and correspond to fast rotation [rotational correlation times ($\tau$) > $10^{-10} - 10^{-11}$ s]. At concentrations > 0.1 mol L$^{-1}$, the spectrum represents one broad signal caused by the spin-exchange interaction of paramagnetic species.[1075] The spectrum of a dilute ($6.5 \times 10^{-5} - 3.9 \times 10^{-3}$ mol L$^{-1}$) solution of spin-labelled cholesterol (3-doxyl-5α-cholestane) in sc-$CO_2$ at 11.2 MPa does not look like a triplet but represents a composition of broad lines that have almost merged into a singlet. The obtained results indicate a high local concentration of the spin-labelled cholesterol in sc-$CO_2$ at these parameters of state.

A radically different type of EPR spectra is characteristic of sc-$CO_2$ containing $0.27 \times 10^{-3}$ mol L$^{-1}$ of 3-doxyl-5α-cholestane in the presence of a small cholesterol excess ($1.4 \times 10^{-3}$ mol L$^{-1}$). At sc-$CO_2$ pressures above 8.9 MPa, the spectrum has three distinct broadened hyperfine structure components, indicating that the local concentration of paramagnetic species in these conditions is much higher than the average value. When the pressure drops from 8.9 to 8.5 MPa, the hyperfine structure almost completely degenerates, and the spectrum looks like a broad asymmetric singlet. Evidently, such pressure drop not only increases the local concentration of spin-labelled molecules but also changes the structure or size of the associates. This is probably explained by the formation of cholesterol aggregates with a higher content of paramagnetic species compared to that in sc-$CO_2$. Within the 8.1 – 8.3 MPa pressure range, the spectral pattern dramatically changes from that characteristic of aggregates to that typical of dilute solutions of fast rotating particles. Adding branched alcohols (2-methylpropan-2-ol and 2-methylpropan-1-ol) stimulates cholesterol aggregation, which is reflected in the EPR spectrum at 10.4 MPa and 308 K as a broad poorly-resolved singlet. Ethanol, n-butanol, acetone, and methanol stimulate cholesterol aggregation to a lesser extent.

At 308 K, the EPR spectrum of the ternary system comprised of 3-doxyl-5-α-cholestane, spin-labelled cholesterol oxidase covalently grafted to glass granules, and sc-$CO_2$ exhibits a broad singlet, the shape of which, in contrast to the previous case, remains practically unchanged within the range of pressure values of 8.17 – 10.4 MPa. Thus, in these conditions, several molecules of the spin-labelled cholesterol and the immobilized enzyme are brought very close to each other, which increases the rate of the enzymatic reaction. Similar regularities were also observed in solutions of stearic acid (the support of transesterification of triglycerides in SCF[1125]) and its spin-labelled analogue, 12-doxylstearic acid, in sc-$CO_2$.[1126]

This approach is applicable to solutions of transition metal salts in sub- and supercritical water. It is known that it is possible to obtain nanocrystalline or amorphous metastable phases of salts and oxides in these condi-

tions.[1127, 1128] The solvation degree of metal ions in supercritical water can become much lower,[1129] which will increase their local concentration. Trukhan *et al.*[1081, 1082] showed that when the temperature rises, the EPR signal intensity of a vanadyl sulfate solution in water increases, and at the critical temperature (608 K), no signal is registered, whereas above 668 K, the spectrum looks like an exchange-broadened singlet, being similar to the spectrum of a concentrated vanadyl sulfate solution in water at room temperature. A spectrum similar to that of dehydrated $VOSO_4$ was obtained in nonisothermal conditions.[1082] The authors suggested that the observed reversible effects of decreasing number of water molecules in the coordination sphere of the metal-containing ions and their local accumulation precede clustering and formation of mainly amorphous oxide particles.

#### 5.2.4. Micelle formation in supercritical fluids

The potential of using sc-$CO_2$ as a reaction medium is limited by low solubility of hydrophilic substances. A method of increasing the content of such substances is the formation of reverse micelles,[1130, 1131] *e.g.*, using the ammonium salt of carboxy-perfluoropolyether (PFPE).[1132, 1133] In the presence of PFPE in dry or water-saturated sc-$CO_2$ ($\rho$ = 3.75–8.55 mol $L^{-1}$, $T$ = 308 K), the rotational correlation time of 4-hydroxy-2,2,6,6-tetramethylpiperidine-1-oxyl (4-OH-TEMPO) is $10^{-10}$ s, whereas in pure sc-$CO_2$, the signal in the spectrum of 4-OH-TEMPO corresponds to fast isotropic rotation of a paramagnetic molecule[1133] [$\tau < 10^{-11}$ s (Ref. 1075)]. If the density of dry $CO_2$ is ~5 mol $L^{-1}$, the HFC constant for 4-OH-TEMPO is equal to ~1.52 mT, and in $CO_2$ in the presence of water and PFPE, it amounts to 1.63 mT, which approaches the value corresponding to water in normal conditions (1.71 mT). The increase in the density of the supercritical solvent to 10 mol $L^{-1}$ and more leads to a considerable decrease in the HFC constant of the nitroxide in the ternary system down to values typical of pure $CO_2$. Heitz *et al.*[1133] believe that these data mean that PFPE promotes the formation of water-filled or 'empty' micelles within a broad range of supercritical solvent density values.

In addition, the $Mn(PFPE)_2$ salt with the average molecular weight of ~2400 Da was used as a compound combining the properties of a surfactant and a spin probe. The spectrum of the metal-containing surfactant in water-saturated solutions in sc-$CO_2$ (water : surfactant = 40 : 1) consists of six lines and indicates the hydration of the manganese ion, supposedly, in the micelles formed. Having analyzed the linewidths and spectrum pattern as a whole, the authors concluded that there was no spin exchange in the system and, consequently, the local concentration of the paramagnetic centres was relatively low.

#### 5.2.5. Polymers in sub- and supercritical solvents

One of the most important areas of SCFT application is modification of polymers, such as their impregnation with small molecules, including molecules of biologically active substances, dyes, *etc.*, or, conversely, extraction of undesirable impurities, preparation of polymer mixtures, foams, and shapes of required architecture.[1134–1139] Despite the obvious importance of determining the mechanisms of these processes, EPR spectroscopy has hardly ever been used to study them. However, the available publications clearly demonstrate the potential of this approach in finding the regularities of polymer interaction with a sub- or supercritical fluid.

Connon *et al.*[1140] used a long-chain molecule of 16-doxyl-stearic acid as a spin probe to determine the $CO_2$ pressure at which poly(D,L-lactide) and its copolymers with glycolic acid undergo a transition from the glassy to viscoelastic state characterized by a sharp increase in the polymer chain mobility. In order to do that, they applied the standard approach [1075] based on measuring the distances between the outermost lines in the nitroxide spectrum. According to estimates,[1075] a distance of 5.0 mT corresponds to the phase transition. The corresponding pressure is designated by P50G. It was found that at 308 K, this transition occurs at a pressure of ~3 MPa, which is much lower than the critical pressure. The authors did not find any differences between the transition pressures for polymers with different lactic to glycolic acid ratios or for semicrystalline poly(L-lactide). In the latter case, the absence of differences was explained by the fact that a spin probe is usually located only in the amorphous regions of the polymer. Similar studies were later carried out for poly(ethyl methacrylate) (PEMA) and poly(vinyl acetate) (PVA).[1141] The authors used 4-benzoyloxy-2,2,6,6-tetramethylpiperidine-1-oxyl (BzONO) and 5,5-dimethyl-2,2-di-n-nonyloxazolidine-3-oxyl (DNOZ) with different sizes of the molecules as the spin probes. DNOZ had been earlier shown[1142] to be virtually insensitive to changes in the polymer free volume. The EPR spectra of this compound recorded at 298 K show a gradual increase in the rotational mobility of the nitroxide moiety.

When the smaller BzONO probe is used, the EPR spectra over a wide range of pressures show a superposition of the spectra of 'slow' (almost identical in the rotational parameters to the BzONO spectra at atmospheric pressure) and 'fast' paramagnetic particles. Most of the authors explain this effect by the free volume size distribution in the polymers.[1143, 1144] Considering the BzONO size (the molecule radius is ~4.1 Å in the spherical approximation[1145]), it is possible to qualitatively evaluate the free volume and its dependence on pressure in different polymers. The rotational correlation times of the 'slow' probe in PVA do not depend on pressure and equal $4.95 \times 10^{-8}$ s, whereas the corresponding values for the fast-rotating probe decrease from $2.55 \times 10^{-8}$ to $1.5 \times 10^{-8}$ s as the pressure rises from 14.8 to 22.9 MPa. Thus, the effect of sc-$CO_2$ on the mobility of the polymer chains at high pressures is similar to the action of standard plasticizers, but the amount of carbon dioxide required to achieve a particular probe mobility is much lower than, for instance, the amount of dibutyl phthalate.[1141]

### 5.3. EPR spectroscopy of intermediates of chemical reactions in supercritical fluids

EPR spectroscopy *in situ* was first applied for studying the mechanisms of chemical reactions before the start of the widespread use of SCFs in synthesis, for example, for investigating the pyrolysis reactions at high temperatures. At pressure values above the critical point, the spin-rotational interaction does not significantly change the EPR spectral linewidth, and it is possible to record well-resolved spectra of radical intermediates.[1084, 1146, 1147] Thus, scientists were able to identify the radical intermediates of thermal decomposition reactions of indene, cumene,[1084] 1,2-diphenylethane,[1084, 1146] and dibenzyl ether.[1147] However, even in model conditions the attempts to collect the

spectra of all the radical intermediates were unsuccessful. For example, the only spectrum measured during the thermal decomposition of 1,2-diphenylethane (**9**) at 460 – 560 °C is that of 1,2-diphenylethyl. However, there is another intermediate, a benzyl radical, formed in the first step.

The spectra of short-lived ( < 1 ms) radical intermediates in supercritical fluids can be recorded with the help of time-resolved electron paramagnetic resonance spectroscopy (TREPR), or time-resolved continuous wave electron paramagnetic resonance spectroscopy [TR(CW)EPR].[1148] This method is often applied to study the mechanisms of photochemical reactions. Using this method, the authors recorded the spectra of the products of photolysis of free radical initiators, azobis(isobutyronitrile), bis(perfluoro-2-propoxypropionyl) peroxide,[1086] dimethoxyphenylacetophenone, and trimethylbenzoyldiphenylphosphine oxide,[1149] in sc-$CO_2$ and estimated the chain initiation rate constant. A serious limitation of this approach is its lower sensitivity compared to that of steady-state EPR spectroscopy.

Generally, these problems, especially those associated with low concentrations and short lifetimes of radical intermediates, are not inherent in the EPR spectroscopy in SCF. Similar problems restrict the application of EPR spectroscopy *in situ* in catalysis.[1150]

The data given above confirm the unique potential of using the EPR method *in situ* for determining the structural features of SCF and physicochemical processes in them. EPR spectroscopy complements the information obtained by other methods with data on the dynamics of rotary and translational motion of paramagnetic centres present in sub- and supercritical fluids or in specially introduced spin probes and labels. Unfortunately, the number of publications addressing *in situ* EPR studies is so far rather small in comparison with that dealing with NMR and IR spectroscopy methods. Hopefully, the development of new instruments such as the so-called EPR-on-a-chip [1151] will considerably expand the scope of applicability of EPR *in situ* in SCF studies.

## 6. Conclusion

The data presented in this review indicate that the application of supercritical fluids in chemistry and chemical engineering opens up great opportunities. The use of supercritical fluid technologies can become the key to synthesizing catalysts, supports, adsorbents, and functional materials with unique properties that are not typical of the systems obtained by traditional methods. Despite the relatively high costs of equipment for operating in supercritical conditions, the rapid development of technologies, appearance of new materials and engineering solutions are gradually making the methods implemented at elevated temperatures and pressures more available and economically attractive.

The number of publications devoted to the synthesis of heterogeneous catalysts using the supercritical state of matter grows quickly. Catalysts prepared by this method often demonstrate unprecedented activity and selectivity in basic bulk chemical and petrochemical processes and also in the synthesis of functional materials with desired properties. Quite promising is the use of SCFs for preparation of supported catalysts. The most interesting supports for generation of active sites with specified structure and morphology are various types of polymer materials that swell in sc-$CO_2$ . However, the use of composites obtained in these conditions and containing metal nanoparticles in the support matrix is still limited to a relatively small range of chemical reactions. Such composites have been mainly tested in hydrogenation processes and in Suzuki – Miyaura coupling reactions, which means that other catalytic processes are yet to be studied.

The unique physicochemical properties and high H-donor activity make sc-alcohols quite promising candidates for the application in reduction reactions of organic compounds and their mixtures. The prospects for using sc-alcohols in processing of substrates, such as lignocellulosic biomass, heavy oil fractions, and bio-oil, seem quite real, especially in view of multifold scalability of these processes. The effective dissolving and wetting capability and excellent diffusion and mass transfer characteristics of sc-alcohols speed up the degradation of the native structure of macromolecules, while the reducing capacity of these alcohols allows them to be used in catalytic and catalyst-free hydrogenolysis of C – O, C – S, C – N, or C – Hal single bonds and hydrogenation of multiple bonds in these substrates.

Excellent results are achieved by SCF application in fine organic synthesis. A number of asymmetric reactions catalyzed by transition metal complexes, such as hydrogenation, hydroformylation, alkylation, cycloaddition, allylation, hydrovinylation, cyclopropanation, epoxidation, and some other reactions that are widely used for preparing bioactive substances, can be efficiently carried out in the sc-$CO_2$ medium. Supercritical fluids are compatible with organocatalysts, which do not require reagent activation with metals and produce a minimum amount of waste (the atom economy principle). Further studies of organocatalytic processes in sub- and supercritical fluids can pave the way for efficient green technologies of obtaining the most active drug enantiomers free of adverse effects.

An extremely important field of sc-$CO_2$ application is the synthesis of polymer materials. This approach has a number of economic, environmental, and technological advantages. It eliminates expensive drying of polymers and removal of polymerization side products and allows obtaining polymers with the desired molecular weight and physicochemical properties by changing the $CO_2$ temperature and pressure.

An important problem is the development of new environmentally safe and inexpensive SCF methods of synthesis of aerogels and other foamed materials. By changing the foaming parameters (pressure, temperature, saturation – decompression time, *etc.*), it is possible to control the porous structure morphology, which determines the set of mechanical and physicochemical properties of a material. Aerogels are highly efficient heat-insulating materials. Besides, they can be used for protection of people and electronic devices from electromagnetic radiation and in medicine.

Quite an effective method for modification of high-molecular-weight compounds to endow them with new functional properties and to fabricate polymer composites is based on polymer impregnation with functional compounds of different nature, including photochromic ones, in a $CO_2$ medium. The simple procedure of sc-$CO_2$ removal from the polymer after the impregnation makes it possible to exclude the undesirable effect of the solvent on the composite properties.

Great opportunities are offered by SCF application in the manufacture of materials for medical purposes. One of

the most promising trends in this field is fabrication of scaffolds for reconstructive surgery, including safe-to-use tissue implants of xenogeneic and allogeneic origin. An effective technique of their decellularization can be based on using a nontoxic, renewable, and available solvent, such as sc-$CO_2$. This approach makes it possible to completely remove the cellular component without serious changes in the structural arrangement and chemical composition of the extracellular matrix and to obtain a product with mechanical properties resembling those of the native tissue. The possibility of combining decellularization and sterilization, together with the ease of fluid removal can significantly reduce the duration and costs of tissue graft production and bring about new opportunities for using sc-$CO_2$ as an effective tool for the design of tissue grafts of the future.

SCFs can be used as media for polymorphic transformations of drug compounds. It is worth noting that in substances characterized by different types of polymorphism, there is a correlation between the structure of conformers in the sc-$CO_2$ phase and the resulting polymorphs. This means that it is possible to obtain microparticles of certain, highly-effective dosage forms possessing high bioavailability.

Useful information about the SCF structure and physicochemical processes that occur in them can be gained by EPR spectroscopy. This method provides data about the dynamics of rotary and translational motion of paramagnetic centres present in sub- and supercritical fluids or spin probes and labels that are introduced into them for a certain purpose. The authors hope that the development of new technologies, such as the so-called EPR-on-a-chip, would considerably expand the applicability of EPR spectroscopy for *in situ* studies of the SCF properties and would make it possible to obtain new data that would promote the use of these promising media in chemistry and chemical engineering.

Section 2.1 was prepared with the financial support of the Russian Foundation for Basic Research (RFBR) (Project No. 18-29-06032); Section 2.2 was supported by the Ministry of Education and Science of the Russian Federation (Project No. 075-15-2019-1876) and the RFBR (Project No.18-29-06022); Section 2.3 was supported by the RFBR (Project 18-29-06072 mk); Section 3.1.1 was supported by the Russian Science Foundation (RSF) (Project No.18-73-10153); Sections 3.1.2, 3.1.3, and 3.1.4 were supported by the Ministry of Education and Science of the Russian Federation (Grant of the Government of the Russian Federation No. 14.W03.31.0018) and the RFBR (Project Nos 18-03-00275 and 18-29-09166); Section 3.2.1was supported by the RSF (Project No. 20-73-10180), Section 3.2.2 was supported by the RSF (Project No. 19-19-00614); Section 3.3 was financed within a state assignment (Theme 0082-2019-0012, No. AAAA-A20-120021190043-7) and was also supported by the RFBR (Project No. 18-29-06019mk); Section 4.1was supported by the RFBR (Project Nos 18-29-06059, 33-00982 mol_a) and the RSF (Project No. 18-15-00401); Section 4.2 was supported by the RFBR (Project Nos 18-29-06008_mk, 18-03-00255); Section 5 was supported by the RFBR (Project No. 18-29-06059).

The authors would like to express their gratitude to the Russian Foundation for Basic Research (Project No. 19-13-50154_Expansion) for the financial support in preparation of this review.

## References

1. I.Chorkendorff, J.W.Niemantsverdriet. In *Concepts of Modern Catalysis and Kinetics*. (New York: Wiley-VCH, 2003). P. 1
2. P.T.Anastas, J.C.Warner. In *Green Chemistry: Theory and Practice*. (Oxford: Oxford University Press, 2000). P. 135
3. R.Noyori. *Chem. Commun.*, 1807 (2005)
4. V.Polshettiwar, R.S.Varma. *Green Chem.*, **12**, 743 (2010)
5. S.Olveira, S.P.Forster, S.Seeger. *J. Nanotechnol.*, Art. ID 324089 (2014)
6. V.I.Bukhtiyarov, B.L.Moroz, I.E.Bekk, I.P.Prosvirin. *Catal. Ind.*, **1**, 17 (2009)
7. F.Tao. In *Metal Nanoparticles for Catalysis: Advances and Applications*. (London: Royal Society of Chemistry, 2014). P. 285
8. P.Claus, A.Brückner, C.Mohr, H.Hofmeister. *J. Am. Chem. Soc.*, **122**, 11430 (2000)
9. K.Okitzu, S.Nagaoka, S.Tanabe, H.Matsumoto, Y.Mizukoshi, Y.Nagata. *Chem. Lett.*, **3**, 271 (1999)
10. J.M.Miller, B.Dunn, T.D.Tran, R.W.Pekala. *J. Electrochem. Soc.* **144**, L309 (1997)
11. F.J.Maldonado-Hodar, C.Moreno-Castilla, J.Rivera-Utrilla, M.A.Ferro-Garcia. *Stud. Surf. Sci. Catal.*, **130**, 1007 (2000)
12. E.Bekyarova, K.Kaneko. *Adv. Mater.*, **12**, 1625 (2000)
13. B.L.Cushing, V.L.Kolesnichenko, C.J.O'Connor. *Chem. Rev.*, **104**, 3893 (2004)
14. D.P.Long, J.M.Blackburn, J.J.Watkins. *Adv. Mater.*, **12**, 913 (2000)
15. D.A.Lemenovskii, V.N.Bagratashvili. *Soros. Obrazov. Zh.*, **10** (10), 36 (1999)
16. M.Polyakov, V.N.Bagratashvili. *Ross. Khim. Zh.*, **43** (2), 93 (1999)
17. D.Yu.Zalepugin, N.A.Til'kunova, I.V.Chernysheva, V.S.Polyakov. *Sverkhkriticheskie Flyuidy: Teoriya i Praktika*, **1** (1), 27 (2006)
18. Y.Zhang, C.Erkey. *J. Supercrit. Fluids*, **38**, 252 (2006)
19. J.M.Campelo, D.Luna, R.Luque, J.M.Marinas, A.A.Romero. *ChemSusChem.*, **2**, 18 (2009)
20. X.-R.Ye, Y.Lin, C.Wang, M.H.Engelhard, Y.Wang, C.M.Wai. *J. Mater. Chem.*, **14**, 908 (2004)
21. Y.Zhang, D.Kang, C.Saquing, M.Aindow, C.Erkey. *Ind. Eng. Chem. Res.*, **44**, 4161 (2005)
22. S.Yoda, A.Hasegawa, H.Suda, Y.Uchimaru, K.Haraya, T.Tsuji, K.Otake. *Chem. Mater.*, **16**, 2363 (2004)
23. M.J.Tenorio, A.Cabañas, C.Pando, C.P.Juan, A.R.Renuncio. *J. Supercrit. Fluids*, **70**, 106 (2012)
24. S.E.Bozbag, S.O.Kostenko, M.A.Kurykin, V.N.Khrustalev, A.R.Khokhlov, L.Zhang, M.Aindow, C.Erkey. *J. Nanopart. Res.*, **14**, 973 (2012)
25. N.G.Smart, T.Carleson, T.Kas, A.A.Clifford, M.D.Burford, C.M.Wai. *Talanta*, **44**, 137 (1997)
26. C.Erkey. *Supercritical Fluids and Organometallic Compounds: from Recovery of Trace Metal to Synthesis of Nanostructured Materials*. Vol. 1. (1st Edn.). (Amsterdam: Elsevier Science, 2011)
27. J.Morère, M.J.Tenorio, C.Pando, J.A.R.Renuncio, A.Cabañas. *J. Chem. Thermodyn.*, **58**, 55 (2013)
28. X.-Q.Bian, J.Li, J.Chen, M.-J.Li., Z.-M.Du. *Chem. Eng. Res. Des.*, **104**, 416 (2015)
29. I.Ushiki, Y.Sato, S.Takishima, H.Inomata. *J. Chem. Eng.*, **52**, 243 (2019)
30. J.J.Watkins, T.J.McCarthy. *Chem. Mater.*, **7**, 1991 (1995)
31. G.L.Weibel, C.K.Ober. *Microelectron. Eng.*, **65**, 145 (2003)

32. Y.Lin, X.Cui, C.H.Yen, C.M.Wai. *Langmuir*, **21**, 11474 (2005)
33. Y.Haldorai, J.-J.Shim, K.T.Lim. *J. Supercrit. Fluids*, **71**, 45 (2012)
34. J.Zhang, M.Chaker, D.Ma. *J. Colloid Int. Sci.*, **489**, 138 (2016)
35. S.Nakahara, S.Stauss, T.Kato, T.Sasaki, K.Terashima. *J. Appl. Phys.*, **109**, 123304 (2011)
36. S.Machmudah, T.Wahyudiono, N.Takada, H.Kanda, K.Sasaki, M.Goto. *Adv. Nat. Sci. Nanosci. Nanotechnol.*, **4**, 045011 (2013)
37. A.O.Rybaltovskii, V.M.Buznik, Y.S.Zavorotny, N.V.Minaev, P.S.Timashev, S.N.Churbanov, V.N.Bagratashvili. *Russ. J. Phys. Chem. B*, **12**, 1160 (2018)
38. A.Singh, T.Salminen, M.Honkanen, J.Vihinen, L.Hyvärinen, E.Levänen. *Appl. Surf. Sci.*, **476**, 822 (2019)
39. E.O.Epifanov, A.G.Shubnyi, N.V.Minaev, A.O.Rybaltovskii, V.I.Yusupov, O.P.Parenago. In *Sverkhkriticheskie Flyuidy: Fundamental'nye Osnovy, Tekhnologii, Innovatsii. (Tez. Dokl. X Nauchno-Prakticheskoi Konferentsii s Mezhdunarodnym Uchastiem)*. [Supercritical Fluids: Fundamentals, Technologies, Innovations (Abstracts of Reports of the Xth Scientific and Practical Conference with International Participation)] (Rostov-on-Don, 2019). P. 367
40. E.O.Epifanov, A.G.Shubnyi, N.V.Minaev, A.O.Rybaltovskii, V.I.Yusupov, O.P.Parenago. *Sverkhkriticheskie Flyuidy: Theory and Practice*, **13** (3), 64 (2019)
41. J.Kim, G.W.Roberts, D.J.Kiserow. *Chem. Mater.*, **18**, 4710 (2006)
42. J.Kim, M.J.Kelly, H.H.Lamb, G.W.Roberts, D.J.Kiserow. *J. Phys. Chem. C*, **112**, 10446 (2008)
43. M.J.Kelly, J.Kim, G.W.Roberts, H.H.Lamb. *Top. Catal.*, **49**, 178 (2008)
44. J.W.Deal, P.Le, C.B.Corey, K.More, C.W.West. *J. Supercrit. Fluids*, **119**, 113 (2017)
45. F.Ulusal, B.Darendeli, E.Erünal, A.Egitmen, B.Guzel. *J. Supercrit. Fluids*, **127**, 111 (2017)
46. B.Wong, S.Yoda, S.M.Howdle. *J. Supercrit. Fluids*, **42**, 282 (2007)
47. X.Wang, H.Kawanami, S.E.Dapurkar, N.S.Venkataramanan, M.Chatterjee, T.Yokoyama, Y.Ikushima. *Appl. Catal. A*, **349**, 86 (2008)
48. A.Zeid, A.L.Othman. *Materials*, **5**, 2874 (2012)
49. J.A.Cecilia, R.M.Tost, M.R.Millán. *Int. J. Mol. Sci.*, **20**, 3213 (2019)
50. J.Morère, M.J.Tenorio, M.J.Torralvo, C.Pando, J.A.R.Renuncio, A.Cabañas. *J. Supercrit. Fluids*, **56**, 213 (2011)
51. A.J.Hunt, V.L.Budarin, J.W.Comerford, H.L.Parker, V.K.Lazarov, S.W.Breeden, D.J.Macquarrie, J.H.Clark. *Mater. Lett.*, **116**, 408 (2014)
52. F.Ulusal, E.Erunal, B.Guzel. *J. Nanopart. Res.*, **20**, 13 (2018)
53. Y.Kai, L.Todd, L.Jiayou, X.Xianmei. *Sci. Adv. Mater.*, **6**, 135 (2014)
54. P.L.Dhepe, A.Fukuoka, M.Ichikawa. *Catal. Lett.*, **81**, 69 (2002)
55. I.Ushiki, N.Takahashi, T.Shimizu, Y.Sato, M.Ota, R.L.Smith, H.Inomata. *J. Supercrit. Fluids*, **120**, 240 (2017)
56. I.Ushiki, M.Koike, T.Shimizu, Y.Sato. *J. Supercrit. Fluids*, **140**, 329 (2018)
57. I.Ushiki, N.Takahashi, M.Koike, Y.Sato, S.Takishima, H.Inomata. *J. Supercrit. Fluids*, **135**, 137 (2018)
58. M.Charoenchaitrakool, M.Chareonpanich, P.Saithongsuk. In *Proceedings of the 3rd World Congress on Mechanical, Chemical, and Material Engineering*. (Rome, Italy, 2017). Paper No. ICCPE 103
59. G.-Y.Qiao, Q.-Q.Xu, J.-Z.Yin, A.-Q.Wang, G.Xu. *J. Supercrit. Fluids*, **128**, 18 (2017)
60. T.Shimizu, I.Ushiki, M.Ota, Y.Sato. *J. Chem. Eng.*, **45**, 615 (2012)
61. C.H.Yen, H.W.Lin, T.D.Phan, C.-S.Tan. *J. Nanosci. Nanotechnol.*, **11**, 2465 (2011)
62. Y.Qiao, N.Said, M.Rauser, K.Yan, F.Qin, N.Theyssen, W.Leitner. *Green Chem.*, **19**, 977 (2017)
63. B.Cangül, L.C.Zhang, M.Aindow, C.Erkey. *J. Supercrit. Fluids*, **50**, 82 (2009)
64. I.V.Elmanovich, A.V.Naumkin, M.O.Gallyamov, A.R.Khokhlov. *J. Nanopart. Res.*, **14**, 733 (2012)
65. C.Wang, S.Guo, X.Pan, W.Chen, X.Bao. *J. Mater. Chem.*, **18**, 5782 (2008)
66. H.B.Pan, C.H.Yen, B.Yoon, M.Sato, C.M.Wai. *J. Synth. Commun.*, **36**, 3473 (2006)
67. Y.Lin, X.Cui, C.Yen, C.M.Wai. *J. Phys. Chem. B*, **109**, 14410 (2005)
68. C.H.Yen, X.Cui, H.-B.Pan, S.Wang, Y.Lin, C.M.Wai. *J. Nanosci. Nanotechnol.*, **5**, 1852 (2005)
69. C.H.Yen, K.Shimizu, Y.Lin, F.Bailey, I.F.Cheng, C.M.Wai. *Energy Fuels*, **214**, 2268 (2007)
70. J.Zhao, Lig.Zhang, T.Chen, H.Yu, Lin Zhang, H.Xue, H.Hu. *J. Phys. Chem. C*, **116**, 21374 (2012)
71. J.Morère, E.Sánchez-Miguel, M.J.Tenorio, C.Pando, A.Cabañas. *J. Supercrit. Fluids*, **120**, 7 (2017)
72. K.S.Morley, P.Licence, P.C.Marr, J.R.Hyde, P.D.Brown, R.Mokaya, Y.Xia, S.M.Howdle. *J. Mater. Chem.*, **14**, 1212 (2004)
73. G.Caputo, I.De Marco, E.Reverchon. *J. Supercrit. Fluids*, **54**, 243 (2010)
74. C.D.Saquing, T.Cheng, M.Aindow, C.Erkey. *J. Phys. Chem. B*, **108**, 7716 (2004)
75. C.D.Saquing, D.Kang, M.Aindow, C.Erkey. *Microporous Mesoporous Mater.*, **80**, 11 (2005)
76. Y.Zhang, D.Kang, M.Aindow, C.Erkey. *J. Phys. Chem. B*, **109**, 2617 (2005)
77. S.E.Bozbag, N.S.Yasar, L.C.Zhang, M.Aindow, C.Erkey. *J. Supercrit. Fluids*, **56**, 105 (2011)
78. S.K.Morley, P.C.Marr, P.B.Webb, A.R.Berry, F.J.Allison, G.Moldovan, P.D.Brown, S.M.Howdle. *J. Mater. Chem.*, **12**, 1898 (2002)
79. M.L.Ge, F.C.Ding, C.Erkey. *Adv. Mater. Res.*, **418 – 420**, 2260 (2012)
80. S.Miao, C.Zhang, Z.Liu, B.Han, Y.Xie, S.Ding, Z.Yang. *J. Phys. Chem. C*, **112**, 774 (2008)
81. N.Y.Baran, T.Baran, A.Menteş. *Carbohydr. Polym.*, **181**, 596 (2018)
82. R.M.Crooks, M.Zhao, L.Sun, V.Chechik, L.K.Yeung. *Acc. Chem. Res.*, **34**, 181 (2001)
83. M.Ooe, M.Murata, T.Mizugaki, K.Ebitani, K.Kaneda. *Nano Lett.*, **2**, 999 (2002)
84. Y.Niu, R.M.Crooks. *C. R. Chimie*, **6**, 1049 (2003)
85. E.A.Karakhanov, A.L.Maximov, V.A.Skorkin, A.V.Zolotukhina, A.S.Smerdov, A.Y.Tereshchenko. *Pure Appl. Chem.*, **81**, 2013 (2009)
86. E.Karakhanov, A.Maximov, A.Zolotukhina, N.Yatmanova, E.Rosenberg. *Appl. Organomet. Chem.*, **29**, 777 (2015)
87. E.Karakhanov, A.Maximov, A.Zolotukhina, A.Mamadlia, A.Vutolkina, A.Ivanov. *Catalysts*, **7**, 86 (2017)
88. E.A.Karakhanov, A.L.Maximov, E.M.Zakharyan, A.V.Zolotukhina, A.O.Ivanov. *Mol. Catal.*, **440**, 107 (2017)
89. A.Maximov, E.Karakhanov, A.Zolotukhina, A.Ivanov. *ChemistryOpen*, **8**, 358 (2019)

90. A.Maximov, E.Kararhanov, A.Zolotukhina. *Mol. Catal.*, **469**, 98 (2019)
91. I.O.Rybakova, A.E.Lazhko, A.V.Zolotuchina, P.S.Timashev, V.N.Bagratashvili, A.L.Maksimov, E.A.Karakhanov, O.P.Parenago. *Russ. J. Phys. Chem. B*, **10**, 1163 (2016)
92. O.P.Parenago, P.S.Timashev, E.A.Karakhanov, A.L.Maksimov, A.E.Lazhko, A.V.Zolotukhina, V.N.Bagratashvili. *J. Supercrit. Fluids*, **140**, 387 (2018)
93. P.M.Gallagher, M.P.Coffey, V.J.Krukonis, W.W Hillstrom. *J. Supercrit. Fluids*, **5**, 130 (1992)
94. E.Reverchon, C.Celano, G.Della Porta, A.Di Trolio, S.Pace. *J. Mater. Res.*, **13**, 284 (1998)
95. E.Reverchon, G.Della Porta, A.Di Trolio, S.Pace. *Ind. Eng. Chem. Res.*, **37**, 952 (1998)
96. E.Reverchon, I.De Marco, G.Della Porta. *J. Supercrit. Fluids*, **23**, 81 (2002)
97. H.Kamiya, A.Kondo, T.Yokoyama, M.Naito, G.Jimbo, S.Nagaya, M.Miyajima, I.Hirabayashi. *Adv. Powder Technol.*, **5**, 339 (1994)
98. P.Chattopadhyay, R.B.Gupta. *Ind. Eng. Chem. Res.*, **39**, 2281 (2000)
99. M.Rueda, L.M.Sanz-Moral, Á.Martín. *Cryst. Growth Des.*, **14**, 4768 (2014)
100. Y.Song, Y.Yang, H.Liang. *J. Chem. Eng. Jpn.*, **42**, 117 (2009)
101. S.Palakodaty, P.York, J.Pritchard. *Pharm. Res.*, **15**, 1835 (1998)
102. I.De Marco, E.Reverchon. *Chem. Eng. J.*, **187**, 401 (2012)
103. E.Reverchon, G.Della Porta, E.Torino. *J. Supercrit. Fluids*, **53**, 95 (2010)
104. A.Montes, M.D.Gordillo, C.Pereyra, N.de la Rosa-Fox, E.J.Martínez de la Ossa. *J. Supercrit. Fluids*, **75**, 88 (2013)
105. Z.-R.Tang, J.K.Bartley, S.H.Taylor, G.J.Hutchings. In *Studies in Surface Science and Catalysis*. (Amsterdam: Elsevier Science, 2006). P. 219
106. Z.Tang, J.Edwards, J.Bartley, S.Taylor, A.Carley, A.Herzing, C.Kiely, G.Hutchings. *J. Catal.*, **249**, 208 (2007)
107. P.J.Miedziak, Z.Tang, T.E.Davies, D.I.Enache, J.K.Bartley, A.F.Carley, A.A.Herzing, C.J.Kiely, S.H.Taylor, G.J.Hutchings. *J. Mater. Chem.*, **19**, 8619 (2009)
108. T.Lu, S.Blackburn, C.Dickinson, M.J.Rosseinsky, G.Hutchings, S.Axon, G.A.Leeke. *Powder Technol.*, **188**, 264 (2009)
109. R.P.Marin, S.Ishikawa, H.Bahruji, G.Shaw, S.A.Kondrat, P.J.Miedziak, D.J.Morgan, S.H.Taylor, J.K.Bartley, J.K.Edwards, M.Bowker,W.Ueda, G.J.Hutchings. *Appl. Catal. A: Gen.*, **504**, 62 (2015)
110. E.P.Da Silva, M.R.Guilherme, E.T.Tenório-Neto, A.F.Rubira, M.H.Kunita, L.Cardozo-Filho, C.G.Alonso. *Mater. Lett.*, **136**, 133 (2014)
111. I.E.Sokolov, I.A.Konovalov, R.M.Zakalyukin, D.V.Golubev, A.S.Kumskov, V.V.Fomichev. *MRS Commun.*, **8**, 59 (2018)
112. N.S.Nesterov, A.S.Shalygin, V.P.Pakharukova, T.S.Glazneva, O.N.Martyanov. *J. Supercrit. Fluids*, **149**, 110 (2019)
113. E.Reverchon, G.Della Porta, D.Sannino, L.Lisi, P.Ciambelli. In *Studies in Surface Science and Catalysis*. (Eds P.A.J.B.Delmon, R.Maggi, J.A.Martens, P.Grange, G.Poncelet). (Amsterdam: Elsevier Science, 1998). P. 349
114. G.J.Hutchings, J.K.Bartley, J.M.Webster, J.A.Lopez-Sanchez, D.J.Gilbert, C.J.Kiely, A.F.Carley, S.M.Howdle, S.Sajip, S.Caldarelli, C.Rhodes, J.C.Volta, M.Poliakoff. *J. Catal.*, **197**, 232 (2001)
115. G.J.Hutchings, J.A.Lopez-Sanchez, J.K.Bartley, J.M.Webster, A.Burrows, C.J.Kiely, A.F.Carley, C.Rhodes, M.Hävecker, A.Knop-Gericke, R.W.Mayer, R.Schlögl, J.C.Volta, M.Poliakoff. *J. Catal.*, **208**, 197 (2002)
116. J.A.Lopez-Sanchez, J.K.Bartley, A.Burrows, C.J.Kiely, M.Hävecker, R.Schlögl, J.C.Volta, M.Poliakoff, G.J.Hutchings. *New J. Chem.*, **26**, 1811 (2002)
117. Z.-R.Tang, C.D.Jones, J.K.W.Aldridge, T.E.Davies, J.K.Bartley, A.F.Carley, S.H.Taylor, M.Allix, C.Dickinson, M.J.Rosseinsky, J.B.Claridge, Z.Xu, M.J.Crudace, G.J.Hutchings. *ChemCatChem.*, **1**, 247 (2009)
118. Z.-R.Tang, S.A.Kondrat, C.Dickinson, J.K.Bartley, A.F.Carley, S.H.Taylor, T.E.Davies, M.Allix, M.J.Rosseinsky, J.B.Claridge, Z.Xu, S.Romani, M.J.Crudace, G.J.Hutchings. *Catal. Sci. Technol.*, **1**, 740 (2011)
119. S.A.Kondrat, T.E.Davies, Z.Zu, P.Boldrin, J.K.Bartley, A.F.Carley, S.H.Taylor, M.J.Rosseinsky, G.J.Hutchings. *J. Catal.*, **281**, 279 (2011)
120. R.P.Marin, S.A.Kondrat, R.K.Pinnell, T.E.Davies, S.Golunski, J.K.Bartley, G.J.Hutchings, S.H.Taylor. *Appl. Catal. B: Environ.*, **140 – 141**, 671 (2013)
121. R.P.Marin, S.A.Kondrat, T.E.Davies, D.J.Morgan, D.I.Enache, G.B.Combes, S.H.Taylor, J.K.Bartley, G.J.Hutchings. *Catal. Sci. Technol.*, **4**, 1970 (2014)
122. S.A.Kondrat, P.J.Smith, P.P.Wells, P.A.Chater, J.H.Carter, D.J.Morgan, E.M.Fiordaliso, J.B.Wagner, T.E.Davies, L.Lu, J.K.Bartley, S.H.Taylor, M.S.Spencer, C.J.Kiely, G.J.Kelly, C.W.Park, M.J.Rosseinsky, G.J.Hutchings. *Nature (London)*, **531**, 83 (2016)
123. P.J.Smith, S.A.Kondrat, J.H.Carter, P.A.Chater, J.K.Bartley, S.H.Taylor, M.S.Spencer, G.J.Hutchings. *ChemCatChem*, **9**, 1621 (2017)
124. D.Jiang, M.Zhang, H.Jiang. *Mater. Lett.*, **65**,1222 (2011)
125. M.Zhang, D.Jiang, H.Jiang. *Mater. Res. Bull.*, **47**, 4006 (2012)
126. H.Jiang, H.Wang, L.Kuang, G.Li, M.Zhang. *J. Mater. Res.*, **29**, 2188 (2014)
127. D.Jiang, M.Zhang, G.Li, H.Jiang. *Catal. Commun.*, **17**, 59 (2012)
128. H.Wang, H.Jiang, L.Kuang, M.Zhang. *J. Supercrit. Fluids*, **92**, 84 (2014)
129. H.Jiang, P.Huang, L.Liu, M.Zhang. *Mater. Charact.*, **63**, 98 (2012)
130. L.Kuang, P.Huang, H.Sun, H.Jiang, M.Zhang. *J. Rare Earths*, **31**, 137 (2013)
131. H.Jiang, L.Zhang, J.Zhao, Y.Li, M.Zhang. *J. Mater. Res.*, **31**, 702 (2016)
132. P.Franco, O.Sacco, I.De Marco, V.Vaiano. *Catalysts*, **9**, 346 (2019)
133. E.P.Da Silva, M.E.G.Winkler, W.M.Giufrida, L.Cardozo-Filho, C.G.Alonso, J.B.O.Lopes, A.F.Rubira, R.Silva. *J. Colloid Interface Sci.*, **535**, 245 (2019)
134. N.S.Nesterov, V.P.Paharukova, V.A.Yakovlev, O.N.Martyanov. *J. Supercrit. Fluids*, **112**, 119 (2016)
135. N.S.Nesterov, V.P.Pakharukova, O.N.Martyanov. *J. Supercrit. Fluids*, **130**, 133 (2017)
136. Patent WO 2018050459A1 (2018)
137. L.W.Hrubesh. *J. Non-Cryst. Solids*, **225**, 335 (1998)
138. H.Maleki, N.Hüsing. *Appl. Catal. B: Environ.*, **221**, 530 (2018)
139. G.M.Pajonk. *Appl. Catal.*, **72**, 217 (1991)
140. M.Schneider, A.Baiker. *Catal. Rev.*, **37**, 515 (1995)
141. G.M.Pajonk. *Catal. Today*, **35**, 319 (1997)

142. J.Engweiler, A.Baiker. *Appl. Catal. A: Gen.*, **120**, 187 (1994)
143. A.E.Gash, T.M.Tillotson, J.H.Satcher Jr., L.W.Hrubesh, R.L.Simpson. *J. Non-Cryst. Solids*, **285**, 22 (2001)
144. S.Bali, G.C.Turpin, R.D.Ernst, R.J.Pugmire, V.Singh, M.S.Seehra, E.M.Eyring. *Energy Fuels*, **22**, 1439 (2008)
145. R.W.Pekala. *J. Mater. Sci.*, **24**, 3221 (1989)
146. O.Barbieri, F.Ehrburger-Dolle, T.P.Rieker, G.M.Pajonk, N.Pinto, A.Venkateswara Rao. *J. Non-Cryst. Solids*, **285**, 109 (2001)
147. C.Moreno-Castilla, F.J.Maldonado-Hódar. *Carbon*, **43**, 455 (2005)
148. F.Rodríguez-Reinoso. *Carbon*, **36**, 159 (1998)
149. X.Liu, L.Dai. *Nat. Rev. Mater.*, **1**, 16064 (2016)
150. P.A.Simonov, A.V.Romanenko, I.P.Prosvirin, E.M.Moroz, A.I.Boronin, A.L.Chuvilin, V.A.Likholobov. *Carbon*, **35**, 73 (1997)
151. N.Keller, N.I.Maksimova, V.V.Roddatis, M.Schur, G.Mestl, Y.V.Butenko, V.L.Kuznetsov, R.Schlögl. *Angew. Chem., Int. Ed.*, **41**, 1885 (2002)
152. S.Ye, A.K.Vijh, Z.-Y.Wang, L.H.Dao. *Can. J. Chem.*, **75**, 1666 (1997)
153. C.Moreno-Castilla, F.J.Maldonado-Hódar, J.Rivera-Utrilla, E.Rodríguez-Castellón. *Appl. Catal. A: Gen.*, **183**, 345 (1999)
154. S.Ye, A.K.Vijh. *Electrochem. Commun.*, **5**, 272 (2003)
155. F.J.Maldonado-Hódar, C.Moreno-Castilla, A.F.Pérez-Cadenas. *Appl. Catal. B: Environ.*, **54**, 217 (2004)
156. A.Smirnova, X.Dong, H.Hara, A.Vasiliev, N.Sammes. *Int. J. Hydrogen Energy*, **30**, 149 (2005)
157. H.-J.Kim, W.-I.Kim, T.-J.Park, H.-S.Park, D.J.Suh. *Carbon*, **46**, 1393 (2008)
158. S.R.Mukai, T.Sugiyama, H.Tamon. *Appl. Catal. A: Gen.*, **256**, 99 (2003)
159. M.A.Worsley, P.J.Pauzauskie, T.Y.Olson, J.Biener, J.H.Satcher, T.F.Baumann. *J. Am. Chem. Soc.*, **132**, 14067 (2010)
160. M.B.Bryning, D.E.Milkie, M.F.Islam, L.A.Hough, J.M.Kikkawa, A.G.Yodh. *Adv. Mater.*, **19**, 661 (2007)
161. D.V.Krasnikov, I.O.Dorofeev, T.E.Smirnova, V.I.Suslyaev, M.A.Kazakova, S.I.Moseenkov, V.L.Kuznetsov. *Phys. Status Solidi*, **255**, 1700256 (2018)
162. L.Peng, Y.Zheng, J.Li, Y.Jin, C.Gao. *ACS Catal.*, **5**, 3387 (2015)
163. Y.Zhao, X.Xie, J.Zhang, H.Liu, H.-J.Ahn, K.Sun, G.Wang. *Chem. – Eur. J.*, **21**, 15908 (2015)
164. Y.Fan, W.Ma, D.Han, S.Gan, X.Dong, L.Niu. *Adv. Mater.*, **27**, 3767 (2015)
165. J.L.Mohanan, S.L.Brock. *J. Non-Cryst. Solids*, **350**, 1 (2004)
166. K.K.Kalebaila, D.G.Georgiev, S.L.Brock. *J. Non-Cryst. Solids*, **352**, 232 (2006)
167. S.Bag, P.N.Trikalitis, P.J.Chupas, G.S.Armatas, M.G.Kanatzidis. *Science*, **317**, 490 (2007)
168. S.Bag, A.F.Gaudette, M.E.Bussell, M.G.Kanatzidis. *Nat. Chem.*, **1**, 217 (2009)
169. J.Staszak-Jirkovský, C.D.Malliakas, P.P.Lopes, N.Danilovic, S.S.Kota, K.-C.Chang, B.Genorio, D.Strmcnik, V.R.Stamenkovic, M.G.Kanatzidis, N.M.Markovic. *Nat. Mater.*, **15**, 197 (2016)
170. N.Leventis, N.Chandrasekaran, C.Sotiriou-Leventis, A.Mumtaz. *J. Mater. Chem.*, **19**, 63 (2009)
171. N.Leventis, N.Chandrasekaran, A.G.Sadekar, S.Mulik, C.Sotiriou-Leventis. *J. Mater. Chem.*, **20**, 7456 (2010)
172. N.C.Bigall, A.-K.Herrmann, M.Vogel, M.Rose, P.Simon, W.Carrillo-Cabrera, D.Dorfs, S.Kaskel, N.Gaponik, A.Eychmüller. *Angew. Chem., Int. Ed.*, **48**, 9731 (2009)
173. L.Kühn, A.-K.Herrmann, B.Rutkowski, M.Oezaslan, M.Nachtegaal, M.Klose, L.Giebeler, N.Gaponik, J.Eckert, T.J.Schmidt, A.Czyrska-Filemonowicz, A.Eychmüller. *Chem. – Eur. J.*, **22**, 13446 (2016)
174. W.Liu, A.-K.Herrmann, N.C.Bigall, P.Rodriguez, D.Wen, M.Oezaslan, T.J.Schmidt, N.Gaponik, A.Eychmüller. *Acc. Chem. Res.*, **48**, 154 (2015)
175. M.R.Lohe, M.Rose, S.Kaskel. *Chem. Commun.*, 6056 (2009)
176. B.Zhu, G.Liu, L.Chen, L.Qiu, L.Chen, J.Zhang, L.Zhang, M.Barboiu, R.Si, C.-Y.Su. *Inorg. Chem. Front.*, **3**, 702 (2016)
177. Z.Ulker, I.Erucar, S.Keskin, C.Erkey. *Microporous Mesoporous Mater.*, **170**, 352 (2013)
178. A.L.Nuzhdin, A.S.Shalygin, E.A.Artiukha, A.M.Chibiryaev, G.A.Bukhtiyarova, O.N.Martyanov. *RSC Adv.*, **6**, 62501 (2016)
179. A.S.Shalygin, A.L.Nuzhdin, G.A.Bukhtiyarova, O.N.Martyanov. *J. Sol-Gel Sci. Technol.*, **84**, 446 (2017)
180. Z.Inonu, S.Keskin, C.Erkey. *ACS Appl. Nano Mater.*, **1**, 5959 (2018)
181. Z.Liu, K.Xu, P.She, S.Yin, X.Zhu, H.Sun. *Chem. Sci.*, **7**, 1926 (2016)
182. M.A.Worsley, S.J.Shin, M.D.Merrill, J.Lenhardt, A.J.Nelson, L.Y.Woo, A.E.Gash, T.F.Baumann, C.A.Orme. *ACS Nano*, **9**, 4698 (2015)
183. W.Lei, V.N.Mochalin, D.Liu, S.Qin, Y. Gogotsi, Y.Chen. *Nat. Commun.*, **6**, 8849 (2015)
184. W.Cheng, F.Rechberger, M.Niederberger. *Nanoscale*, **8**, 14074 (2016)
185. W.Cheng, F.Rechberger, M.Niederberger. *ACS Nano*, **10**, 2467 (2016)
186. F.Rechberger, G.Ilari, M.Niederberger. *Chem. Commun.*, **50**, 13138 (2014)
187. F.Rechberger, F.J.Heiligtag, M.J.Süess, M.Niederberger. *Angew. Chem., Int. Ed.*, **53**, 6823 (2014)
188. S.Chen, G.Liu, H.Yadegari, H.Wang, S.Z.Qiao. *J. Mater. Chem. A*, **3**, 2559 (2015)
189. G.Ozouf, C.Beauger. *J. Mater. Sci.*, **51**, 5305 (2016)
190. L.Yang, J.Huang, L.Shi, L.Cao, W.Zhou, K.Chang, X.Meng, G.Liu, Y.Jie, J.Ye. *Nano Energy*, **36**, 331 (2017)
191. V.P.Pakharukova, A.S.Shalygin, E.Y.Gerasimov, S.V.Tsybulya, O.N.Martyanov. *J. Solid State Chem.*, **233**, 294 (2016)
192. V.P.Pakharukova, D.A.Yatsenko, E.Y.Gerasimov, A.S.Shalygin, O.N.Martyanov, S.V.Tsybulya. *J. Solid State Chem.*, **246**, 284 (2017)
193. A.S.Shalygin, I.V.Kozhevnikov, E.Y.Gerasimov, A.S.Andreev, O.B.Lapina, O.N.Martyanov. *Microporous Mesoporous Mater.*, **251**, 105 (2017)
194. O.V.Klimov, K.A.Leonova, G.I.Koryakina, E.Y Gerasimov, I.P.Prosvirin, S.V.Cherepanova, S.V.Budukva, V.Y.Pereyma, P.P.Dik, O.A.Parakhin, A.S.Noskov. *Catal. Today*, **220 – 222**, 66 (2014)
195. E.Y.Buslaeva, Y.F.Kargin, K.G.Kravchuk, S.A.Sigachev, S.P.Gubin. *Russ. J. Inorg. Chem.*, **46**, 323 (2001)
196. Y.F. Kargin, E.Y.Buslaeva, K.G.Kravchuk, S.P.Gubin. *Russ. J. Inorg. Chem.*, **48**, 103 (2003)
197. J.Kim, D.Kim, B. Veriansyah, J.W.Kang, J.-D.Kim. *Mater. Lett.*, **63**, 1880 (2009)
198. S.P.Gubin, E.Y.Buslaeva. *Russ. J. Phys. Chem. B*, **38**, 1172 (2009)
199. A.V.Egorysheva, V.I.Burkov, E.Y.Buslaeva, Y.F.Kargin, K.G.Kravchuk, S.P.Gubin, V.M.Skorikov. *Russ. J. Inorg. Chem.*, **47**, 891 (2002)

200. Y.F.Kargin, E.Y.Buslaeva, A.V.Egorysheva, K.G.Kravchuk, S.P.Gubin. *Russ. J. Inorg. Chem.*, **48**, 1615 (2003)
201. B.Veriansyah, J.-D.Kim, B.K.Min, Y.H.Shin, Y.-W.Lee, J.Kim. *J. Supercrit. Fluids*, **52**, 76 (2010)
202. J.Kim, Y.-S.Park, B.Veriansyah, J.-D.Kim, Y.-W.Lee. *Chem. Mater.*, **20**, 6301 (2008)
203. K.H.Stern. *High Temperature Properties and Thermal Decomposition of Inorganic Salts with Oxyanions*. (Boca Raton, FL: CRC Press, 2001)
204. S.A.Nikolaev, M.V.Tsodikov, A.V.Chistyakov, P.A.Zharova, D.I.Ezzgelenko. *J. Catal.*, **369**, 501 (2019)
205. T.I.Korányi, X.Huang, A.E.Coumans, E.J.M.Hensen. *ACS Sustain. Chem. Eng.*, **5**, 3535 (2017)
206. S.Ahmadi, Z.Yuan, S.Rohani, C.Xu. *Catal. Today*, **269**, 182 (2016)
207. W.-J.Xu, W.Zhao, C.Sheng, S.-T.Zhong, X.-N.Wu, C.-H.Yan, S.Bai, Z.-M.Zong, X.-Y.Wei. *Energy Fuels*, **24**, 250 (2010)
208. J.Pan, J.Liu, S.Guo, Z.Yang. *Catal. Lett.*, **131**, 179 (2009)
209. A.A.Philippov, A.M.Chibiryaev, O.N.Martyanov. *J. Supercrit. Fluids*, **145**, 162 (2019)
210. H.Choi, B.Veriansyah, J.Kim, J.-D.Kim, J.W.Kang. *J. Supercrit. Fluids*, **52**, 285 (2010)
211. C.Slostowski, S.Marre, O.Babot, T.Toupance, C.Aymonier. *Langmuir*, **28**, 16656 (2012)
212. M.Sato, Z.Fazekas, M.Harada, H.Tomiyasu, Y.Ikeda. *J. Nuclear Sci. Technol.*, **40**, 343 (2003)
213. I.I.Simentsova, A.A.Khassin, G.A.Filonenko, G.K.Chermashentseva, O.A.Bulavchenko, S.V.Cherepanova, T.M.Yurieva. *Russ. Chem. Bull., Int. Ed.*, **60**, 1827 (2011)
214. N.S.Nesterov, I.I.Simentsova, V.F.Yudanov, O.N.Martyanov. *J. Struct. Chem.*, **57**, 90 (2016)
215. M.Kim, B.Y.Lee, H.C.Ham, J.Han, S.W.Nam, H.Lee, J.H.Park, S.Choi, Y.Shin. *J. Supercrit. Fluids*, **111**, 8 (2016)
216. L.Wang, X.Xu, S.Wu, F.Cao. *Catal. Sci. Technol.*, **8**, 1366 (2018)
217. Z.Lou, C.Xue. *CrystEngComm*, **18**, 8406 (2016)
218. D.Evecan, E.Zayim. *Curr. Appl. Phys.*, **19**, 198 (2019)
219. S.Zhuiykov, E.Kats, B.Carey, S.Balendhran. *Nanoscale*, **6**, 15029 (2014)
220. Y.V. Ioni, V.V.Voronov, A.V.Naumkin, E.Y.Buslaeva, A.V.Egorov, S.V.Savilov, S.P.Gubin. *Russ. J. Inorg. Chem.*, **60**, 709 (2015)
221. A.Y.Soloveva, Y.V.Ioni, S.P.Gubin. *Mendeleev Commun.*, **26**, 38 (2016)
222. E.B.Nursanto, A.Nugroho, S.-A.Hong, S.J.Kim, K.Y.Chung, J.Kim. *Green Chem.*, **13**, 2714 (2011)
223. O.Razavizadeh, M.Ghorbani. *Surf. Coat. Technol.*, **363**, 1 (2019)
224. C.Y.Kong, Y.Shiratori, T.Sako, F.Iwata. *Adv. Mater. Res.*, **1004 – 1005**, 1013 (2014)
225. A.Y.Soloveva, Y.V.Ioni, E.Y.Buslaeva, M.A.Zaporozhets, S.V.Savilov, A.V.Naumkin, S.P.Gubin. *Inorg. Mater.*, **51**, 848 (2015)
226. Y.Ioni, E.Buslaeva, S.Gubin. *Mater. Today Proc.*, **3**, S209 (2016)
227. C.Y.Kong, W.-L.Song, M.J.Meziani, K.N.Tackett, L.Cao, A.J.Farr, A.Anderson, Y.-P.Sun. *J. Supercrit. Fluids*, **61**, 206 (2012)
228. S.Liu, K.Chen, Y.Fu, S.Yu, Z.Bao. *Appl. Surf. Sci.*, **258**, 5299 (2012)
229. D.Yoon, K.Y.Chung, W.Chang, S.M.Kim, M.J.Lee, Z.Lee, J.Kim. *Chem. Mater.*, **27**, 266 (2015)
230. W.Li, D.Yoon, J.Hwang, W.Chang, J.Kim. *J. Power Sources*, **293**, 1024 (2015)
231. J.Hwang, D.Yoon, B.Kweon, W.Chang, J.Kim. *RSC Adv.*, **6**, 108298 (2016)
232. M.Choi, S.K.Koppala, D.Yoon, J.Hwang, S.M.Kim, J.Kim. *J. Power Sources*, **309**, 202 (2016)
233. D.Yoon, J.Hwang, W.Chang, J.Kim. *Chem. Eng. J.*, **317**, 890 (2017)
234. D.Yoon, J.Hwang, D.H.Kim, W.Chang, K.Y.Chung, J.Kim. *J. Supercrit. Fluids*, **125**, 66 (2017)
235. M.Choi, W.William, J.Hwang, D.Yoon, J.Kim. *J. Ind. Eng. Chem.*, **59**, 160 (2018)
236. W.Devina, J.Hwang, J.Kim. *Chem. Eng. J.*, **345**, 1 (2018)
237. M.Seo, D.Yoon, K.S.Hwang, J.W.Kang, J.Kim. *Carbon*, **64**, 207 (2013)
238. H.Gao, G.Hu. *RSC Adv.*, **6**, 10132 (2016)
239. S.P.Gubin, V.I.Men'shov, V.M.Kirilets, E.Y.Plopskii, F.Tegai. *Bull. Acad. Sci. USSR. Div. Chem. Sci.*, **32**, 2547 (1983)
240. H.Meerwein, R.Schmidt. *Justus Liebig's Ann. Chem.*, **444**, 221 (1925)
241. T.Kamitanaka, T.Matsuda, T.Harada. *Tetrahedron*, **63**, 1429 (2007)
242. A.Daimon, T.Kamitanaka, N.Kishida, T.Matsuda, T.Harada. *J. Supercrit. Fluids*, **37**, 215 (2006)
243. X.Tang, L.Hu, Y.Sun, G.Zhao, W.Hao, L.Lin. *RSC Adv.*, **3**, 10277 (2013)
244. V.I.Anikeev, V.P.Sivcev, K.R.Valeev, K.P.Volcho, V.A.Sadykov, N.F.Salakhutdinov. *J. Supercrit. Fluids*, **140**, 233 (2018)
245. Z.Sun, G.Bottari, K.Barta. *Green Chem.*, **17**, 5172 (2015)
246. T.Nakagawa, H.Ozaki, T.Kamitanaka, H.Takagi, T.Matsuda, T.Kitamura, T.Harada. *J. Supercrit. Fluids*, **27**, 255 (2003)
247. T.Kamitanaka, K.Yamamoto, T.Matsuda, T.Harada. *Tetrahedron*, **64**, 5699 (2008)
248. G.S.Macala, T.D.Matson, C.L.Johnson, R.S.Lewis, A.V Iretskii, P.C.Ford. *ChemSusChem*, **2**, 215 (2009)
249. T.Kamitanaka, Y.Ono, H.Morishima, T.Hikida, T.Matsuda, T.Harada. *J. Supercrit. Fluids*, **49**, 221 (2009)
250. A.A.Philippov, A.M.Chibiryaev. *Russ. J. Phys. Chem. B*, **13**, 1117 (2019)
251. V.Hach. *J. Org. Chem.*, **38**, 293 (1973)
252. A.M.Chibiryaev, V.I.Anikeev, A.Yermakova, P.E.Mikenin, I.V.Kozhevnikov, O.I.Sal'nikova. *Russ. Chem. Bull., Int. Ed.*, **55**, 987 (2006)
253. V.I.Anikeev, A.Ermakova, A.M.Chibiryaev, I.V.Kozhevnikov. *Kinet. Catal.*, **51**, 162 (2010)
254. T.Aditya, A.Pal, T.Pal. *Chem. Commun.*, **51**, 9410 (2015)
255. H.K.Kadam, S.G.Tilve. *RSC Adv.*, **5**, 83391 (2015)
256. M.M.Trandafir, A.Moragues, P.Amorós, V.I. Parvulescu. *Catal. Today*, (2019); DOI: 10.1016/j.cattod.2019.02.053.
257. D.Formenti, F.Ferretti, F.K.Scharnagl, M.Beller. *Chem. Rev.*, **119**, 2611 (2019)
258. A.Matsunami, Y.Kayaki. *Tetrahedron Lett.*, **59**, 504 (2018)
259. V.P.Sivcev, K.P.Volcho, N.F.Salakhutdinov, V.I.Anikeev. *J. Supercrit. Fluids*, **107**, 179 (2016)
260. V.P.Sivcev, K.P.Volcho, N.F.Salakhutdinov, V.I.Anikeev. *J. Supercrit. Fluids*, **103**, 101 (2015)
261. V.P.Sivcev, D.V.Korchagina, E.V.Suslov, K.P.Volcho, N.F.Salakhutdinov, V.I.Anikeev. *J. Supercrit. Fluids*, **86**, 137 (2014)
262. K.Barta, P.C.Ford. *Acc. Chem. Res.*, **47**, 1503 (2014)
263. D.J.McClelland, P.H.Galebach, A.H.Motagamwala, A.M.Wittrig, S.D.Karlen, J.S.Buchanan, J.A.Dumesic, G.W.Huber. *Green Chem.*, **21**, 2988 (2019)
264. R.Li, B.Li, X.Kai, T.Yang. *Fuel Process. Technol.*, **167**, 363 (2017)

265. S.O.Limarta, J.-M.Ha, Y.-K.Park, H.Lee, D.J.Suh, J.Jae. *J. Ind. Eng. Chem.*, **57**, 45 (2018)
266. M.Zhou, B.K.Sharma, P.Liu, J.Ye, J.Xu, J.-C.Jiang. *ACS Sustain. Chem. Eng.*, **6**, 6867 (2018)
267. Y.N.Regmi, J.K.Mann, J.R.McBride, J.Tao, C.E.Barnes, N.Labbé, S.C.Chmely. *Catal. Today*, **302**, 190 (2018)
268. P.H.Galebach, S.Thompson, A.M.Wittrig, J.S.Buchanan, G.W.Huber. *ChemSusChem*, **11**, 4007 (2018)
269. P.H.Galebach, D.J.McClelland, N.M.Eagan, A.M.Wittrig, J.S.Buchanan, J.A.Dumesic, G.W.Huber. *ACS Sustain. Chem. Eng.*, **6**, 4330 (2018)
270. A.M.Chibiryaev, I.V.Kozhevnikov, A.S.Shalygin, O.N.Martyanov. *Energy Fuels*, **32**, 2117 (2018)
271. B.Sarkar, W.Kwek, D.Verma, J.Kim. *Appl. Catal. A: Gen.*, **545**, 148 (2017)
272. H.Shafaghat, J.M.Kim, I.-G.Lee, J.Jae, S.-C.Jung, Y.-K.Park. *Renew. Energy*, **144**, 159 (2019)
273. I.-G.Lee, H.Lee, S.H.Park, S.-C.Jung, S.C.Kim, C.H.Ko, Y.-K.Park. *J. Nanosci. Nanotechnol.*, **17**, 2674 (2017)
274. S.Cheng, L.Wei, J.Julson, K.Muthukumarappan, P.R.Kharel. *Fuel Process. Technol.*, **167**, 117 (2017)
275. A.Riaz, D.Verma, H.Zeb, J.H.Lee, J.C.Kim, S.K.Kwak, J.Kim. *Green Chem.*, **20**, 4957 (2018)
276. J.-Y.Kim, J.Park, U.-J.Kim, J.W.Choi. *Energy Fuels*, **29**, 5154 (2015)
277. J.-Y.Kim, S.Oh, H.Hwang, T.Cho, I.-G.Choi, J.W.Choi. *Chemosphere*, **93**, 1755 (2013)
278. X.Xu, C.Zhang, Y.Zhai, Y.Liu, R.Zhang, X.Tang. *Energy Fuels*, **28**, 4611 (2014)
279. J.Peng, P.Chen, H.Lou, X.Zheng. *Bioresour. Technol.*, **100**, 3415 (2009)
280. S.Brand, J.Kim. *Energy*, **80**, 64 (2015)
281. J.Zhang. *Green Energy Environ.*, **3**, 328 (2018)
282. S.G.Parto, J.M.Christensen, L.S.Pedersen, A.B.Hansen, F.Tjosås, C.Spiga, C.D.Damsgaard, D.B.Larsen, J.Ø.Duus, A.D.Jensen. *Energy Fuels*, **33**, 1196 (2019)
283. A.M.Chibiryaev, I.V.Kozhevnikov, O.N.Martyanov. *Catal. Today*, **329**, 177 (2019)
284. M.K.Khan, W.Kwek, J.Kim. *Fuel*, **218**, 78 (2018)
285. M.K.Khan, R.Insyani, J.Lee, M.Yi, J.W.Lee, J.Kim. *Fuel*, **182**, 650 (2016)
286. I.V.Kozhevnikov, A.L.Nuzhdin, O.N.Martyanov. *J. Supercrit. Fluids*, **55**, 217 (2010)
287. M.Hosseinpour, S.J.Ahmadi, S.Fatemi. *J. Supercrit. Fluids*, **107**, 278 (2016)
288. K.Arai, T.Adschiri, M.Watanabe. *Ind. Eng. Chem. Res.*, **39**, 4697 (2000)
289. L Wu, B.Li, C.Zhao. *ChemCatChem*, **10**, 1140 (2018)
290. J.-Y.Park, W.Jeon, J.-H.Lee, B.Nam, I.-G.Lee. *Chem. Eng. J.*, **377**, 120312 (2019).
291. B.Jin, P.Duan, Y.Xu, B.Wang, F.Wang, L.Zhang. *Biores. Technol.*, **162**, 341 (2014)
292. Y.Wang, F.-S. Zhang. *J. Hazard. Mater.*, **205** – **206**, 156 (2012)
293. X.Wang, M.Sun, Q.Wang. *Ekoloji*, **28**, 3235 (2019)
294. Q.Li, D.Liu, X.Hou, P.Wu, L.Song, Z.Yan. *Biores. Technol.*, **219**, 281 (2016)
295. S.Saim, B.Subramaniam. *J. Catal.*, **131**, 445 (1991)
296. S.Saim, B.Subramaniam. *J. Supercrit. Fluids*, **3**, 214 (1990)
297. B.Sander, M.Thelen, B.Kraushaar-Czarnetzki. *Catal. Today*, **75**, 119 (2002)
298. T.Funamoto, T.Nakagawa, K.Segawa. *Appl. Catal. A: Gen.*, **286**, 79 (2005)
299. V.I.Bogdan, T.A.Klimenko, L.M.Kustov, V.B.Kazansky. *Appl. Catal. A: Gen.*, **267**, 175 (2004)
300. V.I.Bogdan, A.E.Koklin, V.B.Kazanskii. *Kinet. Catal.*, **48**, 785 (2007)
301. V.I.Bogdan, A.E.Koklin, V.B.Kazanskii. *Sverkhkriticheskie Flyuidy: Teoriya i Praktika*, **2** (4), 60 (2007)
302. V.I.Bogdan, A.E.Koklin, V.B.Kazanskii. *Kinet. Catal.*, **51**, 736 (2010) [*KùÅetùka ù kataöù3*, **51**, 762 (2010)]
303. V.I.Bogdan, A.E.Koklin, Y.A.Pokusaeva, V.B.Kazanskii. *Russ. J. Phys. Chem. B*, **3**, 39 (2010)
304. Z.Dardas, M.G.Süer, Y.H.Ma, W.R.Moser. *J. Catal.*, **162**, 327 (1996)
305. H.M.Minachev, A.A.Dergachev. *Russ. Chem. Rev.*, **59**, 885 (1990)
306. Patent US 5043502 (1991)
307. V.I.Bogdan, E.G.Khelkovskaya-Sergeeva, T.V.Vasina, V.B.Kazanskii. *Kinet. Catal.*, **49**, 115 (2008)
308. A.Corma, A.Martinez. *Catal. Rev. Sci. Eng.*, **35**, 483 (1993)
309. L.Fan, I.Nakamura, S.Ishida, K.Fujimoto. *Ind. Eng. Chem. Res.*, **36**, 1458 (1997)
310. A. L.M.Salinas, G.Sapaly, Y.B.Taarit, J.C.Vedrine, N.Essayem. *Appl. Catal. A: Gen.*, **336**, 61 (2008)
311. A.S.Chellappa, R.C.Miller, W.J.Thomson. *Appl. Catal. A: Gen.*, **209**, 359 (2001)
312. P.Y.Gayraud, I.H.Stewart, S.B.Derouane-Abd Hamid, N.Essayem, E.G.Derouane, J.C.Védrine. *Catal. Today*, **63**, 223 (2000)
313. P.Y.Gayraud, N.Essayem, J.C.Védrine. *Stud. Surf. Sci. Catal.*, **130**, 2549 (2000)
314. M.Clark, B.Subramaniam. *Ind. Eng. Chem. Res.*, **37**, 1243 (1998)
315. C.Lyon, B.Subramaniam, C. Pereira. *Stud. Surf. Sci. Catal.*, **139**, 221 (2001)
316. B.Subramaniam, V.Arunajatesan, C.J.Lyon. *Stud. Surf. Sci. Catal.*, **126**, 63 (1999)
317. D.M.Ginosar, D.N.Thompson, K.Coates, D.J.Zalewski. *Ind. Eng. Chem. Res.*, **41**, 2864 (2002)
318. V.I.Bogdan, V.B.Kazanskii. *Kinet. Catal.*, **46**, 834 (2005)
319. A.E.Koklin, V.M.K.Chan, V.B.Kazanskii, V.I.Bogdan. *Kinet. Catal.*, **51**, 410 (2010)
320. A.E.Koklin, V.M.K.Chan, V.I.Bogdan. *Russ. J. Phys. Chem. B*, **8**, 991 (2014)
321. M.G.Hitzler, F.R.Smail, S.K.Ross, M.Poliakoff. *Chem. Commun.*, 359 (1998)
322. Z.Tian, Z.Qin, G.Wang, M.Dong, J.Wang. *J. Supercrit. Fluids*, **44**, 325 (2008)
323. A.E.Koklin, G.M.Hasyanova, L.M.Glukhov, V.I.Bogdan. *Russ. Chem. Bull., Int. Ed.*, **66**, 488 (2017)
324. S.Van den Hark, M.Härröd. *Appl. Catal. A: Gen.*, **210**, 207 (2001)
325. C.M.Piqueras, G.Tonetto, S.Bottini, D.E.Damian. *Catal. Today*, **133** – **135**, 836 (2008)
326. H.Wang, F.Zhao, S.Fujita, M.Arai. *Catal. Commun.*, **9**, 362 (2008)
327. V.Arunajatesan, B.Subramaniam, K.W.Hutchenson, F.E.Herkes. *Chem. Eng. Sci.*, **56**, 1363 (2001)
328. W.Wei, F.Li, J.Ren, Y.Sun, B.Zhong. *Stud. Surf. Sci. Catal.*, **130**, 2573 (2000)
329. K.Yokota, K.Fujimoto. *Fuel*, **68**, 255 (1989)
330. C.S.Chen, W.H.Cheng, S.S.Lin. *Appl. Catal. A: Gen.*, **257**, 97 (2004)
331. J.A.Loiland, M.J.Wulfers, N.S.Marinkovic, R.F.Lobo. *Catal. Sci. Technol.*, **6**, 5267 (2016)
332. S.Sengupta, A.Jha, P.Shende, R.Maskara, A.K.Das. *J. Environ. Chem. Eng.*, **7**, 102911 (2019)
333. Y.A.Pokusaeva, A.E.Koklin, V.V.Lunin, V.I.Bogdan. *Mendeleev Commun.*, **29**, 382 (2019)
334. B.Dai, G.Zhou, S.Ge, H.Xie, Z.Jiao, G.Zhang, K.Xiong. *Can. J. Chem. Eng.*, **95**, 634 (2017)

335. V.I.Bogdan, A.E.Koklin, S.A.Nikolaev, L.M.Kustov. *Top. Catal.*, **59**, 1104 (2016)
336. N.M.Martin, P.Velin, M.Skoglundh, M.Bauer, P.A.Carlsson. *Catal. Sci. Technol.*, **7**, 1086 (2017)
337. F.Ocampo, B.Louis, A.C.Roger. *Appl. Catal. A: Gen.*, **369**, 90 (2009)
338. H.C.Wu, Y.C.Chang, J.H.Wu, J.H.Lin, I.K.Lin, C.S.Chen. *Catal. Sci. Technol.*, **5**, 4154 (2015)
339. M.Baileraa, P.Lisbon, L.M.Romeo, S.Espatolero. *Renew. Sustain. Energy Rev.*, **69**, 292 (2017)
340. V.I.Bogdan, L.M.Kustov. *Mendeleev Commun.*, **25**, 446 (2015)
341. V.I.Bogdan, A.E.Koklin, D.O.Kozak, L.M.Kustov. *Russ. J. Phys. Chem. A*, **90**, 2352 (2016)
342. V.I.Bogdan, Y.A.Pokusaeva, A.E.Koklin, S.V.Savilov, S.A.Chernyak, V.V.Lunin, L.M.Kustov. *Energy Technol.*, **7**, 1900174 (2019)
343. W.Li, H.Wang, X.Jiang, J.Zhu, Z.Liu, X.Guo, C.Song. *RSC Adv.*, **8**, 7651 (2018)
344. N.Boreriboon, X.Jiang, C.Song, P.Prasassarakich. *Top. Catal.*, **61**, 1551 (2018)
345. Ya.A.Pokusaeva, A.E.Koklin, O.L.Eliseev, R.V.Kazantsev, V.I.Bogdan. *Russ. Chem. Bull., Int. Ed.*, **69**, 237 (2020)
346. J.-H.Lee, N.-R.Foster. *J. Supercrit. Fluids*, **9**, 99 (1996)
347. P.E.Savage, R.Li, J.T.Santini. *J. Supercrit. Fluids*, **7**, 135 (1994)
348. U.Armbruster, A.Martin, A.Krepel. *J. Supercrit. Fluids*, **21**, 233 (2001)
349. B.Kerler, A.Martin. *Catal. Today*, **61**, 9 (2000)
350. L.Fan, Y.Nakayama, K.Fujimoto. *Chem. Commun.*, 1179 (1997)
351. T.Sato, A.Watanabe, N.Hiyoshi, M.Shirai, N.Itoh. *J. Supercrit. Fluids*, **43**, 295 (2008)
352. A.L.Kustov, P.S.Benavente Donaire, A.E.Koklin, V.I.Bogdan. *Kinet. Catal.*, **55**, 93 (2014)
353. A.L.Kustov, A.N.Kalenchuk, V.V.Lunin, A.E.Koklin, V.I.Bogdan. *Russ. J. Phys. Chem. B*, **10**, 1131 (2016)
354. V.I.Bogdan, A.L.Kustov, L.M.Glukhov, A.N.Kalenchuk, L.M.Kustov, I.P. Beletskaya. *Russ. J. Phys. Chem. B*, **7**, 810 (2013)
355. I.I.Mishanin, V.I.Bogdan. *Mendeleev Commun.*, **29**, 455 (2019)
356. O.Yakaboylu, J.Harinck, K.G.Smit, W.De Jong. *Energies*, **8**, 859 (2015)
357. F.L.P.Resende, P.E.Savage. *AIChE J.*, **56**, 2412 (2010)
358. X.Man, K.Okuda, S.Ohara, M.Umetsu, S.Takami, T.Adschiri. *J. Jpn. Inst. Energy*, **84**, 486 (2005)
359. H.Nonaka, M.Funaoka. *Biomass Bioenergy*, **35**, 1607 (2011)
360. T.L.-K.Yong, Y.Matsumura. *J. Supercrit. Fluids*, **87**, 73 (2014)
361. G.J.Di Leo, M.E.Neff, P.E.Savage. *Energy Fuels*, **21**, 2340 (2007)
362. A.K.Goodwin, G.L.Rorrer. *Energy Fuels*, **23**, 3818 (2009)
363. C.M.Huelsman, P.E.Savage. *J. Supercrit. Fluids*, **81**, 200 (2013)
364. V.I.Bogdan, A.V.Kondratyuk, A.E.Koklin, V.V.Lunin. *Russ. J. Phys. Chem. B*, **11**, 1207 (2017)
365. E.S.Alekseev, V.I.Bogdan. *Sverkhkriticheskie Flyuidy: Teoriya i Praktika*, **15** (1), 103 (2020)
366. A.V.Kondratyuk, A.L.Kustov, V.V.Lunin, A.E.Koklin, V.I.Bogdan. In *Book of Abstracts VIII Scientific and Practical Conference with International Participation Supercritical Fluids (SCF): Fundamentals, Technology, Innovation*. (Zelenogradsk, Russia, 2015). P. 200
367. R.A.Sheldon. *Green Chem.*, **7**, 267 (2005)
368. *Handbook of Green Chemistry. Supercritical Solvents*. Vol. 4. (Eds P.G.Jessop, W.Leitner). (Weinheim: Wiley-VCH, 2010)
369. *Ionic Liquids in Synthesis*. (2nd Edn.). (Eds P.Wasserscheid, T.Welton). (Weinheim: Wiley-VCH, 2008)
370. C.Jimeno. *Org. Biomol. Chem.*, **14**, 6147 (2016)
371. S.Bhowmick, K.C.Bhowmick. *Tetrahedron: Asymmetry*, **22**, 1945 (2011)
372. M.A.McHugh, V.J.Krukonis. *Supercritical Fluid Extraction: Principles and Practice*. (2nd Edn.). (Boston: Elsevier, Butterworth-Heinemann, 1994)
373. B.A.S.Machado, C.G.Pereira, S.B.Nunes, F.F.Padilha, M.A.Umsza-Guez. *Sep. Sci. Technol.*, **48**, 2741 (2013)
374. S.Cummings, K.Trickett, R.Enick, J.Eastoe. *Phys. Chem. Chem. Phys.*, **13**, 1276 (2011)
375. A.Baiker. *Chem. Rev.*, **99**, 453 (1999)
376. V.Farina, J.T.Reeves, C.H.Senanayake, J.J.Song. *Chem. Rev.*, **106**, 2734 (2006)
377. D.L.Hughes. *Org. Proc. Res. Dev.*, **22**, 574 (2018)
378. K.Wittmann, W.Wisniewski, R.Mynott, W.Leitner, C.L.Kranemann, T.Rische, P.Eilbracht, S.Kluwer, J.M.Ernsting, C.J.Elsevier. *Chem. – Eur. J.*, **7**, 4584 (2001)
379. V.Laserna, G.Fiorani, C.J.Whiteoak, E.Martin, E.Escudero-Adan, A.W.Kleij. *Angew. Chem., Int. Ed.*, **53**, 10416 (2014)
380. C.M.Rayner, P.M.Rose, D.C.Barnes. In *Handbook of Green Chemistry. Supercritical Solvents*. Vol. 4. (Eds P.G.Jessop, W.Leitner). (Weinheim: Wiley-VCH, 2010). P. 189
381. M.Brookhart, B.Grant, A.F.Volpe Jr. *Organometallics*, **11**, 3920 (1992)
382. M.J.Burk, S.Feng, M.F.Gross, W.Tumas. *J. Am. Chem. Soc.*, **117**, 8277 (1995)
383. K.A.Consan, R.D.Smith. *J. Supercrit. Fluids*, **3**, 51 (1990)
384. D.J.Adams, W.Chen, *E.G.*Hope, S.Lange, A.M.Stuart, A.West, J.Xiao. *Green Chem.*, **5**, 118 (2003)
385. Y.Hu, D.J.Birdsall, A.M.Stuart, *E.G.*Hope, J.Xiao. *J. Mol. Catal. A: Chem.*, **219**, 57 (2004)
386. G.Franciò, K.Wittmann, W.Leitner. *J. Organomet. Chem.*, **621**, 130 (2001)
387. K.Burgemeister, G.Franciò, H.Hugl, W.Leitner. *Chem. Commun.*, **48**, 6026 (2005)
388. K.Burgemeister, G.Franciò, V.H.Gego, L.Greiner, H.Hug, W.Leitner. *Chem. – Eur. J.*, **13**, 2798 (2007)
389. P.G.Jessop, T.Ikariya, R.Noyori. *Chem. Rev.*, **99**, 475 (1999)
390. M.A.Pigaleva, I.V.Elmanovich, Y.N.Kononevich, M.O.Gallyamov, A.M.Muzafarov. *RSC Adv.*, **5**, 103573 (2015)
391. A.Ahosseini, W.Ren, A.M.Scurto. *Ind. Eng. Chem. Res.*, **48**, 4254 (2009)
392. A.B.Paninho, A.L.Ventura, L.C.Branco, A.J.Pombeiro, M.F.C.G.da Silva, M.N.da Ponte, K.T.Mahmudov, A.V.Nunes. *J. Supercrit. Fluids*, **132**, 71 (2018)
393. K.M.Koeller, C.H.Wong. *Nature (London)*, **409**, 232 (2001)
394. B.M.Nest, S.C.Hammer, B.A.Nebel, B.Hauer. *Angew. Chem., Int. Ed.*, **53**, 3070 (2014)
395. C.Cao, T.Matsuda. In *Organic Synthesis Using Biocatalysis*. (Eds A.Goswami, J.D.Stewart). (Amsterdam: Elsevier, 2015). P. 67
396. Z.Knez. *J. Supercrit. Fluids*, **134**, 133 (2018)
397. G.Pupo, R.Properzi, B.List. *Angew. Chem., Int. Ed.*, **55**, 6099 (2016)
398. H.G.Jang, G.R.Kim, G.J.Kim. *Catal. Today*, **185**, 306 (2012)

399. J.Xiao, S.C.Nefkens, P.G.Jessop, T.Ikariya, R.Noyori. *Tetrahedron Lett.*, **37**, 2813 (1996)
400. B.Minder, T.Mallat, K.H.Pickel, K.Steiner, A.Baiker. *Catal. Lett.*, **34**, 1 (1995)
401. *Chemical Synthesis Using Supercritical Fluids*. (Eds P.G.Jessop, W.Leitner). (Weinheim: Wiley-VCH, 1999)
402. P.G.Jessop. In *Supercritical Fluid Technology for Drug Product Development*. (Eds P.York, U.B.Kompella, B.Y.Shekunov). (New York, Basel: Marcel Dekker, 2004). P. 427
403. W.Leitner. *Appl. Organomet. Chem.*, **14**, 809 (2000)
404. E.J.Beckman. *J. Supercrit. Fluids*, **28**, 121 (2004)
405. D.Chouchi, D.Gourgouillon, M.Courel, J.Vital, M.Nunes da Ponte. *Ind. Eng. Chem. Res.*, **40**, 2551 (2001)
406. H.S.Phiong, F.P.Lucien, A.A.Adesina. *J. Supercrit. Fluids*, **25**, 155 (2003)
407. C.Xi, H.Cheng, J.Hao, S.Cai, F.Zhao. *J. Mol. Catal. A: Chem.*, **282**, 80 (2008)
408. M.Arai, S.I.Fujita, M.Shirai. *J. Supercrit. Fluids*, **47**, 351 (2009)
409. X.Dong, C.Erkey. *J. Mol. Catal. A: Chem.*, **211**, 73 (2004)
410. M.Kanakubo, T.Umecky, P.Raveendran, T.Ebina, Y.Ikushima. *J. Solut. Chem.*, **33**, 863 (2004)
411. C.M.Wai, S.Wang, J.-J.Yu. *Anal. Chem.*, **68**, 3516 (1996)
412. M.Ashraf-Khorassani, M.T.Combs, L.T.Taylor. *Talanta*, **44**, 755 (1997)
413. Z.Shen, M.A.McHugh, K.M.Lott, M.E.Wright. *Fluid Phase Equilib.*, **216**, 1 (2004)
414. R.M.Hamdi, J.F.Bocquet, K.Chor, C.Pommier. *J. Supercrit. Fluids*, **5**, 55 (1992)
415. K.E.Laintz, C.M.Wai, C.R.Yonker, R.D.Smith. *J. Supercrit. Fluids*, **4**, 194 (1991)
416. M.Kitamura, M.Tokunaga, T.Ohkuma, R.Noyori. *Tetrahedron Lett.*, **32**, 4163 (1991)
417. S.Lange, A.Brinkmann, P.Trautner, K.Woelk, J.Bargon, W.Leitner. *Chirality*, **12**, 450 (2000)
418. P.W.N.M.van Leeuwen, P.C.J.Kamer, C.Clàver, O.Pamies, M.Diéguez. *Chem. Rev.*, **111**, 2077 (2011)
419. S.E.Lyubimov, A.A.Tyutyunov, V.N.Kalinin, E.E.Said-Galiev, A.R.Khokhlov, P.V.Petrovskii, V.A.Davankov. *Tetrahedron Lett.*, **48**, 8217 (2007)
420. S.E.Lyubimov, I.V.Kuchurov, A.A.Tyutyunov, P.V.Petrovskii, V.N.Kalinin, S.G.Zlotin, V.A.Davankov, E.Hey-Hawkins. *Catal. Commun.*, **11**, 419 (2010)
421. S.E.Lyubimov, E.E.Said-Galiev, A.R.Khokhlov, N.M.Loim, L.N.Popova, P.V.Petrovskii, V.A.Davankov. *J. Supercrit. Fluids*, **45**, 70 (2008)
422. S.E.Lyubimov, V.A.Davankov, E.E.Said-Galiev, A.R.Khokhlov. *Catal. Commun.*, **9**, 1851 (2008)
423. S.E.Lyubimov, I.V.Kuchurov, V.A.Davankov, S.G.Zlotin. *J. Supercrit. Fluids*, **50**, 118 (2009)
424. S.E.Lyubimov, V.A.Olshevskaya, P.V.Petrovskii, E.A.Rastorguev, T.A.Verbitskaya, V.N.Kalinin, V.A.Davankov. *Russ. Chem. Bull., Int. Ed.*, **59**, 1836 (2010)
425. S.E.Lyubimov, E.A.Rastorguev, P.V.Petrovskii, V.A.Davankov. *Russ. Chem. Bull., Int. Ed.*, **60**, 587 (2011)
426. S.E.Lyubimov, E.A.Rastorguev, V.A.Davankov. *Chirality*, **23**, 624 (2011)
427. D.V.Ozolin, S.E.Lyubimov, V.A.Davankov. *Russ. Chem. Bull., Int. Ed.*, **63**, 693 (2014)
428. J.C.Thomas, M.D.Burich, P.T.Bandeira, A.R.M.de Oliveira, L.Piovan. *Biocatalysis*, **3**, 27 (2017)
429. E.Garcia-Verdugo, B.Altava, M.I.Burguete, P.Lozano, S.V.Luis. *Green Chem.*, **17**, 2693 (2015)
430. C.E.Song. *Annu. Rep. Prog. Chem., Sect. C*, **101**, 143 (2005)
431. P.Stephenson, P.Licence, S.K.Ross, M.Poliakoff. *Green Chem.*, **6**, 521 (2004)
432. P.Stephenson, B.Kondor, P.Licence, K.Scovell, S.K.Ross, M.Poliakoff. *Adv. Synth. Catal.*, **348**, 1605 (2006)
433. U.Hintermair, T.Hofener, T.Pullmann, G.Franciò, W.Leitner. *ChemCatChem*, **2**, 150 (2010)
434. L.A.Blanchard, D.Hancu, E.J.Beckman, J.F.Brennecke. *Nature (London)*, **399**, 28 (1999)
435. U.Hintermair, G.Franciò, W.Leitner. *Chem. – Eur. J.*, **19**, 4538 (2013)
436. Z.Zhang, G.Franciò, W.Leitner. *ChemCatChem*, **7**, 1961 (2015)
437. S.Wang, F.Kienzle. *Ind. Eng. Chem. Res.*, **39**, 4487 (2000)
438. O.V.Turova, I.V.Kuchurov, E.V.Starodubtseva, V.A.Ferapontov, N.S.Ikonnikov, S.G.Zlotin, M.G.Vinogradov. *Mendeleev Commun.*, **22**, 184 (2012)
439. M.Kitamura, T.Ohkuma, H.Takaya, R.Noyori. *Tetrahedron Lett.*, **29**, 1555 (1988)
440. J.Theuerkauf, G.Franciò, W.Leitner. *Adv. Synth. Catal.*, **355**, 209 (2013)
441. T.C.Nugent, M.El.Shazly. *Adv. Synth. Catal.*, **352**, 753 (2010)
442. N.Fleury-Brégeot, V.de la Fuente, S.Castillón, C.Claver. *ChemCatChem*, **2**, 1346 (2010)
443. R.Ferraccioli. *Lett. Org. Chem.*, **14**, 461 (2017)
444. H.U.Blaser, F.Spindler. *Top. Catal.*, **4**, 275 (1997)
445. A.Togni. *Angew. Chem., Int. Ed. Engl.*, **35**, 1475 (1996)
446. N.Andrushko, V.Andrushko. In *Stereoselective Synthesis of Drugs and Natural Products*. (Eds V.Andrushko, N.Andrushko). (Hoboken: Wiley, 2013). P. 909
447. S.Kainz, A.Brinkmann, W.Leitner, A.Pfaltz. *J. Am. Chem. Soc.*, **121**, 6421 (1999)
448. M.Solinas, A.Pfaltz, P.G.Cozzi, W.Leitner. *J. Am. Chem. Soc.*, **126**, 16142 (2004)
449. S.E.Lyubimov, E.A.Rastorguev, P.V.Petrovskii, E.S.Kelbysheva, N.M.Loim, V.A.Davankov. *Tetrahedron Lett.*, **52**, 1395 (2011)
450. F.Ungváry. *Coord. Chem. Rev.*, **251**, 2087 (2007)
451. S.Kainz, W.Leitner. *Catal. Lett.*, **55**, 223 (1998)
452. G.Franciò, W.Leitner. *Chem. Commun.*, 1663 (1999)
453. F.Shibahara, K.Nozaki, T.Hiyama. *J. Am. Chem. Soc.*, **125**, 8555 (2003)
454. P.G.Jessop, R.A.Brown, M.Yamakawa, J.Xiao, T.Ikariya, M.Kitamura, S.C.Tucker, R.Noyori. *J. Supercrit. Fluids*, **24**, 161 (2002)
455. Z.Lu, S.Ma. *Angew. Chem., Int. Ed.*, **47**, 258 (2008)
456. J.Qian, G.Jiang. *Curr. Catal.*, **6**, 25 (2017)
457. M.Yoshida. *J. Org. Chem.*, **82**, 12821 (2017)
458. S.E.Lyubimov, I.V.Kuchurov, A.A.Vasilev, S.G.Zlotin, V.A.Davankov. *Mendeleev Commun.*, **20**, 143 (2010)
459. A.Bösmann, G.Franciò, E.Janssen, M.Solinas, W.Leitner, P.Wasserscheid. *Angew. Chem., Int. Ed.*, **40**, 2697 (2001)
460. L.I.Rodríguez, O.Rossell, M.Seco, A.Orejón, A.M.Masdeu-Bultó. *J. Organomet. Chem.*, **693**, 1857 (2008)
461. L.I.Rodríguez, O.Rossell, M.Seco, A.Orejón, A.M.Masdeu-Bultó. *J. Supercrit. Fluids*, **55**, 1023 (2011)
462. C.J.T.Kuster, H.W.Scheeren. In *High Pressure Chemistry: Synthetic, Mechanistic, and Supercritical Applications*. (Eds R.Van Eldik, F.-G.Klarner). (Weinheim: Wiley-VCH, 2002). P. 284
463. S.I.Fukuzawa, H.Matsuzawa, K.Metoki. *Synlett*, 709 (2001)
464. D.C.Wynne, M.M.Olmstead, P.G.Jessop. *J. Am. Chem. Soc.*, **122**, 7638 (2000)

465. M.I.Burguete, A.Cornejo, E.Garcia-Verdugo, M.J.Gil, S.V.Luis, J.A.Mayoral, V.Martinez-Merino, M.Sokolova. *J. Org. Chem.*, **72**, 4344 (2007)
466. M.I.Burguete, A.Cornejo, E.Garcia-Verdugo, J.Garcia, M.J.Gil, S.V.Luis, V.Martinez-Merino, J.A.Mayoral, M.Sokolova. *Green Chem.*, **9**, 1091 (2007)
467. C.Aranda, A.Cornejo, J.M.Fraile, E.Garcia-Verdugo, M.J.Gil, S.V.Luis, J.A.Mayoral, V.Martinez-Merino, Z.Ochoa. *Green Chem.*, **13**, 983 (2011)
468. B.Castano, E.Gallo, D.J.Cole-Hamilton, V.Dal Santo, R.Psaro, A.Caselli. *Green Chem.*, **16**, 3202 (2014)
469. C.Böhm, O.Reiser. *Org. Lett.*, **3**, 1315 (2001)
470. K.Mikami, S.Matsukawa, Y.Kayaki, T.Ikariya. *Tetrahedron Lett.*, **41**, 1931 (2000)
471. L.Liu, Z.T.Liu, Z.W.Liu, D.Xue. *Sci. Chin. Chem.*, **53**, 1586 (2010)
472. L.Qin, L.Zhang, Q.Jin, J.Zhang, B.Han, M.Liu. *Angew. Chem., Int. Ed.*, **52**, 7761 (2013)
473. A.G.Nigmatov, I.V.Kuchurov, D.E.Siyutkin, S.G.Zlotin. *Tetrahedron Lett.*, **53**, 3502 (2012)
474. T.Okino, Y.Hoashi, T.Furukawa, X.Xu, Y.Takemoto. *J. Am. Chem. Soc.*, **127**, 119 (2005)
475. J.-m.Liu, X.Wang, Z.-m.Ge, Q.Sun, T.-m.Cheng, R.-t.Li. *Tetrahedron*, **67**, 636 (2011)
476. C.J.Gao, W.S.Shin, J.M.Han, D.Y.Han, C.Adharvana, H.D.Kim, K.H.Ahn. *Bull. Korean Chem. Soc.*, **30**, 541 (2009)
477. O.Erdem, B.Guzel. *J. Supercrit. Fluids*, **85**, 6 (2014)
478. I.V.Kuchurov, A.G.Nigmatov, E.V.Kryuchkova, A.A.Kostenko, A.S.Kucherenko, S.G.Zlotin. *Green Chem.*, **16**, 1521 (2014)
479. F.Palacios, C.Alonso, J.M.de Los Santos. *Chem. Rev.*, **105**, 899 (2005)
480. *A Guide to Organophosphorus Chemistry*. (Ed. L.D.Quin). (Hoboken: Wiley, 2000)
481. L.F.Tietze, U.Beifuss. *Angew. Chem., Int. Ed. Engl.*, **32**, 131 (1993)
482. E.Teoh, W.R.Jackson, A.J.Robinson. *Aust. J. Chem.*, **58**, 63 (2005)
483. L.F.Tietze, G.Brasche, K.M.Gericke. *Domino Reactions in Organic Synthesis*. (Weinheim: Wiley-VCH, 2006)
484. H.Pellissier. *Adv. Synth. Catal.*, **354**, 237 (2012)
485. Z.Li, J.-G.Chen, L.-P.Song, Z.-W.Liu, D.Xue, Z.-T.Liu. *Russ. J. Org. Chem.*, **49**, 1854 (2013)
486. I.Jacquemond-Collet, S.Hannedouche, N.Fabre, I.Fourast. *Phytochemistry*, **51**, 1167 (1999)
487. K.M.Witherup, R.W.Ransom, A.C.Graham, A.M.Bernard, M.J.Salvatore, W.C.Lumma, P.S.Anderson, S.M.Pitzenberger, S.L.Varga. *J. Am. Chem. Soc.*, **117**, 6682 (1995)
488. E.V.Filatova, O.V.Turova, I.V.Kuchurov, A.A.Kostenko, A.G.Nigmatov, S.G.Zlotin. *J. Supercrit. Fluids*, **109**, 35 (2016)
489. E.V.Filatova, O.V.Turova, A.G.Nigmatov, S.G.Zlotin. *Tetrahedron*, **74**, 157 (2018)
490. M.Kemmere. In *Supercritical Carbon Dioxide: in Polymer Reaction Engineering*. (Eds M.F.Kemmere, T.Meyer). (Weinheim: Wiley-VCH Verlag, 2005). P. 1
491. C.Jérôme, P.Lecomte. *Adv. Drug Deliv. Rev.*, **60**, 1056 (2008)
492. Z.Zhang, K.Huang, Z.Liu. *Supercrit. Carbon Dioxide Macromol.*, **44**, 820 (2011)
493. D.Yuan, J.Bao, Y.Ren, W.Li, L.Huang, X.Cai. *CrystEngComm.*, **20**, 4676 (2018)
494. O.Ihata, Y.Kayaki, T.Ikariya. *Angew. Chem., Int. Ed.*, **43**, 717 (2004)
495. B.Tan, H.M.Woods, P.Licence, S.M.Howdle, A.I.Cooper. *Macromoleules*, **38**, 1691 (2005)
496. T.Tabanelli, D.Bonincontro, S.Albonetti, F.Cavani. *Stud. Surface Sci. Catal.*, **178**, 125 (2019)
497. J.M.DeSimone, Z.Guan, C.S.Elsbernd. *Science*, **257**, 945 (1992)
498. S.Beuermann, M.Imran-ul-Haq. *J. Polym. Sci., Part A: Polym. Chem.*, **45**, 5626 (2007)
499. S.Beuermann, M.Imran-ul-Haq. *Macromol. Symp.*, **259**, 210 (2007)
500. U.Beginn, R.Najjar, J.Ellmann, M.Möller. *Chem. Ing. Tech.*, **83**, 1419 (2011)
501. U.Michel, P.Resnick, B.Kipp, J.M.DeSimone. *Macromolecules*, **36**, 7107 (2003)
502. F.A.Adamsky, E.J.Beckman. *Macromolecules*, **27**, 312 (1994)
503. Y.A.Hussain, T.Liu, G.W.Roberts. *Ind. Eng. Chem. Res.*, **51**,11401 (2012)
504. P.O'Connor, P.B.Zetterlund, F.Aldabbagh. *J. Polym. Sci., Part A: Polym. Chem.*, **49**,1719 (2011)
505. W.Ye, J.M.DeSimone. *Macromolecules*, **38**, 2180 (2005)
506. S.Villarroya, K.J.Thurecht, S.M.Howdle. *Green Chem.*, **10**, 863 (2008)
507. R.Kamrupi, B.Pokhrel, A.Kalita, M.Boruah, S.K.Dolui, R.Boruah. *Adv. Polym. Technol.*, **31**, 154 (2012)
508. T.J.Romack, E.E.Maury, J.M.De Simone. *Macromolecules*, **28**, 912 (1995)
509. T.Liu, J.M.DeSimone, G.W.Roberts. *Chem. Eng. Sci.*, **61**, 3129 (2006)
510. L.Cao, L.Chen, W.Lai. *J. Polym. Sci., Part A: Polym. Chem.*, **45**, 955 (2007)
511. P.O'Connor, P.B.Zetterlund, F.Aldabbagh. *Macromolecules*, **43**, 914 (2010)
512. X.-H.Wang, L.-Q.Cao, L.-J.Zhang, J.-D.Wang. *Polym. Adv. Technol.*, **23**, 529 (2012)
513. G.Hawkins, P.B.Zetterlund, F.Aldabbagh. *J. Polym. Sci., Part A: Polym. Chem.*, **53**, 2351 (2015)
514. S.Zhan, J.Ren, W.Wang, Q.Zhao, J.Zhou. *Polym. Eng. Sci.*, **54**, 704 (2014)
515. H.Minami, Y.Kagawa, S.Kuwahara, J.Shigematsu, S.Fujii, M.Okubo. *Des. Monomers Polym.*, **7**, 553 (2004)
516. B.Grignard, T.Phan, D.Bertin, D.Gigmes, C.Jérôme, C.Detrembleur. *Polym. Chem.*, **1**, 837 (2010)
517. P.F.Oliveira, R.A.F.Machado, D.Barth, E.D.Acosta. *Chem. Eng. Process*, **103**, 46 (2016)
518. M.Haruki, Y.Kodama, K.Tachimori, S.-I.Kihara, S.Takishima. *J. Appl. Polym. Sci.*, **133**, 43813 (2016)
519. M.Okubo, Y.Kitayama, T.Taniyama, X.Liu, J.Zhang, H.Shi. *J. Polym. Sci., Part A: Polym. Chem.*, **57**, 613 (2019)
520. H.Shiho, J.M.DeSimone. *J. Polym. Sci., Part A: Polym. Chem.*, **38**, 3783 (2000)
521. Z.Ma, P.Lacroix-Desmazes. *Polymer (Guildf)*, **45**, 6789 (2004)
522. K.S.Oh, W.Bae, H.Kim. *Eur. Polym. J.*, **44**, 415 (2008)
523. T.Carson, J.Lizotte, J.M.Desimone. *Macromolecules*, **33**, 1917 (2000)
524. R.McHale, F.Aldabbagh, P.B.Zetterlund, M.Okubo. *Macromol. Rapid Commun.*, **27**, 1465 (2006)
525. J.Ryan, F.Aldabbagh, P.B.Zetterlund, M.Okubo. *Polymer (Guildf)*, **46**, 9769 (2005)
526. J.Jennings, M.Beija, J.T.Kennon, H.Willcock, R.K.O'Reilly, S.Rimmer, S.M.Howdle. *Macromolecules*, **46**, 6843 (2013)
527. M.Okubo, Y.Kitayama, T.Taniyama, H.Minami, X.Liu, C.Huang. *Ind. Eng. Chem. Res.*, **58**, 21165 (2019)

528. N.A.Birkin, N.J.Arrowsmith, E.J.Park, A.P.Richez, S.M.Howdle. *Polym. Chem.*, **2**, 1293 (2011)
529. J.M.DeSimone, E.E.Maury, Y.Z.Menceloglu, J.B.McClain, T.J.Romack, J.R.Combes. *Science*, **265**, 356 (1994)
530. R.Ferrari, C.M.Pecoraro, G.Storti, D.Moscatelli. *RSC Adv.*, **4**, 12795 (2014)
531. R.Goddard, S.Pérez-Nieto, T.M.Passos, B.Quilty, K.Carmichael, D.J.Irvine, S.M.Howdle. *Green Chem.*, **18**, 4772 (2016)
532. J.Deng, S.Zhan, J.Wang, Z.Liu, Z.Li. *Aust. J. Chem.*, **70**, 712 (2017)
533. B.Grignard, J.De Winter, P.Gerbaux, B.Gilbert, C.Jerome, C.Detrembleur. *Eur. Polym. J.*, **95**, 635 (2017)
534. N.Mase, Moniruzzaman, S.Mori, J.Ishizuka, F.Kumazawa, S.Yamamoto, K.Sato, T.Narumi. *Tetrahedron Lett.*, **59**, 4392 (2018)
535. C.Schmidt, M.Behl, A.Lendlein, S.Beuermann. *RSC Adv.*, **4**, 35099 (2014)
536. S.R.Rosso Comim, J.G.Veneral, D.de Oliveira, S.R.S.Ferreira, J.V.Oliveira. *J. Supercrit. Fluids*, **96**, 334 (2015)
537. R.D.Santos, S.R.Rosso Comim, D.de Oliveira, H.Treichel, M.Di Luccio, S.R.S.Ferreira, J.V.Oliveira. *Biocatal. Agric. Biotechnol.*, **1**, 280 (2012)
538. M.Yilmaz, S.Eğri, N.Yildiz, A.Çalimli, E.Pişkin. *Polym. J.*, **43**, 785 (2011)
539. H.Kamali, E.Khodaverdi, F.Hadizadeh. *J. Supercrit. Fluids*, **137**, 9 (2018)
540. H.Kamali, R.Mollaee, E.Khodaverdi, F.Hadizadeh, G.H.Zohuri. *J. Supercrit. Fluids*, **145**, 133 (2019)
541. O.García-Valdez, D.G.Ramírez-Wong, E.Saldívar-Guerra, G.Luna-Bárcenas. *Macromol. Chem. Phys.*, **214**, 1396 (2013)
542. B.Grignard, C.Calberg, C.Jerome, C.Detrembleur. *J. Supercrit. Fluids*, **53**, 151 (2010)
543. T.Arita, T.Yoshimura, T.Adschiri. *Bull. Chem. Soc. Jpn.*, **83**, 838 (2010)
544. G.Jaramillo-Soto, P.R.García-Morán, E.Vivaldo-Lima. *Macromol. Symp.*, **289**, 149 (2010)
545. X.Liu, J.Chen, P.Sun, Z.-W.Liu, Z.-T.Liu. *React. Funct. Polym.*, **70**, 972 (2010)
546. P.López-Domínguez, J.C.Hernández-Ortiz, E.Vivaldo-Lima. *Macromol. Theory Simul.*, **27**, 1700064 (2018)
547. P.López-Domínguez, G.Jaramillo-Soto, E.Vivaldo-Lima. *Macromol. React. Eng.*, **12**, 1800011 (2018)
548. T.Ribaut, P.Lacroix-Desmazes, B.Fournel, S.Sarrade. *J. Polym. Sci., Part A: Polym. Chem.*, **47**, 5448 (2009)
549. Z.Y.Huo, P.D.Xia, U.Azhar, J.C.Ma, X.M.Zhang, X.Y.Zhou, S.X.Zhang, A.H.Xu. *IOP Conf. Ser. Mater. Sci. Eng.*, **479**, 012107 (2019)
550. J.de Gooijer, M.Scheltus, H.Lösch, R.Staudt, J.Meuldijk, C.Koning. *J. Supercrit. Fluids*, **29**, 129 (2004)
551. J.de Gooijer, M.Scheltus, C.Koning. *J. Supercrit. Fluids*, **29**, 153 (2004)
552. J.M.de Gooijer, J.Ellmann, M.Möller, C.E.Koning. *J. Supercrit. Fluids*, **31**, 75 (2004)
553. J.M.de Gooijer, M.Scheltus, M.A.G.Jansen, C.E.Koning. *Polymer (Guildf.)*, **44**, 2201 (2003)
554. Z.Liu, L.Song, X.Dai, G.Yang, B.Han, J.Xu. *Polymer (Guildf.)*, **43**, 1183 (2002)
555. D.Li, B.Han, Z.Liu. *Macromol. Chem. Phys.*, **202**, 2187 (2001)
556. Z.Dong, Z.Liu, B.Han, J.He, T.Jiang, G.Yang. *J. Mater. Chem.*, **12**, 3565 (2002)
557. A.L.Mohamed, M.Er-Rafik, M.Moller. *Carbohydr. Polym.*, **98**, 1095 (2013)
558. A.B.Solovieva, A.V.Cherkasova, N.N.Glagolev, A.S.Kopylov, P.S.Timashev, S.I.Tsypina, V.N.Bagratashvili. *J. Mol. Liq.*, **239**, 74 (2017)
559. F.Zou, L.Peng, W.Fu, J.Zhang, Z.Li. *RSC Adv.*, **5**, 76346 (2015)
560. I.V.Elmanovich, T.A.Pryakhina, V.G.Vasil'ev, M.O.Gallyamov, A.M.Muzafarov. *J. Supercrit. Fluids*, **133**, 512 (2018)
561. M.N.Temnikov, Y.N.Kononevich, I.B.Meshkov, M.I.Buzin, V.G.Vasil'ev, G.G.Nikiforova, A.M.Muzafarov. *Polymer*, **138**, 255 (2018)
562. L.Cao, Y.Hu, L.Zhang, C.Ma, X.Wang, J.Wang. *J. Supercrit. Fluids*, **58**, 233 (2011)
563. L.Cao, C.Ma, J.Wang, P.Chen. *J. Supercrit. Fluids*, **75**, 152 (2013)
564. H.Chi, L.Cao, J.Wang. *RSC Adv.*, **6**, 4434 (2016)
565. C.Ma, L.Cao, X.Wang, L.Zhang, M.Shi, J.Wang. *J. Supercrit. Fluids*, **62**, 232 (2012)
566. C.S.Li, J.C.Liang, X.L.Zhu, X.Z.Kong. *Chin. Chem. Lett.*, **22**, 489 (2011)
567. C.Li, J.Liang, X.Zhu, X.Z.Kong. *Colloid Polym. Sci.*, **288**, 1571 (2010)
568. C.Boyère, A.F.Léonard, B.Grignard, A.Favrelle, J.-P.Pirard, M.Paquot, C.Jérôme, A.Debuigne. *Chem. Commun.*, **48**, 8356 (2012)
569. G.Jaramillo-Soto, C.M.Villa-Ávila, E.Vivaldo-Lima. *J. Macromol. Sci., Part A*, **50**, 281 (2013)
570. T.D.McAllister, L.D.Farrand, S.M.Howdle. *Macromol. Chem. Phys.*, **217**, 2294 (2016)
571. G.Jaramillo-Soto, E.Vivaldo-Lima. *Aust. J. Chem.*, **65**, 1177 (2012)
572. Z.Meng, Y.He, P.Liang, J.Nie. *J. Appl. Polym. Sci.*, **125**, 1460 (2012)
573. K.Matsuyama. *J. Supercrit. Fluids*, **134**, 197 (2018)
574. *Aerogels Handbook*. (Eds M.A.Aegerter, N.Leventis, M.M.Koebel). (New York: Springer, 2011)
575. A.Du, B.Zhou, Z.Zhang, J.Shen. *Materials (Basel)*, **6**, 941 (2013)
576. C.Li, L.Qiu, B.Zhang, D.Li, C.-Y.Liu. *Adv. Mater.*, **28**, 1510 (2016)
577. J.L.Gurav, A.V.Rao, D.Y.Nadargi, H.-H.Park. *J. Mater. Sci.*, **45**, 503 (2010)
578. S.Dorcheh, M.H.Abbasi. *J. Mater. Process. Technol.*, **199**, 10 (2008)
579. J.L.Gurav, I.-K.Jung, H.-H.Park, E.S.Kang, D.Y.Nadargi. *J. Nanomater.*, Art. ID 409310 (2010)
580. H.Maleki, L.Durães, A.Portugal. *J. Non-Cryst. Solids*, **385**, 55 (2014)
581. Y.Guo, W.Meyer-Zaika, M.Muhler, S.Vukojević, M.Epple. *Eur. J. Inorg. Chem.*, 4774 (2006)
582. K.K.Kalebaila, S.L.Brock. *Z. Anorg. Allg. Chem.*, **638**, 2598 (2012)
583. T.Hendel, V.Lesnyak, L.Kühn, A.-K.Herrmann, N.C.Bigall, L.Borchardt, S.Kaskel, N.Gaponik, A.Eychmüller. *Adv. Funct. Mater.*, **23**, 1903 (2013)
584. L.Ren, S.Cui, F.Cao, Q.Guo. *Angew. Chem., Int. Ed.*, **53**, 10147 (2014)
585. U.K.H.Bangi, K.-Y.Lee, N.M.N.Maldar, H.-H.Park. *J. Nanosci. Nanotechnol.*, **19**, 1217 (2019)
586. L.Fan, Y.Zhang, Q.Zhang, X.Wu, J.Cheng, N.Zhang, Y.Feng, K.Sun. *Small*, **12**, 5208 (2016)
587. W.Gu, G.Yushin. *Wiley Interdiscip. Rev. Energy Environ.*, **3**, 424 (2014)

588. L.Zuo, Y.Zhang, L.Zhang, Y.-E.Miao, W.Fan, T.Liu. *Materials (Basel)*, **8**, 6806 (2015)
589. Z.Lin, Z.Zeng, X.Gui, Z.Tang, M.Zou, A.Cao. *Adv. Energy Mater.*, **6**, 1600554 (2016)
590. K.Kanamori, K.Nakanishi. *Chem. Soc. Rev.*, **40**, 754 (2011)
591. L.Hu, R.He, H.Lei, D.Fang. *J. Thermophys.*, **40**, 39 (2019)
592. G.D.Sorarù, F.Dalcanale, R.Campostrini, A.Gaston, Y.Blum, S.Carturan, P.R.Aravind. *J. Mater. Chem.*, **22**, 7676 (2012)
593. T.Hu, L.Li, J.Zhang. *ACS Sustain. Chem. Eng.*, **6**, 11222 (2018)
594. G.Zu, K.Kanamori, T.Shimizu, Y.Zhu, A.Maeno, H.Kaji, K.Nakanishi, J.Shen. *Chem. Mater.*, **30**, 2759 (2018)
595. K.Kanamori, R.Ueoka, T.Kakegawa, T.Shimizu, K.Nakanishi. *J. Sol-Gel Sci. Technol.*, **89**, 166 (2019)
596. N.Diascorn, S.Calas, H.Sallée, P.Achard, A.Rigacci. *J. Supercrit. Fluids*, **106**, 76 (2015)
597. N.Diascorn, H.Sallée, S.Calas, A.Rigacci, P.Achard. *Eur. Phys. J. Spec. Top.*, **224**, 1737 (2015)
598. C.Chidambareswarapattar, P.M.McCarver, H.Luo, H.Lu, C.Sotiriou-Leventis, N.Leventis. *Chem. Mater.*, **25**, 3205 (2013)
599. A.Bang, C.Buback, C.Sotiriou-Leventis, N.Leventis. *Chem. Mater.*, **26**, 6979 (2014)
600. A.Shinko, S.C.Jana, M.A.Meador. *RSC Adv.*, **5**, 105329 (2015)
601. S.Malakooti, S.Rostami, H.G.Churu, H.Luo, J.Clark, F.Casarez, O.Rettenmaier, S.Daryadel, M.Minary-Jolandan, L.Sotiriou-Leventis, N.Leventis, H.Lu. *RSC Adv.*, **8**, 21214 (2018)
602. S.Malakooti, H.G.Churu, A.Lee, S.Rostami, S.J.May, S.Ghidei, F.Wang, Q.Lu, H.Luo, N.Xiang, C.Sotiriou-Leventis, N.Leventis, H.Lu. *Adv. Eng. Mater.*, **20**, 1700937 (2018)
603. N.Leventis, C.Sotiriou-Leventis, N.Chandrasekaran, S.Mulik, Z.J.Larimore, H.Lu, H.G.Churu, J.T.Mang. *Chem. Mater.*, **22**, 6692 (2010)
604. S.Członka, M.F.Bertino, J.Kośny, N.Shukla. *J. Sol-Gel Sci. Technol.*, **87**, 685 (2018)
605. Z.Cheng, K.De Gracia, D.A.Schiraldi. *Polymers*, **10**, 1102 (2018)
606. H.-B.Chen, B.Liu, W.Huang, J.-S.Wang, G.Zeng, W.-H.Wu, D.A.Schiraldi. *ACS Appl. Mater. Interfaces*, **6**, 16227 (2014)
607. A.Bang, D.Mohite, A.M.Saeed, N.Leventis, C.Sotiriou-Leventis. *J. Sol-Gel Sci. Technol.*, **75**, 460 (2015)
608. J.C.Williams, B.N.Nguyen, L.McCorkle, D.Scheiman, J.S.Griffin, S.A.Steiner, M.A.B.Meador. *ACS Appl. Mater. Interfaces*, **9**, 1801 (2017)
609. T.Wu, J.Dong, F.Gan, Y.Fang, X.Zhao, Q.Zhang. *Appl. Surf. Sci.*, **440**, 595 (2018)
610. Y.Wu, W.Zhang, R.Yang. *Macromol. Mater. Eng.*, **303**, 1700403 (2018)
611. W.Wu, K.Wang, M.-S.Zhan. *Ind. Eng. Chem. Res.*, **51**, 12821 (2012)
612. X.Pei, W.Zhai, W.Zheng. *Langmuir*, **30**, 13375 (2014)
613. T.Ning, G.Yang, W.Zhao, X.Liu. *React. Funct. Polym.*, **116**, 17 (2017)
614. H.Guo, M.A.B.Meador, L.McCorkle, D.J.Quade, J.Guo, B.Hamilton, M.Cakmak. *ACS Appl. Mater. Interfaces*, **4**, 5422 (2012)
615. H.Guo, M.A.B.Meador, L.McCorkle, D.J.Quade, J.Guo, B.Hamilton, M.Cakmak, G.Sprowl. *ACS Appl. Mater. Interfaces*, **3**, 546 (2011)
616. M.Gawryla, E.Arndt, M.Sánchez-Soto, D.Schiraldi. *Materials (Basel)*, **11**, 233 (2018)
617. Y.Chen, G.Shao, Y.Kong, X.Shen, S.Cui. *Chem. Eng. J.*, **322**, 1 (2017)
618. S.Longo, J.G.Vitillo, C.Daniel, G.Guerra. *ACS Appl. Mater. Interfaces*, **5**, 5493 (2013)
619. M.Joseph, B.Nagendra, P.Shaiju, K.P.Surendran, E.B.Gowd. *J. Mater. Chem. C*, **6**, 360 (2018)
620. S.J.Talley, C.L.A.Schoepe, C.J.Berger, K.A.Leary, S.A.Snyder, R.B.Moore. *Polymer (Guildf.)*, **126**, 437 (2017)
621. X.Wang, L.-L.Lu, Z.-L.Yu, X.-W.Xu, Y.-R.Zheng, S.-H.Yu. *Angew. Chem., Int. Ed.*, **54**, 2397 (2015)
622. S.Yun, H.Luo, Y.Gao. *J. Mater. Chem. A*, **2**, 14542 (2014)
623. M.Wang, I.V.Anoshkin, A.G.Nasibulin, J.T.Korhonen, J.Seitsonen, J.Pere, E.I.Kauppinen, R.H.A.Ras, O.Ikkala. *Adv. Mater.*, **25**, 2428 (2013)
624. C.Wan, Y.Lu, Y.Jiao, J.Cao, Q.Sun, J.Li. *J. Sol-Gel Sci. Technol.*, **74**, 256 (2015)
625. C.Wan, J.Li. *Fibers Polym.*, **16**, 1230 (2015)
626. C.Wan, Y.Lu, Y.Jiao, C.Jin, Q.Sun J.Li. *J. Appl. Polym. Sci.*, **132**, 42037 (2015)
627. M.Kettunen, R.J.Silvennoinen, N.Houbenov, A.Nykänen, J.Ruokolainen, J.Sainio, V.Pore, M.Kemell, M.Ankerfors, T.Lindström, M.Ritala, R.H.A.Ras, O.Ikkala. *Adv. Funct. Mater.*, **21**, 510 (2011)
628. M.Hamedi, E.Karabulut, A.Marais, A.Herland, G.Nyström, L.Wågberg. *Angew. Chem., Int. Ed.*, **52**, 12038 (2013)
629. J.Innerlohinger, H.K.Weber, G.Kraft. *Macromol. Symp.*, **244**, 126 (2006)
630. H.Geng. *Int. J. Biol. Macromol.*, **118**, 921 (2018)
631. N.Lavoine, L.Bergström. *J. Mater. Chem. A*, **5**, 16105 (2017)
632. X.Wang, Y.Zhang, H.Jiang, Y.Song, Z.Zhou, H.Zhao. *Mater. Lett.*, **183**, 179 (2016)
633. V.López Durán, J.Erlandsson, L.Wågberg, P.A.Larsson. *ACS Sustain. Chem. Eng.*, **6**, 9951 (2018)
634. E.S.Ferreira, C.A.Rezende. *ACS Sustain. Chem. Eng.*, **6**, 14365 (2018)
635. D.de Morais Zanata, L.C.Battirola, M.do Carmo Goncalves. *Cellulose*, **25**, 7225 (2018)
636. M.Saraji, A.Shahvar. *Anal. Chim. Acta*, **973**, 51 (2017)
637. P.C.Thapliyal, K.Singh. *J. Mater.*, 1 (2014)
638. J.Choi, D.J.Suh. *Catal. Surv. Asia*, **11**, 123 (2007)
639. A.C.Pierre, G.M.Pajonk. *Chem. Rev.*, **102**, 4243 (2002)
640. N.Hüsing, U.Schubert. In *Ullmann's Encyclopedia of Industrial Chemistry*. (Weinheim: Wiley-VCH, 2012). P. 621
641. G.Reichenauer. *Kirk-Othmer Encyclopedia of Chemical Technology*. (Weinheim: Wiley-VCH, 2008)
642. T.-Y.Wei, S.-Y.Lu. In *Energy Efficiency and Renewable Energy Through Nanotechnology, Green Energy and Technology*. (Ed. L.Zang). (London: Springer-Verlag, 2011). P. 873
643. D.A.Schiraldi. In *Encyclopedia of Polymer Science and Technology*. (New York: Wiley, 2015). P. 1; DOI: 10.1002/0471440264.pst637
644. İ.Şahin, Y.Özbakır, Z.İnönü, Z.Ulker, C.Erkey. *Gels*, **4**, 3 (2017)
645. Z.Qian, Z.Wang, N.Zhao, J.Xu. *Macromol. Rapid Commun.*, **39**, 1700724 (2018)
646. S.Zhao, W.J.Malfait, N.Guerrero-Alburquerque, M.M.Koebel, G.Nyström. *Angew. Chem., Int. Ed.*, **57**, 7580 (2018)
647. *Nanoscale Materials in Chemistry*. (Eds K.J.Klabunde, R.M.Richards). (New York: Wiley-VCH, 2009)
648. *The Sol-Gel Handbook: Synthesis, Characterization, and Applications*. (Eds D.Levy, M.Zayat). (Weinheim: Wiley-VCH, 2015)

649. Y.-W.Zhao, Y.-Z.Gu, P.Huang. *Polym. Compos.*, **39**, 3810 (2018)
650. K.Shang, W.Liao, J.Wang, Y.-T.Wang, Y.-Z.Wang, D.A.Schiraldi. *ACS Appl. Mater. Interfaces*, **8**, 643 (2016)
651. J.Nemoto, T.Saito, A.Isogai. *ACS Appl. Mater. Interfaces*, **7**, 19809 (2015)
652. T.Okada, T.Kato, T.Yamaguchi, T.Sakai, S.Mishima. *Ind. Eng. Chem. Res.*, **52**, 12018 (2013)
653. D.Chen, H.Gao, Z.Jin, J.Wang, W.Dong, X.Huang, G.Wang. *ACS Appl. Nano Mater.*, **1**, 933 (2018)
654. Z.Wang, Z.Dai, J.Wu, N.Zhao, J.Xu. *Adv. Mater.*, **25**, 4494 (2013)
655. M.M.Seraji, N.S.Ghafoorian, A.R.Bahramian. *J. Non-Cryst. Solids*, **435**, 1 (2016)
656. M.M.Koebel, L.Huber, S.Zhao, W.J.Malfait. *J. Sol-Gel Sci. Technol.*, **79**, 308 (2016)
657. A.P.Rao, G.M.Pajonk, A.V.Rao. *J. Mater. Sci.*, **40**, 3481 (2005)
658. A.Fidalgo, J.P.S.Farinha, J.M.G.Martinho, L.M.Ilharco. *Chem. Mater.*, **19**, 2603 (2007)
659. P.R.Aravind, P.Shajesh, G.D.Soraru, K.G.K.Warrier. *J. Sol-Gel Sci. Technol.*, **54**, 105 (2010)
660. J.Wang, Y.Wei, W.He, X.Zhang. *RSC Adv.*, **4**, 51146 (2014)
661. W.Chiappim Jr., C.M.Awano, D.A.Donatti, F.S.de Vicente, D.R.Vollet. *Langmuir*, **30**, 1151 (2014)
662. Z.Wang, D.Wang, Z.Qian, J.Guo, H.Dong, N.Zhao, J.Xu. *ACS Appl. Mater. Interfaces*, **7**, 2016 (2015)
663. H.Maleki, L.Durães, A.Portugal. *J. Phys. Chem. C*, **119**, 7689 (2015)
664. L.Yan, H.Ren, J.Zhu, Y.Bi, L.Zhang. *J. Porous Mater.*, **26**, 785 (2019)
665. D.A.Loy, E.M.Russick, S.AYamanaka, B.M.Baugher, K.J.Shea. *Chem. Mater.*, **9**, 2264 (1997)
666. G.Zu, J.Shen, L.Zou, W.Wang, Y.Lian, Z.Zhang, A.Du. *Chem. Mater.*, **25**, 4757 (2013)
667. A.Fidalgo, J.P.S.Farinha, J.M.G.Martinho, L.M.Ilharco. *J. Mater. Chem. A*, **1**, 12044 (2013)
668. Y.Kobayashi, T.Saito, A.Isogai. *Angew. Chem., Int. Ed.*, **53**, 10394 (2014)
669. Q.Liu, A.W.Frazier, X.Zhao, J.A.De La Cruz, A.J.Hess, R.Yang, I.I.Smalyukh. *Nano Energy*, **48**, 266 (2018)
670. M.H.Bhuiya, A.M.Anderson, M.K.Carroll, B.A.Bruno, J.L.Ventrella, B.Silberman, B.Keramati. *Ind. Eng. Chem. Res.*, **55**, 6971 (2016)
671. B.Qiu, M.Xing, J.Zhang. *J. Am. Chem. Soc.*, **136**, 5852 (2014)
672. S.M.Jung, H.Y.Jung, W.Fang, M.S.Dresselhaus, J.Kong. *Nano Lett.*, **14**, 1810 (2014)
673. A.Grau, A.Baeza, E.Serrano, J.García-Martínez, C.Nájera. *ChemCatChem*, **7**, 87 (2015)
674. M.Power, B.Hosticka, E.Black, C.Daitch, P.Norris. *J. Non-Cryst. Solids*, **285**, 303 (2001)
675. P.Zhang, L.Lv, Z.Cheng, Y.Liang, Q.Zhou, Y.Zhao, L.Qu. *Chem. – Asian J.*, **11**, 1071 (2016)
676. T.Tsutsui, M.Yahiro, H.Yokogawa, K.Kawano, M.Yokoyama. *Adv. Mater.*, **13**, 1149 (2001)
677. F.S.Rodembusch, L.F.Campo, V.Stefani, A.Rigacci. *J. Mater. Chem.*, **15**, 1537 (2005)
678. L.Sorensen, G.F.Strouse, A.E.Stiegman. *Adv. Mater.*, **18**, 1965 (2006)
679. S.Sánchez-Paradinas, D.Dorfs, S.Friebe, A.Freytag, A.Wolf, N.C.Bigall. *Adv. Mater.*, **27**, 6152 (2015)
680. D.R.Chen, X.H.Chang, X.L.Jiao. In *The Role of Colloidal Systems in Environmental Protection*. (Ed. M.Fanun). (Amsterdam: Elsevier, 2014). P. 573
681. S.Cui, W.Cheng, X.Shen, M.Fan, A.(T.)Russell, Z.Wu, X.Yi. *Energy Environ. Sci.*, **4**, 2070 (2011)
682. Q.Ma, Y.Liu, Z.Dong, J.Wang, X.Hou. *J. Appl. Polym. Sci.*, **132**, 41770 (2015)
683. W.Sun, A.Du, B.Zhou, J.Shen, S.Huang, J.Tang. *J. Sol-Gel Sci. Technol.*, **80**, 68 (2016)
684. Z.-S.Wu, S.Yang, Y.Sun, K.Parvez, X.Feng, K.Müllen. *J. Am. Chem. Soc.*, **134**, 9082 (2012)
685. X.-L.Wu, T.Wen, H.-L.Guo, S.Yang, X.Wang, A.-W.Xu. *ACS Nano*, **7**, 3589 (2013)
686. Z.Y.Yang, L.J.Jin, G.Q.Lu, Q.Q.Xiao, Y.X.Zhang, L.Jing, X.X.Zhang, Y.M.Yan, K.N.Sun. *Adv. Funct. Mater.*, **24**, 3917 (2014)
687. X.Guo, J.Shan, Z.Lai, W.Lei, R.Ding, Y.Zhang, H.Yang. *Molecules*, **23**, 945 (2018)
688. H.Bi, X.Huang, X.Wu, X.Cao, C.Tan, Z.Yin, X.Lu, L.Sun, H.Zhang. *Small*, **10**, 3544 (2014)
689. O.Karatum, S.A.Steiner, J.S.Griffin, W.Shi, D.L.Plata. *ACS Appl. Mater. Interfaces*, **8**, 215 (2016)
690. S.M.Jones. *Meteorit. Planet. Sci.*, **45**, 91 (2010)
691. J.P.Randall, M.A.B.Meador, S.C.Jana. *ACS Appl. Mater. Interfaces*, **3**, 613 (2011)
692. S.M.Jones, G.Flynn. *Meteorit. Planet. Sci.*, **46**, 1253 (2011)
693. M.A.B.Meador, S.Wright, A.Sandberg, B.N.Nguyen, F.W.Van Keuls, C.H.Mueller, R.Rodríguez-Solís, F.A.Miranda. *ACS Appl. Mater. Interfaces*, **4**, 6346 (2012)
694. E.Di Maio, E.Kiran. *J. Supercrit. Fluids*, **134**, 157 (2018)
695. H.Li, T.K.Sinha, J.S.Oh, J.K.Kim. *ACS Appl. Mater. Interfaces*, **10**, 14008 (2018)
696. A.Mohebbi, F.Mighri, A.Ajji, D.Rodrigue. *J. Appl. Polym. Sci.*, **134**, 44577 (2017)
697. L.Wang, Y.Hikima, M.Ohshima, A.Yusa, S.Yamamoto, H.Goto. *Ind. Eng. Chem. Res.*, **56**, 13734 (2017)
698. M.Schwan, L.G.A.Kramer, T.Sottmann, R.Strey. *Phys. Chem. Chem. Phys.*, **12**, 6247 (2010)
699. M.Tromm, V.Shaayegan, C.Wang, H.P.Heim, C.B.Park. *Polymer*, **160**, 43 (2019)
700. S.Owusu-Nkwantabisah, C.Staudt, A.J.Lesser. *Polym. Eng. Sci.*, **58**, 1108 (2018)
701. Z.Qu, D.Yin, H.Zhou, X.Wang, S.Zhao. *Eur. Polym. J.*, **116**, 291 (2019)
702. X.Sun, L.-S.Turng. *Polym. Eng. Sci.*, **54**, 899 (2014)
703. N.M.Mehdipour, H.Garmabi, S.Jamalpour. *Polym. Compos.*, **40**, E227 (2019)
704. M.Chauvet, M.Sauceau, J.Fages. *J. Supercrit. Fluids*, **120**, 408 (2017)
705. E.Kiran. *J. Supercrit. Fluids*, **110**, 126 (2016)
706. E.Aram, S.Mehdipour-Ataei. *Int. J. Polym. Mater. Polym. Biomater.*, **65**, 358 (2016)
707. B.Li, G.Zhao, G.Wang, L.Zhang. *Int. J. Biol. Macromol.*, **129**, 171 (2019)
708. D.Banerjee, A.Dutta, K.K.Vimal, G.S.Kapur, A.K.Ghosh. *Ind. Eng. Chem. Res.*, **58**, 12054 (2019)
709. G.Luo, X.Gu, J.Zhang, R.Zhang, Q.Shen, M.Li, L.Zhang. *J. Appl. Polym. Sci.*, **134**, 44434 (2017)
710. M.Xu, H.Yan, Q.He, C.Wan, T.Liu, L.Zhao, C.B.Park. *Eur. Polym. J.*, **96**, 210 (2017)
711. A.Baklavaridis, I.Tsivintzelis, I.Zuburtikudis, C.Panayiotou. *Polym. Eng. Sci.*, **57**, 1005 (2017)
712. Y.X.J.Ong, L.Y.Lee, P.Davoodi, C.Wang. *J. Supercrit. Fluids*, **133**, 263 (2018)
713. C.Yang, Z.Xing, M.Wang, Q.Zhao, G.Wu. *Ind. Eng. Chem. Res.*, **57**, 1498 (2018)
714. W.Tessanan, P.Phinyocheep, P.Daniel, A.Gibaud. *J. Supercrit. Fluids*, **149**, 70 (2019)

715. Z.Yang, T.Liu, D.Hu, Z.Xu, L.Zhao. *J. Supercrit. Fluids*, **147**, 254 (2019)
716. Chaozhi Wang, Chao Wang, J.Li. *J. Appl. Polym. Sci.*, **136**, 48157 (2019)
717. J.Chen, X.Liao, W.Xiao, J.Yang, Q.Jiang, G.Li. *ACS Sustain. Chem. Eng.*, **7**, 9904 (2019)
718. R.Campardelli, P.Franco, E.Reverchon, I.De Marco. *J. Supercrit. Fluids*, **146**, 47 (2019
719. T.Liu, X.-F.Peng, H.-Y.Mi, H. Li, L.-S.Turng, B.-P.Xu. *Polym. Eng. Sci.*, **59**, 1753 (2019)
720. Y.Luo, Y.Ding, C.Wang, L.Tan, S.Ying. *J. Thermoplast. Compos. Mater.*, **30**, 1713 (2017)
721. R.Kumar, B.Patham, S.Mohanty, S.K.Nayak. *J. Polym. Res.*, **26**, 80 (2019)
722. G.Gedler, M.Antunes, J.I.Velasco. *J. Supercrit. Fluids*, **88**, 66 (2014)
723. G.Wang, W.Li, S.Bai, Q.Wang. *ACS Omega*, **4**, 9306 (2019)
724. C.-X.Chen, H.-H.Peng, Y.-X.Guan, S.-J.Yao. *J. Supercrit. Fluids*, **143**, 72 (2019)
725. M.T.Ngo, J.S.Dickmann, J.C.Hassler, E.Kiran. *J. Supercrit. Fluids*, **109**, 1 (2016)
726. D.L.Tomasko, A.Burley, L.Feng, S.-K.Yeh, K.Miyazono, S.Nirmal-Kumar, I.Kusaka, K.Koelling. *J. Supercrit. Fluids*, **47**, 493 (2009)
727. C.Wang, V.Shaayegan, M.Ataei, F.Costa, S.Han, M.Bussmann, C.B.Park. *Eur. Polym. J.*, **119**, 189 (2019)
728. A.Yusa, S.Yamamoto, H.Goto, H.Uezono, F.Asaoka, L.Wang, M.Ando, S.Ishihara, M.Ohshima. *Polym. Eng. Sci.*, **57**, 105 (2017)
729. M.Sauceau, J.Fages, A.Common, C.Nikitine, E.Rodier. *Prog. Polym. Sci.*, **36**, 749 (2011)
730. N.Le Moigne, M.Sauceau, M.Chauvet, J.-C.Benezet, J.Fages. *ACS Symp. Ser.*, **1304**, 171 (2018)
731. C.Okolieocha, D.Raps, K.Subramaniam, V.Altstädt. *Eur. Polym. J.*, **73**, 500 (2015)
732. C.Nikitine, E.Rodier, M.Sauceau, J.Fages. *Chem. Eng. Res. Des.*, **87**, 809 (2009)
733. K.Sudhakar, N.Naryana Reddy, T.Jayaramudu, J.Jayaramudu, A.Babul Reddy, B.Manjula, E.Rotimi Sadiku. In *Design and Applications of Nanostructured Polymer Blends and Nanocomposite Systems*. (Eds S.Thomas, R.Shanks, S.Chandrasekharakurup). (Amsterdam: Elsevier, 2016). P. 75
734. C.Forest, P.Chaumont, P.Cassagnau, B.Swoboda, P.Sonntag. *Prog. Polym. Sci.*, **41**, 122 (2015)
735. M.Antunes, V.Realinho, J.I.Velasco, E.Solorzano, M.-Á.Rodríguez-Pérez, J.A.Saja. *Mater. Chem. Phys.*, **136**, 268 (2012)
736. W.Xiao, X.Liao, Q.Jiang, Y.Zhang, J.Chen, Q.Yang, G.Li. *J. Supercrit. Fluids*, **142**, 52 (2018)
737. J.Yang, X.Liao, J.Li, G.He, Y.Zhang, W.Tang, G.Wang, G.Li. *Compos. Sci. Technol.*, **181**, 107670 (2019)
738. Y.Zhang, Y.Wang, J.Jiang, X.Wang, J.Hou, S.Sun, Q.Li. *J. Mater. Sci.*, **54**, 5112 (2019)
739. C.A.García-González, A.Concheiro, C.Alvarez-Lorenzo. *Bioconjug. Chem.*, **26**, 1159 (2015)
740. R.K.Kankala, Y.S.Zhang, S.-B.Wang, C.-H.Lee, A.-Z.Chen. *Adv. Health. Mater.*, **6**, 1700433 (2017)
741. K.Kosowska, M.Henczka. *Chem. Process Eng.*, **38**.535 (2017)
742. T.Kuang, F.Chen, L.Chang, Y.Zhao, D.Fu, X.Gong, X.Peng. *Chem. Eng. J.*, **307**, 1017 (2017)
743. M.Z.Moghadam, S.Hassanajili, F.Esmaeilzadeh, M.Ayatollahi, M.Ahmadi. *J. Mech. Behav. Biomed. Mater.*, **69**, 115 (2017)
744. Su Hee Kim, J.E.Kim, Soo Hyun Kim, Y.Jung. *J. Tissue Eng. Regen. Med.*, **11**, 3469 (2017)
745. S.Milovanovic, D.Markovic, A.Mrakovic, R.Kuska, I.Zizovic, S.Frerich, J.Ivanovic. *Mater. Sci. Eng. C*, **99**, 394 (2019)
746. H.-Y.Mi, X.Jing, Y.Liu, L.Li, H.Li, X.-F.Peng, H.Zhou. *ACS Appl. Mater. Interfaces*, **11**, 7479 (2019)
747. Y.-W.Fang, J.-B.Bao, H.-K.Yan, W.Sun, L.Zhao, G.H.Hu. *AIChE J.*, **62**, 4182 (2016)
748. L.M.Matuana, C.A.Diaz. *Ind. Eng. Chem. Res.*, **49**, 2186 (2010)
749. I.Tsivintzelis, G.Sanxaridou, E.Pavlidou, C.Panayiotou. *J. Supercrit. Fluids*, **110**, 240 (2016)
750. M.L.Keshtov, E.E.Said-Galiev, D.V.Marochkin, A.R.Khokhlov. *Polym. Sci., Ser. B*, **54**, 275 (2012)
751. S.Costeux. *J. Appl. Polym. Sci.*, **131**, 41293 (2014)
752. J.L.Sumey, J.A.Sarver, E.Kiran. *J. Supercrit. Fluids*, **145**, 243 (2019)
753. R.W.Baker. *Membrane Technology Applications*. (Ed. R.W.Baker). (New York: Wiley, 2012)
754. M. Mulder. *Basic Principles of Membrane Technology*. (Dordrecht: Kluwer, 1991). 372 p.
755. Z.N.Nysenko, V.V.Rusak, A.A.Glazkov, A.M.Sakharov, E.E.Said-Galiev, M.M.Ilyin. *Russ. Chem. Bull., Int. Ed.*, **64**, 2914 (2015)
756. A.Sh.Ramazanov, K.Sh.Shakhbanov. *Russ. J. Phys. Chem. B*, **13**, 1155 (2019)
757. K.L.Parks, E.J.Beckman. *Polym. Eng. Sci.*, **36**, 2404 (1996)
758. X.Liao, H.Zhang, T.He. *J. Nanomater.*, **12**, 836394 (2012)
759. P.S.Timashev, N.N.Vorobieva, N.V.Minaev, Y.A.Piskun, I.V.Vasilenko, S.G.Lakeev, S.V.Kostyuk, V.V.Lunin, V.N.Bagratashvili. *Russ. J. Phys. Chem. B*, **10**, 1195 (2016)
760. X.Jing, X.-F.Peng, H.-Y.Mi, Y.-S.Wang, S.Zhang, B.-Y.Chen, H.-M.Zhou, W.-J.Mou. *J. Appl. Polym. Sci.*, **133**, 43508 (2016)
761. M.Schulze, U.A.Handge, V.Abetz. *Polymer*, **108**, 400 (2017)
762. E.S.Trofimchuk, A.V.Efimov, L.N.Nikitin, N.I.Nikonorova, A.L.Volynskii, A.R.Khokhlov, N.F.Bakeev. *Russ. J. Phys. Chem. B*, **8**, 1019 (2014)
763. A.Wong, L.H.Mark, M.M.Hasan, C.B.Park. *J. Supercrit. Fluids*, **90**, 35 (2014)
764. A.Nistor, M.Topiar, H.Sovova, J.Kosek. *J. Supercrit. Fluids*, **130**, 30 (2017)
765. D.A.Zimnyakov, V.N.Bagratashvili, S.A.Yuvchenko, I.O.Slavnetskov, A.V.Kalacheva, O.V.Ushakova. *Sverkhkriticheskie Flyuidy: Teoriya i Praktika*, **14** (1), 14 (2019)
766. L.J.M.Jacobs, M.F.Kemmere, J.T.F.Keurentjes. *Green Chem.*, **10**, 731 (2008)
767. M.O.Gallyamov, A.Y.Nikolaev, L.N.Nikitin. *Polym. Sci., Ser. A*, **60**, 507 (2018).
768. L.N.Nikitin, A.Y.Nikolaev, E.E.Said-Galiyev, A.I.Gamzazade, A.P.Khokhlov. *Sverkhkriticheskie Flyuidy: Teoriya i Praktika,* **1** (1), 77 (2006)
769. A.Y.Nikolaev, L.N.Nikitin, E.E.Said-Galiyev. *Novoe v Polimerakh i Polimernykh Kompozitakh*, **2**, 111 (2012)
770. J.K.Bal, T.Beuvier, M.S.Chebil, G.Vignaud, Y.Grohens, M.K.Sanyal, A.Gibaud. *Macromolecules*, **47**, 8738 (2014)
771. S.Ma, Y.Wang, Z.Min, L.Zhong, *Adv. Polym. Technol.*, **32**, 21358 (2013)
772. H.-C.Zhang, C.-N.Yu, Y.Liang, G.-X.Lin, C.Meng. *Polymers*, **11**, 89 (2019)
773. A.S.Simonov, M.S.Kondratenko, I.V.Elmanovich, V.E.Sizov, E.P.Kharitonova, S.S.Abramchuk, A.Y.Nikolaev, D.A.Fedosov, M.O.Gallyamov, A.R.Khokhlov. *J. Membr. Sci.*, **564**, 106 (2018)

774. K.A.Arora, A.J.Lesser, T.J.McCarthy. *Macromolecules*, **31**, 4614 (1998)
775. L.N.Nikitin, M.O.Gallyamov, R.A.Vinokur, A.Y.Nikolaev, E.E.Said-Galiyev, A.R.Khokhlov, H.T.Jespersen, K.Schaumburg. *J. Supercrit. Fluids*, **26**, 263 (2003)
776. M.O.Gallyamov, R.A.Vinokur, L.N.Nikitin, E.E.Said-Galiyev, A.R.Khokhlov, K.Schaumburg. *Polym. Sci., Ser. A*, **44**, 581 (2002)
777. R.P.Sear. *J. Phys.: Condens. Matter*, **19**, 033101 (2007)
778. E.I.Blednykh, V.P.Skripov. *Vysokomol. Soedin. Ser. B*, **34** (9), 61 (1992)
779. B.V.Kichatov, A.M.Korshunov. *Theor. Found. Chem. Eng.*, **39**, 643 (2005)
780. S.K.Goel, E.J.Beckman. *Polym. Eng. Sci.*, **34**, 1137 (1994)
781. I.Tsivintzelis, C.Panayiotou. In *Biofoams: Science Applications of Bio-Based Cellular Porous Materials*. (Eds S.Iannace, C.B.Park). (Boca Raton, FL, London, New York: CRC Press, 2015. P. 62
782. I.A.Ronova, A.Alentiev, M.Bruma. In *Physical Chemistry for the Chemical Biochemical Sciences*. (Eds J.L.Lopez-Bonilla, M.I.Abdullin, G.E.Zaikov). (Apple Academic Press, 2016). P. 31
783. S.Mateucci, Y.Yampolskii, B.D.Freeman, I.Pinnau. In *Materials Science of Membranes for Gas Vapor Separation*. (Chichester: Wiley, 2006). P. 1
784. Y.P.Yampolskii. *Macromolecules*, **45**, 3298 (2012)
785. A.F.Ismail, K.C.Khulbe, T.Matsuura. *Gas Separation Membranes. Polymeric Inorganic*. (Springer, 2015)
786. Yu.P.Yampolskii, N.A.Belov, A.Y.Alentiev. *Nanomaterialy: Svoistva i Perspektivnye Prilozheniya*. (Nanomaterials: Properties and Promising Applications). (Ed. A.B.Yaroslavtsev). (Moscow: Nauchnyi Mir, 2014). P. 114
787. S.Kanehashi, K.J.Nagai. *Membr. Sci.*, **253**, 117 (2005)
788. Yu.P.Yampolskii. *Russ. Chem. Rev.*, **76**, 59 (2007)
789. G.Dlubek, J.Pionteck, K.Rätzke, J.Kruse, F.Faupel. *Macromolecules*, **41**, 6125 (2008)
790. A.Alentiev, Y.Yampolskii. *J. Membr. Sci.*, **206**, 291 (2002)
791. V.Ryzhikh, A.Alentiev, Y.Yampolskii. *Polym. Sci., Ser. A*, **55**, 244 (2013)
792. A.Y.Alentiev, N.A.Belov, S.V.Chirkov, Y.P.Yampolskii. *J. Membr. Sci.*, **547**, 99 (2018)
793. S.I.Semenova, H.Ohya, T.Higashijima, Y.Negishi. *J. Membr. Sci.*, **74**, 131 (1992)
794. S.J.Sarrade, G.M.Rios, M.Carles. *Sep. Purif. Technol.*, **14**, 19 (1998)
795. L.A.V.Sarmento, C.B.Spricigo, J.C.C.Petrus, L.H.C.Carlson, R.A.F.Machado. *J. Membr. Sci.*, **237**, 71 (2004)
796. V.E.Patil, L.J.P.van den Broeke, F.F.Vercauteren, J.T.F.Keurentjes. *J. Membr. Sci.*, **271**, 77 (2006)
797. Y.Xiao, B.T.Low, S.S.Hosseini, T.S.Chung, D.R.Paul. *Prog. Polym. Sci.*, **34**, 561 (2009)
798. T.S.Chung, C.Cao, R.Wang. *J. Polym. Sci., Part B: Polym. Phys.*, **42**, 354 (2004)
799. M.R.Coleman, W.J.Koros. *Macromolecules*, **32**, 3106 (1999)
800. S.Kanehashi, T.Nakagawa, K.Nagai, X.Duthie, S.Kentish, G.Stevens. *J. Membr. Sci.*, **298**, 147 (2007)
801. X.Duthie, S.Kentish, C.Powell, K.Nagai, G.G.Qiao, G.Stevens. *J. Membr. Sci.*, **294**, 40 (2007)
802. G.Dlubek, J.Pionteck, Y.Yu, S.Thrunert, M.Elsayed, E.Badawi, R.Krause-Rehberg. *Macromol. Chem. Phys.*, **209**, 1920 (2008)
803. N.R.Horn, D.R.Paul. *Polymer*, **52**, 1619 (2011)
804. P.H.Pfromm. In *Materials Science of Membranes for Gas Vapor Separation*. (Chichester: Wiley, 2006). P. 293
805. C.Zhou, T.S.Chung, R.Wang, S.H.Goh. *J. Appl. Polym. Sci.*, **92**, 1758 (2004)
806. J.H.Kim, W.J.Koros, D.R.Paul. *J. Membr. Sci.*, **282**, 21 (2006)
807. X.Y.Song, H.P.Geng, Q.F.Li. *Polymer*, **47**, 3049 (2006)
808. R.R.Tiwari, Z.P.Smith, H.Lin, B.D.Freeman, D.R.Paul. *Polymer*, **61**, 1 (2015)
809. J.H.Kim, W.J.Koros, D.R.Paul. *J. Membr. Sci.*, **282**, 32 (2006)
810. W.J.Koros, A.Kratochvil, S.Shu, S.Hussein. In *Membrane Industry in Membrane Operations. Innovative Separations Transformations*. (Eds E.Drioli, L.Giorno). (Wiley, 2009). P. 139
811. A.M.Kratochvil, S.Damle-Mogri, W.J.Koros. *Macromolecules*, **42**, 5670 (2009)
812. A.M.Kratochvil, W.J.Koros. *Macromolecules*, **43**, 4679 (2010)
813. T.Koga, Y.-S.Seo, J.L.Jerome, S.Ge, M. H.Rafailovich, J.C.Sokolov, B.Chu, O.H.Seeck, M.Tolan, R.Kolb. *Appl. Phys. Lett.*, **83**, 4309 (2003)
814. T.Oka, K.Ito, Ch.He, C.Dutriez, H.Yokoyama, Y.Kobayashi. *J. Phys. Chem. B*, **112** 12191 (2008)
815. T.Koga, E.Akashige, A.Reinstein, M.Bronner, Y.-S.Seo, K.Shin, M.H.Rafailovich, J.C.Sokolov, B.Chu, S.K.Satija. *Physica B*, **357**, 73 (2005)
816. I.A.Ronova, L.N.Nikitin, E.A.Sokolova, I.Bacosca, I.Sava, M.Bruma. *J. Macromol. Sci., Part A*, **46**, 929 (2009)
817. I.A.Ronova, L.N.Nikitin, E.A.Sokolova, I.Sava, M.Bruma. *High Perform. Polym.*, **21**, 562 (2009)
818. I.A.Ronova, O.V.Sinitsyna, S.S.Abramchuk, A.Y.Nikolaev, S.Chisca, I.Sava, M.Bruma. *J. Supercrit. Fluids*, **70**, 146 (2012)
819. I.A.Ronova, M.Bruma, A.Y.Nikolaev, A.A.Kuznetsov. *Polym. Adv. Technol.*, **24**, 615 (2013)
820. I.A.Ronova, M.Bruma, O.V.Sinitsyna, I.Sava, A.Y.Nikolaev, S.Chisca, N.G.Ryvkina. *Struct. Chem.*, **25**, 1687 (2014)
821. I.A.Ronova, A.Y.Alentiev, S.Chisca, I.Sava, M.Bruma, A.Y.Nikolaev, N.A.Belov, M.I.Buzin. *Struct. Chem.*, **25**, 301 (2014)
822. I.A.Ronova, A.Y.Alentiev, M.Bruma. *J. Char. Develop. Nov. Mater.*, **7**, 497 (2015)
823. V.P.Shantarovich, V.G.Bekeshev, N.A.Belov, I.A.Ronova, A.Y.Nikolaev, V.W.Gustov, I.B.Kevdina, M.K.Filimonov. *High Energy Chem.*, **50**, 287 (2016)
824. N.A.Belov, A.Y.Alentiev, I.A.Ronova, O.V.Sinitsyna, A.Y.Nikolaev, A.A.Zharov. *J. Appl. Pol. Sci.*, **133**, 43105 (2016)
825. A.Y.Alentiev, I.A.Ronova, S.V.Chirkov, A.Y.Nikolaev. In *Polyimide High Performance Polymers*. Vol. 10. (Montpellier: Universite de Montpellier, 2018). P. 81
826. I.A.Ronova, N.A.Belov, A.Y.Alentiev, A.Y.Nikolaev, S.V.Chirkov. *Struct. Chem.*, **29**, 457 (2018)
827. C.A.Scholes, S.Kanehashi. *J. Membr. Sci.*, **566**, 239 (2018)
828. C.A.Scholes, S.Kanehashi. *Membranes*, **9**, 41 (2019)
829. S.V.Chirkov, A.S.Kechekyan, N.A.Belov, S.V.Antonov, A.Yu.Alentiev. *Butlerov. Soobsh.*, **48** (12), 54 (2016)
830. Y.Yampolskii, A.Alentiev, G.Bondarenko, Y.Kostina, M.Heuchel. *Ind. Eng. Chem. Res.*, **49**, 12031 (2010)
831. S.V.Chirkov, N.A.Belov, S.V.Antonov, A.Y.Alentiev, A.S.Kechekyan. *Petrol. Chem.*, **56**, 1074 (2016)
832. L.Dalton. In *Polymers for Photonics Applications I*. (Ed. K.-S.Lee). (*Ser. Advances in Polymer Science*. Vol. 158.) (Heidelberg: Springer-Verlag, 2002). P. 1

833. F.Hussain, M.Hojjati, M.Okamoto, R.E.Gorga. *J. Compos. Mater.*, **40**, 1511 (2006)
834. L.Zimmennann, M.Weibel, W.Caseri, U.W.Suter. *J. Mater. Res.*, **8**, 1742 (1993)
835. G.Carotenuto. *Polymer News (USA)*, **25** (6), 191 (2000)
836. N.N.Glagolev, N.A.Aksenova, V.T.Shashkov, N.L.Zaichenko, L.S.Kol'tsova, A.I.Shienok, P.S.Timashev, B.I.Zapadinsky, A.B.Solov'eva. *Zh. Fiz. Khim.*, **82**, 1759 (2008)
837. K.Binnemans. *Chem. Rev.*, **109**, 4283 (2009)
838. X.Zheng, L.Wang, Y.Guan, Q.Pei, J.Jiang, Z.Xie. *Biomaterials*, **235**, 119792 (2020)
839. C.R.Fontana, D.S.dos Santos Jr., J.M.Bosco, D.M.Spolidorio, R.A.C.Marcantonio. *Drug Deliv.*, **15**, 417 (2008)
840. Q.D.Ling, E.T.Kang, K.G.Neoh, W.Huang. *Macromolecules*, **36**, 6995 (2003)
841. P.Lenaerts, K.Driesen, R.Van Deun, K.Binnemans. *Chem. Mater.*, **17**, 2148 (2005)
842. V.Lokshin, A.Samat, A.V.Metelitsa. *Russ. Chem. Rev.*, **71**, 893 (2002)
843. S.Tate, H.Narusawa. *Polymer*, **37**, 1583 (1996)
844. Y.W.Z.Tang, P.Podsiadlo, N.A.Kotov. *Adv. Mater.*, **18**, 3203 (2006)
845. I.Kikic. *J. Supercrit. Fluids*, **47**, 458 (2009)
846. S.M.Howdle, M.S.Watson, M.J.Whitaker, M.C.Davies, K.M.Shakesheff, V.K.Popov, F.S.Mandel, J.D.Wang. *Chem. Commun.*, 109 (2001)
847. T.P.Bilalov, F.M.Gumerov, Kh.E.Kharlsmpidi, G.I.Fedorov. *Vestn. Kazan. Gos. Tekh. Univ. im. A.N.Tupoleva*, (3), 80 (2008)
848. D.Yu.Zalepugin, N.A.Til'kunova, V.S.Mishin, I.V.Chernyshova, E.N.Glukhan, V.L.Korolev. *Sverkhkriticheskie Flyuidy: Teoriya i Praktika*, **3** (4), 56 (2008)
849. A.Salerno, D.P.Concepción. *Process Biochem.*, **50**, 826 (2015)
850. M.Champeau, J.-M.Thomassin, T.Tassaing, C.Jérôme. *J. Controlled Release*, **209**, 248 (2015)
851. H.Yoon, G.Kim. *J. Pharm. Sci.*, **100**, 424 (2011)
852. Ya.A.Ugai. *Obshchaya i Neorganicheskaya Khimii.* (General and Inorganic Chemistry). (Moscow: Vysshaya Shkola, 1997)
853. *Kurs Fizicheskoi Khimii.* (Course of Physical Chemistry). Vol. 1. (Ed. Ya.I.Gerasimov). (Moscow: Khimiya, 1964)
854. L.E.Fried, W.M.Howard. *J. Chem. Phys.*, **109**, 7338 (1998)
855. B.Wagner, C.B.Kautz, G.M.Schneider. *Fluid Phase Equil.*, **158**, 707 (1999)
856. U.Haarhaus, P.Swidersky, G.M.Schneider. *J. Supercrit. Fluids*, **8**, 100 (1995)
857. A.S.Özcan, A.A.Clifford, K.D.Bartle, D.M.Lewis. *J. Chem. Eng. Data*, **42**, 590 (1997)
858. B.L.West, S.G.Kazarian, M.F.Vincent, N.H.Brantley, C.A.Eckert. *J. Appl. Polym. Sci.*, **69**, 911 (1998)
859. S.E.Barry, D.S.Soane. *Macromolecules*, **29**, 3565 (1996)
860. Y.Li-qiu, Z.Shu-fen, H.Liang, M.Wei, Y.Jin-zong. In *The Proceedings of the 3rd International Conference on Functional Molecules.* (Dalian, China, 2013). P. 99
861. S.Sicardi, L.Manna, M.Banchero. *J. Supercrit. Fluids*, **17**, 187 (2000)
862. J.Yang, T.Hasell, W.Wang, S.M.Howdle. *Eur. Polym. J.*, **44**, 1331 (2008)
863. M.£arrison, S.Kershaw, M.Burt, A.Rogach, A.Kornowski, A.Eychmüller, H.Weller. *Pure Appl. Chem.*, **72**, 295 (2000)
864. W.Z.Xu, P.A.Charpentier. *J. Phys. Chem. C*, **113**, 6859 (2009)
865. T.R.Akhmetzyanov, I.Sh.Khabriev, V.F.Khairutdinov, F.R.Gabitov, F.M.Gumerov. *Vestn. Kasan. Tekhnol. Univ.*, **16**, 93 (2013)
866. L.Kong, H.-L.Wong, A.Y.-Y.Tam, W.H.Lam, L.Wu, V.W.-W.Yam. *ACS Appl. Mater. Interfaces*, **6**, 1550 (2014)
867. V.A.Barachevsky. *J. Photochem. Photobiol., A*, **196**, 180 (2008)
868. T.A.Darwish, R.A.Evans, M.James, N.Malic, G.Triani, T.L.Hanley. *J. Am. ChV.N.Bagratashvili.*, 748 (2010)
869. J.Kohl-Landgraf, M.Braun, C.Ozcoban, D.P.N.Gonçalves, A.Heckel, J.Wachtveitl. *J. Am. Chem. Soc.*, **134**, 14070 (2012)
870. P.J.Castro, I.Gomez, M.Cossi, M.Reguero. *J. Phys. Chem. A*, **116**, 8148 (2012)
871. S.Bénard, E.Rivière, P.Yu, K.Nakatani, J.F.Delouis. *Chem. Mater.*, **13**, 159 (2001)
872. *Photochemistry and Photophysics of Polymeric Materials.* (Ed. N.S.Allen). (New York: Wiley, 2010)
873. F.Ercole, N.Malic, S.Harrisson, T.P.Davis, R.A.Evans. *Macromolecules*, **43**, 249 (2010)
874. B.L.Feringa, R.A.van Delden, N.Koumura, E.M.Geertsema. *Chem. Rev.*, **100**, 1789 (2000)
875. A.Radu, S.Scarmagnani, R.Byrne, C.Slater, K.T.Lau, D.Diamond. *J. Phys. D: Appl. Phys.*, **40**, 7238 (2007)
876. R.Castagna, M.Garbugli, A.Bianco, S.Perissinotto, G.Pariani, C.Bertarelli, G.Lanzani. *J. Phys. Chem. Lett.*, **3**, 51 (2012)
877. L.Angiolini, T.Benelli, L.Giorgini, E.Salatelli, R.Bozio, A.Daurù, D.Pedron. *Macromolecules*, **39**, 489 (2006)
878. S.Kobatake, I.Yamashita. *Tetrahedron*, **64**, 7611 (2008)
879. G.K.Such, R.A.Evans, T.P.Davis. *Macromolecules*, **39**, 1391 (2006)
880. A.Zelichenok, F.Buchholtz, S.Yitzchaik, J.Ratner, M.Safro, V.Krongauz. *Macromolecules*, **25**, 3179 (1992)
881. A.Abdollahi, A.R.Mahdavian, H.Salehi-Mobarakeh. *Langmuir*, **31**, 10672 (2015)
882. D.S.Achilleos, M.Vamvakaki. *Macromolecules*, **43**, 7073 (2010)
883. N.I.Islamova, X.Chen, C.-J.Fan, R.S.Andino, W.J.Lees. *Polym. Degrad. Stab.*, **98**, 1662 (2013)
884. J.Ratner, N.Kahana, A.Warshawsky, V.Krongauz. *Ind. Eng. Chem. Res.*, **35**, 1307 (1996)
885. A.V.Laptev, N.E.Belikov, A.Y.Lukin, Y.P.Strokach, V.A.Barachevskii, M.V.Alfimov, O.V.Demina, V.I.Shvets, D.A.Skladnev, A.A.Khodonov. *Russ. J. Bioorg. Chem.*, **34**, 252 (2008)
886. M.Iftime, R.Ardeleanu, N.Fifere, A.Airinei, V.Cozan, M.Bruma. *Dyes Pigm.*, **106**, 111 (2014)
887. H.R.Allock, C.Kim. *Macromolecules*, **24**, 2846 (1991)
888. L.Zhang, J.Shi, Z.Yang, M.Huang, Z.Chen, Q.Gong, S.Cao. *Polymer*, **49**, 2107 (2008)
889. Z.Li, W.Gong, J.Qin. *Polymer*, **46**, 4971 (2005)
890. H.-G.Liu, F.Xiao, W.-S.Zhang, Y.Chung. *J. Lumin.*, **114**, 187 (2005)
891. T.A.Bykova, B.V.Lebedev, K.V.Kir'yanov, N.N.Smirnova, L.A.Smirnova, O.V.Kameneva, V.A.Barachevskii. *Vysokomol. Soedin. Ser. A*, **45**, 1169 (2003)
892. R.Bonnet, M.A.Krysteva, I.G.Lalov, S.V.Artarsky. *Water Res.*, **40**, 1269 (2006)
893. S.G.Kazarian. *Polym. Sci., Ser. C*, **42**, 78 (2000)
894. A.I.Cooper. *J. Mater. Chem.*, **10**, 207 (2000)
895. M.L.Goni, N.A.Ganan, M.C.Strumia, R.E.Martini. *J. Supercrit. Fluids*, **111**, 28 (2016)

896. D.Markovic, S.Milovanovic, M.Radetic, B.Jokic, I.Zizovic. *J. Supercrit. Fluids*, **101**, 215 (2015)
897. V.I.Gerasimova, Y.S.Zavorotny, A.O.Rybaltovskii, A.Y.Chebrova, N.L.Semenova, D.A.Lemenovskii, Y.L.Slovohotov. *J. Lumin.*, **129**, 1115 (2009)
898. K.Gong, I.U.Rehman, J.A.Darr. *J. Pharm. Biomed. Anal.*, **48**, 1112 (2008)
899. N.N.Glagolev, A.B.Solov'eva, B.I.Zapadinsky, A.V.Kotova, V.A.Barachevsky, P.S.Timashev, V.N.Bagratashvili. *Sverkhkriticheskie Flyuidy: Teoriya i Praktika*, **2** (1), 78 (2007)
900. N.N.Glagolev, A.B.Solovieva, A.V.Kotova, V.T.Shashkova, B.I.Zapadinsky, N.L.Zaichenko, L.S.Kol'tsova, A.I.Shienok, P.S.Timashev, V.N.Bagratashvili. *Zh. Fiz. Khim.*, **83** (5), 1 (2009)
901. A.V.Kotova, N.N.Glagolev, I.A.Matveeva, A.V.Cherkasova V.T.Shashkova, L.A.Pevtsova, B.I.Zapadinsky, A.B.Solovieva, V.N.Bagratashvili. *Vysokomol. Soedin. Ser. A*, **52**, 805 (2010)
902. A.S.Kopylov, V.A.Radtsig, N.N.Glagolev, A.B.Solovieva, V.N.Bagratashvili. *Russ. J. Phys. Chem. B*, **9**, 998 (2015)
903. N.N.Glagolev, A.B.Solovyeva, A.V.Cherkasova, V.P.Mel'nikov, A.Y.Lyapunov, P.S.Timashev, A.V.Kotova, B.I.Zapadinsky, V.N.Bagratashvili. *Russ. J. Phys.Chem. B*, **4**, 1092 (2010)
904. V.N.Bagratashvili, A.B.Solov'eva, N.N.Glagolev, A.V.Cherkasova, I.V.Andreeva, P.S.Timashev. *Russ. J. Phys. Chem. B*, **5**, 1144 (2011)
905. A.V.Cherkasova, N.N.Glagolev, A.S.Kopylov, T.S.Zarkhina, P.S.Timashev, V.N.Bagratashvili, A.B.Solovieva. *Russ. J. Phys. Chem. B*, **9**, 1116 (2015)
906. A.S.Kopylov, N.N.Glagolev, P.S.Timashev, A.V.Cherkasova, S.F.Timashev, A.B.Solov'eva. *Russ. J. Phys. Chem A.*, **89**, 1523 (2015)
907. V.A.Zhorin, A.N.Zelenetskii, M.P.Kiselev, V.S.Marevtsev, A.I.Shienok. *Russ. J. Appl. Chem.*, **78**, 955 (2005)
908. A.S.Kopylov, V.I.Yusupov, A.V.Cherkasova, I.V.Shershnev, P.S.Timashev, A.B.Solovieva. *Russ. J. Phys. Chem. B*, **12**, 1298 (2018)
909. S.F.Timashev. *Flikker-Shumovaya Spektroskopiya. Informatsiya v Khaoticheskikh Signalakh.* (Flicker Noise Spectroscopy. Information in Chaotic Signals) (Moscow: Fizmatlit, 2007)
910. S.F.Timashev, A.B.Solov'eva, E.Yu.Buslaeva, S.P.Gubin. *Russ. J. Phys. Chem. A* , **87**, 153 (2013)
911. V.V.Boldyrev. *Russ. Chem. Rev.*, **75**, 177 (2006)
912. C.McGregor, G.Byrne, B.Rahmani, E.Chisari, K.Kyriakopoulou, G.Burriesci. *Acta Biomater.*, **41**, 204 (2016)
913. E.A.Grebenik, E.R.Gafarova, L.P.Istranov, E.V.Istranova, X.Ma, J.Xu, W.Guo, A.Atala, P.S.Timashev. *Biotechnol. J.*, e1900334 (2020)
914. P.R.Umashankar, T.Arun, T.V.Kumari. *J. Biomed. Mater. Res., Part A*, **97**, 311 (2011)
915. V.Elagin, D.Kuznetsova, E.Grebenik, D.Zolotov, L.Istranov. *Front. Bioeng. Biotechnol.*, **8**, 107 (2020)
916. E.Jorge-Herrero, C.Fonseca, A.P.Barge, J.Turnay, N.Olmo, P.Fernández, M.A.Lizarbe, J.M.Garsia-Paez. *Artificial Organs*, **34** (5), E168 (2010)
917. A.Atala. *Exp. Opin. Biol. Ther.*, **5**, 879 (2005)
918. J.A.Claudio-Rizo, M.Rangel-Argote, L.E.Castellano, J.Delgado, J.L.Mata-Mata, B.Mendoza-Novelo. *Mater. Sci. Eng., C*, **79**, 793 (2017)
919. N.N.Veryasova, A.E.Lazhko, D.E.Isaev, E.A.Grebenik, P.S.Timashev. *Russ. J. Phys. Chem. B*, **13**, 1079 (2019)
920. P.M.Crapo, T.W.Gilbert, S.F.Badylak. *Biomaterials*, **32**, 3233 (2011)
921. B.Mendoza-Novelo, L.Castellano, R.Padilla-Miranda, M.Lona-Ramos, P.Cuellar-Mata, A.Vega-Gonzalez, M.Murguia-Perez, J.Mata-Mata, E.Avila. *J. Biomed. Mater. Res., Part A*, **104**, 2810 (2016)
922. M.B.Ariganello, R.S.Labow, J.M.Lee. *J. Biomed. Mater. Res., Part A*, **93**, 280 (2009)
923. J.Hwang, B.H.San, N.J.Turner, L.J.White, D.M.Faulk, S.F.Badylak, M.S.Yu. *Acta Biomater.*, **53**, 268 (2017)
924. S.B.Seif-Naraghi, M.A.Salvatore, P.J.Schup-Magoffin, D.P.Hu, K.L.Christman. *Tissue Eng., Part A*, **16**, 2017 (2010)
925. S.Park, S.Kim, H.Lim, C.Lim, Y.Kim. *Korean J. Thorac. Cardiovasc. Surg.*, **46** (1), 1 (2013)
926. H.Perme, A.Sharma, N.Kumar, H.Singh, R.Dewangan, K.Maiti. *Indian J. Anim. Sci.*, **79**, 658 (2009)
927. W.Q.Sun, H.Xu, M.Sandor, J.Lombardi. *J. Tissue Eng.*, **4**, 204173141350530 (2013)
928. E.Pagoulatou, I.-E.Triantaphyllidou, D.H.Vynios, D.J.Papachristou, E.Koletsis, D.Deligianni, D.Mavrilas. *J. Mater. Sci.: Mater. Med.*, **23**, 1387 (2012)
929. J.Hülsmann, K.Grün, S.El Amouri, M.Barth, K.Hornung, C.Holzfuß, P.Akhyari. *Xenotransplantation*, **19** (5), 28 (2012)
930. S.Mirsadraee, H.E.Wilcox, S.A.Korossis, J.N.Kearney, K.G.Watterson, J.Fisher, E.Ingham. *Tissue Eng., Part A*, **12**, 763 (2006)
931. G.Orlando, A♀.Farney, S.S.Iskandar, S.-H.Mirmalek-Sani, D.C.Sullivan, E.Moran, T.A.Shwareb, P.De Coppi, K.J.Wood, R.J.Stratta. *Ann. Surg.*, **256**, 363 (2012)
932. S.Cebotari, I.Tudorache, T.Jaekel, A.Hilfiker, S.Dorfman, W.Ternes, A.Lichtenberg. *Artif. Organs*, **34** (3), 206 (2010)
933. K.Sawada, D.Terada, T.Yamaoka, S.Kitamura, T.Fujisato. *J. Chem. Technol. Biotechnol.*, **83**, 943 (2008)
934. S.Guler, B.Aslan, P.Hosseinian, H.M.Aydin. *Tissue Eng., Part C*, **23**, 540 (2017)
935. D.M.Casali, R.M.Handleton, T.Shazly, M.A.Matthews. *J. Supercrit. Fluids*, **131**, 72 (2018)
936. J.K.Wang, B.Luo, V.Guneta, L.Li, S.E.M.Foo, Y.Dai, T.T.Y.Tan, N.S.Tan, C.Choong, M.T.C.Wong. *Mater. Sci. Eng. C*, **75**, 349 (2017)
937. B.Mendoza-Novelo, E.E.Avila, J.V.Cauich-Rodríguez, E.Jorge-Herrero, F.J.Rojo, G.V.Guinea, J.L.Mata-Mata. *Acta Biomater.*, **7**, 1241 (2011)
938. M.Tang, T.Li, E.Pickering, N.S.Gandhi, K.Burrage, Y.Gu. *J. Mech. Behav. Biomed. Mater.*, **86**, 359 (2018)
939. L.G.Bracaglia, M.J.Messina, S.Winston, C.-Y.Kuo, M.Lerman, J.P.Fisher. *Biomacromolecules*, **18**, 3802 (2017)
940. X.Dong, X.Wei, W.Yi, C.Gu, X.Kang, Y.Liu, Q.Li, D.Yi. *J. Mater. Sci.: Mater. Med.*, **20**, 2327 (2009)
941. A.N.Sabirzyanov, A.P.Il'in, A.R.Akhunov, F.M.Gumerov. *High Temp.*, **40**, 203 (2002)
942. A.Zambon, M.Vetralla, L.Urbani, M.F.Pantano, G.Ferrentino, M.Pozzobon, N.M.Pugno, P.De Coppi, N.Elvassore, S.Spilimbergo. *J. Supercrit. Fluids*, **115**, 33 (2016)
943. Y.-H.Huang, F.-W.Tseng, W.-H.Chang, I.-C.Peng, D.-J.Hsieh, S.-W.Wu, M.-L.Yeh. *Acta Biomater.*, **58**, 238 (2017)
944. Y.Hashimoto, S.Funamoto, S.Sasaki, T.Honda, S.Hattori, K.Nam, T.Kimura, M.Mochizuki, T.Fujisato, H.Kobayashi, A.Kishida. *Biomaterials*, **31**, 3941 (2010)
945. Y.Hashimoto, S.Hattori, S.Sasaki, T.Honda, T.Kimura, S.Funamoto, H.Kobayashi, A.Kishida. *Sci. Rep.*, **6**, 27734 (2016)

946. Y.Hashimoto, S.Funamoto, S.Sasaki, J.Negishi, S.Hattori, T.Honda, T.Kimura, H.Kobayashi, A.Kishida. *Mater. Sci. Eng. C*, **102**, 238 (2019)
947. E.A.Grebenik, L.P.Istranov, E.V.Istranova, S.N.Churbanov, B.S.Shavkuta, R.I.Dmitriev, N.N.Veryasova, S.L.Kotova, A.V.Kurkov, A.B.Shekhter, P.S.Timashev. *Xenotransplantation*, **26** (3), e12506 (2019)
948. F.R.Halfwerk, J.Rouwkema, J.A.Gossen, J.G.Grandjean. *J. Mech. Behav. Biomed. Mater.*, **77**, 400 (2018)
949. N.Tovar, L.Witek, R.Neiva, H.F.Marão, L.F.Gil, P.Atria, R.Jimbo, E.A.Caceres, P.G.Coelho. *J. Biomed. Mater. Res., Part B*, **107**, 1320 (2019)
950. J.Antons, M.G.M.Marascio, P.Aeberhard, G.Weissenberger, N.Hirt-Burri, L.A.Applegate, P.E.Bourban, D.P.Pioleti. *Eur. Cells Mater.*, **36**, 81 (2018)
951. L.Chang, Y.-J.Chen, Y.-P.Chen, C.-T.Chen, W.-H.Yu. *Formosan J. Musculoskelet. Disord.*, **2** (2), 55 (2011)
952. Z.Dai, J.Ronholm, Y.Tian, B.Sethi, X.Cao. *J. Tissue Eng.*, **7**, 204173141664881 (2016)
953. T.Baldini, K.Caperton, M.Hawkins, E.McCarty. *Knee Surg. Sports Traumatol. Arthrosc.*, **24**, 3971 (2016)
954. A.B.Yanke, R.Bell, A.Lee, R.W.Kang, R.C.Mather, E.F.Shewman, V.Û.Wang, B.R.Bach. *Am. J. Sports Med.*, **41**, 835 (2013)
955. A.Checinska, I.A.Fruth, T.L.Green, R.L.Crawford, A.J.Paszczynski. *J. Microbiol. Methods*, **87**, 70 (2011)
956. G.J.Van de Pol, F.Bonar, L.J.Salmon, J.P.Roe, L.A.Pinczewski. *Arthroscopy*, **34**, 706 (2018)
957. J.L.Balestrini, A.Liu, A.L.Gard, J.Huie, K.M.S.Blatt, J.Schwan, L.Zhao, T.Broekelmann, R.Mecham, E.Wilcox, L.E.Niklason. *Tissue Eng., Part C*, **22**, 260 (2016)
958. N.A.Russell, A.Rives, M.H.Pelletier, W.J.Bruce, W.R.Walsh. *Cell Tissue Banking*, **14**, 231 (2013)
959. N.A.Russell, A.Rives, M.H.Pelletier, T.Wang, W.R.Walsh. *Cell Tissue Banking*, **16**, 109 (2015)
960. J.L.Wehmeyer, S.Natesan, R.J.Christy. *Tissue Eng., Part C*, **21**, 649 (2015)
961. R.S.Hennessy, S.Jana, B.J.Tefft, M.R.Helder, M.D.Young, R.R.Hennessy, N.J.Stoyles, A.Lerman. *JACC Basic Transl. Sci.*, **2** (1), 71 (2017)
962. R.S.Hennessy, J.L.Go, R.R.Hennessy, B.J.Tefft, S.Jana, N.J.Stoyles, M.A.Al-Hijji, J.J.Thaden, S.V.Pislaru, R.D.Simari, J.M.Stulak, M.D.Young, A.Lerman. *PLoS One*, **12** (8), e0181614 (2017)
963. R.Purohit, P.Venugopalan. *Resonance – J. Sci. Ed.*, **14**, 882 (2009)
964. A.J.Cruz-Cabeza, S.M.Reutzel-Edens, J.Bernstein. *Chem. Soc. Rev.*, **44**, 8619 (2015)
965. A.Nangia. *Acc. Chem. Res.*, **41**, 595 (2008)
966. A.J.Cruz-Cabeza, J.Bernstein. *Chem. Rev.*, **114**, 2170 (2014)
967. S.SeethaLekshmi, T.N.Guru Row. *Cryst. Growth Des.*, **12**, 4283 (2012)
968. C.Wilson. *J. Mol. Struct.*, **405**, 207 (1997)
969. E.B.Burgina, V.P.Baltakhinov, E.V.Boldyreva, T.P.Shakhtschneider. *J. Struct. Chem.*, **45**, 64 (2004)
970. B.B.Ivanova. *J. Mol. Struct.*, **738**, 233 (2005)
971. A.L.Grzesiak, M.Lang, K.Kim, A.J.Matzger. *J. Pharm. Sci.*, **92**, 2260 (2003)
972. J.-B.Arlin, L.S.Price, S.L.Price, A.J.Florence. *Chem. Commun.*, **47**, 7074 (2011)
973. F.N.de Wet, J.J.Gerber, A.P.Lötter, J.G.van der Watt, T.G.Dekker. *Drug Devel. Ind. Pharm.*, **24**, 447 (1998)
974. E.Dudognon, F.Danède, M.Descamps, N.Correia. *Pharm. Res.*, **25**, 2853 (2008)
975. R.K.Gilpin, W.Zhou. *Vibrat. Spectrosc.*, **37**, 53 (2005)
976. R.Panchagnula, P.Sundaramurthy, O.Pillai, S.Agrawal, Y.A.Raj. *J. Pharm. Sci.*, **93**, 1019 (2004)
977. S.K.A.Mudalip, M.R.A.Bakar, P.Jamal, F.Adam, R.C.Man, S.Z.Sulaiman, Z.I.M.Arshad, S.M.Shaarani. *MATEC Web of Conf.*, **150**, 02004 (2018)
978. R.K.Gilpin, W.Zhou. *J. Pharm. Biomed. Anal.*, **37**, 509 (2005)
979. S.Cesur, S.Gokbel. *Cryst. Res. Technol.*, **43**, 720 (2008)
980. G.Nichols, C.S.Frampton. *J. Pharm. Sci.*, **87**, 684 (1998)
981. A.O.Surov, N.A.Vasilev, A.V.Churakov, J.Stroh, F.Emmerling, G.L.Perlovich. *Cryst. Growth Des.*, **19**, 2979 (2019)
982. A.O.Surov, A.V.Churakov, G.L.Perlovich. *Cryst. Growth Des.*, **16**, 6556 (2016)
983. S.Qi, P.Avalle, R.Saklatvala, D.Q.M.Craig. *Eur. J. Pharm. Biopharm.*, **69**, 364 (2008)
984. K.Kachrimanis, K.Fucke, M.Noisternig, B.Siebenhaar, U.Griesser. *Pharm. Res.*, **25**, 1440 (2008)
985. J.Bernstein, R.J.Davey, J.O.Henck. *Angew. Chem., Int. Ed.*, **38**, 3440 (1999)
986. J.D.Dunitz, J.Bernstein. *Acc. Chem. Res.*, **28**, 193 (1995)
987. R.W.Lancaster, P.G.Karamertzanis, A.T.Hulme, D.A.Tocher, T.C.Lewis, S.L.Price. *J. Pharm. Sci.*, **96**, 3419 (2007)
988. D.K.Bučar, R.W.Lancaster, J.Bernstein. *Angew. Chem., Int. Ed.*, **54**, 6972 (2015)
989. J.-O.Henck, J.Bernstein, A.Ellern, R.Boese. *J. Am. Chem. Soc.*, **123**, 1834 (2001)
990. I.Barsky, J.Bernstein, P.W.Stephens, K.H.Stone, E.Cheung, M.B.Hickey, J.-O.Henck. *Cryst. Growth Des.*, **8**, 63 (2007)
991. L.Bhardwaj, P.K.Sharma, S.Visht, V.K.Garg, N.Kumar. *Pharm. Sinica*, **1**, 183 (2010)
992. M.N.Sovilj. *Acta Period. Technol.*, **41**, 105 (2010)
993. O.G.Bhusnure. *Indo Am. J. Pharm. Res.*, **5**, 3785 (2015)
994. N.Esfandiari. *J. Supercrit. Fluids*, **100**, 129 (2015)
995. P.G.Debenedetti, J.W.Tom, X.Kwauk, S.D.Yeo. *Fluid Phase Equilib.*, **82**, 311 (1993)
996. S.H.Soh, L.Y.Lee. *Pharmaceutics*, **11**, 21 (2019)
997. V.M.H.Yoshida, V.M.Balcao, M.M.D.C.Vila, J.M.O.Júnior, N.Aranha, M.P.D.Gremião, M.V.Chaud. *African J. Pharm. Pharmacol.*, **10**, 132 (2016)
998. P.Rabinarayan, S.Padilama. *J. Adv. Pharm. Sci. Technol.*, **1**, 13 (2013)
999. B.S.Sekhon. *Int. J. Pharm. Tech. Res.*, **2**, 810 (2010)
1000. P.B.Deshpande, G.A.Kumar, A.R.Kumar, G.V.Shavi, A.Karthik, M.S.Reddy, N.Udupa. *J. Pharm. Sci. Technol.*, **65**, 333 (2011)
1001. A.M.Vorobei, O.I.Pokrovskii, K.B.Ustinovich, O.O.Parenago, V.V.Lunin. *Vestn. RFFI*, **1**, 84 (2017)
1002. A.H.Harvey. *J. Phys. Chem.*, **94**, 8403 (1990)
1003. A.Ruhan, G.Motonobu, S.Mitsuru. In *Handbook of Food Analysis Instruments*. (Boca Raton, FL: CRC Press, 2008). P. 25
1004. E.Reverchon, G.Della Porta, I.De Rosa, P.Subra, D.Letourneur. *J. Supercrit. Fluids*, **18**, 239 (2000)
1005. P.Gosselin, F.-X.Lacasse, M.Preda, R.Thibert, S.-D.Clas, J.N.McMullen. *Pharm. Devel. Technol.*, **8**, 11 (2003)
1006. S.Wolff, S.Beuermann, M.Türk. *J. Supercrit. Fluids*, **117**, 18 (2016)
1007. M.Perrut, J.-Y.Clavier. *Ind. Eng. Chem. Res.*, **42**, 6375 (2003)
1008. E.Reverchon, I.De Marco, E.Torino. *J. Supercrit. Fluids*, **43**, 126 (2007)
1009. M.Sauceau, J.-J.Letourneau, B.Freiss, D.Richon, J.Fages. *J. Supercrit. Fluids*, **31**, 133 (2004)
1010. Patent US 6998051 (2006)

1011. R.Thakur, R.B.Gupta. *Int. J. Pharm.*, **308**, 190 (2006)
1012. J.Jung, M.Perrut. *J. Supercrit. Fluids*, **20**, 179 (2001)
1013. Z.Knez, E.Weidner. *Curr. Opin. Solid State Mater. Sci.*, **7**, 353 (2003)
1014. N.De Zordi, M.Moneghini, I.Kikic, M.Grassi, A.E.D.R.Castillo, D.Solinas, M.B.Bolger. *Eur. J. Pharm. Biopharm.*, **81**, 131 (2012)
1015. A.Shariati, C.J.Peters. *Curr. Opin. Solid State Mater. Sci.*, **7**, 371 (2003)
1016. E.Reverchon, R.Adami. *J. Supercrit. Fluids*, **37**, 1 (2006)
1017. E.Reverchon, E.Torino, S.Dowy, A.Braeuer, A.Leipertz. *Chem. Eng. J.*, **156**, 446 (2010)
1018. M.Perrut. *J. Supercrit. Fluids*, **66**, 359 (2012)
1019. H.Shinozaki, T.Oguchi, S.Suzuki, K.Aoki, T.Sako, S.Morishita, Y.Tozuka, K.Moribe, K.Yamamoto. *Drug Devel. Ind. Pharm.*, **32**, 877 (2006)
1020. M.Moneghini, B.Perissutti, F.Vecchione, I.Kikic, P.Alessi, A.Cortesi, F.Princivalle. *Curr. Drug Deliv.*, **4**, 241 (2007)
1021. A.Bouchard, N.Jovanović. *J. Supercrit. Fluids*, **44**, 422 (2008)
1022. K.Moribe, Y.Tozuka, K.Yamamoto. *Adv. Drug Deliv. Rev.*, **60**, 328 (2008)
1023. M.A.Rodrigues, J.o.M.Tiago, A.Duarte, V.Geraldes, H.A.Matos, E.Gomes Azevedo. *Cryst. Growth Des.*, **16**, 6222 (2016)
1024. V.N.Bagratashvili, S.E.Bogorodskiy, A.M.Egorov, L.I.Krotova, A.V.Mironov, O.O.Parenago, O.I.Pokrovskiy, K.B.Ustinovich, P.S.Chizhov, D.I.Prokopchuk, V.K.Popov, S.I.Tsypina. *Russ. J. Phys. Chem. B*, **11**, 1163 (2017)
1025. B.Long, G.M.Walker, K.M.Ryan, L.Padrela. *Cryst. Growth Des.*, **19**, 3755 (2019)
1026. Y.Iwai, H.Uchida, Y.Koga, Y.Mori, Y.Arai. *Fluid Phase Equilib.*, **111**, 1 (1995)
1027. N.Matubayasi, N.Nakao, M.Nakahara. *J. Chem. Phys.*, **114**, 4107 (2001)
1028. L.Xu, P.Kumar, S.V.Buldyrev, S.-H.Chen, P.H.Poole, F.Sciortino, H.E.Stanley. *Proc. Natl. Acad. Sci. USA*, **102**, 16558 (2005)
1029. S.Keskin, D.Kayrak-Talay, U.Akman, Ö.Hortaçsu. *J. Supercrit. Fluids*, **43**, 150 (2007)
1030. A.Tenorio, M.D.Gordillo, C.M.Pereyra, E.J.Martínez de la Ossa. *Ind. Eng. Chem. Res*, **46**, 114 (2007)
1031. I.Vyalov, M.Kiselev, T.Tassaing, J.Soetens, M.Federov, P.Damay, A.Idrissi. *J. Mol. Liq.*, **159**, 31 (2011)
1032. Z.Tang, J.-s.Jin, Z.-t.Zhang, H.-t.Liu. *Ind. Eng. Chem. Res*, **51**, 5515 (2012)
1033. S.Foltran, E.Cloutet, H.Cramail, T.Tassaing. *J. Supercrit. Fluids*, **63**, 52 (2012)
1034. E.Schurtenberger, M.Heuberger. *J. Supercrit. Fluids*, **71**, 120 (2012)
1035. V.Brazhkin, Y.D.Fomin, A.Lyapin, V.Ryzhov, K.Trachenko. *Phys. Rev. E*, **85**, 031203 (2012)
1036. S.Varona, J.Fernández, M.Rossmann, A.Braeuer. *Ind. Eng. Chem. Res*, **58**, 1054 (2013)
1037. Y.Medina-Gonzalez, T.Tassaing, S.Camy, J.-S.Condoret. *J. Supercrit. Fluids*, **73**, 97 (2013)
1038. O.Elizalde-Solis, L.A.Galicia-Luna. *Ind. Eng. Chem. Res.*, **50**, 207 (2011)
1039. M.Muntó, N.Ventosa, S.Sala, J.Veciana. *J. Supercrit. Fluids*, **47**, 147 (2008)
1040. S.Bristow, B.Y.Shekunov, P.York. *Ind. Eng. Chem. Res.*, **40**, 1732 (2001)
1041. Z.Huang, G.-B.Sun, S.Kawi, Y.Shi, R.Wen, S.-W.Song. *Fluid Phase Equilib.*, **238**, 26 (2005)
1042. M.Hojjati, Y.Yamini, M.Khajeh, A.Vatanara. *J. Supercrit. Fluids*, **41**, 187 (2007)
1043. J.K.Sabet, C.Ghotbi, F.Dorkoosh, A.Striolo. *Sci. Iran.*, **19**, 619 (2012)
1044. I.V.Kuznetsova, I.I.Gilmutdinov, I.M.Gilmutdinov, A.A.Mukhamadiev, A.N.Sabirzyanov. *Russ. J. Phys. Chem. B*, **7**, 814 (2013)
1045. D.Kostrzewa, A.Dobrzyńska-Inger, E.Rój. *Fluid Phase Equilib.*, **360**, 445 (2013)
1046. M.Lashkarbolooki, A.Z.Hezave, Y.Rahnama, R.Ozlati, H.Rajaei, F.Esmaeilzadeh. *J. Supercrit. Fluids*, **84**, 13 (2013)
1047. C.Tang, Y.-X.Guan, S.-J.Yao, Z.-Q.Zhu. *J. Chem. Eng. Data*, **59**, 3359 (2014)
1048. S.J.Macnaughton, I.Kikic, N.R.Foster, P.Alessi, A.Cortesi, I.Colombo. *J. Chem. Eng. Data*, **41**, 1083 (1996)
1049. R.D.Oparin, A.Idrissi, M.V.Fedorov, M.G.Kiselev. *J. Chem. Eng. Data*, **59**, 3517 (2014)
1050. E.N.Antonov, S.A.Minaeva, V.K.Popo. *Russ. J. Phys. Chem. B*, **7**, 849 (2013)
1051. M.Champeau, J.-M.Thomassin, C.Jérôme, T.Tassaing. *J. Chem. Eng. Data*, **61**, 968 (2016)
1052. R.D.Oparin, E.A.Vorobyev, M.G.Kiselev. *Russ. J. Phys. Chem. B*, **10**, 1108 (2016)
1053. S.Romero, B.Escalera, P.Bustamante. *Int. J. Pharm.*, **178**, 193 (1999)
1054. Y.Kobayashi, S.Ito, S.Itai, K.Yamamoto. *Int. J. Pharm.*, **193**, 137 (2000)
1055. R.Bettini, L.Bonassi, V.Castoro, A.Rossi, L.Zema, A.Gazzaniga, F.Giordano. *Eur. J. Pharm. Sci.*, **13**, 281 (2001)
1056. P.Gosselin, R.Thibert, M.Preda, J.McMullen. *Int. J. Pharm.*, **252**, 225 (2003)
1057. M.Tuerk, D.Bolten. *J. Supercrit. Fluids*, **116**, 239 (2016)
1058. A.Martin, K.Scholle, F.Mattea, D.Meterc, M.J.Cocero. *Crys. Growth Des.*, **9**, 2504 (2009)
1059. Y.-M.Chen, M.Tang, Y.-P.Chen. *Chem. – Eng. J.*, **165**, 358 (2010)
1060. S.Clercq, A.Mouahid, P.Gérard, E.Badens. *J. Supercrit. Fluids*, **141**, 29 (2018)
1061. R.D.Oparin, M.Moreau, I.De Waele, M.Paolantoni, A.Idrissi, M.G.Kiselev. *Eur. J. Pharm. Sci.*, **77**, 48 (2015)
1062. R.D.Oparin, D.V.Ivlev, A.M.Vorobei, A.Idrissi, M.G.Kiselev. *J. Mol. Liq.*, **239**, 49 (2017)
1063. R.D.Oparin, Y.A.Vaksler, M.A.Krestyaninov, A.Idrissi, S.V.Shishkina, M.G.Kiselev. *J. Supercrit. Fluids*, **152**, 104547 (2019)
1064. Y.E.Gorbaty, G.V.Bondarenko, E.Venardou, S.J.Barlow, E.Garcia-Verdugo, M.Poliakoff. *Vibrat. Spectrosc.*, **35**, 97 (2004)
1065. Y.E.Gorbaty. *Sverkhkriticheskie Flyuidy: Teoriya i Praktika,* **2** (1), 40 (2007)
1066. Y.E.Gorbaty, G.Bondarenko. *Rev. Sci. Instrum.*, **64**, 2346 (1993)
1067. Y.E.Gorbaty. *Rev. Sci. Instrum.*, **65**, 505 (1994)
1068. Y.E.Gorbaty, G.Bondarenko, S.Mileiko. *Rev. Sci. Instrum.*, **65**, 2739 (1994)
1069. S.Rey. Ph.D. Thesis. Institut de Chimie de la Matière Condensée de Bordeaux, Bordeaux, 1999
1070. P.Di Martino, A.M.Guyot-Hermann, P.Conflant, M.Drache, J.C.Guyot. *Int. J. Pharm.*, **128**, 1 (1996)
1071. G.P.Johari, S.Kim, R.M.Shanker. *J. Pharm. Sci.*, **96**, 1159 (2007)
1072. P.Derollez, E.Dudognon, F.Affouard, F.Danede, N.T.Correia, M.Descamps. *Acta Crystallogr., Sect. B*, **66**, 76 (2010)
1073. R.D.Oparin, A.M.Vorobei, M.G.Kiselev. *Russ. J. Phys. Chem. B*, **13**, 1139 (2019)

1074. J.E.Wertz, JR.Bolton *Electron Spin Resonance. Elementary Theory and Practical Applications*. (Dordrecht: Springer, 1986)
1075. A.M.Vasserman, A.L.Kovarskii. *Spinovye Metki i Zondy v Fizikokhimii Polimerov*. (Spin Labels and Probes in the Physicochemistry of Polymers) (Moscow: Nauka, 1986)
1076. W.M.Walsh, N.Bloembergen. *Phys. Rev.*, **107**, 904 (1957)
1077. N.Edelstein, A.Kwok, A.H.Maki. *J. Chem. Phys.*, **41**, 179 (1964)
1078. N.Edelstein, A.Kwok, A.H.Maki. *J. Chem. Phys.*, **41**, 3473 (1964)
1079. T.Sakurai, S.Okubo, H.Ohta. *J. Magn. Reson.*, **280**, 3 (2017)
1080. A.Y.Shaulov, Y.K.Shaulov, A.G.Sklyarova, N.I.Andreeva, N.S.Buchachenko, A.L.Enikolopov. *J. Exp. Theor. Phys.*, **36**, 82 (1973)
1081. S.N.Trukhan, V.F.Yudanov, O.N.Martyanov. *J. Supercrit. Fluids*, **57**, 247 (2011)
1082. S.N.Trukhan, V.F.Yudanov, O.N.Mart'yanov. *Russ. J. Phys. Chem. B*, **7**, 924 (2013)
1083. I.T.Horvath, J.M.Millar. *Chem. Rev.*, **91**, 1339 (1991)
1084. R.Livingston, H.Zeldes, M.S.Conradi. *J. Am. Chem. Soc.*, **101**, 4312 (1979)
1085. R.Livingston, H.Zeldes. *Rev. Sci. Instrum.*, **52**, 1352 (1981)
1086. K.E.Dukes, E.J.Harbron, M.D.E.Forbes, J.M.DeSimone. *Rev. Sci. Instrum.*, **68**, 2505 (1997)
1087. S.N.Batchelor. *J. Phys. Chem. B*, **102**, 615 (1998)
1088. C.R.Yonker, T.S.Zemanian, S.L.Wallen, J.C.Linehan, J.A.Franz. *J. Magn. Reson., Ser. A*, **113**, 102 (1995)
1089. D.M.Pfund, T.S.Zemanian, J.C.Linehan, J.L.Fulton, C.R.Yonker. *J. Phys. Chem.*, **98**, 11846 (1994)
1090. J.McCoy, W.L.Hubbell. *Proc. Natl. Acad. Sci. USA*, **108**, 1331 (2011)
1091. T.W.Randolph, C.Carlier. *J. Phys. Chem.*, **96**, 5146 (1992)
1092. S.Ganapathy, C.Carlier, T.W.Randolph, J.A.O'Brien. *Ind. Eng. Chem. Res.*, **35**, 19 (1996)
1093. P.R.Marriott, D.Griller. *J. Am. Chem. Soc.*, **103**, 1521 (1981)
1094. T.W.Randolph, D.S.Clark, H.W.Blanch, J.M.Prausnitz. *Proc. Natl. Acad. Sci. USA*, **85**, 2979 (1988)
1095. H.Yamada, K.Nishikawa, M.Honda, T.Shimura, K.Akasaka, K.Tabayashi. *Rev. Sci. Instrum.*, **72**, 1463 (2001)
1096. Y.Sueishi, N.Nishimura, K.Hirata, K.Kuwata. *Bull. Chem. Soc. Jpn.*, **61**, 4253 (1988)
1097. Y.Sueishi, S.Yamamoto, N.Nishimura. *Measure Sci. Technol.*, **4**, 1171 (1993)
1098. D.C.Roe. *J. Magn. Reson. (1969)*, **63**, 388 (1985)
1099. I.T.Horváth, E.C.Ponce. *Rev. Sci. Instrum.*, **62**, 1104 (1991)
1100. S.Bai, C.M.Taylor, C.L.Mayne, R.J.Pugmire, D.M.Grant. *Rev. Sci. Instrum.*, **67**, 240 (1996)
1101. S.Cannistraro. *Rev. Sci. Instrum.*, **55**, 996 (1984)
1102. S.L.Wallen, L.K.Schoenbachler, E.D.Dawson, M.A.Blatchford. *Anal. Chem.*, **72**, 4230 (2000)
1103. N.B.Minaev, O.I.Gromov, E.N.Golubeva, A.Kh.Vorob'ev, V.N.Bagratashvili. *Pribory i Tekhnika Eksperimenta*, **62**, 151 (2019)
1104. T.Umecky, M.Kanakubo, Y.Ikushima, N.Saito, J.Yoshimura, H.Yamazaki, J.Yana. *Chem. Lett.*, **31**, 118 (2002)
1105. C.R.Yonker, R.D.Smith. *J. Phys. Chem.*, **92**, 235 (1988)
1106. O.Kajimoto. *Chem. Rev.*, **99**, 355 (1999)
1107. S.C.Tucker. *Chem. Rev.*, **99**, 391 (1999)
1108. M.P.Heitz, F.V.Bright. *J. Phys. Chem.*, **100**, 6889 (1996)
1109. M.P.Heitz, M.Maroncelli. *J. Phys. Chem. A*, **101**, 5852 (1997)
1110. K.P.Johnston, S.Kim, J.Combes. In *Supercritical Fluid Science and Technology*. (Eds K.P.Johnston, J.M.L.Penninger). (Washington,DC: ACS, 1989). P. 52
1111. N.Wada, M.Saito, D.Kitada, R.L.Smith, H.Inomata, K.Arai, S.Saito. *J. Phys. Chem. B*, **101**, 10918 (1997)
1112. M.Kanakubo, T.Aizawa, T.Kawakami, O.Sato, Y.Ikushima, K.Hatakeda, N.Saito. *J. Phys. Chem. B*, **104**, 2749 (2000)
1113. T.Abe, S.Tero-Kubota, Y.Ikegami. *J. Phys. Chem.*, **86**, 1358 (1982)
1114. O.H.Griffith, P.J.Dehlinger, S.P.Van. *J. Membr. Biol.*, **15**, 159 (1974)
1115. A.H.Reddoch, S.Konishi. *J. Chem. Phys.*, **70**, 2121 (1979)
1116. C.Carlier, T.W.Randolph. *AIChE J.*, **39**, 876 (1993)
1117. T.Tachikawa, K.Akiyama, C.Yokoyama, S.Tero-Kubota. *Chem. Phys. Lett.*, **376**, 350 (2003)
1118. W.Song, R.Biswas, M.Maroncelli. *J. Phys. Chem. A*, **104**, 6924 (2000)
1119. R.F.Curl. *Mol. Phys.*, **9**, 585 (1965)
1120. J.L.de Grazia, T.W.Randolph, J.A.O'Brien. *J. Phys. Chem. A*, **102**, 1674 (1998)
1121. R.M.Anderton, J.F.Kauffman. *J. Phys. Chem.*, **98**, 12117 (1994)
1122. D.A.Hammond, M.Karel, A.M.Klibanov, V.J.Krukonis. *Appl. Biochem. Biotechnol.*, **11**, 393 (1985)
1123. T.W.Randolph, H.W.Blanch, J.M.Prausnitz, C.R.Wilke. *Biotechnol. Lett.*, **7**, 325 (1985)
1124. T.W.Randolph, D.S.Clark, H.W.Blanch, J.M.Prausnitz. *Science*, **239**, 387 (1988)
1125. J.C.Erickson, P.Schyns, C.L.Cooney. *AIChE J.*, **36**, 299 (1990)
1126. D.Miller, D.S.Clark, H.W.Blanch, J.M.Prausnitz. *J. Supercrit. Fluids*, **4**, 124 (1991)
1127. A.A.Galkin, B.G.Kostyuk, V.V.Lunin, M.Poliakoff. *Angew. Chem., Int. Ed.*, **39**, 2738 (2000)
1128. A.Cabanas, J.A.Darr, M.Poliakoff, E.Lester. *Chem. Commun.*, 901 (2000)
1129. S.L.Wallen, B.J.Palmer, J.L.Fulton. *J. Chem. Phys.*, **108**, 4039 (1998)
1130. K.Harrison, J.Goveas, K.P.Johnston, E.A.O'Rear. *Langmuir*, **10**, 3536 (1994)
1131. J.L.Fulton, D.M.Pfund, J.B.McClain, T.J.Romack, E.E.Maury, J.R.Combes, E.T.Samulski, J.M.DeSimone, M.Capel. *Langmuir*, **11**, 4241 (1995)
1132. K.P.Johnston, K.L.Harrison, M.J.Clarke, S.M.Howdle, M.P.Heitz, F.V.Bright, C.Carlier, T.W.Randolph. *Science*, **271**, 624 (1996)
1133. M.P.Heitz, C.Carlier, J.De Grazia, K.L.Harrison, K.P.Johnston, T.W.Randolph, F.V.Bright. *J. Phys. Chem. B*, **101**, 6707 (1997)
1134. E.N.Golubeva, N.A.Chumakova. *Russ. J. Phys. Chem. B*, **13**, 1088 (2019)
1135. M.Champeau, J.-M.Thomassin, T.Tassaing, C.Jérôme. *J. Controlled Release*, **209**, 248 (2015)
1136. O.R.Davies, A.L.Lewis, M.J.Whitaker, H.Tai, K.M.Shakesheff, S.M.Howdle. *Adv. Drug Deliv. Rev.*, **60**, 373 (2008)
1137. N.A.Chumakova, E.N.Golubeva, T.A.Ivanova, N.N.Vorobieva, P.S.Timashev, V.N.Bagratashvili. *Russ. J. Phys. Chem. B*, **12**, 1255 (2018)
1138. S.E.Bogorodski, L.I.Krotova, S.V.Kursakov, S.A.Minaeva, V.K.Popov, V. I.Sevast'yanov. *Russ. J. Phys. Chem. B*, **9**, 1011 (2015)
1139. A.Torres, E.Ilabaca, A.Rojas, F.Rodríguez, M.J.Galotto, A.Guarda, C.Villegas, J.Romero. *Eur. Polym. J.*, **89**, 195 (2017)
1140. C.S.Connon, R.F.Falk, T.W.Randolph. *Macromolecules*, **32**, 1890 (1999)
1141. E.J.Harbron, W.C.Bunyard, M.D.E.Forbes. *J. Polym. Sci., Part B: Polym. Phys.*, **43**, 2097 (2005)

1142. I.S.Miles, G.G.Cameron, A.T.Bullock. *Polymer (Guildf)*, **27**, 190 (1986)
1143. F.Tsay, S.D.Hong, J.Moacanin, A.Gupta. *J. Polym. Sci., Polym. Phys. Ed.*, **20**, 763 (1982)
1144. Z.Veksli, W.G.Miller. *Macromolecules*, **10**, 1245 (1977)
1145. F.-D.Tsay, A.Gupta. *J. Polym. Sci., Part B: Polym. Phys.*, **25**, 855 (1987)
1146. H.Zeldes, R.Livingston. *Fuel*, **61**, 1254 (1982)
1147. R.Livingston, H.Zeldes. *J. Phys. Chem.*, **87**, 1086 (1983)
1148. M.D.E.Forbes. *Photochem. Photobiol.*, **65**, 73 (1997)
1149. M.D.E.Forbes, H.Yashiro. *Macromolecules*, **40**, 1460 (2007)
1150. A.Brückner. *Adv. Catal.*, **51**, 265 (2007)
1151. A.Chu, B.Schlecker, K.Lips, M.Ortmanns, J.Anders. In *Proceedings of 2018 IEEE International Solid-State Circuits Conference*. (San Francisco, CA, 2018). P. 354